9-9-2016

Characterization of Biopolymeric Micro- Nano Structured 3D Porous Matrices in Combination with Bone Marrow Derived Mesenchymal Stem Cells for Bone Regeneration

Aja Aravamudhan
University of Connecticut - Storrs, aja@uchc.edu

Characterization of Biopolymeric Micro- Nano Structured 3D Porous Matrices in Combination with Bone Marrow Derived Mesenchymal Stem Cells for Bone Regeneration

Aja Aravamudhan, PhD
University of Connecticut -2016

Approximately half a million individuals suffer from fractures every year and the demand for bone graft procedures is on a continuous increase. Scaffold based bone tissue engineering (BTE) has made great progress in regenerating lost bone tissue. Several materials are used for fabrication of scaffolds for BTE. Biopolymers apart from being a cost effective alternative to conventional synthetic polymers used for fabrication of scaffolds, offer advantages such as greater bioactivity and biocompatibility with mammalian tissue. A clinically relevant cell type proven to improve bone healing is bone marrow derived mesenchymal stem cells (MSCs). The biomaterial used to deliver these stem cells can induce their differentiation into the osteoblastic lineage and hasten bone healing.

In this project we used polysaccharide and protein chemistry in a hierarchical scaffold design to accomplish structural stability and bioactivity. In these scaffolds, a cellulose derivative formed the micro scale structures, while collagen the most abundant osteogenic extracellular matrix (ECM) protein of bone, formed the self assembled nanostructures. This dissertation aims at characterizing these three- dimensional (3D) porous biopolymeric scaffolds of cellulose acetate (CA) and cellulose acetate coated with Nano-fibrous collagen (CAc), in terms of their ability to induce bone healing in combination with MSCs.

The CA and CAc scaffolds were compared to similar polyester (Poly-lactic acid co-glycolic acid) (PLGA) 3D porous scaffolds for their material properties and biological performance. It was seen that the CA scaffolds had greater hydrophilicity and when functionalized with collagen led to a more biomimetic self-assembly of collagen nanofibers. During the induced differentiation of seeded human bone marrow derived mesenchymal stem cells (hMSCs) *in vitro*,

the cells on polysaccharide scaffolds showed higher levels of osteoblastic progression than the cells on the polyester scaffolds.

The polysaccharide scaffolds also showed greater biocompatibility at twelve weeks of subcutaneous implantation in rats. On the other hand, polyester scaffolds started exhibiting increased foreign body response (FBR) by later time points. Finally, when implanted into critical sized calvarial defects of mice, the polysaccharide scaffolds seeded with bone marrow stromal cells showed greater bone formation and greater levels of collagen content, along with a more even distribution of osteoblastic markers throughout the scaffold structure than the control polyester scaffolds. Hence these findings demonstrated the potential of cellulose acetate and collagen, micro- nano structured biopolymeric scaffolds to be used in combination with MSCs as a biomaterial for bone regeneration.

Characterization of Biopolymeric Micro- Nano Structured 3D Porous Matrices in Combination with Bone Marrow Derived Mesenchymal Stem Cells for Bone Regeneration

Aja Aravamudhan

B.S., Anna University, **2008**

A Dissertation

Submitted in Partial Fulfillment of the

Requirements for the Degree of

Doctor of Philosophy

at the

University of Connecticut

2016

APPROVAL PAGE

Doctor of Philosophy Dissertation

Characterization of Biopolymeric Micro- Nano Structured 3D Porous Matrices in Combination with Bone Marrow Derived Mesenchymal Stem Cells for Bone Regeneration

Presented by
Aja Aravamudhan, B.S.

Major Advisor

Sangamesh G Kumbar

Associate Advisor

Cato T Laurencin

Associate Advisor

Barbara E Kream

Associate Advisor

Gloria A Gronowicz

Associate Advisor

Mina Mina

University of Connecticut
2016

“Dream is not that which you see while sleeping, it is something that does not let you sleep.”
- A.P.J Abdul Kalam

I dedicate this thesis to my loving parents Mr. Aravamudhan, and Mrs. Prema, for supporting me throughout my journey, for their unconditional love and for believing in my dreams.

Acknowledgements

Firstly, I would like to thank my advisor Dr. Sangamesh Kumbar. Dr. Kumbar welcomed me into the lab and gave me the opportunity to try varied things and implement new ideas. Dr. Kumbar always encouraged me to work hard and to never accept failure. His go-getter attitude and goal-oriented approach have always inspired me. I am truly indebted to you for the training, support, opportunities and mentorship you have provided me during my Ph.D.

I would like to thank my thesis committee for all their help and guidance. I would like to than Dr. Kream for helping me steer through the toughest times with her wisdom. Dr. Gronowicz had provided me with immensely valuable suggestions that helped me achieve success in my experiments. I would like to thank Dr. Laurencin for his time, inputs with material chemistry and for his constant encouragement. I would like to thank Dr. Mina for her thoughtful questions and inputs that made me think clearly through experiments, presentation and interpretation of data. I would not be completing this thesis without all their guidance, and I truly appreciate it.

I would like to thank the past and present members of Dr. Kumbar's lab and at the I.R.E. for their constant support. In particular, I would like to thank my lab mates Ms. Daisy Ramos, Mr. Matthew Harmon, Dr. Sean Peach, Dr. Meng Deng and Dr. Udaya Toti for being very encouraging and supportive during my early years in the lab. I would also like to thank Dr. Namdev Shelke and Dr. Roshan James. I would like to thank Ms. Eva Kan for always being ready to offer suggestions with experiments and share her expertise. I would also like to thank Dr. Jiang Tao, Dr. Kevin Lo, Dr. Syam Nukavarapu, Dr. Yusuf Khan and Dr. Lakshmi Nair. I would like to thank Ms. Hillary Stevens for her optimistic conversations.

I am very thankful to all my friends at the I.R.E. like Ms. Deborah Dorcemus, Ms. Xiaoyan Tang, Mr. Paulos Mengsteab, Dr. Farzana Sharmin, Mr. Jimmy Veronick, Dr. Shalini Gohil, Dr. Clarke Nelson, Dr. Paiyz Mikael, Ms. Erica Carbone, Ms. Koyal Rampura, Ms. Fayekah Assanah, Dr. Ashley Amini-Sami and Dr. Ami Amini. I am thankful to Dr. Nelson for sharing his thoughts on the calvarial defect model.

I would like to thank Dr. David Rowe and all his lab members for their support and suggestions. Though there were technical challenges involved in the histological evaluation of materials used in my project, members of Dr. Rowe's group were always ready to help me when I had questions or ran into problems. In particular I would like to thank Ms. Xi Jiang, Ms. Li Chen, and Dr. Liping Wang, for all the help with histology and the calvarial defect implantation surgery. I would like to thank Dr. Nathaniel Dyment for help with the two-photon imaging of collagen and for his valuable suggestions. I would like to thank Dr. Peter Maye for letting me use his imaging facilities so generously. I would like to thank Ms. Suzan Krueger, Dr. Anne Cowan and the confocal microscopy core at University of Connecticut Health Center. I am extremely thankful to the SBR area of concentration at the University of Connecticut Health Center, for training me in skeletal biology.

I would like to thank Institute of Material Science, University of Connecticut, Storrs. In particular I'd like to thank Dr. Gary Lavigne, Dr. Jack Gromek, Dr. Mark Dudley, Dr. Laura Pinatti, and Dr. Daniela Morales for being so welcoming and for teaching me material characterization techniques. My special thanks to Dr. Marie Cantino and Dr. Xuanhao Sun at the Bioscience Electron Microscopy Laboratory at the University of Connecticut, Storrs for teaching me the principles and working of electron microscopy.

I am also very thankful to the students who worked with me for their summer projects, namely Ms. Reyna Deese, Mr. Nathaniel Jenkins and Ms. Sydney Keise. I thank Mr. Jenkins for his help with histological biocompatibility analysis. I would also like to thank Dr. Mary Sanders from the clinical pathology department at the University of Connecticut Health Center for her guidance with the biocompatibility analysis. I also thank Mr. Matthew Harmon and Ms. Daisy Ramos for being instrumental in performing the animal surgeries with rats.

I would like to thank my teachers from school and college who taught me the wonder of science, for encouraging me to think deeply and solve problems. I would like to dedicate my thesis to my parents who have always supported me throughout my life. My parents believed in my dreams and gave me the freedom to chase them even if that meant I was going far away from them. I thank them for building me as a woman of values. I thank them infinitely for their unwavering belief in me.

List of Tables

TABLE 1.1 POPULAR SYNTHETIC POLYMERS, THEIR PROPERTIES AND APPLICATIONS 13
TABLE 1.2 TYPES OF CHONDROITIN SULPHATE (CS) 28
TABLE 2.1 QUANTIFICATION OF COLLAGEN ON SCAFFOLD AND COATING EFFICIENCY 86
TABLE 2.2 SACFFOLD COMPRESSIVE MECHANICAL PROPERTIES IN DRY AND HYDRATED STATE 86

Table of Figures

CHAPTER 1

FIGURE 1.1. STUCTURE OF PGA 8
FIGURE 1.2 STRUCTURE OF PLA 9
FIGURE 1.3 PLGA STRUCTURE. 10
FIGURE 1.4 STRUCTURE OF PCL 11
FIGURE 1.5 POLYSACCHARIDES IN BIOMEDICAL APPLICATIONS 20
FIGURE 1.6 STRUCTURE OF HYALURONIC ACID (HA) 22
FIGURE 1.7 CHAIN LENGTH OF HA 23
FIGURE 1.8 STRUCTURE OF CHONDROITIN SULPHATE (CS) 30
FIGURE 1.9 STRUCTURE OF CHITIN AND CHITOSAN 36
FIGURE 1.10 NANOFIBERS OF CITIN AND CHITOSAN 38
FIGURE 1.12 GELLATION OF ALGINIC ACID 43
FIGURE 1.12 STRUCTURE OF CELLULOSE 52
FIGURE 1.13 ANHYDROGLUCOSE UNIT OF CELLULOSE 52
FIGURE 2.1 OPTIMIZATION OF SINTERING SOLUTION 87
FIGURE 2.2 MORPHOLOGY OF CA-COLLAGEN SCAFFOLDS 88
FIGURE 2.3 MORPHOLOGY OF EC-COLLAGEN SCAFFOLDS 89
FIGURE 2.4 COLLAGEN NANOFIBER STABILITY *IN VITRO* 90
FIGURE 2.5 METABOLIC ACTIVITY OF SEEDED HOBS 91
FIGURE 2.6 PROLIFEARTION OF SEEDED HOBS 92
FIGURE 2.7 ALP ACTIVITY OF SEEDED HOBS 93
FIGURE 2.8 MINERALIZATION BY SEEDED HOBS 94
FIGURE 2.9 VIABILITY OF SEEDED HOBS 95
FIGURE 3.1 CHARACTERIZATION OF COLLAGEN NANOFIBERS 118
FIGURE 3.2 HYDRATION PROPERIES 119
FIGURE 3.3 CHANGES IN PLGA CHEMISTRY ON COLLAGEN TREATMENT 120
FIGURE 3.4 CHANGES IN CA CHEMISTRY ON COLLAGEN TREATMENT 121
FIGURE 4.1 VIABILITY, PROLIFERATION AND OSTEOBLASTIC MARKERS OF SEEDED HMSCS 138
FIGURE 4.2 OSTEOBLASTIC GENE AND PROTEIN EXPRESSION BY HMSCS 139
FIGURE 4.3 VIABILITY OF SEEDED HMSCSS 144
FIGURE 4.4 PROLIFERATION OF SEEDED HMSCS 145
FIGURE 4.5 OSTEOCHONDRAL GENE EXPRESSION BY SEEDED HMSCS 146
FIGURE 5.1 STAAINED HISTOLOGICAL SECTIONS AT EARLY TIME POINTS 152
FIGURE 5.2 STAINED HISTOLOGICAL SECTIONS AT LATE TIME POINTS 153
FIGURE 5.3 HISTOMORPHOMETRIC ANALYSIS OF SUBCUTANEOUS IMPLANTS 154
FIGURE 6.1 MORPHOLOGY OF SCAFFOLD 172
FIGURE 6.2 CALVARIAL SURGERY AND SCAFFOLD GROUPS IMPLANTED 173
FIGURE 6.3 CALVARIAL IMPANTS WITH MATERIAL ONLY 174
FIGURE 6.4 CALVARIAL IMPLANTS WITH MATERIALS AND DONOR CELLS 175
FIGURE 6.5 HISTOLOGICAL SECTIONS OF SCAFFOLDS WITHOUT CELLS (GROUP 2) 176
FIGURE 6.6 ECM MARKERS IMMUNOSTAINED ON CELL SEEDED SCAFFOLDS (GROUP 2) 177
FIGURE 6.7 ECM PROTEIN CONTENT ON SEEDED IMPLANTS 178
FIGURE 6.8 STAINED HISTOLOGICAL SECTIONS OF CELL SEEDED SCAFFOLDS (GROUP 2) 179
FIGURE 6.9 QUANTIFICATION OF BONE FORMATION, HOST AND DONOR CELLS 180
FIGURE 6.10 OSTEOBLASTIC ACTIVITY ON CELL SEEDED SCAFFOLDS (GROUP 2) 181
FIGURE 6.11 OSTEOCLASTIC ACTIVITY ON CELL SEEDED SCAFFOLDS (GROUP2) 181
FIGURE 6.12 QUANTIFICATION OF OSTEOBLASTIC AND OSTEOCLASTIC ACTIVITY ON SEEDED IMPLANTS 182
FIGURE 6.13 HISTOLOGICAL SECTIONS OF SCAFFOLDS WITHOUT CELLS (GROUP 1) 191
FIGURE 6.14 HISTOLOGICAL SECTIONS OF SCAFFOLDS WITHOUT CELLS (GROUP 3) 192
FIGURE 6.15 ECM MARKERS IMMUNOSTAINED ON CELL SEEDED SCAFFOLDS (GROUP 1) 193
FIGURE 6.16 ECM MARKERS IMMUNOSTAINED ON CELL SEEDED SCAFFOLDS (GROUP 3) 194
FIGURE 6.17 STAINED HISTOLOGICAL SECTIONS OF CELL SEEDED SCAFFOLDS (GROUP 1) 195
FIGURE 6.18 STAINED HISTOLOGICAL SECTIONS OF CELL SEEDED SCAFFOLDS (GROUP 3) 196
FIGURE 6.19 OSTEOBLASTIC ACTIVITY ON CELL SEEDED SCAFFOLDS (GROUP 1) 197

FIGURE 6.20 OSTEOBLASTIC ACTIVITY ON CELL SEEDED SCAFFOLDS (GROUP 3) 198
FIGURE 6.21 OSTEOCLASTIC ACTIVITY ON CELL SEEDED SCAFFOLDS (GROUP 1 AND 3)..... 199

Table of content

Acknowledgements ..... i.v
List of Tables vii
Table of Figures viii
Table of Content ..... …x

1 Chapter 1 1
1.1 Bone Loss and demand for implants 1
1.2 Clinical treatment of critical sized bone defects 1
1.2.1 Autograft 1
1.2.2 Allograft 2
1.2.3 Xenograft 3
1.2.4 Other materials 3
1.3 Bone Tissue Engineering (BTE) 4
1.4 Scaffolds in BTE 4
1.5 Attributes of a successful BTE scaffold 5
1.5.1 Osteoconduction 5
1.5.2 Osteoinduction 5
1.5.3 Osteointegration 6
1.6 Materials used as scaffolds for BTE 6
1.6.1 Synthetic polymers in BTE 6
1.6.1.1 Poly(α-hydroxy acid)s 7
1.6.1.1.1 Polyglycolides (PGA) 8
1.6.1.1.2 Polylactides (PLA) 8
1.6.1.1.3 Poly(lactide-co-glycolide) 9
1.6.1.1.4 Polycaprolatone 10
1.6.1.2 Poly (ortho esters) 11
1.6.1.3 Polyanhydrides 12
1.6.2 Natural polymers in BTE 15
1.6.2.1 Polysaccharides in tissue engineering and drug delivery 15
1.6.2.1.1 Hyaluronic acid 21
1.6.2.1.1.1 1.6.2.1.1.1 Chemical structure, properties and sources 21
1.6.2.1.1.2 Attempts made in Tissue Engineering and Drug delivery 23
1.6.2.1.1.2.1 Hyaluronic acid alone 23
1.6.2.1.1.2.2 HA derivatives and combinations with other polymers 24
1.6.2.1.1.3 Promises and challenges with HA 27
1.6.2.1.2 Chondroitin sulfate 28
1.6.2.1.2.1 Chemical structure, properties and sources 28
1.6.2.1.2.2 Attempts made in Tissue engineering and drug delivery 30
1.6.2.1.2.2.1 Chondroitin sulfate alone 30
1.6.2.1.2.2.2 Chondroitin sulfate derivatives and combination with other polymers 31
1.6.2.1.2.3 Promises and challenges with Chondroitin sulfate 34
1.6.2.1.3 Chitin and chitosan 35
1.6.2.1.3.1 Chemical structure, properties and sources 35
1.6.2.1.3.2 Attempts made in Tissue engineering and drug delivery 38
1.6.2.1.3.2.1 Chitosan alone 38
1.6.2.1.3.2.2 Chitosan derivatives and combination with other polymers 39
1.6.2.1.3.3 Promises and challenges with Chitosan in tissue engineering 42
1.6.2.1.4 Alginic acid 42
1.6.2.1.4.1 Chemical structure, properties and sources 42
1.6.2.1.4.2 Attempts made in Tissue engineering and drug delivery 44
1.6.2.1.4.2.1 Alginate alone 44
1.6.2.1.4.2.2 Alginate Derivatives and combinations with other polymers 45
1.6.2.1.4.3 Promises and challenges with Alginates in tissue engineering 50

1.6.2.1.5 Cellulose 50
1.6.2.1.5.1 Chemical structure, properties and sources 50
1.6.2.1.5.2 Attempts made in Tissue engineering and drug delivery 53
1.6.2.1.5.2.1 Cellulose alone 53
1.6.2.1.5.2.2 Cellulose derivatives and combination with other polymers 54
1.6.2.1.5.3 Promises and challenges with cellulose 59
1.6.2.2 Proteins in tissue engineering 60
1.6.2.2.1 Collagen 60
1.6.2.2.2 Fibronectin 61
1.6.2.2.3 Fibrin 62
1.6.2.2.4 Vitronectin 62
1.6.2.2.5 Keratin 62
1.6.2.2.6 Silk 63
1.7 Design of Scaffolds for BTE 63
1.7.1 Processes used for fabrication of macro and microporous BTE scaffolds 63
1.7.1.1 Thermally induced phase separation (TIPS) 63
1.7.1.2 Solvent casting and particle leaching 64
1.7.1.3 Solid freeform fabrication techniques (SFFT) 65
1.7.1.4 Microsphere sintering 65
1.7.1.5 Coated scaffolds 66
1.7.1.6 3D Printing 66
1.7.2 Processes used for fabrication of nanoscale BTE scaffolds 67
1.7.2.1 Self assembly 67
1.7.2.2 Electrospinning 67
1.8 Cells used in BTE 68
1.8.1 Somatic cells in BTE 68
1.8.1.1 Cells used in analysis of BTE scaffolds 68
1.8.1.2 Cells used in vivo 68
1.8.2 Stem cells in BTE 69
1.8.2.1 Embryo derived stem cells 69
1.8.2.1.1 Embryonic stem cells 69
1.8.2.1.2 Amniotic fluid derived stem cells (AFSCs) 69
1.8.2.2 Adult stem cells 70
1.8.2.2.1 Induced pluripotent stem cells (iPSCs) 70
1.8.2.2.2 Bone marrow derived mesenchymal stem cells (BM-MSCs) 70
1.8.2.2.3 Adipose derived stem cells (ADSCs) 70
2 Chapter 2 Preliminary Studies 72
2.1 Introduction 72
2.2 Materials and Methods 75
2.2.1 Materials 75
2.2.2 Polysaccharide Microsphere Fabrication 75
2.2.3 3D Porous Scaffold Fabrication 76
2.2.4 Functionalization of 3D Scaffolds: Micro-Nano Structured Scaffolds 76
2.2.5 Collagen Content in Micro-Nano Structured Scaffolds 77
2.2.6 Scanning Electron Microscopy (SEM) 77
2.2.7 Micro-Nano Structured Scaffolds: Collagen Nanofiber Stability in Solution 78
2.2.8 Compressive Mechanical Properties 78
2.2.9 Porosimetry 79
2.2.10 Cell Culture 79
2.2.11 Cell Viability Assay 80
2.2.12 Cell Proliferation (Picogreends DNA Assay) 80
2.2.13 Alkaline Phosphatase Activity 81
2.2.14 Mineralized Matrix Deposition Assay 81

2.2.15 Live/Dead Cell Viability 82
2.2.16 Statistical Analysis 82
2.3 Results *83*
2.3.1 Fabrication of Sintered Microsphere Scaffold and Effect of Solvent Composition on Sintering Morphology 83
2.3.2 Morphology of Functionalized Microsphere Scaffolds with Collagen to Form Micro-Nano Structures 83
2.3.3 Temporal Stability of Nanofibers on the Scaffold Surface Under Culture Condition 84
2.3.4 Mechanical Property and Porosity of Scaffolds Under Dry and Wet Conditions 84
2.3.5 Cell Survival and Proliferation 84
2.3.6 Differentiation Measured by Alkaline Phosphatase Content and Mineral Deposition 85
2.3.7 Cell viability and morphology 85
2.4 Discussion *96*
2.5 Conclusions *104*
2.6 SPECIFIC AIMS *105*
2.6.1 Specific Aim 1: To characterize and contrast the unmodified and collagen functionalized CA scaffolds for their material properties 106
2.6.2 Specific Aim2: To test the performance of CA-collagen, micro-nano structured scaffolds *in vitro* using bone marrow derived MSCs. 106
2.6.3 Specific Aim3: To test the performance of CA-collagen, micro-nano structured scaffolds in vivo 106
2.6.3.1 Specific Aim3a: To test the biocompatibility of CA-collagen, micro-nano structured scaffolds in vivo in a subcutaneous implantation. 106
2.6.3.2 Specific Aim3b: To test the performance of CA-collagen, micro-nano structured scaffolds in vivo in a bone defect in mouse calvarium. 107

3 Chapter 3 108
3.1 Introduction *108*
3.2 Materials and Methods *109*
3.2.1 Materials 109
3.2.2 Preparation of microspheres 109
3.2.3 Preparation of micro-porous sintered microsphere scaffolds 110
3.2.4 Preparation of micro-nano structured scaffolds 110
3.2.5 Quantification of Scaffold collagen Content 111
3.2.6 Morphology of collagen by two- photon microscopy 112
3.2.7 Characterization internal structure of scaffolds by SEM 112
3.2.8 Scaffold water uptake by gravimetric analysis 112
3.2.9 Microsphere surface chemistry by ATR-FTIR analysis 113
3.2.10 Microsphere surface crystallinity by XRD analysis 113
3.2.11 Polymer molecular weight by GPC analysis 113
3.2.12 Statistical analysis 114
3.3 Results *115*
3.3.1 Characterization of collagen nanofibers 115
3.3.2 Analysis of hydration property 116
3.3.3 Characterization of Materials properties 116
3.4 Discussion *123*
3.5 Conclusions *126*

4 Chapter 4 127
4.1 Introduction *127*
4.2 Materials and Methods *128*
4.2.1 Materials 128

4.2.2 Preparation of microspheres 129
4.2.3 Preparation of micro-porous sintered microsphere scaffolds 129
4.2.4 Preparation of micro-nano structured scaffolds 130
4.2.5 *In Vitro* human Mesenchymal Stem Cells (hMSCs) culture on scaffolds 130
4.2.6 Cell viability 131
4.2.7 Cell proliferation 131
4.2.8 Alkaline phosphatase activity 132
4.2.9 Mineralized matrix deposition by cells 132
4.2.10 Gene expression 133
4.2.11 Osteogenic marker Immunostaining 134
4.2.12 Statistical analysis 135
4.3 Results *136*
4.3.1 Characterization of hMSC response 136
4.4 Discussion *140*
4.5 Conclusions *142*
4.6 Supplemental Figures *144*

5 Chapter 5 147
5.1 Introduction *147*
5.2 Materials and Methods *148*
5.2.1 Subcutaneous implantation 148
5.2.2 Histological staining 148
5.2.3 Histomorphometric analysis 149
5.2.4 Statistical analysis 149
5.3 Results *150*
5.3.1 Cellularity in the scaffolds 150
5.3.2 Immune response to scaffolds 151
5.3.3 Vascularity in scaffolds 151
5.4 Discussion *155*
5.5 Conclusions *156*

6 Chapter 6 157
6.1 Introduction *157*
6.2 Materials and Methods *161*
6.2.1 Materials 161
6.2.2 Preparation of microspheres 161
6.2.3 Preparation of micro-porous sintered 3D microsphere scaffolds 161
6.2.4 Preparation of collagen naonfiber infused cellulose 3D microporous scaffolds 162
6.2.5 Characterization of internal structure of scaffolds by SEM 162
6.2.6 Design of calvarial implantation studies 163
6.2.7 BMSC Culture 164
6.2.8 Calvarial surgery 164
6.2.9 Sample harvest 165
6.2.10 Histomorphometric analysis of calvarial implants 166
6.3 Results *167*
6.3.1 Scaffold Morphology 167
6.3.2 Radiological examination of bone formation with scaffolds alone and scaffolds along with BMSCs 167
6.3.3 Histological analysis of implantation of scaffolds alone 168
6.3.4 ECM protein deposition by scaffolds and BMSCs 169
6.3.5 Osteoblastic and osteoclastic activity in scaffolds seeded with BMSCs 170
6.4 Discussion *183*

6.5 Conclusions *189*
6.6 Supplemental Figures *191*

7 Chapter 7 ..... **200**
7.1 Stabilizing self- assembled collagen in vivo and uncovering the mechanism of material- protein interactions *200*
7.2 Mechanism of bone formation in calvarial defects in the presence of BMSCs *201*
7.3 Scaffold degradation properties *202*

8 Appendix **204**
8.1 Journal Articles *204*
8.1.1 Research Articles 204
8.1.2 Review Article 204
8.2 Book Chapters *204*
8.3 Conference Abstracts *204*
8.3.1 Conference Posters 204
8.3.2 Conference Podium Presentations 205

9 References **206**

1 Chapter 1

1.1 Bone Loss and demand for implants

High impact trauma, pathological conditions such as tumors and infections and conditions such as osteoporosis can lead to massive defects of the bone(*1*). About 5- 10% of the total number of bone fractures result in delayed or non-union and surgical intervention is needed(*2-4*). The ease of handling combined with the huge demand renders bone as one of the most transplanted organs(*5*). About 0.5 million bone grafts are carried out in the U.S. alone, while more than two million procedures are performed around the globe (*6-8*) per annum(*5*). Though using bone from the patient itself (autografting) is considered the golden standard for achieving bone healing, it is restricted by availability and discomfort to the patient. Allografts on the other hand help overcome these limitations, but carry the threat of low remodeling due to excessive processing and possibility of disease transmission(*9*). Hence bone tissue engineering, where biomaterial scaffolds, biological factors and cells are used alone or in a combination promises better bone regeneration(*9*). The demand for bone graft subsititutes is constantly increasing at a rate of 3.8% every year(*10*).

1.2 Clinical treatment of critical sized bone defects

1.2.1 Autograft

Autograft is bone harvested from a non- essential site in the host. Hence the donor and the host are the same in the case of autografts. This grafted bone could be obtained most commonly from the iliac crest or fibula, chin, ribs, mandibles and parts of the skull from the patient(*11, 12*). The outcomes of autografting of bone are seen to be superior to any other

bone grafting technique. There is regeneration with new bone formation at the defect site, with complete remodeling of the implanted autograft, with no immune issues(*13*). Hence autografts are termed the 'golden standard'. On the flipside, there are two surgeries needed on the patient, one for explantation of the autograft and another for implantation of the graft into the defect site(*14*). Therefore the procedures are complicated by morbidity at the donor site. Additionally the availability of non-essential bone is limited in very young and very old patients, posing another limitation(*12, 15*).

1.2.2 Allograft

Allograft is bone obtained from another human donor, different from the patient undergoing the transplantation. This source could be alive as seen with patients who have a total hip replacement, where the extracted bone could be processed and implanted as a bone graft in a patient requiring an allograft implantation. The source could be cadaveric and such bone could be banked, processed and used in patients as an allograft(*16*). While allografts overcome limitations of autografts such as no excessive pain to the patient associated with explantation of the bone to be grafted, and is not limited by availability, they have their set off limitations. The allografts have been documented to have issues of disease transmission and immune rejection by host tissue(*17, 18*). Hence they tend to be treated by extreme measures to ensure the elimination of biologics that may ensue in disease transmission or rejection of the allograft. This processing leaves the allograft with poor biological properties for bone regeneration. Hence unlike autografts, allografts tend to be mildly osteogenic, but pose a challenge to remodeling and regeneration of lost bone(*19*).

1.2.3 Xenograft

Xenograft is a graft obtained from species other than human. Most of these xenografts are highly processed materials, with high calcium content to favor bone formation. Some popular products are a coral based xenograft called coral derived granules (CDG)(*20*), bovine(*21*) and porcein processed bone materials. Interpore and Pro-osteon (Interpore International, Inc., Irvine, CA) are coral based products available in the market. Bio-Oss (Geistlich Biomaterials, Geistlich, Switzerland), Osteograf-N (CeraMed Co., Denver, CO), and Endobon (Merck Co., Darmstadt, Germany) are bovine-based products in the market(*22*). While encouraging results have been seen in dentistry with the use of xenografts(*23*), orthopaedic outcomes have been limited. There are also concerns of disease transmission and hence xenografts are not a popular clinical option as bone grafts(*24, 25*).

1.2.4 Other materials

Other materials used as bone grafts are ceramics, and composites of calcium phosphate such as HA and tri calcium phosphate (TCP)(*25*), calcium phosphate cements(*26*), and calcium sulphate(*27*). Since bone contains calcim and phosphate as its mineral component, these materials are biocompatible and osteoconductive(*28*). They are however brittle with mechanical strength far below that of cortical bone. Hence though these ceramic and calcium phosphate based fillers are used in smaller defects, they are not used in the case of load bearing long bone defects.

1.3 Bone Tissue Engineering (BTE)

Though the concept of application of materials to replace lost tissue started, as early in the 17th century when artificial legs were made out of wood and metal(*29*), the concept of tissue engineering is relatively young as it has been around for only the past twenty-five years(*30*). The term 'tissue engineering' was coined in 1987(*30, 31*). Tissue engineering involves the integration of engineering, chemistry and biology to achieve tissue regeneration(*29*). Rather than the earlier concept of using an inert material that acts as a mechanical replacement for the lost tissue, the tissue-engineering concept takes advantage of the knowledge gained from multiple fields and applies it to formulate a platform made of biomaterials, cells, factors and design considerations to achieve complete healing of lost bone(*32*).

1.4 Scaffolds in BTE

The scaffold for BTE act as a template for regeneration to occur and the properties of the biomaterial can dictate the nature of bone regeneration achieved(*33*). It is well known that the scaffold's material properties such as moderate hydrophilicity(*34*), morphology(*35*), porosity(*36*), chemical functionalities(*37, 38*) and biomechanical properties(*39*) can be used to direct effective bone healing, by influencing the resident osteoblasts and by inducing the homing, growth and differentiation of progenitor cells. BTE scaffolds act as the delivery vehicle for stem cells and growth factors, and their design considerations can lead to controlled delivery of these agents in order to elicit maximum regeneration of lost bone(*40*). Therefore the selection of an appropriate material to formulate the scaffold and have a smart design are important for a biomaterial scaffold for BTE to perform well.

1.5 Attributes of a successful BTE scaffold

There are three essential attributes for a scaffold for BTE: Osteoconductivity, osteoinductivity and osteointegrativity.

1.5.1 Osteoconduction

Osteoconduction is the ability of the scaffold to allow the resident cells in bone to grow into the scaffold(*41*). Hence osteoconductive materials provide a conducive environment that allows the bone to grow on the biomaterial's surface(*42*). An important consideration in achieving osteoconduction is vascularization of the biomaterial to maintain live osteoblasts on the scaffold surface(*43*). A number of pro-proliferative growth factors like Insulin-like growth factor (IGF-I, II), fibroblast growth factors (FGFs), transforming growth factor β (TGF-β), and platelet-derived growth factor (PDGF) are known to be osteoconductive(*44*). Collagen and calcium phosphate based materials are known to be osteoconductive(*30*).

1.5.2 Osteoinduction

Osteoinduction is the ability of the scaffold to facilitate the differentiation of progenitor cell population into the osteoblastic lineage. This property is important to the scaffold system as these progenitor cells can further recruit other cell types and secrete factors that hasten the process of bone healing(*45*). The first instance of osteoinduction was seen with bone formation by the implantation of demineralized bone matrix in the muscle, termed extopic bone formation. Bone morphogenetic proteins (BMPs) were the factors isolated and found to be responsible for osteoinduction(*46*). Progenitor cells are found to secrete this growth factor in response to bone injuries as well(*29*). Hence most systems utilize BMPs or progenitor cells to make the systems osteoinductive.

1.5.3 **Osteointegration**

Osteointegration is the ability of the scaffold to establish and maintain intimal contact with the living bone tissue(*47, 48*). Osteointegration can be seen as an extension of the scaffold's ability to be osteoconductive and osteoinductive. A material that allows for progenitor cell recruitment, differentiation and allows for the proliferation of cells in the bone forms a good contact with the neighboring bone tissue(*49*). Rough surfaces and mineral (HA deposited) scaffold surfaces are known to show greater osteointegration(*49*). The layer of integration is about 40- 150 nm thick and hence it is tough to examine by microscopic examination(*50*).

1.6 Materials used as scaffolds for BTE

Materials of many different properties and origin are used to formulate scaffolds for tissue engineering. Though initially the idea was to have an inert matrix that allows the lost tissue to be mechanically replaced, and the expectation from the material was to be immune acceptable, nowadays smart materials capable of inducing bone regeneration are sought. Polymers of both natural and synthetic origin have been used for a variety of bone BTE applications. A way of categorizing these polymers used for BTE is based on their origin- 1. Synthetic polymers and 2. Natural polymers.

1.6.1 Synthetic polymers in BTE

Most synthetic polymers used in tissue engineering are designed to be degradable, so as to transfer the load onto the regenerating tissue as they dissolve away. Most of these polymers have chemical groups that have chemical bonds that are break on the action of water (hydrolytically degradation) or due to enzymes (enzymatic degradation). Most synthetic polymers undergo hydrolytic degradation(*51*). However there are a few engineered polymers that use amino acid monomers and are engineered to degrade enzymatically. Hydrolytically degradable polymers are synthesized by condensation (step) polymerization or chain

(addition) polymerization reaction(*52*). The classes of hydrolytically degradable synthetic polymers used in tissue engineering are:

1. Poly(α-hydroxy acid)s
2. Poly(ortho esters)
3. Polyanhydrides

Though a number of scaffolds have been made with each of these polymers and their combinations there are a few polymers that have been approved by regulatory authorities for use in biomedical devices(*53*). These polymers are:

1.6.1.1 Poly(α-hydroxy acid)s

Poly (α-esters) are polymers that have a labile aliphatic ester linkage in their chemical backbone. Ring opening and condensation polymerization reactions lead to the synthesis of poly (α-esters). Poly (α-hydroxy acid)s constitute the most popular and well studied group of Poly(α-esters). Though polycondensation of monomers could be employes to synthesize these poly(α-hydroxy acid)s, ring opening polymerization (ROP) reaction offers greater control over the molecular weight of the product formed. Additionally the reaction conditions seen with ROP process render it mild in contrast to polycondensation and hence the process is industrially relevant for scale up of production(*54*). Poly -**lactides, glycolides** and **caprolactones** are the most widely used poly(α-hydroxy acid)s in BTE applications.

1.6.1.1.1 Polyglycolides (PGA)

Polyglycolides were some of the earliest degradable polymers employed in tissue engineering(*55*). The chemical structure of PGA is given above (Figure 1.1). The high tensile strength and the solubility of polyglycolides can be attributed to their highly crystalline nature (45- 55%). Some matrices made of polyglycolide exhibit a modulus of 12.5 GPa. Due to their great initial mechanical property, Biofix^{R} has been developed as a polyglycolide based device for bone. Polyglycolides however undergo bulk degradation of the polymer matrix(*56*). The end product of degradation is glycine. These degradation products are highly acidic, but can be shuttled into the tricarboxylic acid metabolic cycle. The buildup of the acidic pH could be overwhelming for the tissue and hence this polymer is most commonly used in combination with other polymers to combat the disadvantage(*57*).

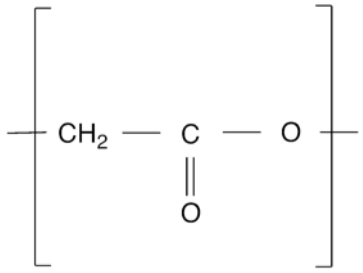

Figure 1.1. Stucture of PGA

1.6.1.1.2 Polylactides (PLA)

Polylactide is a chiral molecule. The L- and D- optically active isoforms are seen in polylactide as a racemic micture of (D, L)- lactide. The L- lactide isoform is the naturally occurring one. Poly (L- lactide) (PLLA) is also a crystalline (37% crystallinity) polymer. The general chemical structure of PLA is shown above (Figure 1.2) PLLA is slow degrading and has a high modulus of 4.8 GPa. Hence a number of implants and devices for orthopaedic application have been developed using PLLA. Phantom Soft Thread Soft Tissue Fixation

Screws, Phantom Suture Anchors (DePuy), Full Thread Bio Interference Screws (Arthrex), BioScrews, Bio-Anchors, Meniscal Stingers (Linvatec), and

Clearfix Meniscal Darts (Innovasive Devices) are some examples of such orthopaedic devices(*58, 59*). Since PLLA is more hydrophobic than polyglycolides, it has a very long degradation time of more than five years in the body. Hence poly (DL-lactides) (PDLLA) has also been investigated for tissue engineered device formulation. PDLLA has a lower modulus than PLLA (1.9 GPa). Mass loss occurs at 12- 16 months in the case of PDLLA(*57*). All polylactides exhibit bulk degradation properties(*60*). Lactic acid is the end product from their degradation and this can be shuttled into the tricarboxylic acid metabolic cycle for elimination(*57*).

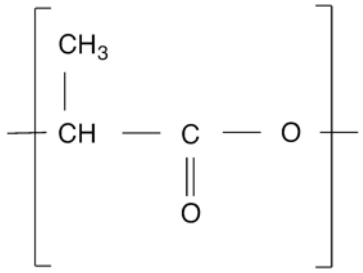

Figure 1.2 Structure of PLA

1.6.1.1.3 Poly(lactide-co-glycolide)

The chemical structure of Poly(*lactide-co-glycolide*) (PLGA), is given above (Figure 1.3). PLGA is the co-polymer of L / -DL- Lactide and glycolide. Different ratios of lactide and glydolide have been used to formulate PLGA of various molecular weights and degradation rates. In the case of PLGA, polymers with an intermediate composition (50/50) were more susceptible to degradation (1-2 months *in vivo*) than compositions at the either extreme ends of the compositional spectrum (75/ 25 PLGA: 4-5 months *in vivo*, and 85/15 PLGA: 5-6 months *in vivo* for degradative mass loss)(*61*). Many studies have used PLGA to create micro

and nanoscale featured scaffolds for BTE(*62*). PLGA due to its ease of being engineered to desired qualities lends itself to be fabricated using a number of scaffold fabrication techniques such as gas foaming(*63*), 3D sintered microspheres(*64*) and electrospun nanofiber scaffolds(*65*) . Hence PLGA is a polymer under extensive investigation for BTE and the United States Food and Drug Administration (U.S.F.D.A) has approved it for several drug delivery applications. However the degradation kinetics and the degradation products associated with PLGA continue to pose limitations on achieving controlled release(*66*) of factors from the polymer and sometimes pose the threat of loss of activity of factors due to change in pH.

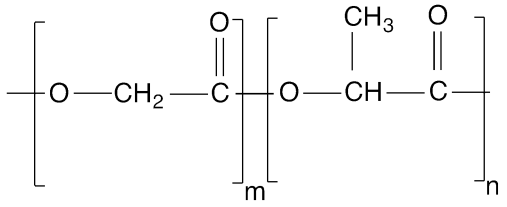

Figure 1.3 PLGA Structure.

The chemical structure of Poly(lactide-co-glycolide) (PLGA) (Ratio of PGA: PLA is m:n and it can be modulated to achieve different kinds of PLGA copolymer).

1.6.1.1.4 Polycaprolatone

Polycaprolatone (PCL) is a polymer of ε-caprolactone formed by ring opening polymerization reaction. It takes around two to three years to degrade in the body. The chemical strcture of PCL is given above (Figure 1.4). PCL too has good mechanical properties. It has an excellent elongation coefficient of seven hundred percent its original

length at break. Composites of PCL with calcium phosphate may be suitable scaffolds for BTE(*67*).

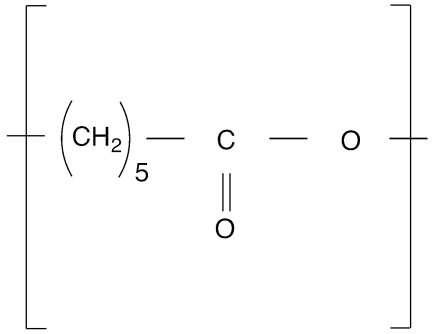

Figure 1.4 Structure of PCL

1.6.1.2 Poly (ortho esters)

Poly (ortho ester) (POE) was developed to be a hydrophobic polymer with surface erosion characteristics by ALZA corporation (Alzamer). The polymer's hydrophobic nature combined with its ester linkage that is hydrolytically labile render them slow to degradation and better at achieving slow and sustained delivery of molecules entrapped into its matrix. The unique feature of POEs is their ability to be engineered into pH sensitive matrices. Thus this class of polymer was developed as an ideal platform for drug delivery applications by tuning the pH of excipients used to control the temporal release of encapsulated drug. There are four classes of POEs:

POE class I: Diol and diethoxytetrahydrofuran tranesterification yielded POE I. One of their degradation products acted as an autocatalyst and accelerated the degradation of the polymer. Hence class II POEs were developed.

POE class II: Diols reacted with diketene acetal led to the synthesis of POE II. Acidic excipients were needed to accelerated their degradation rate.

POE class III: Reaction of a triol with an orthoester led to the synthesis of viscous POE III. However their consistency posed problems with scale-up of production at an industrial levels and hence the POE class IV polymers were synthesized.

POE class IV: Adding short segments of lactic or glycolic acid to POE II led to the formulation of POE IV. This gave POE IV the advantage of accelerated degradation without the addition of pH modulating excipients. These POE IV polymers are being considered for formulation of BTE scaffolds(*68*).

1.6.1.3 Polyanhydrides

Polyanhydrides are surface eroding polymers that have aliphatic anhydride bonds in their backbone that are sensitive to attack by water. However they are highly hydrophobic, confining the degradation to their surface. Due to their surface eroding property, this class of polymer is highly suitable for controlled release of drugs. FDA had approved the use of a Polyanhydride for drug delivery in 1996(*69*). Many different kinds of polymerization reactions including melt condensation, ring opening polymerization, interfacial condensation, and dehydrochlorination can produce polyanhydrides. Polymers such as poly(sebacic anhydride) (PSA) due to their fast rate of degradation and highly crystalline nature have limited applications(*70*). However, poly ((carboxy phenoxy propane)-(sebacic acid)) (PCPP-SA) is a well characterized polyanhydride approved by US FDA for drug delivery applications(*71*). A 1:1 sebacic acid and erucic acid dimeric copolymer system has been approved for drug delivery in osteomyeltis(*72*).

Table 1.1 Popular synthetic polymers, their properties and applications

Polymer	**Degradation Mechanism**	**Degradation time**		**Modulus (GPa)**	**Area of application**	**Commercial products**
		Molecular weight / mechanical property loss (months)	Mass loss (months)			
PDLLA (70/30)	Bulk erosion	5-6	12-18	1.9-2.4 (Film or disk)	Oral and Maxillofacial Surgery, Orthopedic Surgery	ResorPin, Leadfix MacroSorb System (screws and plates, mesh, nails, pins) PolyPin
PLLA	Bulk erosion	9-15	36-48	1.2–3.0 (Film or disk)	Orthopedic Surgery, Oral and Maxillofacial Surgery	FixSorb System (screws, nails, pins) Neofix

						(screws, nails, pins)
PGA	Bulk erosion	0.5-1	3-4	7–14 (Fiber)	Orthopedic Surgery	Biofix
PLGA	Bulk erosion			1.4–2.8		
10/ 90		1-2	3-4		Periodontal suture	Vicryl suture
85/ 15		1-2	4-5			
75/ 25		1-2	4-5			
50/ 50		1-2	3-4			
PCL	Bulk and surface erosion	9-12	24-36		Drug delivery and composite orthopedic devices	Capranor
Poly(ortho-esters)	Surface erosion	4-6	12-18	2.5–4.4		
Poly(anhydrides)	Surface erosion	4-6	12-18	0.14–1.4	Animal experiments	

1.6.2 Natural polymers in BTE

Polysaccharides, proteins and polyesters derived from both plant and animal kingdoms constitute the family of natural polymers. Several of these polymers are part of our diet and have been used in a variety of human applications in pharmaceutical excipients, prosthetics, drug delivery and imaging applications. These polymers are known to be recognized by the biological environment and channeled into metabolic degradation. Due to the similarity that natural polymers share with the ECM components, these materials may also avoid the stimulation of chronic immunological reactions and toxicity, often detected with synthetic polymers(*73*).

1.6.2.1 Polysaccharides in tissue engineering and drug delivery[1]

Polysaccharides consist of monosaccharides (sugars) linked together by O-glycosidic linkages. Differences in the monosaccharide composition, linkage types and patterns, chain shapes and molecular weight dictates their physical properties, such as solubility, viscosity, gelling potential and/or surface and interfacial properties. Polysaccharides are derived from renewable resources, like plants, animals and microorganisms and are therefore widely distributed in nature. In addition, polysaccharides perform different physiological functions and hence have great potential applications in the fields of tissue engineering and regenerative medicine(*73*)(**Figure 1.5**).

There are hundreds of known polysaccharides. A list of polysaccharides from varying sources is listed below:

[1] This section was published as a book chapter: **Aravamudhan A**, Ramos D, Nada AA, Kumbar SG, Natural Polymers: Polysaccharides and Their Derivatives for Biomedical Applications, Natural and Synthetic Biomedical Polymers; pg. 67-90, Elsevier Science; 2014.

Examples of polysaccharides from higher plants include starch, cellulose, exudate gums like arabinogalactan, gaur gum, and gum arabic.

Examples of algal polysaccharides: Alginates, galactans, and carrageenan.

Examples of polysaccharides from animals: chitin, chitosan, glycosaminoglycans, and hyaluronic acid

Examples of polysaccharides from microorganisms: dextran, gellan gum, pullulan, xanthan gum, and bacterial cellulose.

Their monomer composition and biological source provides these polysaccharides with different sets of physico-chemical properties. Often, polymers of natural origin have limitations in terms of their solubility and industrially acceptable processability factors such as high temperature of melting, which are commonly applied to synthetic polymers. For instance, majority of polysaccharides are water-soluble and oxidize at elevated temperatures beyond their melting point. These limitations have to be overcome prior to designing any products using polysaccharides. For instance techniques to crosslink polymer chains have been developed to stabilize polysaccharide structures in order to give structural stability in aqueous environments(*74, 75*). Polysaccharide chitin in its native form cannot be produced into desired sizes and shapes due to its inability to dissolve in most common industrial solvents. Thus, chitosan, the deacetylated form of chitin, was produced and applied widely instead of native chitin itself, as chitosan is water-soluble polymer at low pH. Due to its properties, chitosan is widely used for biomedical applications(*76*). The following sections will summarize these efforts in the context of biomedical applications (as shown in Figure 1.5) of polysaccharides invoking native polysaccharides, semi-synthetic polysaccharide derivatives and their blends with other synthetic polymers.

Polymers derived from plants and animal kingdoms have been widely researched as biomaterials for a variety of biomedical applications including drug delivery and regenerative medicine. These polymers have biochemical similarity with human ECM components and hence readily accepted by the body. Additionally, these polymers inherit several advantages including natural abundance, relative ease of isolation and room for chemical modification to meet the technological needs. In addition, these polymers undergo enzymatic and/or hydrolytic degradation in the biologic environment with body friendly degradation byproducts. Natural polymers include the list of polysaccharides (carbohydrates) and animal-derived proteins. Polysaccharides are an important class of biomaterials with significant research interest for a variety of drug delivery and tissue engineering applications due to their assured biocompatibility and bioactivity. Polysaccharides are often isolated and purified from renewable sources including plants, animals and microorganisms. Essentially these polymers have structural similarities, chemical versatility and their biological performance with the ECM components; often mitigate issues associated with biomaterial toxicity and host immune responses. The building blocks of carbohydrate monosaccharide are joined together by O-glycosidic linkages to form a polysaccharide chain. Polysaccharides offer a diverse set of physicochemical properties based on the monosaccharide that constitutes the chain, its composition and source. The popular list of polysaccharides used for a variety of biomedical applications cellulose, chitin/chitosan, starch, alginates, hyaluronic acids, pullulan, gaur gum, xanthan gum, and glycosaminoglycans. In spite of many merits as biomaterials these polysaccharides suffer from various drawbacks including variations in material properties based on the source, microbial contamination, uncontrolled water uptake, poor mechanical strength and unpredictable degradation pattern. These inconsistencies have limited their

usage and biomedical application related technology development. Numerous synthetic polymers with well-defined mechanical and degradation properties have been developed to meet the technological needs in the biomedical applications. However, these polymers from the biologic stand point, lack much-desired bioactivity and biocompatibility and may cause toxicity and immune response. Polysaccharide structure offers freely available hydroxyl and amine functionalities that makes it possible to alter its physicochemical properties by chemically modifying polysaccharide structure. For instance, grafting synthetic monomers on the polysaccharide chain offers an easy way to control polymer solubility in desired solvents, water uptake and degradation. These semi-synthetic polymers offer best features of the both natural and synthetic polymers. Various crosslinking techniques to restrict the polysaccharide chain movement to control their water uptake, degradation and mechanical properties have also been developed. Polysaccharide-based porous scaffolds, fiber matrices, hydrogels, micro and nanoparticles have been developed for a variety of tissue regeneration and drug delivery applications. In the recent years glycochemistry has gained research momentum for understanding carbohydrate biological functions and development of carbohydrate-based drugs and vaccines. Engineered carbohydrate based polymeric structures may serve as an alternative material platform for a variety of regenerative medicine and drug delivery applications.

A new non-petroleum based biomaterial platform to meet the versatile needs in biological science and biomedical engineering could be achieved by collaborative efforts between academia, government, and industry partnership. The collaborative efforts should include bringing scientists working in different disciplines of chemistry, biology, polymers, materials sciences and engineering to work towards these activities. These collaborative efforts could

lead to the development of a methodology for synthesis of natural polymer based semi-synthetic polymers and provide a greater depth of understanding of carbohydrate biological functions, polymer structure, material properties, degradation and mechanical properties. Further development of modeling tools to predict structure-property and biological activity of carbohydrates for biomedical applications. The goal of the new initiatives should focus on the development of natural polymer based orthopaedic fixation devices, biomedical implants, drug delivery vehicles, carbohydrate based drugs, hydrogels, surfactants, coagulants and absorbents for a variety of biomedical applications. The research activities in this area could generate commercially available technologies and products from the renewable resources and contribute immensely towards economic development.

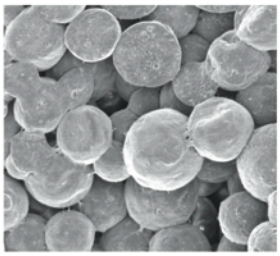

Scaffolds

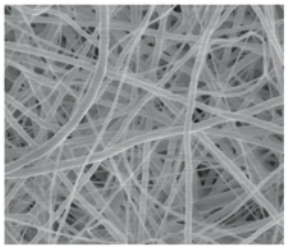

Nanostructures

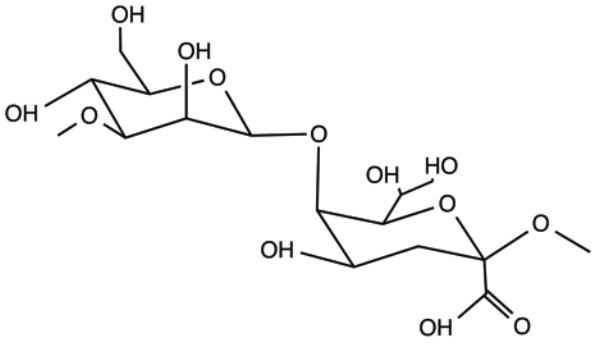

Polysaccharide

Drug delivery
-Hydrogels
-Scaffolds

Hydrogels

Figure 1.5 Polysaccharides in biomedical applications

1.6.2.1.1 Hyaluronic acid

1.6.2.1.1.1 1.6.2.1.1.1 Chemical structure, properties and sources

Chemically HA is a linear polysaccharide made up of: D-glucoronic acid and N-Acetyl-D-Glucosamine that are linked to one another by a β-(1->3) linkage. There could be 250-25000 such basic disaccharide units in a polymer chain of hyaluronic acid, connected by β-(1-> 4) linkage (Figure 1.6). The disaccharide units of hyaluronic acid are extended, forming a rigid molecule whose many repelling anionic groups bind cations and water molecules. In solution, hyaluronate occupies a volume approximately 1000 times that in its dry state. Hyaluronate solutions exhibit clear viscoelastic properties that make them excellent biological absorbers and lubricants. These properties also attribute to its preferred form of fabrication into hydrogels. Because of its hydration properties, HA has the ability to bear compressive loads *in vivo*, and provide lubrication at the same time. *In vitro*, HA has been shown to facilitate cell migration and pericellular matrix formation(*77*).

Biologically, HA are an important glycosaminoglycan (GAG) component of connective tissue, synovial fluid (the fluid that lubricates joints) and the vitreous humor of the eye in mammals(*78*). The biological roles of HA are widespread and widely appreciated(*79-81*). They range from development, angiogenesis, cellular migration and receptor mediated signaling through receptor CD44 and receptor for HA-mediated motility (RHAMM) in ECM remodeling and mediation of inflammatory responses(*82, 83*). HA chain length plays an essential role in the biological functions elicited in native and hence the engineered tissues. Therefore the molecular weight of HA is an important consideration for the response elicited. For instance, while the low molecular HA (less than $3.5X10^4$ Da) is known to be involved in cytokine activity implicated in inflammatory responses(*84*), the higher molecular weight HA (above $2X10^5$ Da) is known to inhibit cell proliferation(*85*). Similarly, (1-4KDa) smaller

fragments of HA have a positive effect in promoting vascularization during injury, whereas the (1-9KDa) large fragment showed no significant effects(*85, 86*). Not only is the usage of HA at the correct molecular weight and chain length, but also the hyaluronidas (HAS) isozyme (Figure 1.7) that is responsible for degradation of HA in the tissue, determines the chain length of the degradation product. Therefore the enzymes in the tissue where the HA material is to be implanted is a factor for consideration while using the material in tissue engineering(*87*).

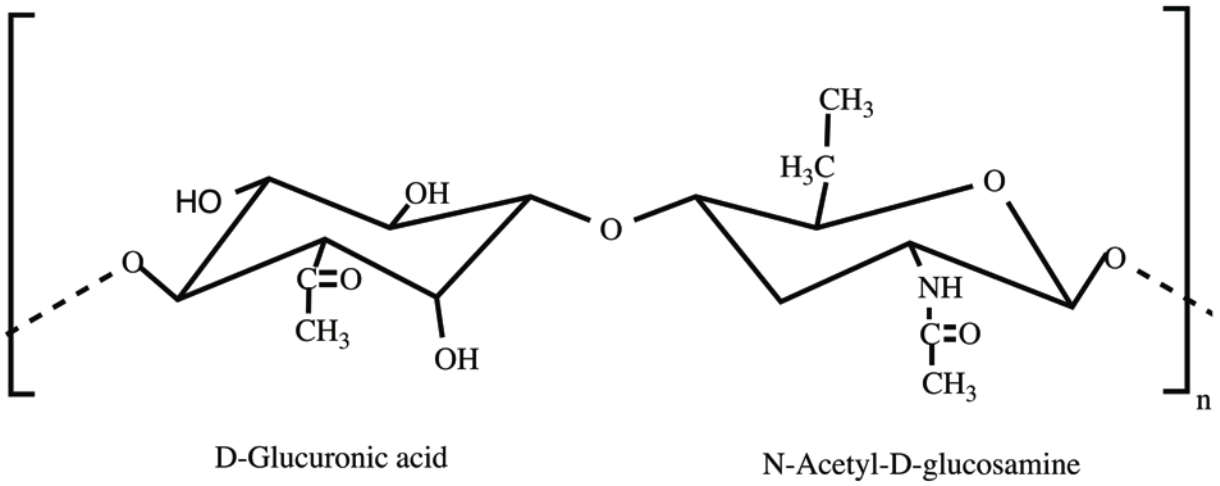

Figure 1.6 Structure of Hyaluronic Acid (HA)

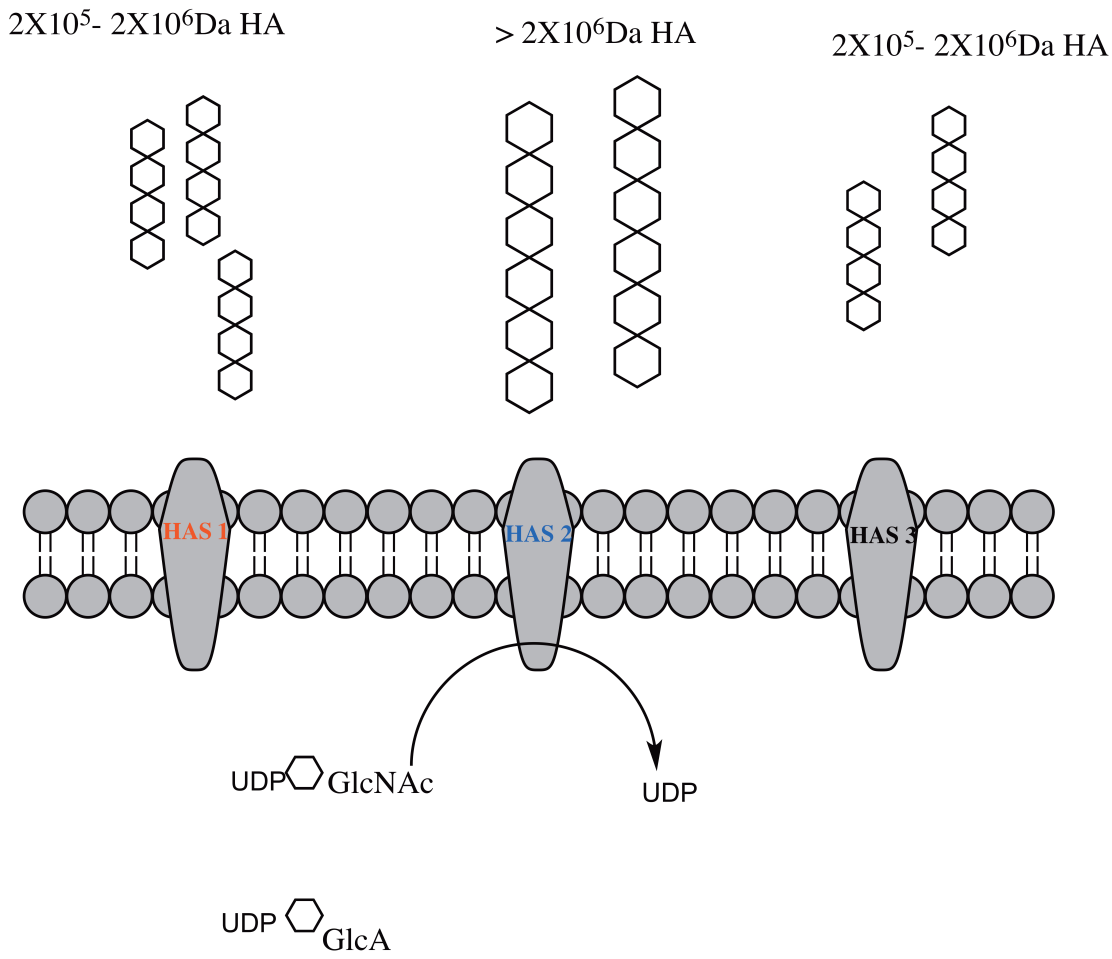

Figure 1.7 Chain length of HA

The 3 HAS isozymes produce distinct chain lengths of HA. HAS1 and HAS3 can produce chains of 2X10^5-2X10^6 Da, while HAS2 produces HA of chain length greater than 2X10^5 Da (Modified from Allison *et al*., 2006(*88*)).

1.6.2.1.1.2 Attempts made in Tissue Engineering and Drug delivery

1.6.2.1.1.2.1 Hyaluronic acid alone

HA is highly water soluble at room temperature and at acidic pH values, and exhibits high rates of turnover *in vivo* (half-life varies from only minutes in the blood to weeks in cartilage(*80, 81, 88-90*). These properties pose challenges for the material's integrity *in vivo*. Therefore the usage of HA in its native form in tissue engineering and drug delivery applications is pretty limited. Several crosslinking methods are used to increase the stability of HA in such applications. Some of them are as follows: water-soluble carbodiimide

crosslinking, polyvalent hydrazide crosslinking, divinyl sulfone cross-linking, disulfide crosslinking, and photocrosslinking hydrogels through glycidyl methacrylate–HA conjugates(*87*). Hence these techniques of covalent crosslinking provide the opportunity to combine HA with more mechanically stronger polymers.

1.6.2.1.1.2.2 HA derivatives and combinations with other polymers

The early usage of HA was in ophthalmic drug delivery systems where it provided an ideal matrix for covalent attachment of drugs and showed as much as twice the retention in contrast to free drug (methylprednisolone esters of HA)(*91, 92*). Different formulations such as such as gels, solutions and hydrogels with several model drugs such as pilocarpine (Pi) and tropicamide (Tr) showed that HA ester systems were effective ophthalmic drug delivery systems(*92*). HA has also been employed in liposomal dermal drug delivery. HA was conjugated to the surface of liposomes by carbodiimide crosslinking of its surface carboxyl residues to the amine residues on the liposome. The epidermal growth factor showed an encapsulation efficiency of >87% in these HA conjugated liposomes(*93*). Avid binding of these HA conjugated liposomes to a cellular monolayer in culture were seen that did not occur with the unmodified liposomes(*93*). Sodium butyrate used as an anti proliferative drug in treatment of cancer has an extremely short half-life of five minutes *in vivo*. In order to bypass this constrain butyratic ester derivatives of HA were synthesized by stepwise chemical treatment of HA. The degree of substitution (DS) varied from 0.1 to 2.24 (1.8-28.4%). MCF breast cancer cell lines showed maximum anti- proliferative response with DS of 0.2. It was seen that complete internalization of the HA vehicle occurred in two hours through CD44 receptors that are frequently over expressed on cancer cells(*94*). From these and several other systems where HA and its derivatives have been used to deliver drugs, its

innate role that facilitates binding of HA to receptors/ specific cell types helps achieve efficient targeted delivery of intended drug to a tissue while its activity is preserved.

Another major application of modified HA is in formulation of tissue engineering scaffolds. Radiation mediated crosslinked HA networks have been used as scaffolds for cell growth with positive outcomes(*95*). HA modified with methacrylic anhydride (MA) was photopolymerized to produce HA–MA hydrogels containing porcine chondrocytes(*96*). The chondrocytes within the HA scaffolds were viable and were able to produce neo-cartilage within the porous networks. Photopolymerizable HA–MA hydrogels have also been used in heart valve applications, in which the HA hydrogels were designed to mimic the cardiac ECM from which the heart valves develop(*97*). HA has been combined with other natural/ synthetic polymers to produce scaffolds. For example, HA has been combined with polypyrrole to create a multifunctional copolymer(*98, 99*). When implanted into rats, there was a marked early increase in local vascularization(*99*). On the other hand it was observed that polypyrrole–HA polymers were subsequently sulfonated, which was shown to significantly reduce platelet and cell adhesion(*98*).

Benzyl derivatives of HA (Hyalograft C and HYAFF-11) are used as polymeric scaffolds for tissue engineering of cartilage(*100*). Though the laboratory tests have given mixed results, the human clinical results show normal cartilage formation when implanted into previously damaged tissue(*101*). Hence benzyl esters of HA have a great potential as scaffolds and drug delivery vehicles for chondrocytes in tissue engineering. Another HA-based scaffold examined for tissue engineering–based cartilage regeneration is auto-crosslinked polysaccharide polymer (ACP). While comparing ACP with HYAFF-11, poly (L- lactic acid) (PLLA) and poly (DL- lactic- glycolic acid) (PLGA) in an osteochondral defect, faster

degrading scaffolds of ACP, PLGA had greatest regeneration, while it was slower in HYAFF-11, PLLA that had slower degradation rates. These *in vivo* data revealed that the scaffolds degraded within 4 months and were able to repair the osteochondral lesions, again emphasizing the selection of type of HA and the consideration of hyaluronidase system in the tissue that would degrade it(*102, 103*). HYAFF-11 scaffolds have shown very positive effects as scaffolds for engineering of vascular and hepatic tissue and showed great ability for maintenance of cell phenotype indicating that it could be used as scaffolds for many tissue engineering applications(*104, 105*).

Combining chitosan and high molecular weight HA ($2.4X10^6$ Da) in a three-dimensional (3D) copolymer system promoted chondrocyte adhesion. The production of aggrecan and the native rounded morphology of seeded chondrocytes increased with the concentration of added HA and the scaffolds with HA performed better than scaffolds of chitosan alone(*106*). Incorporation of chondrocytes and HA into orthopedic implants by crosslinking HA to amine terminated PLGA–poly (ethylene glycol) (PEG) scaffolds allowed the attachment and proliferation of donor chondrocytes. It was also observed that collagen II expression, a marker of healthy cartilage phenotype, and DNA synthesis were significantly increased in polymers that incorporated HA(*107*). Combining HA with divinyl sulfone (DVS), and crosslinking with ultraviolet light, created suitable surfaces for cell adhesion. When a DVS-crosslinked HA scaffold was dehydrated before seeding with smooth muscle cells, gels were more porous and conducive to cell migration and infiltration, but did not lose their non-immunogenic properties(*108-110*). Follow up studies conducted on the same material showed that smooth muscle cells increased the synthesis of ECM components elastin and collagen of aortic valve tissues, over cells cultured on tissue culture plastic; this synthesis

was controlled by HA fragment size and dose(*108, 111*). Such studies have shown that HA is a suitable material for vascular and cardiac tissue engineering. HA was also introduced directly to engineered structures exogenously. For example, collagen matricides implanted in rabbits have shown greater numbers of chondrocytes (1.5 times control values) after the addition of soluble HA. The addition of HA fragments increased the amounts of proteoglycans, a desirable component of remodeling(*112*). However, small HA oligosaccharides (4–16 disaccharides), on the other hand can prevent cell proliferation *in vivo(113)*. These findings could have implications for improving the potency of implanted small diameter vascular grafts and preventing stenotic lesions after graft implantation in cardiovascular tissue engineering.

With the knee osteoarthritis patients increasing to a staggering 19 million in 2010, treatment by visco-supplimentation has become popular. Visco-supplementation refers to the concept of synovial fluid replacement with intra-articular injections of hyaluronan mainly for the relief of pain associated with osteoarthritis(*114, 115*). Intra-articular injections of hyaluronan ameliorate pain and increase function, generally for up to 3 months with no serious adverse events. In the US, the first single-injection hyaluronan for visco-supplementation, Synvisc-One®, was approved in early 2009. The global market for dermal fillers is constantly increasing with 100 different dermal fillers on the market for aesthetic plastic surgery and about half of them are based on hyaluronan(*116*). Thus it can be summed up that hyaluronic acid has already stepped into clinical treatments in tissue engineering and will gain greater importance in the future.

1.6.2.1.1.3 Promises and challenges with HA

HA has had a profound impact on the field of tissue engineering. The incorporation of HA into biomaterials and scaffolds has yielded a new class of biocompatible, controllable, and

readily degradable materials. These new scaffolds have been tested with multiple types of cells and have been shown to promote beneficial remodeling of engineered tissues, as well as the gross preservation of cell phenotypes. However harnessing the endogenous activity of the hyaluronan synthases to stimulate endogenous HA production may be another useful strategy for the future. Recent research developments regarding HA as a molecular delivery vehicle for pharmacological and oncological applications, as well as in the orthopedic and cardiovascular arenas, have the potential to transform the clinical future of tissue engineering.

1.6.2.1.2 Chondroitin sulfate

1.6.2.1.2.1 Chemical structure, properties and sources

Chemically, Chondroitin sulfate (CS) is a sulphated GAG derivative. Alternating units of N-acetylgalactosamine and glucuronic acid are the monomers that constitute the basic unit of CS (Figure 1.8). Hundreds of these alternating units could be present together in a CS polymer chains. CS is a GAG seen associated with proteins in living systems termed proteoglycan. CS is classified according to the position of sulfation of the monomer unit. The types of CS and their chemical structure are listed below

Table 1.2 Types of Chondroitin Sulphate (CS)

S.no.	Name (Type)	Synthetic name (Sulphation of GalNAc)
1.	Chondroitin sulfate A	chondroitin-4-sulfate
2.	Chondroitin sulfate C	chondroitin-6-sulfate
3.	Chondroitin sulfate D	chondroitin-2,6-sulfate
4.	Chondroitin sulfate E	chondroitin-4,6-sulfate

Biologically, CS is a major structural component of the ECM of several tissues of the body, like cartilage. The biological function and efficacy of CS seems to be highly dependent on

the chain length of the polymer. For instance, CS extracted from the trachea is usually shorter Ca. 20-25 kDa, and considered to be of lower quality. On the other hand, CS polymer extracted from shark is considered more bioactive and of higher quality with longer chain length Ca. 50-80 kDa. Even CS extracted from a single source could have variable polymer chain length(*117*). Hence the type and chain length of CS is likely to determine its biological functions, such as interaction with growth factors, proteins in GAG complexes of the ECM and its ability to influence cellular function(*118, 119*). CS is also an indispensible component of tissues for maintaining their mechanical properties. The resistance of cartilage to compression is attributed to the tightly packed, charged sulphate groups of CS. This leads to osmotic water retention and swelling of the cartilage and hence endows it with the weight-bearing mechanical properties(*120*). Apart from its structural role, CS has also been an important player in basic biological processes including cell division and development of nervous system. Such biological roles are mediated by the binding of CS to growth factors, cytokines and regulating signaling pathways in neurons(*121, 122*). Age related changes in sulphation of the CS chains indicate their fundamental biochemical role in tissues(*123*) during age related pathological changes. Loss of CS has been implicated in pathological conditions. For example, osteo arthritis (OA) in cartilage is seen to occur due to the loss of CS leading to cartilage degeneration. Many studies on the impact of CS administration in patients suffering from OA along with *in vitro* results suggest that CS could improve pathology of OA through promoting proteoglycans synthesis, usually lost during cartilage degeneration(*124*), inhibiting elastase(*125-127*) and cathepsin G activity(*128*), and reducing gene expression for a number of proteolytic enzymes(*129*).

The reason for a high variability in the outcomes of treating OA with CS is due to the variation in the chain length of the polymer used in these studies. While the high quality, long chain CS is more effective, the low quality, short chain CS have minimal effects on the pathogenesis of OA. Apart from its effects of improving OA, the anti-inflammatory effects of CS have led to improvement in conditions such as psoriasis and inflammatory bowel disease. These effects seem to be related to the inhibition of cytokines such as TNF-α*(130)*, and IL-1β induced translocation of NF-κB(*131*). However most of the effects are dependent on the type of CS determined by degree and position of sulphation, as well as the chain length of the polymer(*122*).

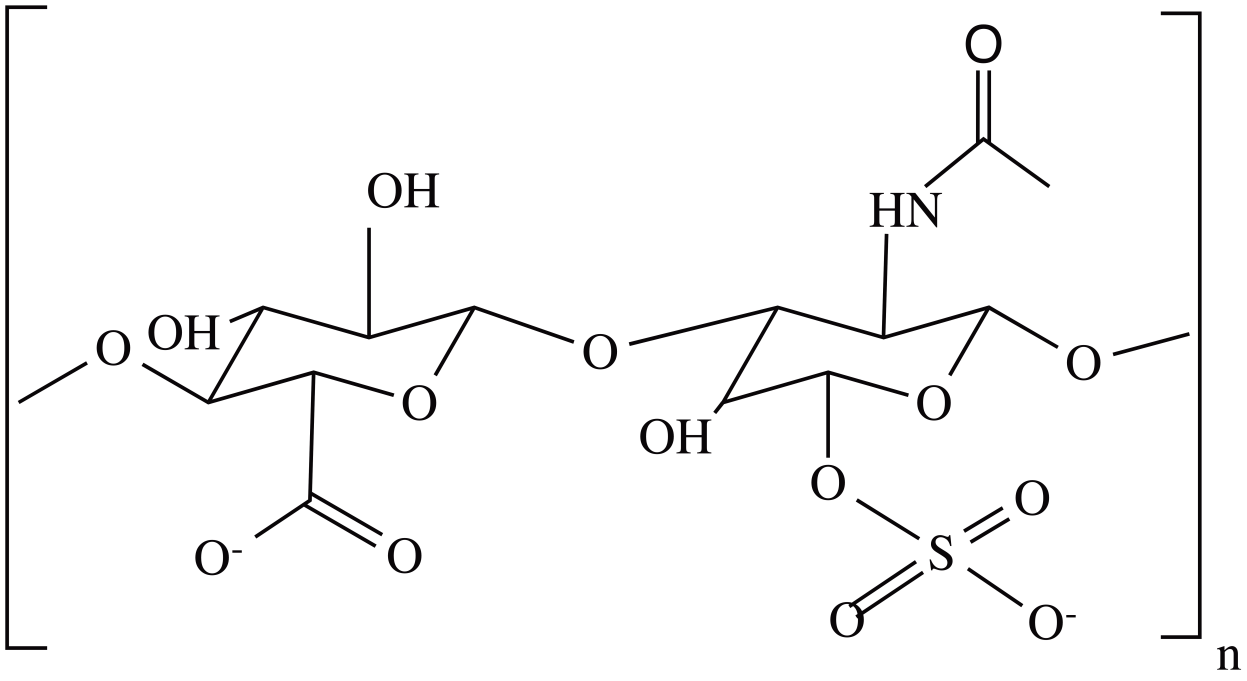

Figure 1.8 Structure of Chondroitin Sulphate (CS)

1.6.2.1.2.2 Attempts made in Tissue engineering and drug delivery

1.6.2.1.2.2.1 Chondroitin sulfate alone

CS is often administered orally as it is seen to improve joint-related pathologies(*117*). The intact polymer is often consumed and several studies have examined the levels of the CS in

blood plasma after consumption(*132, 133*) in humans, mice and horses. The degree of sulphation and chain length of the polymer were seen to determine the rate of uptake, retention and clearance from these biological systems. For instance, tracheal CS with lower molecular weight is absorbed quickly within 1-5 hours and reached a peak plasma concentration at around 10 hours. On the other hand shark CS of high molecular weight is seen to be have a slower rate of uptake at around 8.7 hours and was retained in the system for as long as 16 hours(*133*). It was also observed that desulphated chondroitin had quick uptake rate (15 minutes) and was also cleared within 3 hours(*134*). Further, *in vitro* experiments showed that there was a direct correlation between the polymer size and the rate at which it crossed the gut wall(*135*). This in turn reflected as the rate of uptake and retention of the polymer in the biological system. Therefore smaller CS polymer is taken up and cleared quickly, while the larger CS polymer takes longer time to be absorbed and cleared from a system.

1.6.2.1.2.2.2 Chondroitin sulfate derivatives and combination with other polymers

CS is a water-soluble polymer. Early attempts of using CS as a vehicle for colonic drug delivery, crosslinked the polymer to different degrees to achieve a biodegradable system for controlled release of model drugs, indomethacin. A linear correlation between degree of crosslinking and rate of drug release emerged, indicating that the level of crosslinking of CS can be used to regulate the kinetics of drug delivery(*136, 137*). Still, crosslinking of CS is used as a strategy to decrease the dissolution of CS in water. For example, treatment of water-soluble CS polymer with different proportions of trisodium trimetaphosphate (TMFS) achieved crosslinking of CS and reduced solubility for the usage of the polymer in drug delivery applications(*138*).

Mostly due to its highly water-soluble nature and lack of mechanical stability, CS has been modified with or used along with other polymers for drug delivery and tissue engineering applications. Porous sponge of CS-chitosan was used for the delivery of Platelet Derived Growth Factor (PDGF), aimed at achieving greater bone regeneration. Aqueous CS-Chitosan solution was subjected to freeze drying followed by crosslinking to form a porous sponge with 100-150μm pore size. PDGF-BB was incorporated into the CS–chitosan sponge by soaking CS–chitosan sponge into the PDGF-BB solution. Amount of CS could act a factor to control the release of PDGF-BB from the sponge(*139*). It was also seen that presence of CS increased the osteoconductive characteristics of the material. Hence, the bioactive CS could be used in combination with other polymers in the formulation of materials for delivery of growth factors.

As CS has biological roles that are advantageous and is a water-soluble and enzymatically biodegradable polysaccharide, it has been used in combination with materials such as collagen in preparation of scaffold matrices. Addition of CS to collagen type I matrix was achieved by using 1-ethyl-3- (3-dimethyl aminopropyl) carbodiimide (EDC) as a crosslinking agent. The CS bound matrix had increased water-binding capacity, with decreased tensile strength and temperature of denaturation(*139*). Apart from imparting advantageous biological properties to the scaffold, CS also presented the opportunity to control the scaffold's mechanical and degradation characteristics.

As explained in the previous section, CS is an important component of joint ECM and known to play crucial roles in development and amelioration of joint/cartilage pathologies. Hence, it is used extensively in osteochondral tissue engineering. Here again a number of CS variants such as modified CS or CS in combination with other natural and/or synthetic polymers have

been utilized for the formulation of scaffolds. Scaffolds of different formats were utilized. Both fibrous spongy scaffolds and hydrogel scaffolds have been formulated utilizing CS. While employing CS in combination with Collagen type I in the form of fibrous sponge matrix, a clear advantage in chondrocyte proliferation and phenotype maintenance were seen(*140*). Similarly sponges with a pore diameter of 180μm were synthesized using natural polymers gelatin, CS and HA together. When these scaffolds were seeded with chondrocytes, they maintained their morphology for up to 5 weeks and showed higher levels of aggrecan production than scaffolds that did not contain CS and HA components. These *in vitro* studies clearly point to the potential of scaffolds incorporating CS for cartilage tissue engineering(*141, 142*).

A number of hydrogel scaffolds have also been formulated using CS for cartilage. Chondrocytes have a rounded morphology and this is seen to be best preserved in hydrogels, and therefore hydrogel scaffolds are an ideal option for cartilage regeneration. Polymers such as poly ethylene glycol (PEG), poly vinyl alcohol (PVA), and poly (3-hydroxybutyrate) (PHB) have been used with CS to formulate hydrogels. While PVA hydrogels alone could not support cell adhesion, the addition of CS lowered the extreme hydrophilicity of the hydrogel and facilitated greater cell attachment in the scaffold(*143*). When CS containing Collagen hydrogel was conjugated to a fabric of PHB, it showed greater osteogenic potential than the parent fabric, on the seeded osteoblasts(*144*). The presence of CS in PEG hydrogels, promoted the chondrogenic differentiation of seeded bone marrow derived mesenchymal stem cells (MSCs), but did not allow them to proceed onto a hypertrophic state. This was an optimal outcome suitable for chondrocyte differentiation, to achieve cartilage regeneration(*145*). In a recent study, the polysaccharide backbone was modified with

methacrylate and aldehyde groups to form an adhesive gel. This modification led to better integration of the hydrogel with the implanted tissue *in vivo*, as seen in a rat model. This was due to greater scaffold-protein interaction brought about by the addition of modified CS(*146*). Efforts have been made to deliver CS using scaffolding principles to joints affected by OA. For instance, a scaffold with 40% chitosan and 60% CS was designed to serve as a carrier of CS proved effective(*147*). Hence CS by itself after certain modifications and in combination with other synthetic and natural polymers has a great potential in scaffolding and drug delivery for osteochondral regeneration.

1.6.2.1.2.3 Promises and challenges with Chondroitin sulfate

There have been many promising outcomes with CS as a drug and as a matrix for tissue engineering, both *in vitro* and *in vivo*. However clinical outcomes have been inconsistent and have variable results. Better experimental design and ways to determine the polymer length and level of sulphation would be crucial to determining to the fate of exogenously administered CS. Better experimental design and greater understanding of the biological role of CS are important factors for determining the polymer's role and most suitable type of CS polymer that lend the desirable biological outcomes.

1.6.2.1.3 Chitin and chitosan

1.6.2.1.3.1 Chemical structure, properties and sources

Chitin is a structural polysaccharide found in nature. Chemically, chitin is made monomer units of 2-acetamido-2-deoxy-b-D-glucose connected through β (1->4) linkages (Figure 1.9). The C-2 position in the glucose ring in the monomers has an acetamido group. The N-deacetylation of this chitin leads to the formation of chitosan. The degree of conversion of the acetamido group to amine group is never really complete. This is given by the degree of deacetylation (DD) of the chitosan. The DD of chitosan can vary from 30- 95%. This conversion of chitin to chitosan renders the material more readily soluble and processable for various applications (Figure 1.10). Though crystalline chitosan is insoluble in aqueous solution at a pH> 7.0, in dilute acid where pH <6.0, the positively charged amino group facilitates its solubility(*148, 149*). There are three reactive functional groups in chitosan- the amino group at C-2, a primary and secondary –OH group at C-3 and C-6 positions respectively. These reactive groups allow for chemical modification of chitosan such as covalent and ionic modifications.

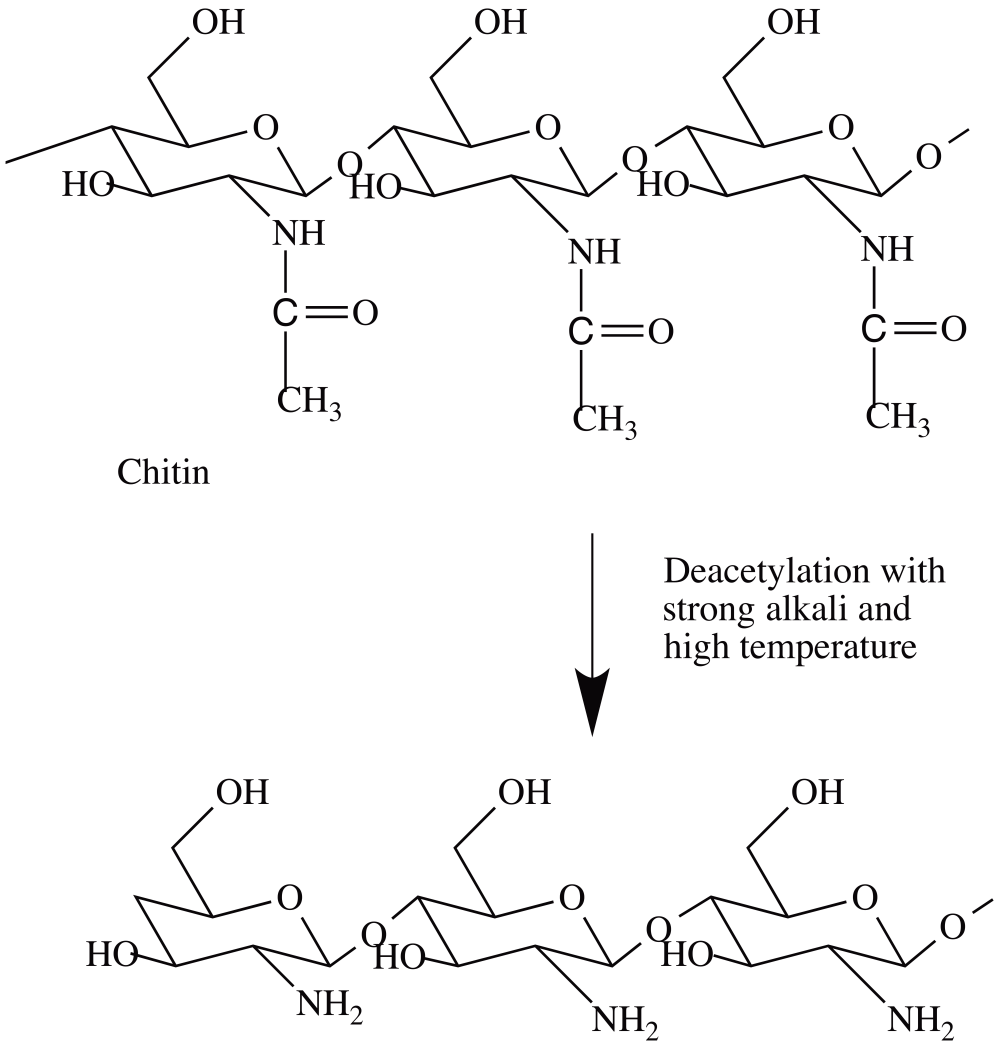

Figure 1.9 Structure of Chitin and Chitosan

Chitosan is one of the highly studied and utilized polysaccharide for tissue engineering. A process called "internal bubbling process (IBP)" can be used to form porous structures from chitosan by freezing and lyophilizing a solution of chitosan. The addition of $CaCO_3$ to chitosan is used in this process to create porous chitosan gels(*150*). This processability of chitosan is attributed to its cationic nature. The cationic property also leads to interaction of the material with negatively charged small molecules and proteins in biological systems. This

is structurally very similar to native GAGs and hence plays crucial role in stimulating favorable responses in biological systems. Chitosan's mechanical properties are determined by the pore sizes, the molecular weight and crystallinity of the polymer. High porosity, lower molecular weight and less crystalline polymers are mechanically less competent and vice versa. Apart from these properties, chitosan is biodegradable. The acetylated residues of chitosan are targeted by lysozyme *in vivo* and this seems to be the major mechanism of chitosan degradation. Therefore DD, and crystallinity of the polymer are inversely related to degradation. Thus the higher DD (>85%), the more crystalline the chitosan polymer and the slower its degradation in the body(*151-153*).

Chitosan is known to have antibacterial properties that(*154*) are attributed to the attack of negatively charged groups on the cell wall by the positively charged chitosan polymer. This leads to lysis of bacterial cell wall, and hence its bactericidal activity. Inhibition of bacterial growth by chitosan is also attributed to its binding of bacterial DNA and interference of bacterial transcription(*155*). Chitosan is also seen to have minimal immune rejection. Chitin is the major source for chitosan (Figure 1.10). It is the most abundant polymer to undergo biosynthesis, next to cellulose. It is a constituent of the exoskeleton in animals, like crustaceans, molluscs and insects. It is also a polymer found in the cell wall of certain fungi. Most of the polymer used for commercial source comes as a byproduct of the fishery industry(*156*).

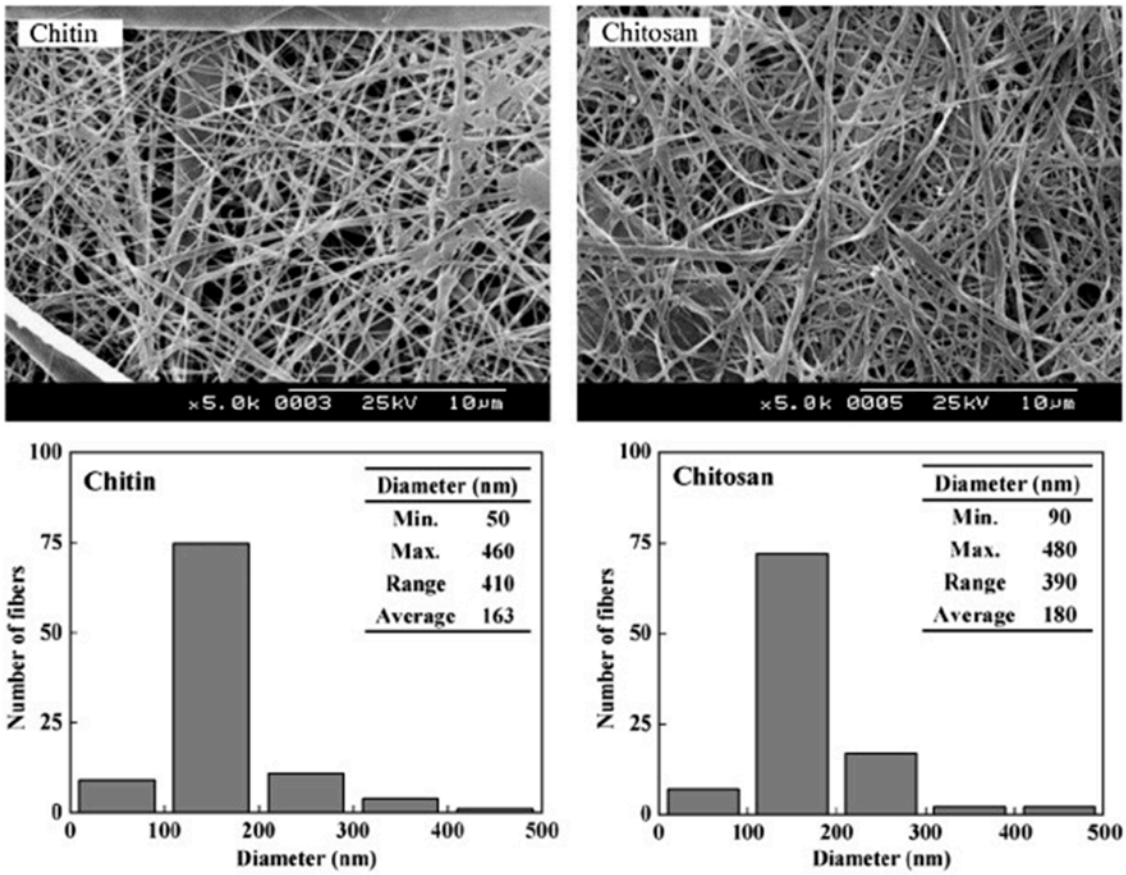

Figure 1.10 Nanofibers of Citin and Chitosan

Chitin (on left) and Chitosan after deacetylation (on right) Nanofibers(*157*).

1.6.2.1.3.2 Attempts made in Tissue engineering and drug delivery

1.6.2.1.3.2.1 Chitosan alone

The various biological properties of chitosan have been discussed above. Chitosan has also been used as a dietary supplement. It is seen to lower low-density cholesterol and is helpful in weight loss(*158*). Apart from its direct consumption, chitosan is used in drug formulations of different types such as microparticles, liposomes, granules, gels for oral and parenteral drug delivery. In most of these applications chitosan is physically or chemically crosslinked to obtain stability. The degree of crosslinking and drug loading are parameters used to control drug delivery(*159, 160*). In tissue engineering, chitosan alone was used initially. Since the mechanical and dissolution properties of the polymer make it tough to work with

and formulate scaffolds, chemical modifications and their combinations with other natural and synthetic polymers is at present the more popular strategy. Common strategies are discussed in the following section.

1.6.2.1.3.2.2 Chitosan derivatives and combination with other polymers

Some of the limitations chitosan suffers from are those of insolubility at neutral pH and high water absorption by the polymer at a rapid rate. These factors pose problems of processability and also lead to rapid drug release from chitosan. Hence chitosan is modified to overcome these limitations. Most modifications are brought about by reactions with the amine or hydroxyl groups of the glucoseamine unit in chitosan. Using the reactive amine group a number of modifying reactions are carried out. A simple example is a reaction in which an aldehyde functional group reacts with $–NH_2$ group of chitosan by reductive amination(*161*). The introduction of N-cyanoethyl groups into the side chain of glucosamine in chitosan is a good example of this process. This reaction produced some crosslinking through a reaction between the nitrile group and the amine group of chitosan(*162*). Examples of covalent modifications of chitosan include acylation and quarternization. When two oppositely charged polymers (a polycation and a polyanion) in a solution phase, separate out in a solution, a dense polymer phase called coacervate and a supernatant with low polymer content separate out. This process is termed polyelectrolyte complex formation. Polyelectrolyte complex formation has been used in a number of chitosan drug delivery systems(*163, 164*) where controlled release of the loaded drug was desired. Modified chitosan and its blends with other polymers have been used in different formats. Nanoparticles and microparticles of chitosan and its derivatives have been formulated using techniques such as emulsification/solvent evaporation(*157*), spray drying(*165*), ionotropic gelation and coacervation(*166*), emulsion crosslinking(*167*) and sieving(*168*). Thin films

have been produced using solution casting, while crosslinking and gelation processes have been applied to produce hydrogels of chitosan for drug delivery(*169*). Chitosan drug delivery vehicles in the form of tablets and gels are applied in dental, buccal, gastrointestinal, colon-specific, and gene delivery applications due to their favorable biological properties(*169*). In tissue engineering, chitosan had been used mostly in minimally modified forms. The focus presently has shifted to improving the properties by introducing chemical modifications to form derivatives of chitosan for specific tissue regeneration purposes. Some of them are listed below:

Introduction of sugars

Synthesis of chitosan bound to sugar has many applications in drug delivery and tissue engineering. This is due to the fact that cells, viruses and bacteria recognize these sugar moieties and hence render these polymers good agents for targeting several target components in tissue engineering. For example, galactosylated chitosan (GC), worked as a good ECM for hepatocytes(*170*). Specific antigen presenting B cells were recognized by mannosylated chitosan (MC)(*171*).

Graft polymerization

Chemical grafting of chitosan can be used to functionalize chitosan and obtain important derivatives. Ceric ion, fenton's reagent, gamma-irradiation, various radicals, and ring opening reactions are the various routes used to achieve graft polymerization of chitosan(*172*). Cell morphology and function were controlled by chitosan graft-polymerized onto poly (L-lactide) (PLA) by plasma coupling reaction(*173*). Further cooperative complementation through graft copolymerization or blend with poly (α- hydroxy acids) using a photosensitive crosslinking agent led to attachment of chitosan onto PLA films. These films

showed improved cell attachment(*174*). On the other hand copolymerization of chitosan with heparin inhibited platelet adhesion(*175*). Therefore graft polymerization can help modulate chitosan's properties to elicit a desired cellular response.

Immobilization of specific sequences

Specific amino acid sequences promote cell adhesion. The most commonly used sequence is the arginine-glycine-aspartic acid (RGD) from adhesion proteins, such as collagen and fibronectin that bind cells through cellular integrin receptors. Photo crosslinking RGD peptides to chitosan improved the adhesion of human endothelial cells, compared to unmodified chitosan scaffolds(*176*). In another approach the –COOH group of amino acids such as lysine, arginine, aspartate, phenylalanine react to the $–NH_2$ group of chitosan. These functionalized chitosan polymers were entrapped onto the surface of PLA to improve cellular responses(*177*).

Production of nanofibers

Nanofibers mimic the structure of natural ECM closely. Hence enhanced cellular responses are achieved on electrospun nanofiber scaffolds. Chitosan nanofibers ranging from several down to a few nanometers have been produced by electrospinning technique(*178, 179*)

Thermal gelation

Thermal gelling is a technique of injecting a polymeric aqueous solution, while keeping the temperature above the polymer's sol-gel transition temperature and allow the polymer to form a gel as it reaches the body temperature. A thermal gelling chitosan polymer was formed by neutralizing highly deacetylated chitosan solution with glycerol phosphate (GP). Chitosan remained in solution at physiological pH. Chitosan/GP solution gelled at body temperature and hence was an attractive, injectable hydrogel drug delivery system local

delivery of antineoplastic drugs like pachlitaxal(*180*). Derivatives of chitosan have been used in skin, bone, cartilage, liver tissue engineering. A detailed description of chitosan is given elsewhere in this book.

1.6.2.1.3.3 Promises and challenges with Chitosan in tissue engineering

Chitin and its derivatives have a number of applications in drug delivery and tissue engineering. While being an abundantly available polymer, chitosan is also biodegradable inside the body, mostly by the enzymatic activity of lysozyme. However chitosan/chitin by itself lacks good mechanical properties required in certain structural applications. Chemical modifications of chitosan and blending the polymer with other natural and synthetic polymers are done to overcome this limitation. On the whole, chitosan has a huge potential in tissue engineering and drug delivery applications.

1.6.2.1.4 Alginic acid

1.6.2.1.4.1 Chemical structure, properties and sources

Alginic acid is an anionic, strictly linear (unbranched) copolymer of mannuronic acid (M block) and guluronic acid (G block) units arranged in an irregular pattern of varying proportions of GG, MG, and MM blocks (Matsumoto, Kawai, & Masuda, 1992) (Figure 1.11). C5 epimerization and flipping of sugar ring to $^{1}C_{4}$ position (Christensena, 2011) is seen to occur for steric stability in the polymer. The M residues are linked at $^{4}C_{1}$ (diequatorial links). The G residues are the C-5 epimers of M. These G residues are linked at $^{1}C_{4}$ with diaxial links(*181*). The G and M blocks are present as similar or strictly alternating (GG, MM, or GM). Due to the diaxial linkage, G blocks (GG) are stiffer than alternating blocks (GM), and hence more soluble at lower pH. The content of G in alginates varies from 40-70 % depending on the source and determines the quality of the alginate polymer. The

molecular weight of alginate can vary widely between 50-100,000 kDa. It is generally seen that alginates with high G block content are highly suitable for biomedical application due to the ease of processiblity, and low immunogenicity in the body. Hence the content of G and M blocks is a crucial factor that determines the properties and applications of the resultant alginate(*182*). Alginates are polysaccharides produced by a wide variety of brown seaweeds (*Laminaria* sp., *Macrocystis* sp., *Lessonia* sp., etc.). Additionally bacteria also synthesize alginates and these can be used as tools to tailor alginate production, by understanding the biosynthesis of the polymer in these bacteria. A family of enzymes termed mannuronan-C5-epimerases that convert M into G at the polymer level. By genetically selecting and engineering *Pseudomonas* strains that contain only a single epimerase for the production of high G containing alginates has been possible. Using such strategies, alginates with up to 90% G content and extremely long G-blocks have been produced(*183-185*).

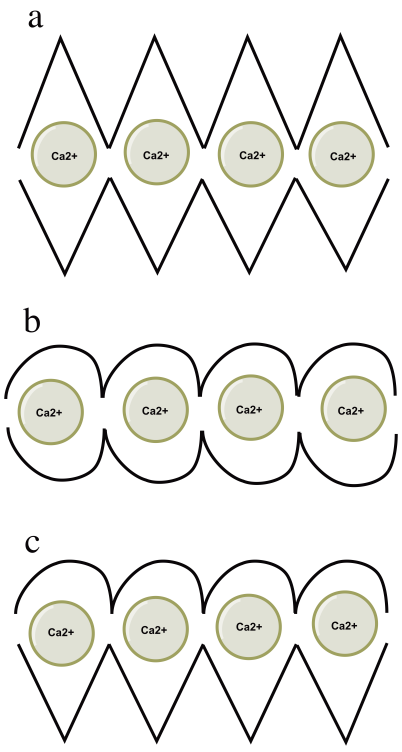

Figure 1.11 Gellation of Alginic Acid

Mechanism of gellation of alginic acid in the presence of Ca^{2+}. Possible junctions: (a) GG/GG junctions, (b) MG/MG junctions, and (c)mixed GG/MG, with Ca^{2+}.

Though such strategies are useful to engineer alginates, most of the alginates extracted for large-scale applications originate from natural sources such as seaweeds. The quality is determined by the species and even the seasonal variations. The alginate could contain from 10-70% G. Techniques of separation such as fractionation and precipitation in calcium can help separate the G-block and M-block rich alginates. The molecular weight of alginate is a critical factor to influence its viscosity in solution, besides the concentration of the polymer. The most important property of alginate is its ability to gel in the presence of cations (like Ca^{2+}, and Ba^{2+}) (Figure 1.12). The carboxylic acid groups of sugars in G blocks of adjacent polymer chains crosslink with multivalent cations to form a gel. Factors that influence the stiffness of the gel are molecular weight distribution of the alginate polymer (dependent on M/G ratio), and the stoichiometry of alginate with the chelating cation(*186, 187*).

1.6.2.1.4.2 Attempts made in Tissue engineering and drug delivery

1.6.2.1.4.2.1 Alginate alone

The usage of polymers in biomedical applications such as drug delivery and tissue engineering are highly dependent on its ability to degrade in the body(*188*). There are enzymes that can degrade alginate in the human body. The mechanism of degradation of alginate in the body happens in multiple ways as described below:

Disintegration of the alginate material occurs by exchange of gelling calcium ion with sodium. Acid hydrolysis and alkali hydrolysis are two possible processes that can lead to disintegration. At a physiological pH of 7.4, β-elimination by alkali hydrolysis is the predominant mechanism of alginate polymer length reduction. Oxidation of the gels, by

agents such as peroxides(*189*) help hasten the process, but also weaken the gel, in a ring opening reaction of the polymer.

Degradation by reactive oxygen species (ROS). Most polymers including alginates undergo 'free radical de-polymerization' or 'oxidative-reductive de-polymerization'. Water molecules or molecular oxygen generates free radicals in living systems. Exposure of polymer to gamma irradiation hastens this process and can be used to enhance the rate of degradation(*190*).

Thus the major disadvantages of alginate are the lack of enzymatic degradation and its inert nature that makes it non-adherent for cells. To overcome these limitations, alginate is widely used as its derivative in combination with other polymers in drug delivery and tissue engineering applications. Alginate by itself is used widely in many industries. It is used as a stabilizer and emulsifier in food industry, as it interacts with proteins, fats and fibers. Alginate-pectin mixtures are used as gelling agents independent of sugar content in foods. Hence, alginate is used in many low calorie substitute foods. The high hydrophilicity of alginates renders the material biocompatible and non-immunogenic. Therefore it is used widely in pharmaceutical industry as drug excipient(*181*), dental impression material(*191*), and as a material for wound dressing(*192*).

1.6.2.1.4.2.2 Alginate Derivatives and combinations with other polymers

In general alginates are formed into gels either by using multivalent cations or by covalent crosslinking. These modifications will be discussed further, here. The major purpose in subjecting algnates to chemical and physical modifications is to tailor their physical properties such as degradation, mechanical strength, and biological properties such as enhanced interaction with cells. Mechanical properties like stiffness and strength of alginate gels can be controlled by physical factors. Concentration of polymer(*193*) and its molecular

weight(*186*) can be used to determine the density of polymer solution for formulation of gels. Increase of both these factors leads to higher viscosity of the polymer solution and hence a stiffer and mechanically strong gel. Cationicpoly- (ethyleneimine) (PEI)(*194*) addition leads to improvement of alginate gel's mechanical properties. High molecular weight PEI increases the resistance of the gel to de- crosslinking agents and thus improves the gel's stiffness. Gelling conditions such as temperature, type and concentration of crosslinker also affect the mechanical properties of alginate gels. Low temperature cross-linking(*195*) leads to slow crosslinking, due to reduced rate of calcium ion diffusion. This results in the formation of gels with enhanced mechanical properties. Apart from these factors, the presence of cells in the gels is also shown to improve its mechanical strength(*196*).

As discussed above in the previous section there are many methods used to control the degradation of alginates. Gamma irradiation(*197*) and partial oxidation(*198*) can be used to reduce the molecular weight of polymer and accelerate degradation rates. These techniques also affect the mechanical strength of alginate gels. Gels with bimodal molecular weight distribution have been formulated with one molecular weight polymer being oxidized, and the other left untreated. This approach also accelerated gel degradation rate. In gels that are covalently crosslinked, the linker density(*199*) determines the rate of degradation as well as the strength of the gel. As alginates are not conducive to cell adhesion, covalent modification of the polymer, coupling whole (like fibronectin and collagen)(*200, 201*) or parts of cell adhesion molecules (like RGD peptides) is a popular strategy used to increase cellular responses. Here the concentration(*202*) of these adhesion molecules and the composition of the gel (M/G ratio) determine the effectiveness of the gel in inducing cell adhesion.

Alginate based hydrogels have been used as drug delivery vehicles for low molecular weight (small) molecule drugs as well as proteins such as growth factors. Drug-alginate interactions play a crucial role in determining the rate of drug release from alginate gel matrices. Drug release rate can be completely controlled by charge polarity (hydrophilic molecules will be released quickly and hydrophobic ones more slowly), when there is no chemical interaction between the drug and the alginate matrix. Carbodiimide chemistry is used to link hydrophilic drugs(*203*) to alginate matrices to delay their release. In such a scenario the rate of drug release is determined by polymer degradation. Here a linker such as AAD could be used to attach the drug to alginate and the rate of release would be controlled by the concentration of the spacer. Ionic complexes can also be used to attach drugs to alginate(*204*). Proteins such as growth factors have been successfully delivered by alginate gel systems. It was seen that such deliver systems preserved the bioactivity of the factors. Hence angiognic growth factors like *β*- Fibroblast Growth Factor (FGF-*β*)(*205*), and Vascular Endothelial Growth Factor (VEGF) loaded into alginate beads were successful in inducing angiogenesis to a greater extent than free administration of the growth factors. Ionic complexes were used to link VEGF(*206, 207*) to alginate matrix and the dissolution of this complex along with diffusion acted to control the release of active VEGF from the gels over several weeks *in vivo*.

In most tissue engineering applications alginates with modified physical, chemical and biological properties are desirable. These characteristics can be achieved by chemically modifying alginate to form its derivatives and blends with other polymers. Alginate has a number of hydroxyl and carboxyl groups along its polymer backbone and these are ideal candidates for its chemical modification. Chemical modifications that can be carried out using the hydroxyl group are as follows:

Oxidation: Oxidation of alginate polymer chain produced a decrease in the stiffness of the polymer by breaking C_2–C_3 bond. Here sodium alginate is usually the substrate to be reacted with sodium periodate. This leads to oxidation on the –OH group at C-2 and C-3 position of the uronic acid on sodium alginate. Two aldehyde groups result in each oxidized monomeric units. The resultant oxidized alginate has reactive groups on its backbone and large rotational freedom of the molecule. This renders the polymer more amenable to further chemical modifications and greater biodegradation(*208, 209*).

Reductive amination of oxidized alginate: Oxidized alginate can be used as a substrate for chemical reactions such as reductive amination. Reductive amination is performed with alkyl amine by using $NaCNBH_3$ as reducing agent. This reaction is favorable at a pH of 6-7 and byproducts such as aldehyde/ ketone are negligible under the reaction conditions(*210*).

Sulfation: On sulfation, alginate structurally resembles heparin and attains anti coagulant properties, alongside high blood compatibility(*211*). Reacting sodium alginate with formamide and chlorosulfuric acid ($ClSO_3H$) at 60°C can sulfate it.

Copolymerization: Microwave irradiation of sodium alginate and acrylamide led to synthesis of various grades of grafted polymers(*212*). Alginate-*g*-vinyl sulfonic acid prepared by employing potassium peroxydiphosphate/thiourea redox system has also been reported(*213*). These synthesized graft copolymer exhibit better results for swelling, metal ion uptake, and resistance to biodegradability in comparison to parent alginates themselves.

Linking Cyclodextrins: α-cyclodextrin (α-CD) can be covalently linked to alginate. This reaction can be targeted to the hydroxyl groups of the alginate by cyanogen bromide (CNBr) method to prevent reaction at the carboxyl group. This specificity was necessary to form the

calcium–alginate beads that have great potential in encapsulating bacteria for environmental remediation(*214*).

Chemical modifications that can be carried out using the carboxyl group are as follows:

Esterification: Alkyl group is attached to a molecule during esterification. Addition of alkyl group to the backbone of alginate results in increasing the hydrophobicity of alginate. Alginate can be modified by direct esterification using several alcohols in the presence of catalyst. The alcohol is present in excess to ensure that the equilibrium is in favour of product formation. Propene glycol ester of alginate (PGA) was obtained by esterification of alginate with propyleneoxide. This is a commercially useful derivative of alginate(*215*).

Ugi Reaction: Hydrophobically modified alginate can be prepared by the Ugi multicomponent condensation reaction. The Ugi reaction is amulti-component reaction in organic chemistry involving a ketone or aldehyde, an amine, an isocyanide and a carboxylic acid to form a bis-amide(*216*).

Amidation: In amidation reaction, a coupling agent, 1-ethyl-3-(3-dimethylaminopropyl) carbodiimide hydrochloride (EDC-HCl) is reacted with alginate to form amide linkages between amine-containing molecules and the carboxylate moieties on the alginate polymer backbone. This results in hydrophobic modification of the alginate(*217*).

A general outline of reactions used to modify alginate for biomedical applications was summed up above. Though mostly hydrogel of alginate is the most popular form of application of the polymer, other formats have also been formulated. Alginate foams(*218*), fibers(*219, 220*) and nanofibers(*221*) are other forms in which alginates are fabricated(*182*). Bioartificial pancreas, bone(*222*), vasculature and liver(*223*) are some of the tissue-engineered organs where alginate materials have been used successfully.

1.6.2.1.4.3 Promises and challenges with Alginates in tissue engineering

Alginates are a versatile class of polysaccharides that present a great tool as materials for tissue engineering. They have been formulated as gels, microspheres, foams and fibers in tissue engineering and for delivery of drugs and biological factors. Some constraints posed by the material are its non- enzymatic degradation in the human body and its extremely hydrophilic nature that discourage cell anchorage. However, these limitations have been overcome by subjecting its –OH and –COOH functionalities to chemical modifications. Understanding of the biosynthetic pathways leading to alginate biosynthesis in bacterial systems has been very useful in tailoring their polymer chain composition and the molecular weight of the polymer. Yet, more work needs to be done in improving these systems. Alginate hence serves as a low cost biopolymer that is a good tool in biomedical engineering.

1.6.2.1.5 Cellulose

1.6.2.1.5.1 Chemical structure, properties and sources

Cellulose, the "sugar of plant cell wall" is the most abundant biopolymer in the biosphere. The basic monomer unit of cellulose is β-D-anhydroglucopyranose. These units are joined together covalently by acetal functions between the equatorial group of the C4 carbon atom and the C1 carbon atom (β-1,4-glycosidic bonds). These β-1,4-glycosidic linkages bestow cellulose with its resistance to chemical/ enzymatic attack(*224*) (Figure 1.13). Therefore cellulose is a linear-chain polymer with a large number of hydroxyl groups (three -OH groups per anhydrous AGU unit). This linear structure can be extended to molecules containing 1000–1500 β-D-glucose monomer units, in a cellulose polymer chain. This chain length of cellulose is expressed in terms of number of constituent AGUs, termed degree of polymerization (DP). The degree of linearity and the presence of extensive –OH groups throughout the cellulose chain are responsible for formation of inter and intra molecular hydrogen bonds throughout the polymer

chain. This causes cellulose chains to organize in parallel arrangements into crystallities and crystallite strands, the basic elements of the supramolecular structure of the cellulose fibrils and the cellulose fibers. This arrangement of fibers in the polymer is termed its supramolecular structure and it in turn influences its physical and chemical properties. Cellulose is known to exist in at least five allomorphic forms. Cellulose I is the form found in nature. Cellulose may occur in other crystal structures denoted cellulose II, III and IV. Cellulose II is the most stable structure of technical relevance. This structure can be formed from cellulose I by treatment with an aqueous solution of sodium hydroxide. This leads to regeneration of native cellulose from solutions of semi-stable derivatives. This crystalline structure is modified from cellulose I. A parallel chain arrangement of cellulose in cellulose I form undergoes a change to form cellulose II. This renders the cellulose II more accessible to chemical treatments and hence more reactive. A fringe fibrillar model is used to describe the microfibrillar structure of cellulose polymer. It describes the structure to be made of crystalline regions of varying dimensions called crystallites and noncrystalline regions. This structure explained the partial crystallinity and reactivity of cellulose in relation to its microfibrillar structure(*225*).

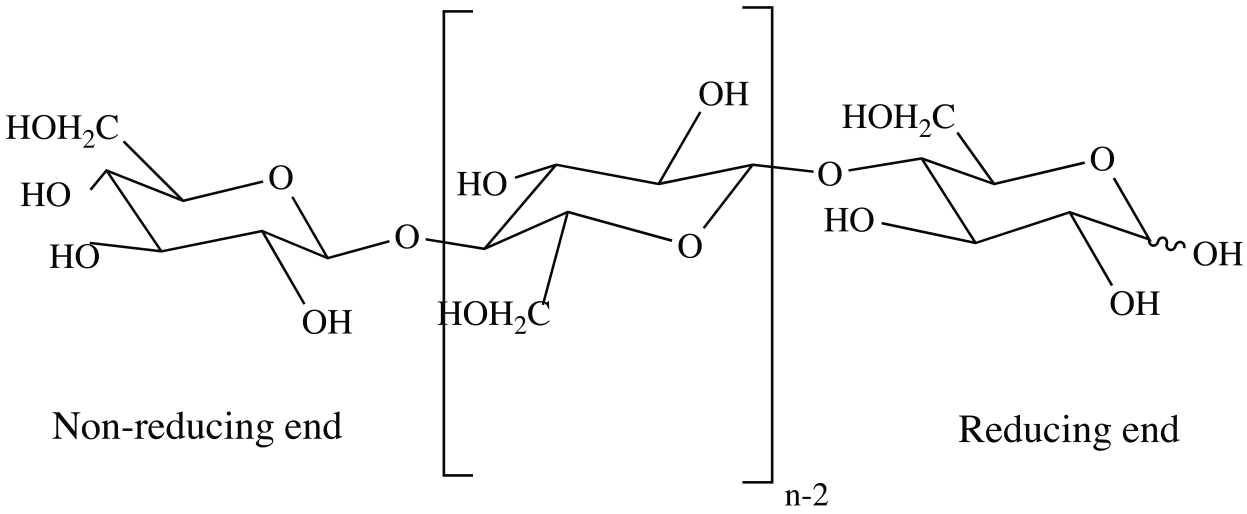

Figure 1.12 Structure of Cellulose

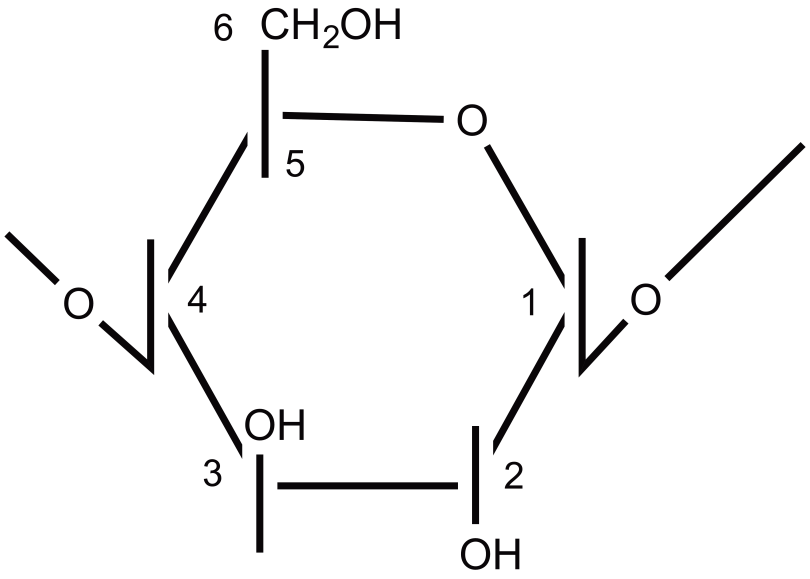

Figure 1.13 Anhydroglucose unit of Cellulose

Numbering of carbon atoms in anhydroglucose unit of cellulose

Cellulose behaves an active chemical due to the three-hydroxyl groups in each glucose residue. The hydroxyl groups at the second and third positions behave as secondary alcohols, while the hydroxyl group at the sixth position acts as a primary alcohol (Numbering as shown in Figure 1.14). These –OH groups are the responsible for the reactivity of cellulose. Degree of substitution (DS) is the term used to indicate the average number of –OH groups

substituted in an anhydroglucose unit of a cellulose molecule. That is, a DS of 3 indicates that all the 3 –OH groups have been substituted in the anhydroglucose units of the cellulose derivative. In general, the relative reactivity of the hydroxyl groups can be expressed as OH–C_6 >> OH–C_2 > OH–C_3(*226*).

Cellulose, like the polysaccharides above, has certain drawbacks. These include poor solubility in common solvents, poor crease resistance, poor dimensional stability, lack of thermoplasticity, high hydrophilicity and lack of antimicrobial properties. To overcome such drawbacks, the controlled physical and/or chemical modification of the cellulose structure is essential(*226*). Introduction of functional groups into cellulose can alleviate these problems, while maintaining the desirable intrinsic properties of cellulose. Apart from the conventional plant source, cellulose is also obtained from bacteria, termed bacterial cellulose. Understanding and engineering these biological systems has opened further doors for bringing in desired modifications into cellulose.

1.6.2.1.5.2 Attempts made in Tissue engineering and drug delivery

1.6.2.1.5.2.1 Cellulose alone

As cellulose in its native form has extensive hydrogen bonds, it is not very processible. Most of the early attempts resorted to viscose process of regenerating (restoring cellulose structure back) cellulose from its derivatives. Regenerated cellulose has been used as a matrix for wound dressing. Early results indicated that implanted viscose cellulose sponges led to increased granulation tissue formation over a period of time and that the pore structure of the scaffold could influence cell infiltration within a certain limit(*227*). On the other hand it was seen that a lower content of cellulose and lower pore diameter induced greater tissue invasion of the implant and later on it also proved to be a matrix conducive for bone formation in a rat model(*228*). However, cellulose sponges were seen to be slow degrading matrices taking up to

sixty weeks for them to be degraded(*229*). Cellulose also was used successfully as an enzyme carrier by dissolving cellulose in ionic liquid and regenerating it. Usage of a hydrophobic ionic liquid preserved the enzymatic activity to a greater extent(*230*). While biodegradation remains a challenge for the absorption of cellulose, it was seen that treatments that markedly reduced crystallinity led to degradation as well as high biocompatibility of regenerated cellulose(*231*). In recent years, microbial cellulose (MC) produced by bacterial species such as *Acetobacter xylinum* has gained much attention as a material for use in biomedical appliances. Though chemically similar to plant cellulose, MC has a microfibrillar and nanostructured arrangement that enables higher water retention by the material. This property is conducive in its application in wound dressing, production of vascular conduits etc(*232*). This cellulose was also seen to have a high degree of biocompatibility(*233*).

1.6.2.1.5.2.2 Cellulose derivatives and combination with other polymers

The supramolecular structure of cellulose and the extensive hydrogen bonded chemical structure of cellulose render it insoluble in water and organic compounds. Therefore most of the reactions involving cellulose are carried out in solid or swollen state as heterogeneous reactions. Here, the limiting factors for the hetrogenous reaction are the breakage of hydrogen bonds (by alkaline treatment) and degree of interaction with the reaction media (by swelling). Therefore, specific solvents that disrupt the hydrogen bonds in cellulose such as N, N-dimethylacetamide and lithium chloride (DMA/LiCl), Dimethyl Sulfoxide/Tetrabutylammonium Fluoride (DMSO/ TBAF)(*234*) are used widely for the purpose. Hence, even though using such strategies, cellulose alone has been employed for different purposes as a material, its derivatives are easier to work with as they overcome the limitations posed by cellulose. The following section gives an overview of derivatives of cellulose and its combination with other polymers:

Cellulose Esters:

Esters of cellulose with interesting properties such as bioactivity, thermal and dissolution behavior can be obtained by esterification of cellulose with nitric acid in the presence of sulfuric acid, phosphoric acid or acetic acid. Commercially important cellulose esters are cellulose acetate, cellulose acetate propionate and cellulose acetate butyrate. Cellulose esters of aliphatic, aromatic, bulky, and functionalized carboxylic acidscan be synthesized through the activation of free acids in situ with tosyl chloride, N, N'-carbonyldiimidazole, and iminium chloride under homogeneous acylation with DMA/LiCl or DMSO/ TBAF. A wide range of cellulose esters that vary in their degree of substitution, various substituent distributions and several desirable properties can be obtained through these reactions. Recently a number of enzymes that degrade cellulose esters have been reported. Some of them are acetyl esterases, carbohydrate esterase (CE) family 1, and Esterases of the CE 5(*235-238*) family.

Cellulose esters have been put to use in many biomedical applications. Hemodialysis membranes used in purification of blood, for patients with renal failure have employed melt-spun cellulose diacetate membrane. These membranes have been produced by Altin (company) and used successfully. They were advantageous and had less toxicity than synthetic polymer based membranes(*239*). Cellulose acetate is seen as a preferred material for the fabrication of blood filration devices that are used to separate a fraction of the blood such as red blood cells and leukocytes(*240, 241*). Cellulose acetate and regenerated cellulose fibrous matrices have been successful in supporting the growth of cardiac myocytes and present a potential scaffold platform for cardiac regeneration(*242*) (Entcheva *et al*., 2004).

Cellulose Ethers:

Carboxymethyl cellulose (CMC) is the major cellulose ether. By activating the non-crystalline regions of cellulose, selective regions of alkylating reagents can attack the cellulose. This is termed the concept of reactive structure fractions and is used widely for the production of CMC. Another route for carrying out the same reaction is by derivatization of cellulose in reactive microstructures, formed by induced phase separation. This process involves the usage of NaOH in anhydrous state in combination with solvents like DMA/LiCl. These CMC products have a distribution of substituents that deviate significantly from statistical prediction of the product theoretically.

CMC is used in several drug delivery and tissue engineering purposes. The release of apomorphine, a drug used to regulate motor responses in Parkinson's disease was successfully incorporated into CMC powder formulation exhibited a sustained nasal release, and it performed better than starch based delivery vehicle(*243*). Sodium CMC has been used successfully in gastrointestinal drug delivery(*244*). Hence CMC is seen as a successful drug delivery system for mucosal tissue(*245*). Apart from drug delivery, CMC is useful as a scaffold in tissue engineering too. pH dependent swelling of CMC hydrogels, were capable of releasing drugs at the right pH present in the tissue of interest and showed potential as a wound dressing material(*246*). CMC hydrogels could be used for encapsulating cells of nucleus pulposis and hence are a potential replacement for intervertebral disc degeneration(*247*). CMC has been combined with chitosan(*248*) and hydroxyapatite(*249*) for bone and dental regeneration purposes too.

Silyl Cellulose:

Silyl ethers of cellulose are characterized by a remarkable increase in thermal stability, lipophilic behavior and a lack of hydrogen bonds. They can be used as selective protecting

groups in organic synthesis, due the simple cleavage of the silyl ethers under acidic conditions or through nucleophilic attack. Therefore, the silyl ethers of cellulose are very attractive for engineering polysaccharide chemistry(*250*). The silylation of polar protic -OH groups of cellulose with chlorosilanes and silazanes leads to these silyl ethers. The degree of substitution (DS) and position of silyl substitution is determined by the reaction condition. All the three –OH groups will be substituted when trimethyl silylation with hexamethyldisilazane (HMDS) in liquid ammonia, is used in the reaction. Dissolution of cellulose in DMA/LiCl (homogeneous reaction) makes the –OH groups more accessible. Following this, if the synthesis takes place in the presence of imidazole, the bulky silylation reagent thexyldimethylchlorosilane (TDSCl) leads to complete silylation at O_6 and O_2 (DS value=2.0). Here, the primary and the most reactive secondary -OH groups are converted. If silyl ether formation starts with the same reagent in cellulose suspension in aprotic dipolar media like N-methylpyrrolidone (NMP), which contain gaseous ammonia, silylation of all primary C_6-OH groups takes place. This state does not permit any further reaction of the secondary hydroxy groups(*251*).

Cellulose Sulfonates:

The most frequently synthesized and used cellulose sulfonates are the p-toluenesulfonates (tosylates), methanesulfonates (mesylates), p-bromobenzenesulfonates (brosylates), and trifluoromethanesulfonates (triflates). The synthesis of sulfonates is through simple esterification of the -OH groups of cellulose with the corresponding sulfonic acid chlorides or anhydride is a way to attach nucleofuge groups to cellulose(*252*). By varying the solvent and reaction conditions, the DS of the polymer can be controlled. For instance, at temperatures of 7°C, cellulose tosylate with a maximum DS of 2.3 can be formed with tosyl chloride in the

presence of triethylamine. The DS of sulfonated cellulose can also be controlled by the molar ratio of tosyl chloride to glucose units of the cellulose.

Aminocellulose:

Aminocellulose are aminodeoxy derivatives bearing the nitrogen function directly on the cellulose skeleton. These are useful in immobilization of enzymes and other proteins. By having a specific structural design based on cellulose tosylates. Aminodeoxycellulose are synthesized with corresponding halogen derivatives and sulfonates as starting materials. PDA cellulose is a material used successfully for immobilization of enzymes like oxidoreductases, glucose oxidases, peroxidases using gluteraldehyde. Diazo coupling and redox coupling have also been utilized to link ascorbates, and dyes. Here too, the solvent composition and reaction conditions can determine the reaction chemistry (S_N2) and hence the DS of the product formed(*253*).

Resinification of cellulose:

Resinification of cellulose can impart crease-resistance termed ‘‘durable press’’ properties to cellulose. The reaction of cellulose with bi- or poly-functional compounds leads to formation of crosslinked cellulose matrix, called resinified cellulose(*224*).

Graft polymerization of cellulose:

A new approach to modification of cellulose is by graft polymerization. A graft copolymer generally consists of a long sequence of one monomer, referred to as the backbone polymer (main chain) (cellulose in this case) with one or more branches (grafts) of long sequences of a different monomer(*254*). Graft copolymerization permits the combination of the best properties of two or more polymers in one physical unit(*226*). The aim with cellulose graft polymerization is to retain the inherent properties of cellulose and incorporate qualities from

the polymer grafted onto it. Depending on the nature of the grafted polymer, properties such as dimensional-stability, resistance to abrasion and wear, wrinkle recovery, oil and water repellence, elasticity, sorbancy, ion exchange capabilities, temperature responsiveness, thermal resistance and resistance to microbiological attack can be incorporated into cellulose(*255-259*).

The methods for graft polymerization of cellulose can be generally classified into three major groups such as (i) free radical polymerization, (ii) ionic and ring opening polymerization and (iii) living radical polymerization.

Strategies used in cellulose graft polymerization can be divided into three categories:

The 'grafting to' approach- here the functional pre-formed polymer with its reactive end-group is coupled with the functional groups located on the backbone of cellulose, the major polymer. The inherent weakness of this approach is a hindrance to diffusion caused by crowding of polymer chains on the surface (Odian, 2004).

The 'grafting-from' approach- here the growth of polymer chains occurs from initiating sites on the cellulose backbone. This is the most commonly used approach. Easy access of the reactive groups to the chain end of the growing polymer is achieved in 'grafting-from' approach. This makes it possible to attain high graft density(*260*).

The 'grafting through' approach- in this approach, a vinyl macromonomer of cellulose, is copolymerised with a low molecular weight co-monomer. Though this approach is more convenient, a cellulose-derived macromonomer has to be synthesized. This poses a limitation to this technique (Odian, 2004).

1.6.2.1.5.3 Promises and challenges with cellulose

Cellulose and other polysaccharides discussed above have been gaining importance as polymeric materials. Increasing the knowledge of organic, polymer chemistry and the

chemistry of low-molecular weight polysaccharides can greatly help us understand more about the chemistry of cellulose and control the different processing techniques for cellulose to a greater extent. Having a multidisciplinary approach will further help us utilize the polymer more in biomedical applications. The development of derivatives and grafted polymers of cellulose have been important steps towards the utilization of cellulose, which is considered as a renewable resource. Processes such as lyocell processing of cellulose are environment friendly techniques and promise a safer polymer processing technology. New insights are still being obtained on the process of wood pulping and biosynthetic pathways in cellulose synthesis. By using this knowledge, engineering cellulose and utilizing bacteria for production of the polymer are the advances we could expect in the future.

1.6.2.2 Proteins in tissue engineering

Proteins are the building blocks of life and their sophisticated chemistry makes them excellent scaffolding materials for BTE. Some common proteins used in BTE are:

1. Collagen
2. Fibronectin
3. Fibrin
4. Vitronectin
5. Keratin
6. Silk

1.6.2.2.1 Collagen

About 20- 30% of mammalian protein is collagen and therefore it is the most abundant animal protein biopolymer(*261*). There are around 28 types of collagen found in various tissues(*262*). All of the collagen shares a structural similarity. Their basic unit is termed tropocollagen and consists of 3 parallel polypeptide chains- GXY, where G is glycine, X is usually proline, and

Y is usually 4-hydroxyproline, arranged to form a triple helical structure. This tropocollagen further forms the fibrous collagen structure seen in different tissues(*263*). The natural source of collagen is animal tissue like skin, tail and tendon. Collagen can be formulated into hydrogels, fibers and microspheres. These matrices have been used for drug delivery(*264*) and in BTE applications(*265*). In the case of bone 60% of its weight is attributed to the mineral content. The remaining 40% of bone weight comes from the proteins and water. Of the proteins found in bone, collagen constitutes 90%. Hence many BTE scaffolds use collagen as a biomaterial by itself or in combination with other materials. Collagen acts as a ligand to the cellular integrin that act as their receptors like α2β1 and α1β1 integrin. This binding of collagen to integrin elicits a signaling cascade that is conducive to cell survival, adhesion, proliferation and osteoblastic differentiation(*266*). Though collagen has excellent tissue compatibility and osteoconductive properties, collagen matrices lack mechanical strength to be used for BTE. Therefore, oftentimes collagen is combined with other natural/ synthetic polymers for BTE applications(*267*).

1.6.2.2.2 Fibronectin

Fibronectin too is an ECM protein. It provides structural support, and also acts as ligand to certain integrin receptors, apart from recruiting other biological factors(*268*). These functionalities of fibronectin offer it the ability to induce cell adhesion, proliferation and differentiation. There are two forms of Fibronectin- the secreted, soluble form produced by hepatocytes in the liver and the insoluble form secreted by cells such as fibroblasts. The soluble form of fibronectin is a major component of blood plasma. The secreted fibronectin from cells is composed of two non- identical polypeptide chais linked by a disulfide bond at the carboxy terminal end of the peptides. There are three modules in each subunit of fibronectin. Each subunit is about 230- 270 KDa in molecular weight. The three modules

forming each of these subunits are: type I, type II and type III(*269*). Owing to its biocompatibility and cell adhesion properties, fibronectin and the adhesion subunits of fibronectin have been coated onto many BTE implants(*268, 270*).

1.6.2.2.3 Fibrin

Fibrin is an ECM protein formed during blood clot. The polymerization of soluble fibrinogen turns to insoluble fibrin by the action of thrombin(*271*). Fibrinogen is made of three pairs of polypeptides Aα, Bβ and γ, bridged by disulfide bonds(*272*). When thrombin cleaves Aα and Bβ chains at their N- termini, the polymerization of fibrinogen to fibrin ensues(*273*). The fibrin fibrils aggregate to form a clot. The FDA has approved fibrin sealants for use as medical adhesives. Fibrin biomaterials are used as drug delivery and wound healing scaffolds(*274*).

1.6.2.2.4 Vitronectin

Glycoprotein vitronectin is also a ligand for integrin receptors on cells(*275*). Vitronectin is found both in circulation and in different tissues. It is also seen that vitronectin plays a role in linking cell adhesion, humoral immunity and cell invasion into tissues. Vitronectin mediates cell adhesion and spread and hence coating scaffolds with fibronectin induced cell adhesion and spreading(*276*).

1.6.2.2.5 Keratin

Keratin is a protein found in animal tissues such as nail, hair, and horns. It presents a filamentous structure made of hierarchically arranged structures. Cell adhesion domains termed LDV domains were found in keratin(*277*). It was seen that keratin biomaterials led to growth and differentiation of MC3T3-E1 preosteoblasts. Hence keratin is seen as a potential scaffolding platform for BTE(*278*).

1.6.2.2.6 Silk

Silk is a protein produced by insects like worms and spiders. It is also a hierarchically structured filamentous protein(*279*). A glycoprotein matrix called sericin embeds the two microfilaments of silk and this constitutes the basic structure of silk. The sericin protein in silk fibroi is shown to have immunogenic effects. Therefor, this protein is removed from silk while using the material for biomedical applications. Silk is a 370 kDa fibroin protein, with a lighter chain fibroin of 25 kDa and a P25 protein of 325 kDa form the microfilament structure(*280*). The presence of α-helix and β-turns in the protein structure of silk renders the material mechanically strong. The silk produced by silk worm *B. mori* is the most polular source of the protein. Silk based materials are being developed as various tissue engineered scaffolds including materials for bone(*281*).

1.7 Design of Scaffolds for BTE

There are several processing techniques used in BTE for the formulation of 3D porous scaffold structures. These processing techniques facilitate the inclusion of more than one material into a desired shape and form with pore sizes that are needed for the particular tissue engineered application. Some of the most common techniques are as follows(*282*).

1.7.1 Processes used for fabrication of macro and microporous BTE scaffolds

1.7.1.1 Thermally induced phase separation (TIPS)

In this technique, a homogenous solution of the polymer used for scaffolding is dissolved in dimethylcarbonate overnight. Ceramics are added to the polymer solution and dispersed into the polymer phase by sonication. This mixture is then maintained at -196°C for two hours after quenching in liquid nitrogen. This mixture is transferred into a cooling bath at -10°C with the application of vacuum. The solvent evaporates after the mixture is subjected to 48

hours of -10°C, followed by 48 hours of exposure to 0°C. Finally it is transferred to an oven at room temperature for the material to reach its equilibrium mass(*283*).

The TIPS technique can produce scaffolds with macro and microstructures, with a high degree of porosity for various tissue engineering applications(*284, 285*). It is possible to gain control over the porosity of the scaffold formulated by modulating the parameters like concentration of the polymer and ceramic used, the solvent used for the system and the temperature of quenching(*284*). PDLLA/ Bioglass scaffolds prepared by TIPS have shown to support MG-63 osteosarcoma cell line viability and proliferation and hence can be seen as potential scaffolds for BTE(*286*). Scaffolds of PDLLA or PLGA/ 45S5 Bioglass with high porosity hold promise as a scaffold for BTE(*286, 287*). Scaffolds formulated using TIPS have shown to have nanotopographical features and hence greater bioactivity(*288, 289*).

1.7.1.2 Solvent casting and particle leaching

The solvent casting technique involves casting of a well-dissolved polymer or a polymer/ seramic composit solution to allow the solvent to evaporate. The casting mould can be used to design the 3D shape of the resulting scaffold material. While the technique is very simple to carry out, there are some disadvantages to it as well. Only a few shapes can be formulated and the process could lead to entrapment of solvent in the matrix. The entrapped solvents could attribute to the scaffold's toxicity as well as denaturation of bioactive molecules in a composite scaffold system(*290*).

Polymer microsphere constructs made by water oil/water emulsions can further be sovent sintered with the inclusion of salt or sugar during the sintering step. These porogens can be leached once the sintering is achieved. This technique gives tissue engineers the scope of engineering matrices with controlled porosity(*288*). However particle leaching has disadvantages such as limitations of dimensionality achieved in the scaffold, solvent retention,

and loss of bioactivity of encapsulated biomolecules. BTE scaffolds that incorporate calcium phosphate with graded porosity have been formulated using this technique(*291*). Optimally porous salt leached PLGA microsphere 3D sintered matrices have been used to improve the oxygen transfer in an otherwise less porous 3D porous sintered microsphere matrix(*36*).

1.7.1.3 Solid freeform fabrication techniques (SFFT)

Scaffolds with controlled macro and micro porous architecture are created by conventional foam fabrication procedures such as phase separation, porogen leaching and emulsion-solvent diffusion(*292, 293*). Computer aided imaging by micro CT and magnetic resonance (MR) has aided with production of scaffolds with programmed porosities, using SFFT(*293*). A PLLA/ TCP composite scaffold with about 90% porosity was successfully developed using SFFT(*285*). Its porosity was programed to be 400 μm in between the multiple layers of the scaffold along with micropores of 10 μm diameter. Similarly PLA scaffolds developed by SFFT combined computer aided programed macropore size of 500–800 μm, with solvent derived 50–100 μm void size(*292*). Though SFFT gives better control over the scaffold architecture, it may be a time consuming technique.

1.7.1.4 Microsphere sintering

Applying thermal(*294*) or solvent sintering(*295*) can sinter polymeric microspheres formed by emulsion solvent evaporation technique. This leads to the formation of 3D porous matrices with a porosity of 30- 40%, with pore diameter around 90 μm(*294*), as reported in literature. The polymer solutions could be made to incorporate bioactive molecules like ceramics and growth factors(*296*). The mechanical properties of these matrices can be constructed so that it is close to cancellous bone. The microsphere platform also offers scope for other modifications such as incorporation of nanofibers to be used in BTE(*297*).

1.7.1.5 Coated scaffolds

Porous scaffolds prepared by any of the above techniques can be coated by dipping in a slurry of polymer or by electrophoretic deposition (EPD). The slurry could contain ceramics or growth factors. The slurry dipping technique performs better than EPD technique of coating(*298*). Deposition of biomineral by SBF solution using the slurry dipping technique has been used successfully in many BTE scaffolds to make them more osteoconductive(*299*).

1.7.1.6 3D Printing

3D Printing is an extension of SFF technology, where complex free structures can be created using a computer-aided design (CAD). Unlike many other machining processes that are subtractive in nature to create a desired scaffold structure, the 3D Printing technique uses an additive manufacturing approach (AM). The rapid prototyping (RP) system used in 3D printing combines liquids, powders and sheets to form the parts of the scaffold(*300*). Depending on the polymer used, the process can be tailored and performed at high or room temperature. This flexibility allows for incorporation of factors, hydroxyapatite and cells into the scaffold structure(*301*). In fused deposition molding (FDM) a CAD design is created using the information from CT and MR imaging data(*302*). The CAD data is input into the printer's software that slices the data to form instructive printable layers. This information is sent to the polymer extrusion head and it prints the entire design one layer after another. Many polymers such as PCL(*303*), PDLLA and PLLA(*304*) have been used and in a combination with TCP and AH for producing BTE scaffolds using 3D printing(*305*). Some constraints of polymer processing parameters still exist with 3D printing, but progress is being made at a rapid pace with 3D printing technology.

1.7.2 Processes used for fabrication of nanoscale BTE scaffolds

TIPS (described above), self-assembly of polymers, and electrospinning can be used to fabricate BTE scaffolds with nanoscale features.

1.7.2.1 Self assembly

Using the principles of protein folding can be applied towards the formation of an orderly nanofibrillar network. As few as two to three peptides can self assemble through their hydrophobic end groups to form nanofibers(*306-308*). Hydrogels(*309*) formulated by peptide molecule self assembly and nanofibers incorporated into scaffolds are examples of BTE scaffolds where the self assembly of proteins and peptides has been employed(*310*).

1.7.2.2 Electrospinning

Electrospinning is a popular technique for formulating polymeric nanofibrillar scaffolds for BTE. When an electric field is applied to a polymer solution, to over come the forces of surface tension, a continuous jet of polymer solution is obtained. This jet of polymer is allowed to collect at a grounded collector plate and the solvent evaporates leaving back the polymeric nanofibers at the collector plate(*311*). Electrospinning is a versatile technique that is simple and can be used to produce nanofibers of different fiber diameter(*312*), alignment(*312*) and could be fabricated to incorporate minerals(*313*). However nanofibers suffer from a few constraints. The electrospun nanofiber matrices have a surface to volume ratio that leads to burst release of encapsulated factors. Another issue is that the fibers form a 2D mat rather than a 3D scaffold. Hence electrospinning alone cannot be used to formulate scaffolds for BTE as these matrices are not 3 dimensional and have no mechanical compatibility with bone(*289*).

1.8 Cells used in BTE

Though scaffolds can act as the support structures, including cells and factors into tissue engineered constructs is essential for complete bone regeneration. While the incorporation of growth factors has proved to be beneficial, there are challenges of non-targeted bone formation and problems of maintaining the bioactivity of the factors while delivering them. Hence using cells is a clinically relevant and a simpler option in BTE. There are two cell types that could be used in tissue engineering. These two types of cells are somatic cells and stem cells.

1.8.1 Somatic cells in BTE

1.8.1.1 Cells used in analysis of BTE scaffolds

Transfected cells that are immortalized are used to test a number of BTE scaffolds in culture. They can replicate osteoblastic proliferation and differentiation in the body. Studies with these cell types have indicated the potential of the BTE scaffold to perform in the body. Examples of such cell types are the murine MC3T3-E1 cells that are preostoblats derived from mouse calvaria(*314*) and the MG-63, Saos-2 and U-2 OS human osteosarcoma cell lines(*315*). They however have limited use with scaffolds implanted into the body, as these cells are capable of causing cancers due to the presence of transfected genes in them.

1.8.1.2 Cells used in vivo

Primary calvarial osteoblasts from rats(*316*), mice and humans(*317*) are used to determine the osteoconductive potential of BTE scaffolds. These are more reflective of the environment in the body and the responses may be more clinically relevant when examining the response of bone to a biomaterial being tested(*316*). They can also be transplanted into the body of animals of the same species. However their availability may be a limiting factor for their usage *in vivo*.

1.8.2 Stem cells in BTE

While somatic cells like osteoblasts and periosteal cells can be used in BTE constructs, they have limited potential for expansion and avoiding de-differentiation. Hence stem cells hold great potential in BTE. The scaffolds can include features like nanoscaled dimensions and chemical functionalities that can direct the differentiation of stem cells. Stem cells could be of two types based on their source:

1. Embryo derived and
2. Adult derived

1.8.2.1 Embryo derived stem cells

1.8.2.1.1 Embryonic stem cells

Embryonic stem cells (ESCs) are totipotent stem cells with the ability to differentiate into multiple lineages. They also have the ability to maintain this potential while proliferating greatly. They have shown great potential towards osteoblastic differentiation. ESCs offer a great differentiation potential, but also have the ability to form tumors when implanted in vivo. This is termed teratogenicity. Apart from this, obtaining ESCs would involve their harvest from unborn embryos. Therefore using them in humans is challenging due to ethical, clinical and regulatory concerns associated with ESCs.

1.8.2.1.2 Amniotic fluid derived stem cells (AFSCs)

Amniotic fluid derived stem cells (AFSCs), are partly embryonic in origin and have are a little less multipotent than ESCs. They can maintain their potential while dividing upto 250 times. They can differentiate well in the osteoblastic lineage. Studies have used AFSCs to characterize the performance of BTE scaffolds *in vitro*.

1.8.2.2 Adult stem cells

1.8.2.2.1 Induced pluripotent stem cells (iPSCs)

Induced pluripotent stem cells (iPSCs) were formulated to overcome the limitations of ESCs. By the transfection of the reprogramming factor genes (Oct4, Sox2, cMyc and Klf4) into somatic cells, the cells are reprogrammed to stem cells (iPSCs). These cells are being investigated for use in BTE(*318*).

1.8.2.2.2 Bone marrow derived mesenchymal stem cells (BM-MSCs)

The bone marrow has multipotent stem cells that can differentiate into cells of the mesodermal lineage including bone, cartilage, adipose, and skeletal muscle(*319*). These BM-MSCs, are used widely both in research and in clinical procedures(*320*). The ease of accessibility, their large potential for self renewal, and minimal ethical and regulatory issues concerning BM-MSCs, makes these cells an attractive option for application in BTE(*321*). MSCs are found in the bone marrow and thought to play an essential role in bone healing(*322*). Their participation could be direct (they can differentiate into cells of the osteochondral lineage) and indirectly too by secretion of cytokines that allow for progenitor cells to home into the site of injury and help with processes like angiogenesis(*323*). BM-MSCs are also known to have immunomodulatory effect when implanted into an osseous defect(*324, 325*).

1.8.2.2.3 Adipose derived stem cells (ADSCs)

The fat tissue in the body contains a population of multipotent stem cells called Adipose derived stem cells (ADSCs)(*326, 327*). These cells have a great proliferative and multilineage differentiation potential. Several experiments have shown the potential of ADSCs to differentiate in the osteogenic lineage when given the right media *in vitro(328)*.

ADSCs have shown to be osteogenic when implanted into animals along with biodegradable BTE scaffold. Ectopic ossification by ADSCs that turned into osteoblasts under subcutaneous implantation(*329*) in mice and the capability of ADSCs to heal cranial defects by intramembranous ossification demonstrated their potential to be used in BTE(*330*). Hence the first phases of clinical trials combining ADSCs with autologous materials to induce bone formation were successful(*331*). Hence BM-MSCs and ADSCs are the most clinically relevant stem cell sources, presently.

2 Chapter 2 Preliminary Studies

Cellulose and Collagen Derived Micro-Nano Structured Scaffolds for Bone Tissue Engineering[2]

2.1 Introduction

Scaffold based tissue engineering strategy has emerged as an alternative to autografts and allografts to regenerate damaged or lost tissue(*332, 333*). Bone graft substitutes or scaffolds are routinely used as viable alternatives to biological grafts due to ease of fabrication, handling and storage. Scaffolds often utilize a biodegradable three-dimensional (3D) architecture to serve as a temporary ECM to support tissue ingrowth. In particular, scaffolds for BTE are desired to have osteoconductive (promote osteoblast proliferation), osteoinductive (promote osteoblastic differentiation of progenitor cells) and osteointegrative (form an intimate contact and anchor into the surrounding bone) properties to promote bone regeneration(*334*). In the repair of a bone defect, the scaffold is designed to maintain the structure of the defect and restore the functions of the lost bone. Ideally the scaffold should satisfy a number of design criteria to achieve comparable properties present in autologous grafts: The scaffold should be (1) biocompatible so that it is integrated with the host tissue without any adverse immune response, (2) mechanically competent in order to tolerate the local forces. This is most critical for protecting the tissues and transmitting the compressive, tensile forces and mechanical cues across the defect to the regenerating cells, (3) biodegradable with non-toxic degradation products that can be metabolized and excreted by

[2] This study was published as a research article: **Aravamudhan A**, Ramos DM, Nip J, Harmon M, James R, Deng M, Laurencin CT, Yu X, Kumbar SG. Cellulose and Collagen Derived Micro-Nano Structured Scaffolds for Bone Tissue Engineering. *J. Biomed. Nanotechnology*, 9 (4), 719-731, 2013

the body, and with controllable degradation kinetics to match the rate of bone formation so that the newly produced tissue compensates the mechanical and mass loss of the degraded matrix, (4) osteoconductive with porous structures to allow cell infiltration, proliferation, neovascularization, and nutrient transport. It is desirable for BTE scaffolds to have highly interconnected pores with a minimum pore size of >100 μm to promote ingrowth of tissue and vasculature(*335*). The interconnected pore spaces enable the transport of oxygen and nutrients. Surface roughness of the scaffold promotes cellular adhesion, proliferation, and differentiation of anchorage-dependent cells(*336, 337*). (5) Lastly, scaffolds should be able to integrate with the surrounding osseous tissue through the formation of bonds with the bone. Scaffold chemical composition and topographical properties play an important role in guiding cell behavior and tissue regeneration *in vivo*. For instance, scaffolds presenting acrylate groups have been reported to maintain multipotency of progenitors(*338*) while functional groups such as amine, hydroxyl and carboxyl, lead to greater differentiation in the osteochondral lineage(*38, 339*), both in the absence and presence of inductive media. Recent studies have demonstrated the importance of topographical features in regulating cell behavior, including preferential adhesion, migration, proliferation and expression of cell-specific phenotype(*340*). Several studies have reported the role of nano, micro and combination of micro-nano dimensional patterns in regulating stem cell differentiation into osteogenic lineage even in the absence of inductive media(*64, 341, 342*). In our previous studies we have reported enhanced cell migration and mature osteoblast phenotype development on the hierarchical structures comprised of micro-nano dimensions for BTE applications(*297*).

Biomaterials of both synthetic and natural biodegradable polymers have shown great promise in tissue engineering. Though synthetic polymers such as polyesters can be synthesized with desired molecular weight and elasticity, their degradation pattern often is reported to have a negative impact on tissue healing due to acidic degradation products(*343*). Different buffering systems made of polymer–polymer or polymer-calcium phosphates have been developed to neutralize acidic degradation products(*344*). On the other hand, polymers of natural origin due to their compositional similarity with native ECM components offer greater biocompatibility in tissue healing(*335, 345*). It is often a challenge to produce load-bearing scaffolds using natural polymers due their limited solubility and processability. For example, collagen(*346, 347*), chitosan(*345*), polysaccharide(*348*) and protein based scaffolds are often presented in the form of porous sponges, fiber matrix or hydrogels. These scaffolds lack the mechanical stability and require chemical crosslinking to produce stable scaffolds. During scaffold fabrication, extensive processing and crosslinking compromises the biological functionality of these scaffolds(*349-351*). In this work we report the fabrication and characterization of mechanically stable micro-nano structured scaffolds based on a derivative of cellulose and type I collagen for bone tissue engineering. Sintered microspheres of cellulose acetate microstructure contribute towards ideal mechanical and pore property of the scaffolds for BTE. Scaffold surface functionalization with collagen nanofibers combines the nano fiber structures with the microsphere based scaffold framework to enhance the surface area as well as bioactivity. In this work we report the fabrication, optimization and characterization of cellulose acetate, and collagen functionalized scaffolds for BTE application.

2.2 Materials and Methods

2.2.1 Materials

Cellulose acetate (Mn 30 K) (CA), ethyl cellulose (Mn 30 K) (EC), and poly(vinyl alcohol) (30,000–70,000) (PVA) were procured from Sigma-Aldrich (St. Louis, MO, USA). Poly(lactic-co-glycolic acid) 85:15 (PLGA) was purchased from Alkermes (Wilmington, OH). Acetone, dichloromethane, cyclohexane, 10% formalin in PBS and gluteraldehyde were purchased from Fisher Scientific (Fair Lawn, NJ, USA). Promega MTS reagent kit (Madison, WI, USA), Bio-Rad Alkaline phosphatase (ALP) substrate kit (Hercules, CA, USA) and Invitrogen quantity PicoGreen dsDNA assay kit (Eugene, Oregon, USA) were used in this study. Alizarin Red and cetylpyridinium chloride were procured from Acros Organics (New Jersey, USA). Cell culture media was prepared by mixing 1:1 ratio of F-12 Nutrient Mixture (Invitrogen, Greens Island, NJ) and DMEM (Invitrogen, Greens Island, NJ, USA). Basal media was prepared by adding 10% FBS (Invitrogen, Greens Island, NJ, USA) and 1% Penicillin-Streptomycin (Invitrogen, Greens Island, NJ, USA) to 1:1 mixture of F-12 and DMEM. Osteogenic media was prepared by adding 0.05 mM L-ascorbic acid (Sigma, St. Louis, MO, USA) and 3.15 mM glycerol 2-phosphate disodium salt (Sigma, St. Louis, MO, USA) to basal media. RNAse and DNAse free water and 7.4 pH PBS buffer used were purchased from Invitrogen (Greens Island, NJ, USA). Human osteoblasts used in this study were purchased from PromoCell (Heidelberg, Germany).

2.2.2 Polysaccharide Microsphere Fabrication

Microspheres of CA and EC were fabricated via an oil-inwater solvent-evaporation technique. In brief, 20% EC or 13% (w/v) CA solutions in methylene chloride and acetone at a ratio 9:1 were emulsified into an aqueous phase containing 1% (w/v) PVA. Emulsion was stirred at a

constant stirring rate of 250 rpm overnight and hardened microspheres were collected following solvent evaporation. Microspheres were washed repeatedly with deionized (DI) water and segregated into different sizes namely: 300–425, 600–710 and 710–800 m using sieves. Control PLGA microspheres were also prepared using a similar protocol.

2.2.3 3D Porous Scaffold Fabrication

Polysaccharide microspheres were sintered together into 3D porous scaffolds at the room temperature using a mixture of solvent and non-solvent(*352, 353*). In brief, a Teflon mould was filled with CA or EC microspheres to which 200 μL of an optimized solvent/non-solvent composition was added to cover the microspheres to achieve sintering. The solvent/non-solvent composition of acetone: cyclohexane ratio was varied from 1:0, 2:1, 3:1, 4:1 and 5:1 to achive microsphere sitering. The solvent and non-solvent mixture was allowed to evaporate in a fume hood for 30 minutes followed by vacuum drying for an additional 24 hours. Cylindrical scaffolds measuring 10 mm by 5 mm were fabricated to characterize compressive mechanical properties and porosity while 8 mm by 2 mm tablet type cylindrical scaffolds were made for evaluating in vitro osteocompatibility studies. Control PLGA microsphere scaffolds were fabricated by heating the stainless steel mold at 95°C for 2 h to achieve sintering.

2.2.4 Functionalization of 3D Scaffolds: Micro-Nano Structured Scaffolds

Sintered microsphere scaffolds were surface functionalized with collagen type I nanofibers using principles of molecular self-assembly(*354*). Optimization studies used different aqueous collagen concentrations, solution pH and incubation time. These studies were aimed to achieve uniform collagen functionalization without compromising the pores in the sintered microsphere scaffolds. In a typical study scaffolds were incubated in a 0.1% (w/v) solution of

collagen type I with a pH adjusted to 5.2 at 37°C for 24 h(*355*). These nanofiber-functionalize scaffolds were washed with DI water and stored in a desiccator until further use.

2.2.5 Collagen Content in Micro-Nano Structured Scaffolds

The amount of collagen present on each scaffold was quantified with a calorimetric bicinchoninic acid (BCA) Protein Assay Reagent kit (Pierce). Proteins form a purple colored chelation complex with BCA via reduction of cupric ions to cuprous ions. The purple color of this complex is directly proportional to the protein concentration and the absorbance was read at 562 nm using a BioTek plate reader. In brief, collagen coated micro-nano structured scaffolds were transferred to a new 48 well plate and incubated with 1 mL of aqueous 1% acetic acid for 1 hour followed by mixing with the aid of a pipette to extract all collagen from the scaffold. Similarly collagen remaining on the TCPS surface during coating experiment was also extracted for the estimation of collagen content. A 25 μL of the collagen extract was mixed with 200 μL of BCA reagent followed by 30 min incubation at 37°C and analyzed at 562 nm using a plate reader. A sample size of n = 6 was used for all these estimations. The absorbance of six known collagen concentrations: 62.5, 125, 250, 500, 1000 and 2000 μg/mL were used to construct a standard curve to convert absorbance readings to collagen concentrations.

2.2.6 Scanning Electron Microscopy (SEM)

Surface morphology of the scaffolds was characterized by using SEM and field emission SEM (FESEM). Scaffold surfaces were sputter coated with Au/Pd using a Hummer V sputtering system (Technics Inc., Baltimore, MD) prior to imaging. The samples were viewed using JSM 6400 scanning electron microscope (JEOL, Boston, MA, USA) operated at an accelerating voltage of 20 kV at various magnifications. Uncoated micro-nano structured

scaffolds were imaged using a tabletop TM-1000 (Hitachi, Closter, New Jersey) at various magnifications. Nanofiber diameter was measured using Image J, NIH software. For each fiber diameter measurement 3 different samples at 3 different locations were considered (average of 100 fibers).

2.2.7 Micro-Nano Structured Scaffolds: Collagen Nanofiber Stability in Solution

Collagen nanofiber stability on the micro-nano structured scaffolds, in culture media up to 28 days, was qualitatively determined by using SEM. In brief, micro-nano structured scaffolds were incubated in 1.8 mL of basal media up to 28 days and media was changed every other day. At predetermined time points of 1, 3, 7, 14, 21 and 28 days scaffolds (n = 3) were taken out and gently washed with DI water and dried. Scaffolds were imaged at various magnifications to qualitatively estimate nanofiber stability.

2.2.8 Compressive Mechanical Properties

Cylindrical scaffolds (10×5 mm) of CA, both in dry and wet (n = 12) conditions were tested under compression until failure using an Instron® tester (model 5544; Instron, Canton, MA). Dry scaffolds were incubated in PBS overnight and held at a temeprature of 37°C in the water bath to produce scaffolds for testing under wet conditions. Prior to testing, excess of PBS from the sacffolds was wiped using a Kimwipes ^{TM}. Both dry and wet samples were subjected to compression testing at a rate of 1 mm/min at ambient conditions until failure.

From the load and displacement values a stress–strain curve was constructed. For each scaffold the following parameters were calculated:

(1) Compressive modulus = slope of the linear region of the stress versus strain curve,

(2) Compressive strength = maximum force/the original cross-sectional area,

(3) Maximum compressive load = maximum force applied, and

(4) Energy absorbed at failure = area under the stress–strain curve at the point of failure.

2.2.9 Porosimetry

Both simple polysaccharide microsphere scaffolds and micro-nano structured scaffolds were characterized for median pore diameter and porosity. Micromeritics Autopore III porosimeter (Norcross, GA) was employed to measure the volume of mercury intrusion at specific pressures for the scaffolds (n = 6). The scaffold pore volume and the pore size were calculated by substituting this information into the Washburn equation. A set of 6 scaffolds (10×5 mm) in a 5 mL penetrometer was used for each measurement.

2.2.10 Cell Culture

HOB were plated in tissue culture flasks (125 cm^2) and cultured in basal media as specified in the materials section. The media was replaced every other day, and culture was maintained in a tissue culture incubator at 37°C and 5% carbon dioxide. Cells were trypsinized at 90% confluency and cells at passage 6 were used for scaffold seeding. Both CA and EC scaffolds were autoclave sterilized at 121°C for 30 min. Control PLGA scaffolds were sterilized by incubation in 70% ethanol for 15 min and 30 min UV light exposure on both sides. Optimized collagen concentration and pH conditions were used for collagen nanofiber functionalization of scaffold. Functionalization experiments were carried out using sterile microsphere scaffolds and collagen solution in the cell culture hood and maintained in a tissue culture incubator at 37 °C for 24 hours. Scaffolds were placed in 24-well plates and incubated with 2 mL of basal medium for 30 min prior to cell seeding. Each scaffold was seeded with 50,000 cells and allowed to stand for 2 h in the incubator prior to adding 1.8 mL of basal media to allow HOB adhesion onto scaffolds. Following 24 hours of incubation, the medium was changed from basal to osteogenic. Cultures were maintained for 28 days and media was changed every other

day. One set of scaffolds was cultured in basal media up to 28 days to establish HOB viability using MTS assay. For all these experiments a sample size of n=5 was used.

2.2.11 Cell Viability Assay

The cell viability on these scaffolds was measured using MTS assay at culture times of 1, 3, 7, 14, 21 and 28 days. The metabolically active cells react with the tetrazolium salt in the MTS reagent to produce a formazan dye that can be observed at 490 nm. At each time point the cellular constructs were washed twice with PBS to removenon-adherent cells and then transferred to a new 24-well plate. These constructs were incubated with 200 μL of MTS reagent with 1 mL of basal medium for 2 hours. Aliquots were taken and their absorbance was read on a plate reader (BioTek Synergy HT, USA). The absorbance of six known cell numbers 10,000, 30,000, 50,000, 75,000,100,000, and 150,000, were used to construct a standard curve to convert absorbance readings to cell numbers. The absorbance values of the samples were fitted with the standard curve to determine the cell number on the scaffolds.

2.2.12 Cell Proliferation (Picogreends DNA Assay)

HOB proliferation after changing to osteogenic media was quantified by measuring the amount of cellular DNA content at various culture points using a PicoGreen® dsDNAassay(*297, 356*). In brief, at different culture times of 1, 3, 7, 14, 21 and 28 days the cellular constructs were washed twice with PBS, transferred to new well plates and 1mL of 1% Triton X-100 solution was added to lyse the cells. The well plates underwent three freeze-thaw cycles, between −70°C and room temperature. The contents were mixed individually with the aid of a pipette to extract cell lysate from the 3D scaffolds prior to analysis. 125 μL of sample DNA was transferred into a new well plate to which 375 μL (component B) and 500 μL (Component A) kit reagents were added. Well plates were covered with aluminum foil

to prevent light exposure and incubated for 5 min. A BioTek plate reader was used to measure fluorescence (485 nm/535 nm). Optical readings were converted in DNA concentration using a standard curve(*352*).

2.2.13 Alkaline Phosphatase Activity

ALP expression by HOB cultured scaffolds at various time points was evaluated as an early marker of the retention of osteoblast phenotype using an ALP substrate kit(*357*). A 100 μL of cell lysate was transferred into a well plate to which a 400 μL of P-NPP (para-nitro phenol phosphate) substrate and buffer solution were added and incubated at 37 °C for 30 min. After 30 minutes, adding a 500 μL of 0.4 N of sodium hydroxide stopped the reaction. The intensity of the color produced though the reaction is proportional to ALP activity. The optical density of the solution was measured at 405 nm using a BioTek plate reader. The results for ALP activity optical density were normalized to DNA content determined in a companion DNA assay(*352*).

2.2.14 Mineralized Matrix Deposition Assay

Mineralized matrix deposition on the scaffolds by HOB was evaluated using an Alizarin Red staining method for calcium deposition(*358*). This colorimetric analysis is based on solubilizing the red matrix precipitate with cetylpyridinium chloride (CPC) to yield a purple solution. In brief, at 7, 14, 21 and 28 days of cell culture, cellular constructs were fixed in 10% formalin at 4 °C for 1 h and then stained with 40 mM alizarin red solution for 10 min at room temperature. After washing 5–10 times with distilled water to remove the adsorbed/absorbed dye, chemically bound red matrix precipitate was solubilized in 1 mL of 10% CPC until color was stable. The optical density of the solution was read at 562 nm using

BioTek plate reader. The results for calcium deposition were also normalized with DNA content determined in a companion DNA assay(*297*).

2.2.15 Live/Dead Cell Viability

Cell viability on scaffolds was performed using a live/dead cell viability kit and then imaged. In brief, calcein AM enters live cells and reacts with intracellular esterase to produce a bright green fluorescence, while ethidium homodimer-1 enters only dead cells with damaged membranes and produces a bright red fluorescence upon binding to nucleic acids. Scaffolds were imaged at 3 days using a BioRad Radiance 2100 Multiphoton/Laser Scanning Confocal Microscope (LSCM) at magnifications of 10× and 20× with and without transmitted light to view cells independently and alongside the scaffold.

2.2.16 Statistical Analysis

All results were first evaluated using one-way analysis of variation (ANOVA) followed by Tukey's (HSD) analysis of the differences between groups with a confidence range of 95.00%.

2.3 Results

2.3.1 Fabrication of Sintered Microsphere Scaffold and Effect of Solvent Composition on Sintering Morphology

In general cellulose microspheres had a rough morphology as opposed to control PLGA microspheres as evidenced by SEM images. These microspheres were segregated into different sizes using sieves(*295*). Figure 1 illustrates the morphology of the microsphere scaffolds at different sintering conditions. For instance, scaffolds sintered with higher solvent content in the solvent/non-solvent composition lead to greater bonding between adjacent microspheres (**Figures 2.1(A)–(H)**). Increasing the solvent content resulted in distorted microsphere structure with compromised pore properties. Based on the morphology and pore property measurement studies, scaffolds sintered at a ratio of 3:1 acetone: cyclohexane was found to be optimal for further characterization (**Figures 2.1(C) and (D**)).

2.3.2 Morphology of Functionalized Microsphere Scaffolds with Collagen to Form Micro-Nano Structures

Figure 2.2 and **2.3** indicate the morphology of the CA and EC cellulose collagen micro-nano structured scaffolds respectively, at various magnifications and scaffold depths. Collagen nanofiber assembly was found to be uniform throughout the scaffold architecture. These fibers were in the diameter range of 140±40 nm for CA scaffolds and 120±34 nm for EC scaffolds(*355*). We also characterized the quantity of collagen present in each scaffold using a calorimetric BCA protein assay. The average collagen content on each polysaccharide scaffold and the encapsulation efficiency are presented in **Table 2.1**.

The porous microsphere scaffold could retain only 42% of the collagen on the scaffold and rest was deposited on the TCPS. Functionalizing scaffolds of different materials with collagen nanofibers may present different morphologies and material properties. Uniform collagen

nanofiber functionalization around the cellulose microsphere surfaces without compromising in the pore properties was evident in the images (**Figures 2.2** and **2.3**).

2.3.3 Temporal Stability of Nanofibers on the Scaffold Surface Under Culture Condition

Collagen nanofiber functionalized scaffolds were incubated in culture media for three weeks, and imaged at different time points (**Figure 2.4**) using SEM at 50 and 500× magnifications in order to determine the stability of collagen nanofibers. These scaffolds were imaged on Day 1 (**Figures 2.4(A), (B)**), Day 3 (**Figsures 2.4(C), (D)**), Day 7 (**Figures 4(E), (F**)), Day 14 and (**Figures 4(G), (H)**), Day 21 (**Figures 2.4(I), (J)**). It is apparent from the images that collagen nanofibers not only remained stable but supported passive mineralization with time.

2.3.4 Mechanical Property and Porosity of Scaffolds Under Dry and Wet Conditions

Dry CA scaffolds under compression testing showed an average maximum compressive modulus of 266.75 ± 33.22 MPa, strength 12.15 ± 2.23, load 225.14 ± 42.09 and energy at failure 0.34±0.13 J. The same scaffolds under wet conditions showed an average maximum compressive modulus of 130.53±13.97 MPa, strength 7.15 ± 1.24 MPa, load 144.76 ± 24.43 N and energy at failure 0.36±0.12 J (Table 2.2). Under wet conditions, the compressive mechanical properties of the scaffolds reduced to almost half that of the scaffold under dry condition. Nanofiber functionalized scaffold porosity was found to be 33.9±5.2% with an average pore diameter 185.4± 8.6 μm.

2.3.5 Cell Survival and Proliferation

Figure 2.5 showed osteoblast survival measured up to 28 days on micro-nano structured scaffolds, control PLAGA scaffolds and TCPS. At all time points TCPS showed significantly higher cell number based on metabolic activity compared to test scaffolds and control PLGA

(**Figure 2.5**) in basal media. However, cell numbers on test and PLAGA control scaffolds were comparable. The observed differences in cell metabolic activity may be due to the difference in number of cells that initially adhered to the scaffold and the change in scaffold environment (2D and 3D). For instance, a fraction of the seeded cells may attach to the 3D porous scaffold while the rest will attach to the TCPS container. Higher metabolic activity on 2D TCPS compared to 3D scaffold environment may reflect the inverse relationship between cellular proliferation and phenotypic differentiation. HOB proliferation in osteogenic media showed significantly higher DNA content on the micro-nano structured scaffolds than TCPS (**Figure 2.6**).

2.3.6 Differentiation Measured by Alkaline Phosphatase Content and Mineral Deposition

Osteoblasts cultured on micro-nano structured scaffolds resulted in the higher levels of ALP expression as compared to TCPS controls (Figure 2.7). Expression of ALP on polysaccharide micro-nano structures was either higher or comparable to PLAGA micro-nano structures. Scaffold mineralization also followed a similar ALP expression trends where significantly higher amounts of calcium were deposited on the micronano structured scaffolds as compared to TCPS control (Figure 2.8). In general, calcium deposition on polysaccharide structures was either higher or comparable to PLAGA micro-nano structures. osteoblasts seeded on EC scaffolds start showing very early expression of phenotypic markers (ALP and Calcium deposition) while CA scaffolds make up towards the later time points (Figures 2.7 and 2.8).

2.3.7 Cell viability and morphology

In **Figure 2.9**, the cell viability at different planes and locations of the scaffold can be seen. For instance, for similar cell seeding densities micro-nano structured scaffolds showed significantly

higher number of viable cells distributed uniformly throughout scaffold architecture (**Figures 2.9(C), (D)**) while the viable cells were only at the microsphere junctions on the microsphere scaffolds (**Figures 2.9(A), (B)**).

Table 2.1 Quantification of Collagen on Scaffold and Coating Efficiency

Total Collagen Concentration used for coating	**Collagen per scaffold**		**Collagen on TCPS**		**Scaffold coating Efficiency**
	AVG	**STD**	**AVG**	**STD**	
2000 μg/mL	847.5	171.7	1146.7	166.8	42.3%

Table 2.2 Sacffold Compressive mechanical properties in dry and hydrated state

Dry Scaffold	**Wet Scaffold**
Compressive Modulus (Mpa)	
266.75±33.22	**130.53±13.97**
Maximum Compressive Load (N)	
225.14±42.09	**144.76±24.43**
Compressive Strength (MPa)	
12.15±2.23	**7.15±1.24**
Energy at Failure (J)	
0.34±0.13	**0.36±0.12**

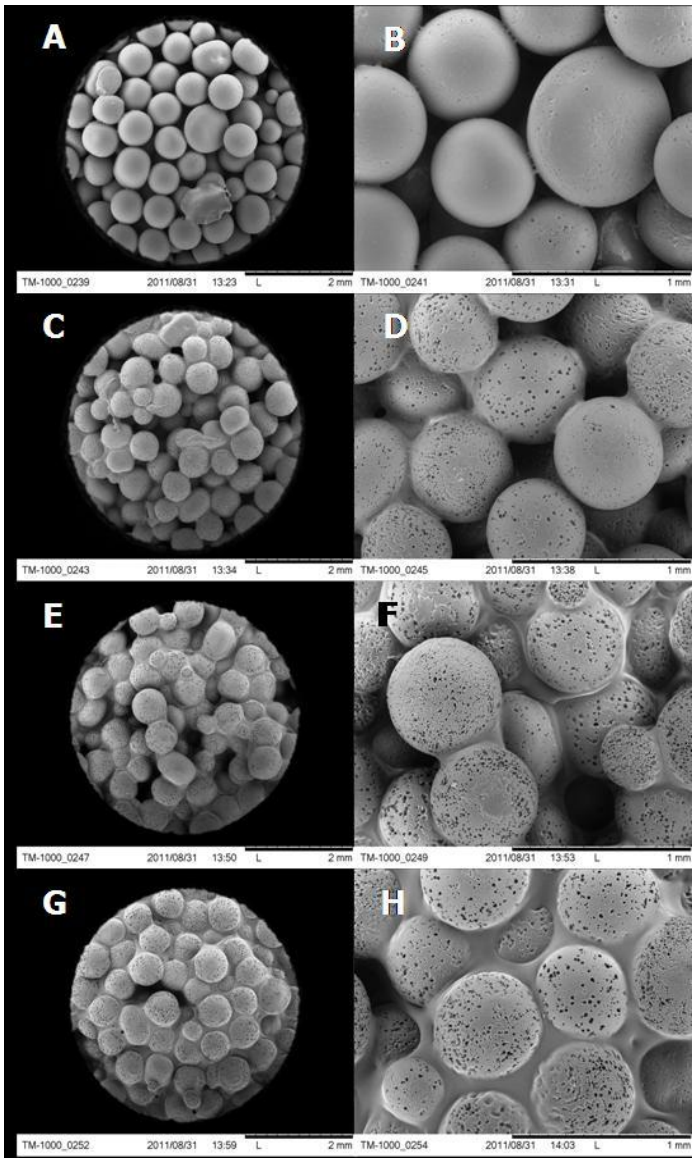

Figure 2.1 Optimization of Sintering solution

Effect of solvent/non-solvent composition on the morphology of the resulting sintered microsphere scaffolds. Anetone is a solvent for CA while cyclohexane is a non-solovent. Acetone:cyclohexane ratio was varied from 1:0, 2:1, 3:1, 4:1 and 5:1. The 30× and 100× SEM images of CA scaffolds with varying acetone/cyclohexane sintering solution concentrations: **A. 2:1 30×, B. 2:1 100× C. 3:1 30×, D. 3:1 100×, E. 4:1 30×, F. 4:1 100×, G. 5:1 30×, H. 5:1 100×.** Higher solvent compositions led to greater bonding between adjcent microspheres.

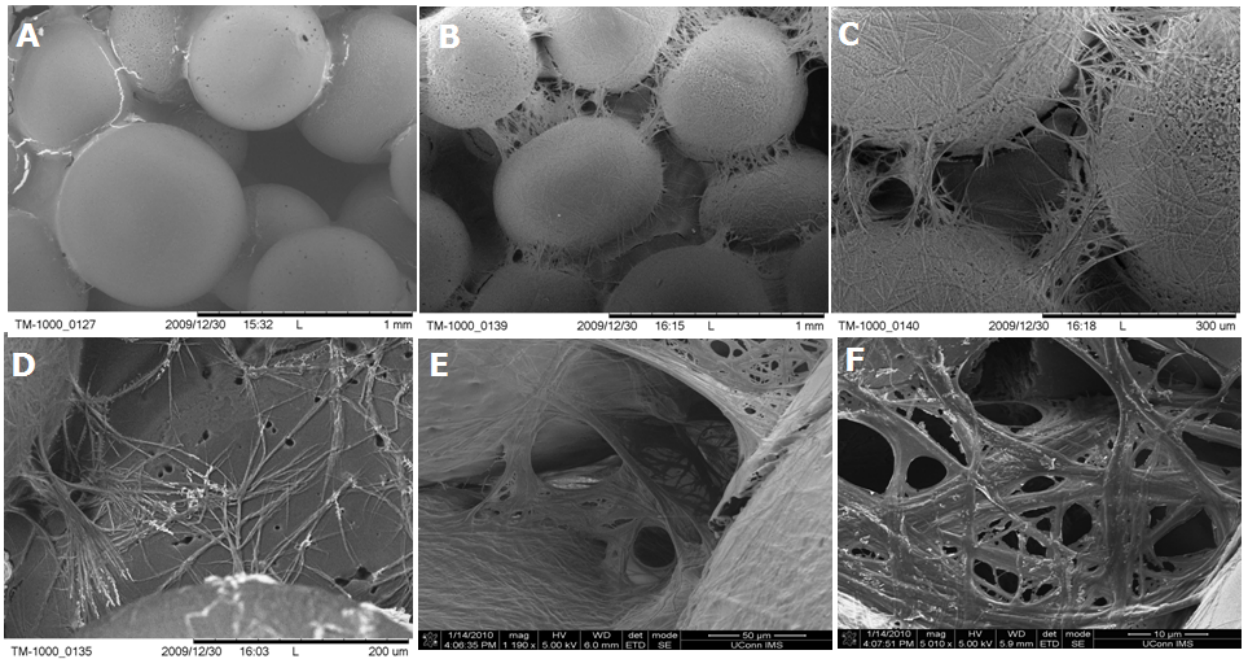

Figure 2.2 Morphology of CA-collagen scaffolds

SEM micrographs (B and C) illustrate the top view of CA-composite scaffold surface morphology where A is a control CA scaffold without collagen. Micrographs A-D were recorded on an environmental SEM without applying Au-Pd coating. Representative micrographs D-F illustrates the deep interior surface morphology of the composite scaffolds taken on several randomly broken pieces of the different scaffolds. Micrographs E and F at higher magnifications were imaged after coating with Au-Pd using a FESEM. Preferred Collagen nanofiber (140 ± 40nm) assembly on the microsphere surface may be attributed to polysaccharide hydrophilic nature as well as slower water evaporation during scaffold drying process. Collagen coating was uniform throughout the scaffold 3D architecture with enhanced surface area as compared to neat CA scaffolds.

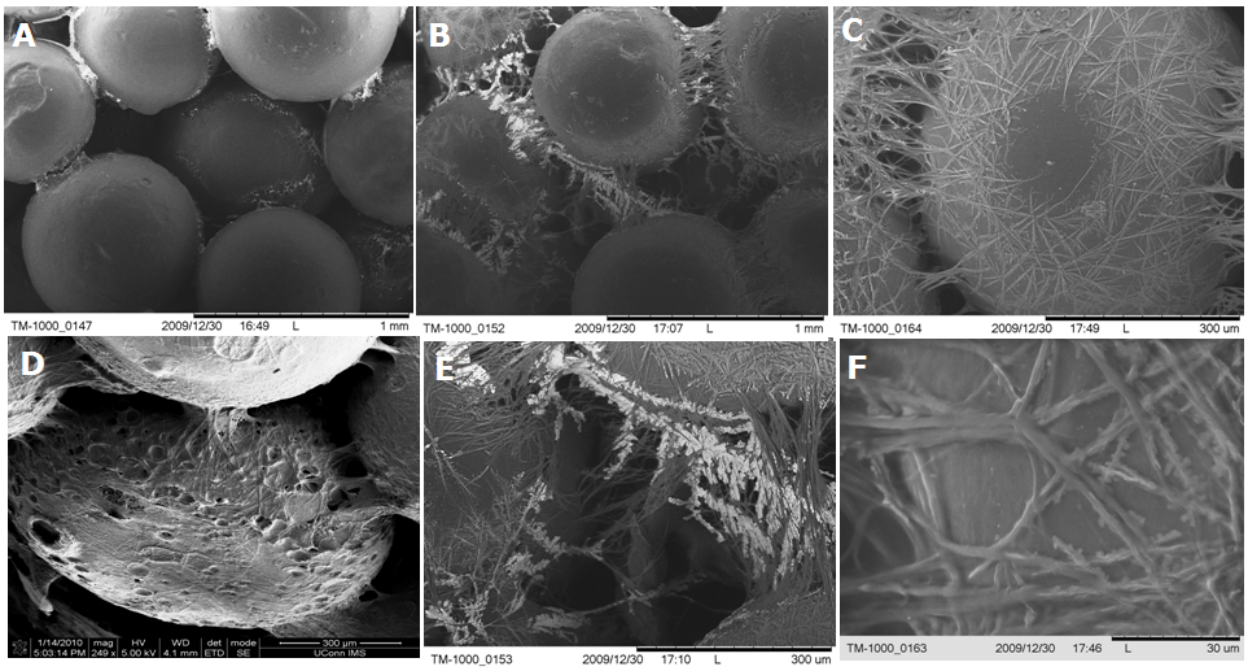

Figure 2.3 Morphology of EC-collagen scaffolds

SEM micrographs (B and C) illustrate the top view of EC-composite scaffold surface morphology where A is a control EC scaffold without collagen. Micrographs A-C, E and F were recorded on an environmental SEM without applying Au-Pd coating. Representative micrographs D-F illustrates the deep interior surface morphology of the composite scaffolds taken on several randomly broken pieces of the different scaffolds. Micrograph D was imaged after coating with Au-Pd using a FESEM. Collagen nanofibers (120 ± 34 nm) coating was uniform throughout the scaffold 3-D architecture. Composite scaffolds in general present enhanced surface area as compared to EC scaffolds.

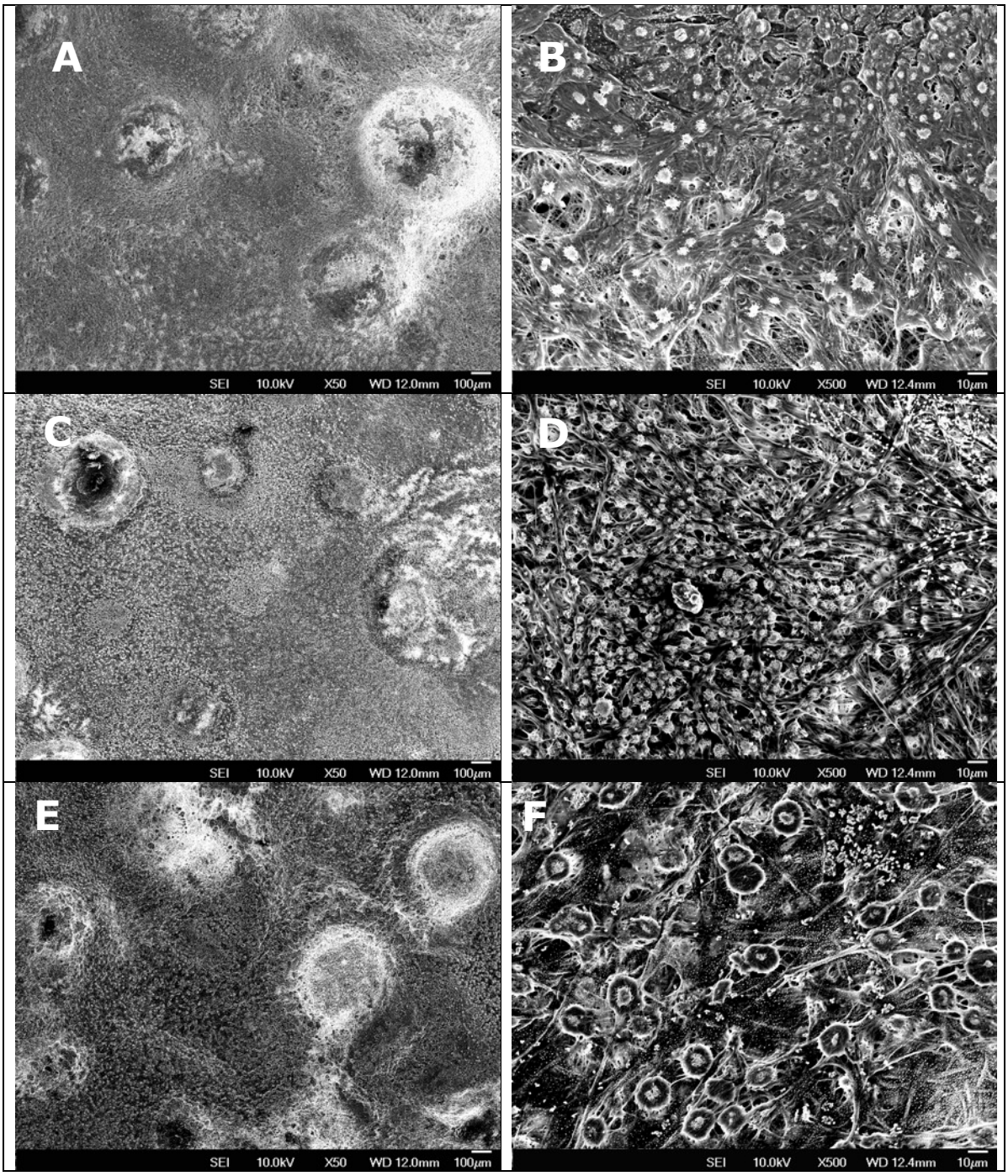

Figure 2.4 Collagen Nanofiber stability *in vitro*

Stability of collagen nanofibers in composite scaffolds following incubation in culture media. Representative SEM micrographs (A B) Day 1, (C,D) Day 3, (E,F) Day 7, (G,H) Day 14 and (I, J) Day 21 illustrates the deep interior surface morphology of the composite scaffolds taken on several randomly broken pieces of the different scaffolds at two different magnifications of 50 and 500 X. Culture media was replaced every other day just to mimic cell culture conditions. Scaffolds were imaged after coating with Au-Pd using a FESEM. Collagen nanofibers act like a nucleating agent and favored salt deposition from the culture media which seemed to increase

with culture time. It was difficult to image samples with increasing culture time due to increased amount of salt deposition that lead to charging and destroyed the image quality.

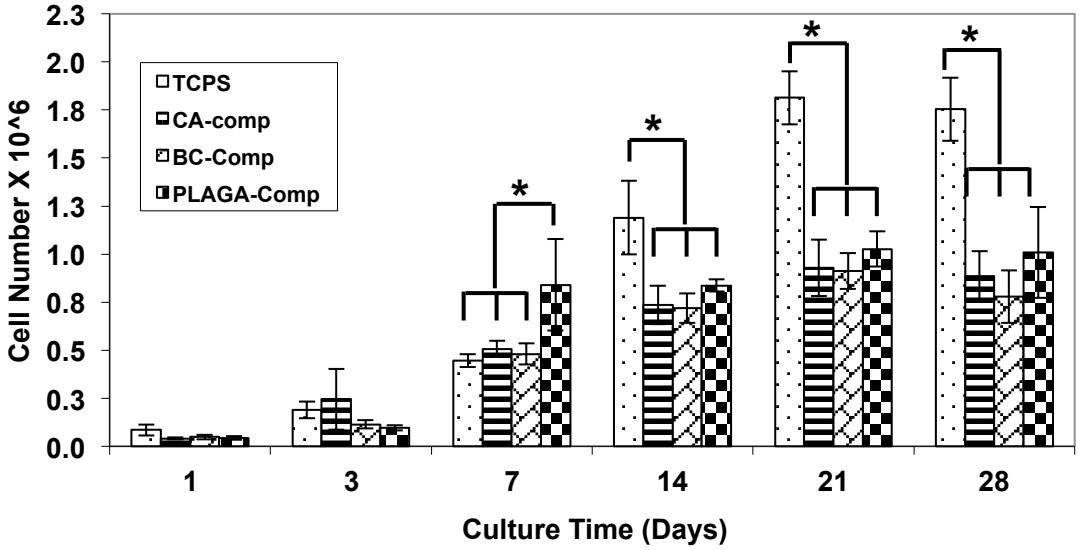

Figure 2.5 Metabolic activity of seeded HOBs

Proliferation of HOB seeded on polysaccharide composite scaffolds in basal media measured using MTS assay. At each time point quintuplicate samples were measured and comparisons were made within the group. (*) indicates the statistical significance within the group at $p<0.05$. These studies were designed to establish composite cellulose material compatibility with HOB. In general HOB proliferation on cellulose composite scaffolds was comparable to PLAGA composite scaffolds and attained confluency by day14. TCPS control showed significantly higher cell number beyond 7days as compared to composite scaffolds.

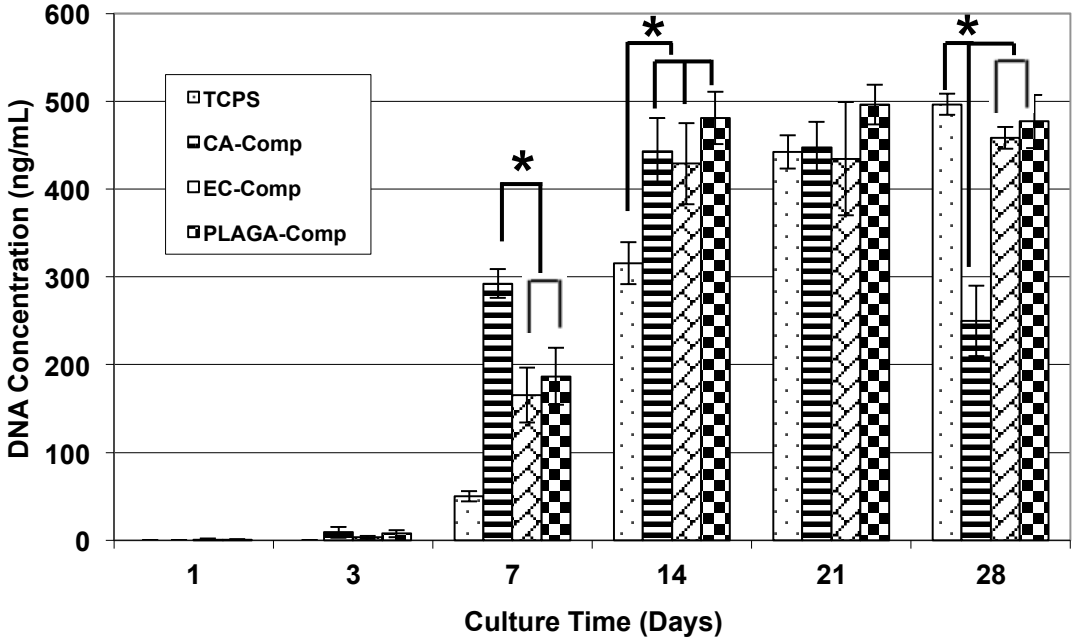

Figure 2.6 Prolifeartion of seeded HOBs

Proliferation of HOB seeded on polysaccharide composite scaffolds in osteogenic media following day 1 culture in basal media. At each time point quintuplicate samples were measured and comparisons were made within the group. (*) indicates the statistical significance within the group at $p<0.05$. Cell proliferation was significantly higher on composite scaffolds up to day 14 as compared to TCPS 2D control. CA composite scaffolds showed significantly higher amount of DNA at day 7 and the composite scaffolds achieved confluency by day 14. Higher amount of DNA content on composite scaffolds can be attributed to material bioactivity, 3D environment and higher surface area offered by nanofiber structures.

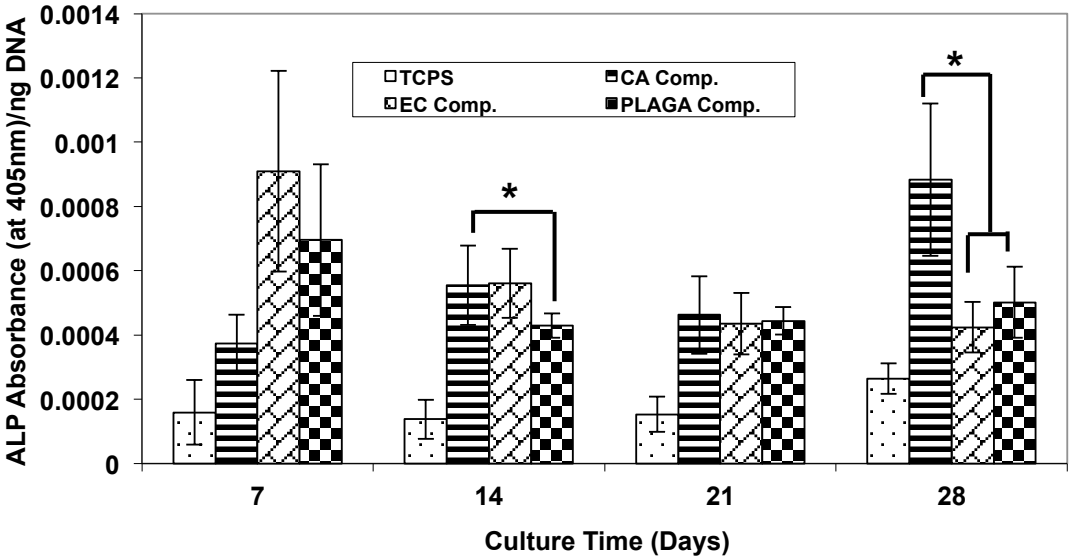

Figure 2.7 ALP activity of Seeded HOBs

Normalized alkaline phosphatase activity expressed by HOB cultured on polysaccharide composite scaffolds in osteogenic media following day 1 culture in basal media. At each time point quintuplicate samples were measured and comparisons were made within the group. (*) indicates the statistical significance within the group at $p<0.05$. In general significantly higher levels of ALP activity were observed on composite scaffolds as compared to TCPS controls. ALP activity was polysaccharide composites was either higher are comparable to PLAGA composites.

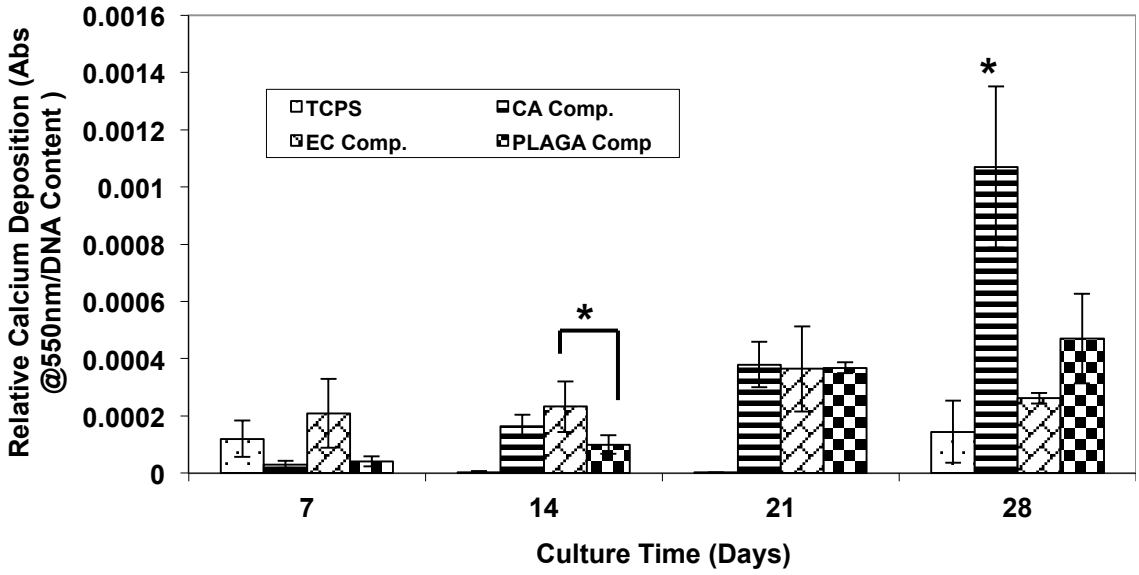

Figure 2.8 Mineralization by seeded HOBs

Relative mineralized matrix deposited on scaffolds at various culture points normalized with DNA content. Significantly higher amount of Calcium was deposited on the composite scaffolds as compared to TCPS control. Calcium deposition on polysaccharide composites was either higher are comparable to PLAGA composites. At each time point quintuplicate samples were measured and comparisons were made within the group. (*) indicates the statistical significance within the group at $p<0.05$.

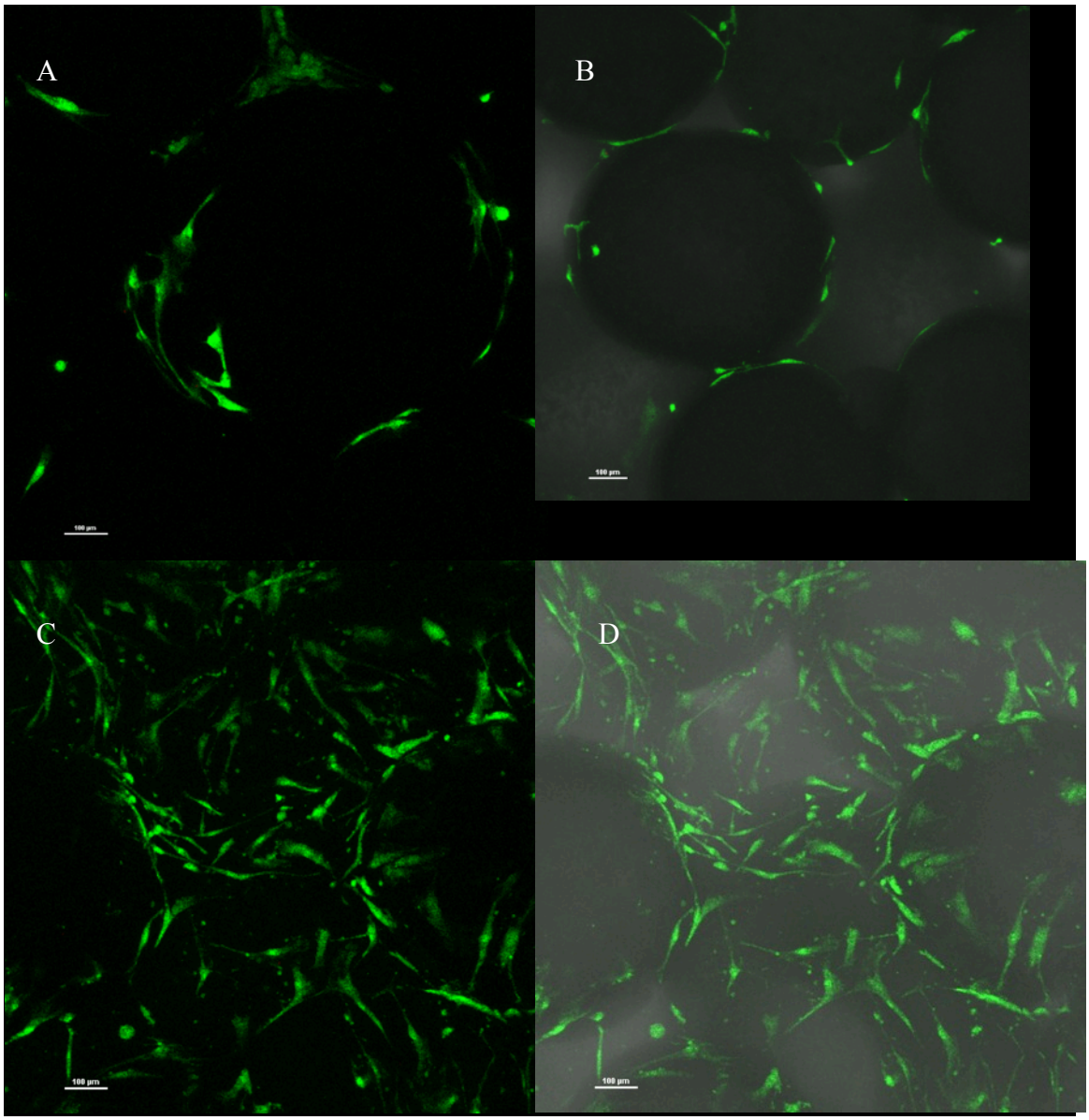

Figure 2.9 Viability of seeded HOBs

Representative confocal micrographs showing survival and morphology of HOB cultured on polysaccharide CA (A), (B) and micro-nano structured scaffolds (C), (D) without (A), (C) and with (B), (D) transmitted light at 3 days after cell seeding. Confocal images clearly indicated the higher cell number on composite scaffolds as compared to neat scaffolds. Majority of the cells were viable had a well-spread morphology and distributed uniformly throughout the microsphere surface and microsphere junctions. Cell survival was determined by viability assay where live cells appear as fluorescent green color and dead cells as fluorescent red.

2.4 Discussion

Scaffolds are designed to serve as a temporary ECM and hence are required to provide structural support and a physical environment for cells to attach, grow, migrate and respond to signals(*332, 333*). Additionally scaffolds for BTE should provide mechanical properties similar to bone(*359*). A variety of scaffolds in various forms and pore properties have been fabricated and characterized for bone tissue engineering applications using polymers of both natural and synthetic origin(*346, 360*). In particular, biodegradable polyesters including PLA, PGA, and their copolymer (PLAGA) based scaffolds and orthopedic fixation devices in the form of screws and plates have been widely researched(*361*). Reproducible mechanical and degradation properties obtained by the precise control over molecular weight and crystallinity during polyester synthesis makes them attractive for scaffolding applications(*353, 362, 363*). However, acidic degradation products may cause inflammation depending on the anatomical compartment and their clearance from those locations(*364*). A comprehensive 9-year clinical study reported several inflammatory foreign body reactions and severe osteoarthritis in the joints near α-hydroxyester implants(*365*). To achieve mechanical and degradation properties ideal for implant performance, high molecular weight and crystalline polymers were used(*362*) with degradation varying from 2–6 years based on the molecular weight and crystallinity(*362*). However, a six-year evaluation of ankle fractures stabilized with PLA screws showed the absence of osseous replacement(*366*). Faster degrading implants show delayed tissue replacement with evidence of an osteolytic lesion during the final stages of degradation. Polyester blends with other class of polymers and ceramics have been reported to neutralize acidic degradation products and support tissue healing(*344, 367, 368*). Scaffolds derived from polymers of natural origin, namely polysaccharides and proteins, are known to be bioactive and highly biocompatible(*369*). Further these scaffolds support cell

attachment, proliferation and differentiation in vitro and during *in vivo* implantation(*370*).

In our earlier publications we have demonstrated the benefits of sintered microsphere scaffold platform in terms of controlling mechanical and pore properties as well as cell and tissue infiltration using both in vitro and in vivo experiments(*64, 363*). Sintered microsphere scaffolds are designed as a negative template of trabecular bone. For instance, trabecular bone is 70% porous with 30% material content while sintered microsphere scaffolds present about 30% porosity with 70% material content(*371*). We have also demonstrated that scaffolds fabricated using microspheres in the size range of 600–710 μm present optimal pore volume and mechanical strength to support bone repair and promote tissue ingrowth(*353*). In our previous study we have reported the feasibility of fabricating mechanically strong sintered microsphere scaffolds using cellulose derivatives and evaluated their ability to support HOB growth and mineralized matrix production(*352*). Collagen is the most abundant protein within the ECM.

The most abundant type-I collagen readily forms fibrils in a self-assembly process. Hence collagen has been popularly used to coat non-biological surfaces to simulate native ECM fibrous structures. Numerous pre-clinical and human clinical studies have utilized ECM scaffolds of both allogeneic and xenogeneic origin for the repair and regeneration of different tissue types with a huge success. These scaffolds promote angiogenesis, recruitment of circulating progenitor cells and complete scaffold degradation coupled with damaged tissue remodeling. This study evaluates micro-nano structured biomimetic scaffolds with correct combination of mechanical properties and ECM mimicry obtained by surface functionalization of cellulose based sintered microsphere scaffolds with collagen nanofiber for BTE applications.

Sintered microsphere scaffold platforms have been shown to offer several advantages over conventional salt leaching andelectrospun nanofiber scaffolds scaffolds for load bearing bone

healing applications(*295, 371*). This technique creates 100% interconnected porous structures with a great control over mechanical and pore properties(*363*). Scaffold mechanical properties greatly depend on the number of bonds and extent of bonding between adjacent microspheres(*295*). For instance, use of larger microspheres creates larger pores with lesser number of bonds with adjacent microspheres in the scaffold and hence results in reduced mechanical properties. Two cellulose derivatives, namely cellulose acetate and ethyl cellulose, were used to fabricate microspheres using an oil-in-water-emulsion-solvent evaporation method(*352*).

In general cellulose microspheres had a rough morphology as opposed to control PLAGA microspheres as evidenced by SEM images. Scaffold mechanical and pore properties are inversely proportional and therefore a balance between these two important parameters needs to be optimized for BTE application(*371*). Hence, we chose microspheres in the diameter range of 300–425, 600–710 and 710–800 μm for fabricating 3D porous structures via a solvent/non solvent sintering technique and characterized their mechanical properties(*295*). This study concluded that scaffolds fabricated from 600–710 μm sized microspheres resulted in optimal mechanical and pore properties as well as osteoblast response(*352*). In this study we wanted to optimize the combination of solvent/non-solvent composition and sintering conditions to fabricate scaffolds using 600– 710 μm sized microspheres of both CA and EC. For these polymeric systems acetone was used as a solvent and cyclohexane as a non-solvent. Solvent/non solvent assisted polymeric microsphere sintering based on Flory-Huggins solution theory is published elsewhere(*295*). According to this theory a greater affinity between the solvent and polymer allows the solvent to dissolve progressively longer chains causing the surface of the microspheres to swell and intertwine with each other(*295*). Hence at an optimal solvent/non-

solvent composition microsphere surfaces turn sticky, bond with adjacent microspheres and harden as the solvent evaporates(*295*). Very few attempts have been made to create natural polymer based sintered microsphere scaffolds for BTE applications. One of these studies combined chitosan with PLAGA and produced the heat sintered microsphere scaffolds and evaluated its cellar response *in vitro(372)* and the response when implaned into the body(*373*). These scaffolds showed superior osteoblast phenotype expression as compared to PLAGA control scaffolds but clearly failed to have significant effect *in vivo* bone healing(*373*). Such an oberved effect may be due to crosslinking of chitosan to produce Schiff base at elevated temperature during sintering(*161, 349*). Often crossliked natural polymers tend to loose their bioactivity due to utilization of available functional groups to produce crosslinked bonds(*161*). In general hydrogels, sponges or fiber matrices created using natural polymers were reported to be bioactive, but clearly lacked mechanical competence(*346*). As such cellulose and chosen cellulose derivatives are practically isoluble in water in spite of being hydrophillic, which makes them attractive for creating microspheres and their scaffolds without crosslinking(*253*).

Type I collagen is the major organic ECM component of bone offering bioactivity and strength(*369*). On the other hand, the role of topographic features including pores, fibers, ridges, grooves and their combinations in the nanometer scale have been shown to influence cell function and consequent regenerative capacity(*374*). Therefore, presentation of this bioactive collagen in nanofibrillar form is intended to endow the greatest biomimetic properties possible to the scaffold(*375*). Collagen nanofiber functionalization was carried out to improve the bioactivity(*297, 355*) of the 3D porous scaffolds fabricated as above.. The collagen nanofibers presented a uniform coating of the cellulose (CA and EC) microspheres (**Figures 2.2**, and **2.3**). Functionalizing scaffolds of different materials with collagen nanofibers may present different

morphologies and material properties. For instance, water contact angles for CA, EC and PLAGA are roughly 55, 35 and 80°, which makes cellulose scaffolds relatively hydrophilic than the control PLAGA(*375-377*). This lead to uniform collagen nanofiber functionalization around the microsphere surfaces without compromising the pores (**Figures 2.2**, **2.3**). Such a difference in hydrophilicity of the scaffold material may reflect in different levels of cell adhesion, proliferation and differentiation in spite of both the test and control scaffolds being coated with collagen nanofibers compromising the pores(*378, 379*). In our earlier communication we have reported micronano structured scaffolds using two synthetic polymers on the sintered microsphere scaffold platform(*297*). The PLLA nanofibers were created in the open pores of the poly phosphazene microsphere scaffold using thermally induced phase separation technique(*297*). These scaffolds were successful in promoting the osteoblast phenotype development but compromised scaffold pore properties to some extent. The hydrophilic nature of polysaccharide microspheres promote uniform deposition of collagen nanofiber adhesion on the microsphere surface without affecting the pore properties of the scaffold, a factor that is critical for tissue ingrowth while increasing the surface area for cell adhesion and biomimetics at the same time(*297*). In a similar approach polysaccharide microfibers functionalized with collagennanofibers acted as an ECM equivalent and promoted osteogenesis and angiogenesis in vitro(*380*) . Several studies reported the use of collagen in the form of hydrogel to deliver cells and tissue void filler where they clearly lacked the mechanical properties(*355*). Micro-nano structured scaffolds effectively combine the benefits two natural polymers without compromising pore and mechanical properties. Sustainment of the functionalized collagen nanofibers in culture as well as *in vivo* implantation can predict the scaffold bioactivity and performance. It is apparent from the images that collagen nanofibers not only remained stable

but increased passive mineralization with time(*335*). This form of biomineralization is a prerequisite for proper osteoinduction *in vivo* by a biomaterial(*381*), and points to the possible bioactivity of the material towards directing osteogenesis *in vivo(335).*

Mechanical properties of degradable polymers significantly vary under physiological conditions as opposed to dry samples(*382*). Hence we observed that the mechanical properties of the cellulose based scaffolds halved. These values were superior to several polysaccharidebased tissue-engineering scaffolds and PLAGA-based heat sintered microsphere scaffolds of similar pore properties earlier reported in literature(*353, 363*). These polysaccharide scaffolds showed compressive mechanical properties are comparable to those in the mid range of human trabecular bone and ideally suited for bone tissue engineering applications(*359*). This mechanical property is

highly desirable to serve the functional role of replacing lost bone tissue and the biological role of directing progenitor cell differentiation into osteoblastic lineage(*383*). Nanofiber functionalized scaffold porosity was found to be with an average pore diameter 185.4°+/_8.6 μm. Nanofiber functionalization neither compromised the mechanical property nor the porosity of the microsphere scaffolds. These micro-nano structures made of natural polymers may significantly improve the scaffold performance both as a supporting material as well as a bioactive platform for bone regeneration(*371*).

Osteoconductivity, the ability of a material to support the survival of osteoblasts, is an important basic characteristic of a scaffold in bone tissue engineering. **Figure 2.5** shows osteoblast survival measured up to 28 days on micro-nano structured scaffolds, control PLAGA scaffolds and TCPS. At all time points TCPS showed significantly higher cell number based on metabolic activity compared to test scaffolds and control PLAGA in basal media. However, cell numbers

on test and PLAGA control scaffolds were comparable. Such observed differences in cell metabolic activity may be due to the differences in number of cells that initially adhered to the scaffold and the difference in scaffold environment (**2.2D and 2.3D**). For instance, a fraction of the seeded cells may attach to the 3D porous scaffold while the rest will attach to the TCPS container. Higher metabolic activity on 2D TCPS as compared to 3D scaffold environment may reflect the inverse relationship between cellular proliferation and phenotypic differentiation. HOB proliferation in osteogenic media showed significantly higher DNA content on the micro-nano structured scaffolds than TCPS (**Figure 2.6**). Higher DNA content observed on the micro nano structured scaffolds presumably due to increased surface area and bioactivity provided by collagen nanofiber. Type-I collagen is known to enhance osteoblast viability and proliferation. Hence collagen coated implants supported the osteoblast spreading through rapid formation of focal adhesions and their associated stress fibers(*347*). Often 2D surfaces such as TCPS could induce greater number of focal adhesions but clearly fails to mimic the desired 3D environment. Collagen functionalized scaffolds present a 3D environment and brings about a desirable cellular response(*384*). In general higher DNA content is an indication of higher levels of mitotic (proliferative) cellular activity. Higher DNA content was observed on the TCPS as compared to test scaffolds (CA, and EC). This may represent a scenario where cells are at different stages of maturity on scaffolds than on TCPS. For instance, as osteoblasts progress towards mature osteocyte lineage, they are seen to be in the interphase state of cell cycle(*385-387*). Hence DNA content may not be a true indicator of cell division during an interphase stage wherein DNA content is likely to be more than cell number. Such an observation was made on the scaffolds using MTS assay (metabolic activity) and pico green DNA assay in the current study. In this

situation, it may translate into a greater level of cellular activity towards the differentiation program than cell division on test scaffolds.

Osteogenic differentiation is characterized by the robust ALP expression at early stages while mineralization occurs at later stages(*388, 389*). It is clear from the literature that a robust ALP expression inevitably leads to mineralization of the regenerated tissue(*388*). Osteoblasts cultured on

micro-nano structured scaffolds resulted in the higher levels of ALP expression as compared to TCPS controls (**Figure 2.7**). Expression of ALP on polysaccharide micro-nano structures was either higher or comparable to PLAGA micro-nano structures. Scaffold mineralization also followed a similar ALP expression trend where significantly higher amounts of calcium were deposited on the micronano structured scaffolds as compared to TCPS control (**Figure 2.8**). In general calcium deposition on polysaccharide structures was either higher or comparable to PLAGA micro-nano structures. Similar observations were also made on the polymeric scaffolds coated with cell matrix derived proteins where these scaffolds lead to higher levels of ALP expression as well as calcium deposition *in vitro*. The two cellulose derivatives EC and CA by virtue of their structure present different physical, mechanical and chemical properties. For instance, osteoblasts seeded on EC scaffolds start showing very early expression of phenotypic markers (ALP and Calcium deposition) while CA scaffolds make up towards the later time points (**Figures. 2.7** and **2.8**). Such an observed phenomenon may be due to the differences in relative hydrophilicity of the two materials. It has been reported that hydrophilic functionalities such as hydroxyl and methyl groups (as seen in EC) favor osteoinduction(*37*) compared to the more neutral acetate groups, which translates into early osteoblast maturation on EC scaffolds in

contrast to CA scaffolds. Often in addition to material chemistry and surface topography, mechanical properties of the scaffolds contribute towards cell differentiation(*390*).

2.5 Conclusions

In this work we report fabrication and characterization of cellulose and collagen based micro-nano structured scaffolds for BTE applications. This natural polymer based scaffolds show compressive mechanical properties in the mid range of human trabecular bone and may be ideally suited for bone tissue engineering applications. Collagen nanofiber functionalization did not compromise mechanical and pore properties of the microsphere scaffolds. Better human osteoblast adhesion, proliferation, alkaline phosphatase expression and mineralized matrix synthesis on these scaffolds as compared to that on control tissue culture plastic and PLAGA scaffolds confirm the potential for use in bone tissue engineering.

2.6 SPECIFIC AIMS

Tissue engineering seeks to design functional substitutes to achieve regeneration of lost tissue. Biodegradable three-dimensional (3D) porous structures called scaffolds are an important component of engineered tissue**.** Scaffolds derived from polymers of natural origin, like polysaccharides and proteins have improved biocompatibility over synthetic scaffolds due to their biochemical similarity to the native ECM. However, due to limitations of solubility and processing, polysaccharide and protein scaffolds have been fabricated as porous sponges or fiber matrices that do not have mechanical properties essential for bone tissue-engineering (BTE) applications. Polysaccharide, cellulose that forms the primary structural component of plant cell walls is analogous to the structural protein, collagen in the ECM of bone. Extensive hydrogen bonding between hydroxyl functionalities gives cellulose strength that makes it suitable for load bearing applications. This bonding also makes the polymer difficult to process due to its limited solubility in common solvents and instability at higher temperature. This limitation can be overcome by the use of derivatives of cellulose for scaffold fabrication. Previously we have reported fabrication of mechanically strong cellulose acetate (CA) and their collagen nanofiber functionalized scaffolds for BTE applications. These scaffolds have shown to have osteocoductive (support growth of osteoblast) abilities. *The present project aims to characterize the response of seeded mesenchymal stem cells (MSCs) on these scaffolds and to examine the regenerative potential of polysaccharide and collagen based micro- nano structured scaffolds.* We **hypothesize** that polysaccharide chemistry and collagen nanofibers offer bioactivity to **induce the osteogenic differentiation of (MSCs *in vitro,* would be biocompatible and mediate effective bone regeneration *in vivo*.** This project will be conducted by performing the following three specific aims:

2.6.1 Specific Aim 1: To characterize and contrast the unmodified and collagen functionalized CA scaffolds for their material properties

The CA and CA-collagen scaffolds will be contrasted with PLGA and PLGA-collagen scaffolds for the efficiency of collagen nanofiber functionalization. Further, the change in material crystallinity and surface morphology will be determined, in order to understand the difference in physical properties of the test and control scaffolds after being functionalized with collagen nanofibers. The hydration property of all the materials subjected to different treatments will be studied.

2.6.2 Specific Aim2: To test the performance of CA-collagen, micro-nano structured scaffolds *in vitro* using bone marrow derived MSCs.

The CA and CA-collagen scaffolds will be tested for their ability to support adhesion, proliferation and differentiation of MSCs in the presence of basal and osteogenic media *in vitro* and contrasted with PLGA and PLGA-collagen scaffolds. We will assess cell viability, proliferation, expression of osteogenic genes, proteins, ALP activity (early osteogenic differentiation marker) and mineralization (later stage marker).

2.6.3 Specific Aim3: To test the performance of CA-collagen, micro-nano structured scaffolds in vivo

2.6.3.1 Specific Aim3a: To test the biocompatibility of CA-collagen, micro-nano structured scaffolds in vivo in a subcutaneous implantation.

The scaffolds would be tested for their biocompatibility *in vivo.* The scaffolds would be implanted subcutaneously in rats. Results will be compared with control scaffolds. At 4, 8, and 12-week time points, animals will be sacrificed and implant will be evaluated for cytocompatibility, and cellularization by histological examination.

2.6.3.2 Specific Aim3b: To test the performance of CA-collagen, micro-nano structured scaffolds in vivo in a bone defect in mouse calvarium.

The CA, CA-collagen and PLGA scaffolds will be tested for their functional performance *in vivo*. At 8-week time point, the animals will be sacrificed and new bone formation will be evaluated by X-ray radiography and histological analyses.

3 Chapter 3

Characterize of the Material Properties of Unmodified and Collagen Functionalized CA Scaffolds

3.1 Introduction

Several scaffold fabrication techniques and materials are used in constructing the scaffolds for BTE. It is crucial to achieve a mechanically strong, porous, three dimensional scaffold that allows cells of the organ to infiltrate into the materials as well as induce the stem cells to differentiate and heal a defect, once the material is implanted. A sintered microsphere microsphere scaffold serves the needs of mechanical strength and material transfer (33(*391*)-40%(*392*) porosity is usually observed), in a 3D environment. However, most bodily ECM components are presented as nanofibers(*393*). A number of studies have shown the biological efficacy of nanofiber matrices in inducing favorable tissue healing response(*289, 310*). Hence taking this factor into consideration, we formulated a two-component system made of a base 3D porous sintered CA scaffold further functionalized with collagen nanofibers(*391*). The principle of protein self-assembly was employed to achieve the formation of collagen nanofibers on these 3D porous structures of CA(*355*). Synthetic polymer PLGA was used as the control material due to its widespread application in BTE(*394-396*). PLGA has also been approved for several applications like drug delivery and suture formulations(*397*). The PLGA materials were formulated into 3D porous sintered microspheres with similar dimensions as CA and functionalized with collagen nanofibers similarly. It has been shown in literature that protein assembly on hydrophilic and polar surfaces may be more biomimetic than on hydrophobic, nonpolar surfaces(*398*). We hypothesized that the CA material due to its hydrophilic and polar nature may lead to more effective collagen nanofiber presentation, with nanofibers decorating

the microspheres(*391*) rather than significantly occupying the pores in contrast to PLGA which is known to be a much more hydrophobic material. In this study CA and PLGA microspheres were subjected to incubation in the functionalizing buffer (without collagen) and the functionalizing solution (with collagen). The changes in the scaffold's wettability, chemical nature, and crystallinity with treatment were examined. Additionally quantification of total amount of collagen functionalizing the materials and the presentation of these fibers were examined. As the material characteristics of a scaffold dictate its biological performance, it is important to examine the change in the phiso- chemical nature of a matrix when subjecting it to a modification such as collagen nanofiber functionalization of scaffolds by self-assembly.

3.2 Materials and Methods

3.2.1 Materials

Cellulose acetate (Mw: 30K) (CA), and Polyvinyl Alcohol (30,000-70,000) (PVA) were procured from Sigma -Aldrich (St. Louis, MO, USA). Poly (lactic-co-glycolic acid) 85:15 (PLGA) was purchased from lakeshore biomaterials (Birmingham, USA). Acetone, Dichloromethane, Cyclohaxane, Paraformaldehyde and Gluteraldehyde were purchased from Fisher Scientific (Fair Lawn, NJ, USA).

3.2.2 Preparation of microspheres

Oil in water solvent- evaporation, followed by sintering of formed microspheres using a solvent/non-solvent mixture was used for producing microsphere of i) Cellulose acetate (CA), ii) poly (lactic-co-glycolic acid) 85:15 (PLGA). In brief, 13 (w/v) % of CA polymer was dissolved in a solvent mixture containing methylene chloride and acetone at a ratio of 9:1 to produce microspheres. A 20 (w/v) % solution in methylene chloride was used in the case of PLGA

polymer to produce the microspheres. The polymer solutions were then poured in a thin stream into an aqueous media containing 1.25(w/v) % PVA as a surfactant, with constant stirring at 250rpm to form an oil-in-water emulsion. These suspensions were stirred overnight to evaporate the solvent to obtain hardened microspheres. Isolated microspheres were washed repeatedly with deionized (DI) water, dried, and sieved into different microsphere sizes. Microspheres in the size range of 600-710 and 710-800μm were mixed at a weight ratio of 1:1 and sintered into micro porous scaffolds using either solvent-non-solvent or heat sintering based on the polymer(*352, 391*).

3.2.3 Preparation of micro-porous sintered microsphere scaffolds

Teflon molds of different dimensions were filled with CA microspheres to which a 200μL volume of an optimized solvent/non-solvent composition, acetone: cyclohexane in the ratio of 3:1 (v/v), was added to cover the microspheres. Solvent was allowed to evaporate at room temperature to obtain sintered microsphere scaffolds. Cylindrical scaffolds measuring 5mm diameter X 10mm height were used for the characterization of hydration properties. The control PLGA micro porous scaffolds with identical micro-particle sizes were produced by heat sintering at 95^{o}C for 45 minutes using Teflon molds(*352*).

3.2.4 Preparation of micro-nano structured scaffolds

A modified biomimetic approach was used to functionalize micro porous scaffolds with type I collagen. In brief, both control and test scaffolds were incubated in a 0.1 (w/v) % collagen type I solution with a pH adjusted to 4.2 at 37°C for 7 days to promote molecular collagen self-assembly. The dried scaffolds were treated with UV light for 30 min each side to achieve collagen nanofiber stability and washed repeatedly with DI water to remove buffer salts. Microspheres in the size range of 300-425μm diameters were functionalized with collagen and

used for material characterizations presented in this study. The effect of coating buffer pH was studied by incubating scaffolds in the buffer alone without collagen (*391*).

3.2.5 Quantification of Scaffold collagen Content

Amount of collagen present on each scaffold was estimated with a calorimetry using a bicinchoninic acid (BCA) Protein Assay Reagent kit (Pierce). Proteins form a purple colored chelation complex with BCA via reducing the cupric ions to cuprous ions. The purple color of this complex is directly proportional to the protein concentration and the absorbance was read at 562 nm using a BioTek plate reader. In brief, collagen coated composite scaffolds were transferred to a new 48 well plate and incubated with 500μL of aqueous 1% acetic acid overnight with agitation followed by mixing with the aid of a pipette to extract all collagen from the scaffold. Similarly collagen remaining on the TCPS surface during the coating experiment was also extracted and quantified. A volume of 25μL of the collagen extract was mixed with 200μL of BCA reagent followed by 30 min incubation at 37^{o}C and analyzed at 562 nm using a plate reader. A sample size of n=4 was used for all estimations. The absorbance of six known collagen concentrations 0, 62.5, 125, 250, 500, and 1000 μg/mL were used to construct a standard curve to convert absorbance readings to collagen concentrations. The content of collagen on the scaffolds and the plates used for incubation were measured and the percentage of collagen on the scaffold against that on the plate was calculated to obtain the collagen coating efficiency on each scaffold.

3.2.6 Morphology of collagen by two- photon microscopy

Micro-nano structured scaffolds namely PLGAc and CAc were imaged at an excitation wavelength of 890nm and the collagen second harmonic generation (SHG) signal along with autofluorescent signal from the scaffold material were acquired with bandpass filters of 435–485nm (SHG), 500–550nm (scaffold autofluorescence), and 570–620nm (scaffold autofluorescence). The SHG signal is generated from the triple helical structure of collagen.

3.2.7 Characterization internal structure of scaffolds by SEM

Scanning electron microscopy (SEM) was used to characterize scaffold morphology and evaluate collagen fiber diameter and distribution. Scaffolds were sputter coated with Au/Pd using a Polaron E5100 sputtering system (Quorum Technologies, East Sussex, UK) to achieve an eighteen nanometer thick coating before viewing under SEM. The samples were viewed using FEI Nova NanoSEM 450 scanning electron microscope (FEI, Hillsboro, OR, USA) operated at an accelerating voltage of 2kV at various magnifications. Collagen fibers at different locations were selected randomly on the functionalized samples and these images were used for measuring the fiber diameter using FIJI, NIH software and averaged (an average of 100 fibers).

3.2.8 Scaffold water uptake by gravimetric analysis

Scaffolds of 10mm X 5mm size were used for analysis of weight and volume changes on hydration over 72hours. Scaffolds dry weight and dimensions were noted prior to testing for hydration studies (0h). All groups namely CA and PLGA (treated with DI water), CA- buffer/ PLGA-buffer (treated with buffer without collagen) and CAc/PLGAc (treated with collagen solution) were individually placed in microcentrifuge tubes with 1mL of PBS (pH 7.4) (n=6/group) and incubated at 37°C. At the end of 24h, 48h and 72h, the scaffolds were isolated and the changes in weight were noted with a Mettler Toledo® (XP56C-Mass Comparator)

balance with an accuracy of 0.01mg and dimensional changes were measured with a digital calipers (at six different points on the scaffold). The volume changes in the individual cylindrical scaffolds were calculated using the relation=π X (diameter/2)^2 X height.

3.2.9 Microsphere surface chemistry by ATR-FTIR analysis

Fourier Transform Infrared Spectroscope (FTIR), Nicolet Magna 560, using ZnSe and Ge crystal (Nicolet Instrument Corporation, Madison, WI, USA) was used to measure the Attenuated Total Reflection (ATR)-infrared red (IR) spectra of the CA, CA-buffer, CAc and PLGA, PLGA-buffer, PLGAc treated microsphere surfaces. The Nicolet OMNIC^R software was used to blank the runs every time before samples were placed on the pedestal for measurement of their spectra. Sample scans were run at 320 scans per specimen to extract the spectra in the range 400-4000cm^{-1}.

3.2.10 Microsphere surface crystallinity by XRD analysis

A Bruker D2 Phaser powder diffractometer (Bruker axs, Inc., Madison, WI, USA), was used to measure the wide angle x-ray diffraction of CA, CA-buffer, CAc and PLGA, PLGA-buffer, PLGAc microspheres. A 2θ between 10-60° with an increment of 0.02° was captured, for all the polymers.

3.2.11 Polymer molecular weight by GPC analysis

A Waters GPC system with Jordi Gel fluorinated DVB columns (1-100K, 2-10K & 1-500Å) was used for running the PLGA, PLGA-buffer and PLGAc microparticles. Tetrahydrofuran (THF) was used as a mobile phase along with Varian 380-LC Evaporative Light Scattering Detector (ELSD) detector. In brief, 0.1 (w/w) % polymer solutions in THF were filtered through 0.2µm nylon filter prior to testing. A flow rate of 1.25mL/min with an injection volume of 100µl was

used for the analysis. The molecular weight distributions were compared with polystyrene standards with molecular weight ranges 450- 200,000 Da. For CA based samples, a Waters GPC system with two mixed bed Jordi Gel DVB columns were used with dimethylacetamide (DMAC) as the mobile phase. For this analysis 0.2 (w/w) % CA in DMAC was used with at an injection volume 200µL and a flow rate of 1.25mL/min. Samples were analyzed using a Waters 2414 refractive index detector (RI) detector. The molecular weight distributions were compared with poly (methyl methacrylate) (PMMA) standards with molecular weight ranges 2000- 1100,000Da.

3.2.12 Statistical analysis

All data are reported as the mean ± standard deviation (SD) of results from at least three independent runs. In case of experiments with two groups a student t- test was performed. In the case of experiments with multiple groups and multiple time points a 2- way- ANOVA with Bonferroni posttest was performed. In the case of experiments that focused on one time point and several groups, a one- way- ANOVA with Tukey posttest was performed. 95% Confidence interval was employed to arrive at the p values. The denotation of significances given by p values are- *$p<0.001$ (extremely significant), $^{\#}p<0.01$ (very significant), $^{@}p<0.05$ (significant). Analyses were performed using GraphPad Prism Software (GraphPad Software, San Diego, CA).

3.3 Results

3.3.1 Characterization of collagen nanofibers

Scanning electron microscopic (SEM) images showed a smoother microsphere surface for PLGA while CA scaffolds presented a rougher surface with many features (**Figure 3.1a**). Similar quantity of collagen content was observed on both PLGA and CA scaffolds as determined by protein assay (**Figure 3.1b**). However, major differences were observed in terms of collagen assembly, fibril diameter and collagen distribution on PLGA and CA micro-nano structures. Collagen fibers on PLGA showed a wider range of fiber diameter distribution with a mean fiber diameter of 150nm, while the collagen fibers on CA showed a narrow range of distribution with a mean fiber diameter of 80nm (**Figure 3.1c**).). At 50,000X magnification, the collagen fibers of CAc presented a D-band like pattern of triple helical collagen. Such banding patterns were very sparse in the case of the collagen fibers on PLGA (**Figure 1d**). On subjecting the PLGAc and the CAc scaffolds to two-photon excitation, the second harmonic signal derived from the collagen fibers on CAc was stronger than that of PLGAc (**Figure 1e**). In addition, the CAc group typically had collagen fibers arranged in co-operative sheets while the collagen fibers in the PLGAc group were more dispersed.

3.3.2 Analysis of hydration property

The volumetric changes on hydration between PLGA and CA groups also showed a significant volume gain by all the CA groups in contrast to PLGA (**Figure 2d**). The volume changes on the PLGA groups occurred in the first 24h of hydration (**Figure 2e**), are also in agreement with weight gain profiles (**Figure 2b**). Volumetric changes for both PLGA and CA based scaffolds were stabilized by 24 hours. However at 72 hours, only PLGAc and PLGA-buffer groups showed volumetric changes (**Figure 2e**), which remained unaltered for all CA groups (**Figure 2f**).

3.3.3 Characterization of Materials properties

To investigate the changes in material properties due to treatment with the collagen solution, the ATR-FTIR spectra of both PLGA and CA were probed after incubation in water (PLGA, CA), aqueous buffer without collagen (PLGA-buffer, CA-buffer) and with collagen (PLGAc, CAc). The characteristic alkyl groups (2800-2900cm^{-1}), C-O ester group (1050- 1450cm^{-1}) and C=O stretch (1750cm^{-1}) of PLGA remained unaffected. However, major differences in absorbance frequencies were noted around 1600cm^{-1} and 3300cm^{-1} following treatment with acidic collagen solution (Figure 3.3a). The XRD spectra of the PLGA groups treated with buffer and collagen showed a steeper peak at around a 2θ angle of 20°, in contrast to the non- treated PLGA (Figure 3.3b). In the case of CA groups, all treatments showed characteristic bands of ether (1040cm^{-1}), acetyl ester (1220cm^{-1}) and carbonyl (1740cm^{-1}) groups that were unaffected following acidic collagen solution treatment(*399*). However, the treatments lead to an additional band around 1600cm^{-1} (Figure 3.4a). Following treatment CA showed a steeper peak at around a 2θ angle of 20° in its XRD pattern (**Figure 3.4b**).

Scaffolds derived from PLGA showed significant decline in weight average molecular weight (Mw) and Z-average molecular weight (Mz) with no change in polydispersity index (PI) (**Figure 3.5 a, b, c, d**). On the other hand in the case of CA the buffer and the collagen treatments resulted in a decrease in number average molecular weight (Mn) that affected the PI ((**Figure 3.5 e, f, g, h**).

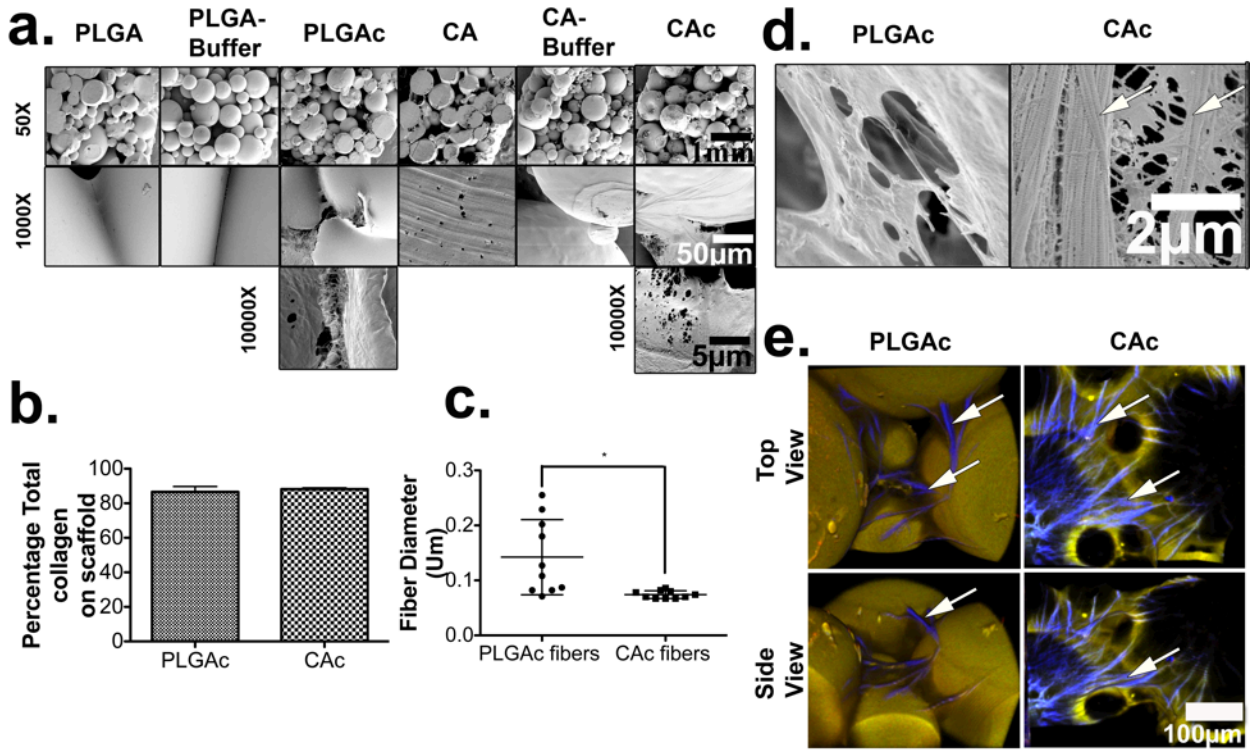

Figure 3.1 Characterization of collagen nanofibers

SEM images of a) PLGA, PLGA- buffer treated and PLGAc, CA, CA-buffer treated and CAc scaffold interiors. Scale bar on top = 1mm, middle =50µm, and bottom = 5µm b) Percentage of total collagen on scaffolds after coating (coating efficiency), n=4, Unpaired t-test done and no statistical significance was seen. c) Diameter of collagen fibers on PLGAc and CAc at magnifications of 50,000X, n=10, Unpaired t-test done and a *P<0.001 was obtained. d) SEM images of collagen nanofibers on PLGAc and CAc at 50,000X (D- band-like patterns indicated by arrows on CAc), scalebar = 2 µm and e) Second harmonic signals from collagen fibers on PLGAc and CAc at 10X (blue color indicated by arrows), scalebar = 100 µm.

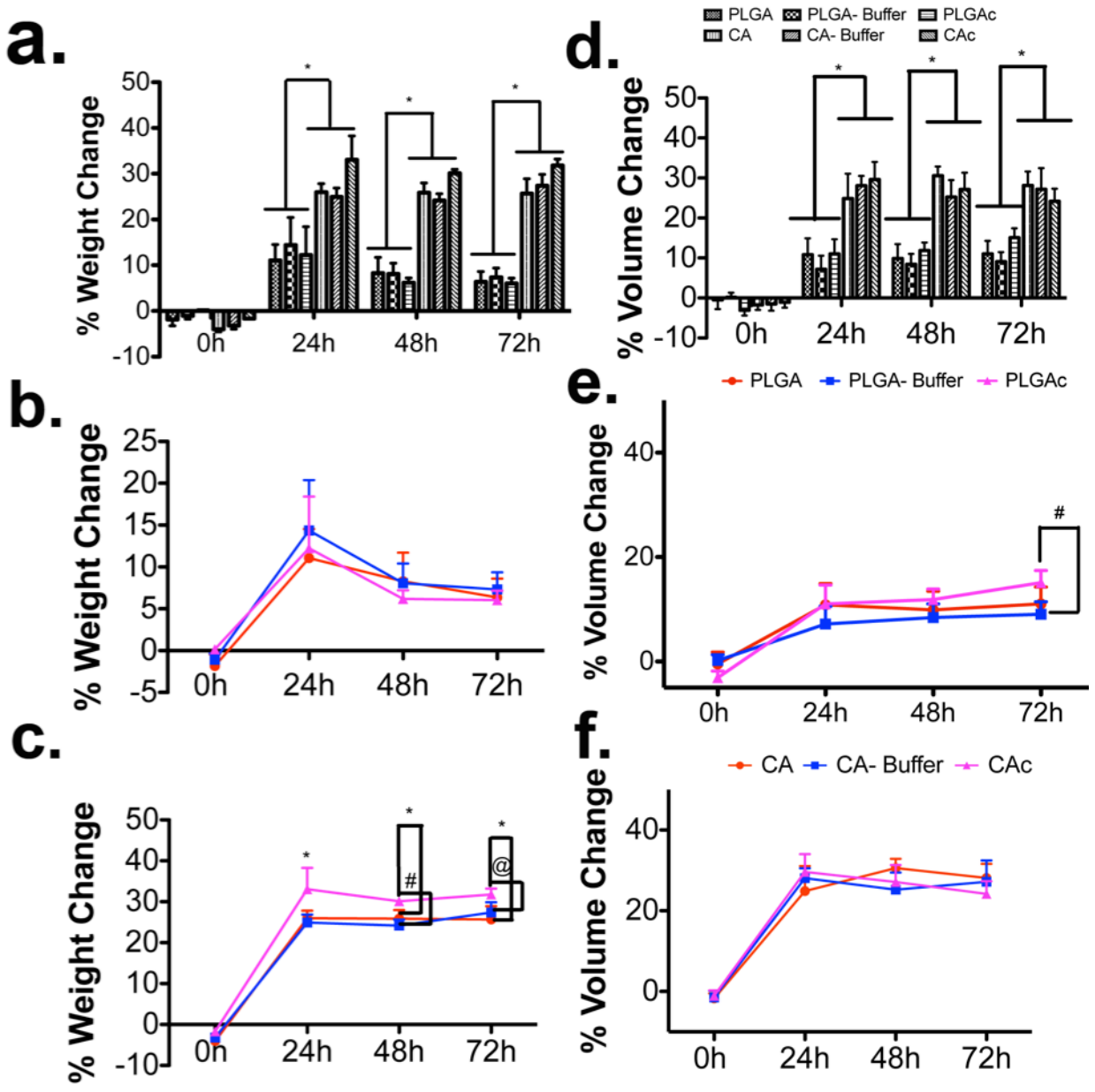

Figure 3.2 Hydration properies

Effect of hydration on the scaffold weight and volume changes over 72 hours of incubation in PBS at 37°C. Changes in scaffold weight a) PLGA and CA groups, b) PLGA, PLGA- Buffer treated and PLGAc, c) CA, CA- Buffer treated and CAc. Changes in scaffold volume d) PLGA and CA groups e) PLGA, PLGA- Buffer treated and PLGAc, f) CA, CA- Buffer treated and CAc. Two- way ANOVA with Bonferroni post- test, with 95% confidence intervals, $^{*}P<0.001$, $^{\#}P<0.01$, $^{@}P<0.05$.

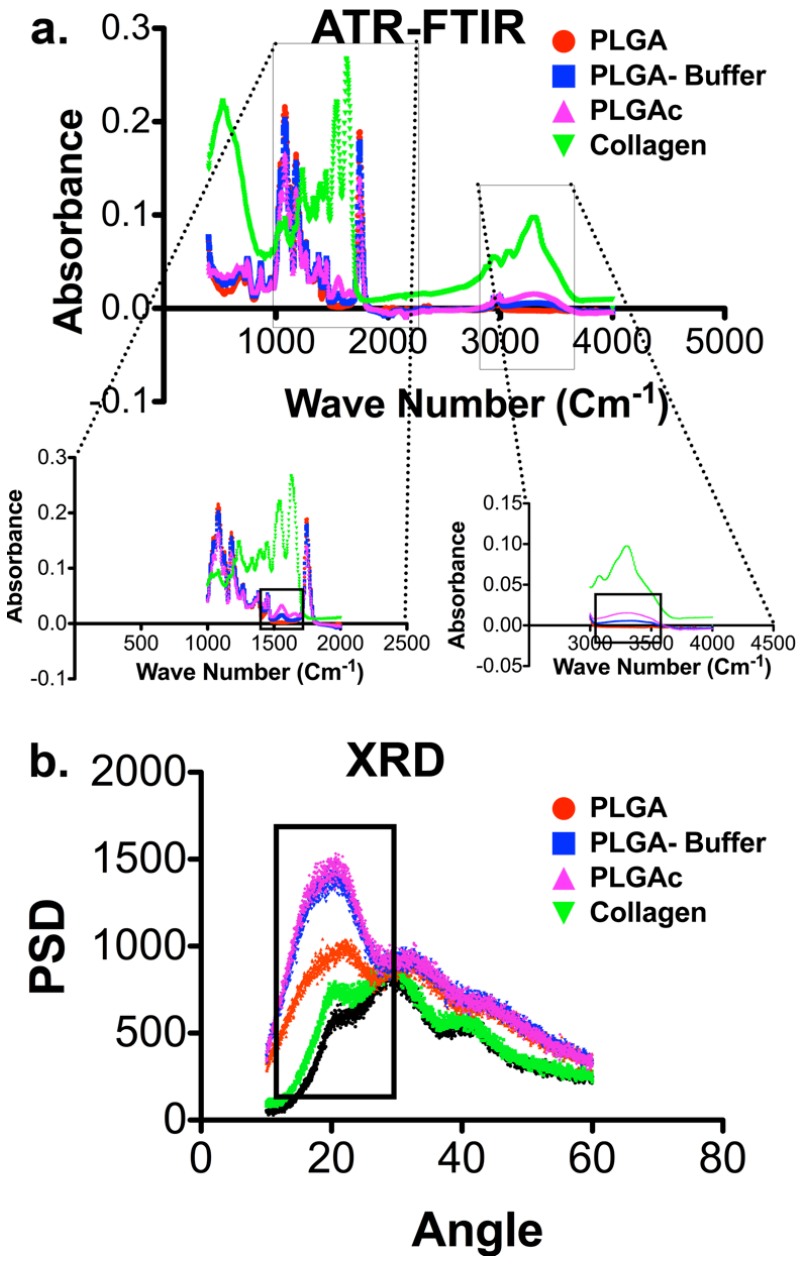

Figure 3.3 Changes in PLGA chemistry on collagen treatment

a) ATR- FTIR (from 400- 4000 cm-1) and b) XRD spectra (2θ= 10-60^{O}) of PLGA, PLGA-buffer treated and PLGAc (Red- PLGA, blue- PLGA buffer treated, pink- PLGAc, green-lyophilized collagen).

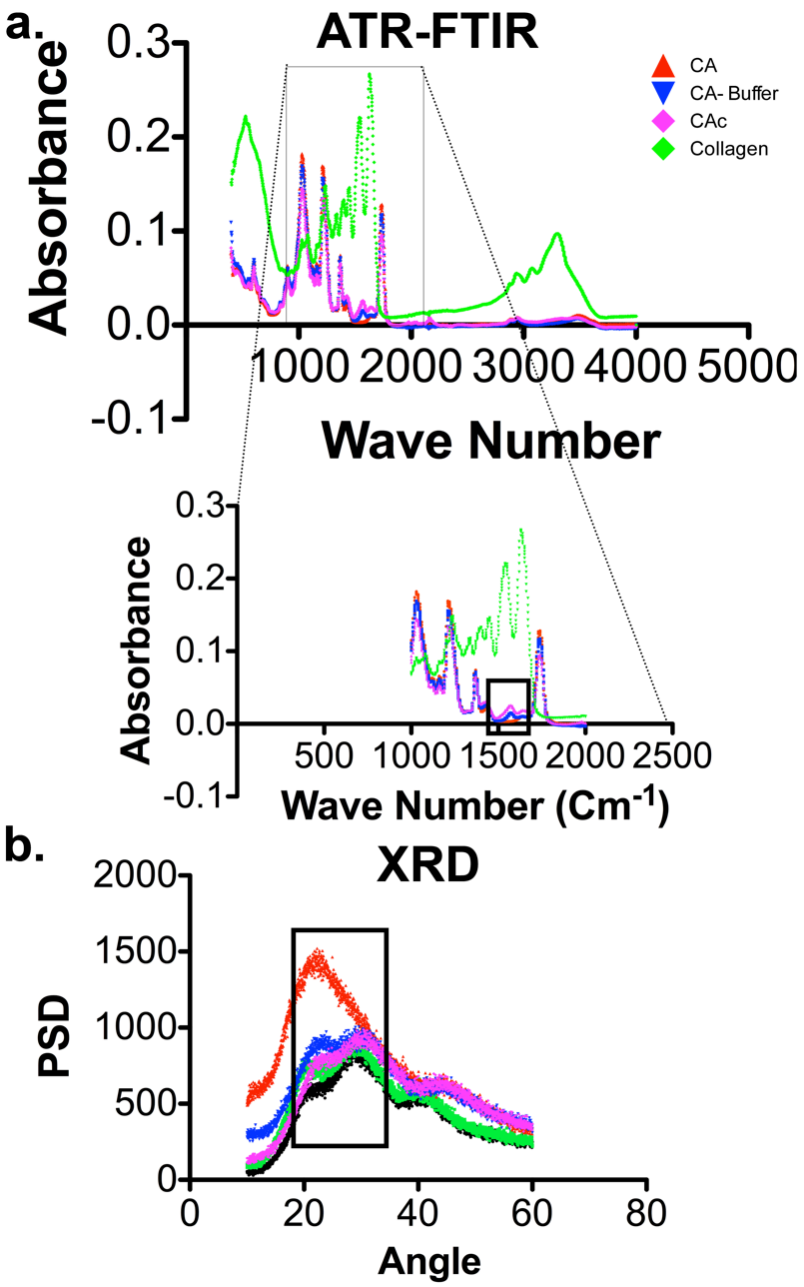

Figure 3.4 Changes in CA chemistry on collagen treatment

a) ATR- FTIR (from 400- 4000 cm^{-1}) and b) XRD spectra (2θ= 10-60^{O}) of CA,CA- buffer treated and CAc. (Red- CA, blue- CA buffer treated, pink- CAc, green- lyophilized collagen)

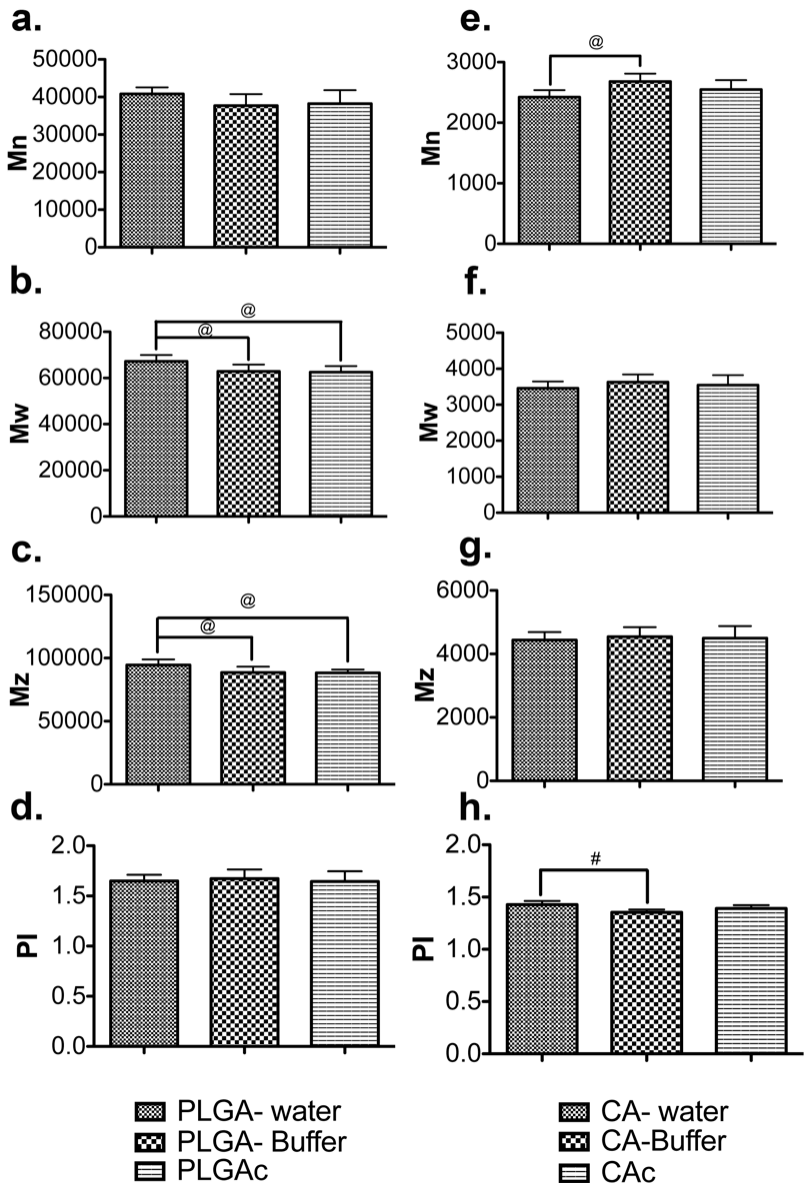

Figure 3.5 Molecular weight changes on collagen treatment

Molecular weights determined by Gel permeation chromatographic analysis of a), b), c), d) PLGA and e), f), g), h) CA polymers after treatments: a), e) Mn- Number average molecular weight, b), f) Mw- weight average molecular weight, c), g) Mz- z average molecular weight, d), h) PI- Polydispersity index= Mw/Mn). One – way ANOVA with Tukey post test, with 95% confidence intervals, $^{*}P<0.001$, $^{\#}P<0.01$, $^{@}P<0.05$.

3.4 Discussion

In our scaffold system, the 3D porous sintered CA and PLGA matrices are exposed to a mildly acidic buffer solution (pH 4.2) dissolving the collagen, for a prolonged period of time to allow the solution to evaporate and to allow the nanofibers to self assemble. The effect of this treatment on the material may be important as there could be certain physical and chemical changes happening to the parent polymer during the treatment.

A smoother microsphere surface was observed for PLGA while CA scaffolds presented a rougher surface with many features (**Figure 3.1a**). The surface topography of materials could play an important instructive role in directing cellular responses. For instance osteoblasts were seen to maintain their phenotype(*400*) and respond more towards signaling factors like BMP-2(*401*), and vitamin D3(*402, 403*) when cultured on microscale and nanoscale(*404*) rough surfaces. Hence the CA materials may be more osteoconductive in nature than the PLGA materials due to the rougher topography presented by them.

The total collagen content was not very different when the CA and the PLGA 3D porous sintered microsphere scaffolds were functionalized with collagen nanofibers (**Figure 3.1b**). However the morphology of the fibers was very different between the PLGAc and CAc groups (**Figure 3.1c, d, e)**. The D- banding patterns (**Figure 3.1d)** and the greater levels of second harmonic signal generated by the collagen on CAc than PLGAc (**Figure 3.1e)** may indicate a more native presentation of the functionalizing collagen nanofibers on the CA surface than on the PLGA surface. It has also been shown that collagen nanofiber in its native form is far more inductive towards bone formation than collagen that is denatured(*405, 406*). Hence we hypothesize that CAc matrices may be more osteoinductive than the PLGAc scaffolds.

The water uptake by all the CA groups was significantly higher than PLGA groups (**Figure 3.2.a, d**). All CA structures gained significant weight in the first 24 hours and achieved equilibrium weight by 72 hours. The CA-buffer and CAc groups showed progressive weight gain at all time points between 24-72h. The addition of collagen in CAc (**Figure 3.2c**) and the presence of additional carboxylic acid groups in CA-buffer samples (**Figure 3.4a**) increased exposure to acidic pH resulting in greater hydrophilicity and weight gain than CA structures.

Exposure of CA to highly acidic or alkaline environment may lead to deacetylation(*399*), by showing changes at ether ($1040cm^{-1}$), acetyl ester ($1220cm^{-1}$) and carbonyl ($1740cm^{-1}$) groups. In the case of CA groups, all treatments showed characteristic bands of ether ($1040cm^{-1}$), acetyl ester ($1220cm^{-1}$) and carbonyl ($1740cm^{-1}$) groups that were identical and thus these chemical groups were unaffected following acidic collagen solution treatment(*399*). However, treatment lead to an additional band around $1600cm^{-1}$ on CA microsphere surface due to the presence of carboxylic acid salts. Hence the mild acidic environment did not have a degradative effect on CA due to its more robust chemistry (**Figure 3.4a, b**).

However, PLGA-buffer groups appear to be more hydrophobic as the acidic pH treatment may lead to degradation on the surface (**Figure 3.3a**). The intensity of absorbance around $1600cm^{-1}$ increased due to the cleavage of ester bond resulting in carboxylic acid salts (O=C-ONa) of PLGA following treatment. Likewise the increase in absorbance around $3300cm^{-1}$ in PLGA was attributed to an increase in hydroxyl content from alcohol groups (**Figure 3.3a, b**), probably due to a mild degradative change on the surface of the polymer(*407, 408*). Lee *et al* also observed such changes with the degradation of PLGA when it was exposed to irradiation(*407*).

The wettability of surfaces also plays an important role in determining cellular responses like cell adhesion(*409*). Cells adhere to materials through adhesion mediating proteins that adsorb onto

biomaterial surface. While highly hydrophobic surfaces favor high level of protein adsorption, they also mediate more material- protein and protein-protein interactions, but minimal protein-cell interaction due to masking of the active protein domains responsible for cell adhesion(*410*). This is explained by the rigid conformation of proteins achieved on hydrophobic non- polar surfaces against a more flexible protein conformation achieved on hydrophilic non- polar surfaces(*398*), which may quantitatively adsorb less protein(*410*). On the other hand highly hydrophilic surfaces may not allow for protein adhesion on their surface at all and hence such surfaces too are not good for cell adhesion on materials(*411, 412*). Hence the hydration behavior of material would dictate protein adsorption and self- assembly on it.

The chemical functional groups on a material can influence cellular responses immensely. For instance Curran et al. cultured bone marrow derived mesenchymal stem cells (MSCs) on glass substrates modified to contain the functional groups: like -CH_3, -SH, –COOH, –OH, and –NH_2, under basal and octeogenic and chondrogenic conditions. They found that the -CH_3 functional groups helped maintain the multipotency of MSCs, while the –OH and –NH_2 groups were conducive for osteogenic differentiation, and the –COOH and –SH groups on the substrate supported chondrogenic differentiation. These differences were observed both under basal and stimulated conditions(*413*). Many other studies have used materials that varied only by the chemical functional groups on the biomaterial's surface and all of them have shown that the chemical functionalities on the material surface can have a profound influence on stem cell behavior(*37, 340*). These changes can be attributed to the resulting material surface energy and hydration characteristic that determine the conformation of adsorbed proteins and in turn cellular adhesion(*414*).

From these observations in literature that state the importance of chemical functionalities, hydrophilic characteristics and their relationship to the conformation of adsorbed proteins, we conclude that the hydrophilic characteristics of CA scaffolds presumably induced the adsorbed collagen nanofibers to be presented in a more native conformation than on PLGA. We hypothesize that these may translate into better cell adhesion and differentiation responses *in vitro* and *in vivo*.

3.5 Conclusions

We conclude that the process of collagen nanofiber functionalization on CA and PLGA scaffolds had very different outcomes. While the quantity of collagen present in both the scaffolds was similar the native structure of collagen nanofibers was apparent on CA scaffolds than on PLGA. On examining the water uptake behavior of these matrices, it was seen that the PLGA matrices did not have significant improvement in their hydrophilic nature, while the CA matrices showed greater water uptake on treatment with the collagen solution. The stable nature of CA against the more readily degradative nature of PLGA led to preserving the chemistry of CA, while inducing a mild degradation on the surface of PLGA microspheres that nullified the effect of collagen that usually renders the material more hydrophilic upon its incorporation.

4 Chapter 4

Characterization of Human Bone Marrow Derived Mesenchymal Stem Cell (hMSC) Response to CA-Collagen, Micro-Nano Structured Scaffolds *in vitro*

4.1 Introduction

In BTE the scaffold plays an important role. But in order to achieve complete bone healing, the delivery of cells and/ or growth factors(*397*) and/ or small molecules is necessary(*415*). While growth factors like BMP-2(*416*), VEGF(*417*), FGF-2(*418*) have been very effective in inducing tissue responses like bone formation, angiogenesis and homing and proliferation of stem/ progenitor cells, a number of constrains still exist in the delivery of these factors(*415*). For instance BMP-2 is very effective in inducing bone formation, but ectopic bone formation has also shown to occur at non-target sites that can lead to pathological outcomes(*419*). Yet another constraint in delivering proteins such as growth factors is the challenge of retaining their biological activity during the process of their targeted delivery. On the other hand small molecules that are easier to handle and pose less threat of denaturation or loss of function during processing, but induce many different cellular signaling pathways and targeting a specific therapeutic outcome without side effects is a challenge(*420*). However delivering the patient's autologous bone marrow derived stem cells is a simple and clinically relevant strategy to improve the outcomes of bone healing. It has been demonstrated that bone marrow derives mesenchymal stem cells (MSCs) are capable of differentiating in the osteochondral lineage. Additionally, the phisio- chemical nature of the biomaterial has dictated the differentiation of stem cells in the specific lineage. A detailed description of the mechanisms by which materials dictate protein adsorption and in turn cell adhesion is given in the **Discussion** section of **chapter 3**. Briefly, the various factors influencing the differentiation of MSCs(*421*) are the mechanical

property of the matrix(*422*), chemical functionalities(*37*) on the surface of the scaffold, the hydration properties(*410*) and the surface topography of the biomaterial(*379, 400*). Many studies have used these mechanical and phisio- chemical properties alone and in combination with inductive media to differentiate stem cells in the osteochondral lineage. In **Chapter 3**, the higher hydrophilicity of all the CA materials over PLGA was established. The collagen nanofibers on the CAc 3D- porous scaffolds presented a more native triple helical presentation than on PLGAc. We hypothesized that these differences in material charecteristics between the PLGA and CA (uncoated and collagen coated) scaffolds may positively influence MSC differentiation in the osteo-chondral lineage *in vitro*. Hence, here in this chapter high density cultures of MSCs were seeded onto PLGA, CA, PLGAc and CAc 3D- porous scaffolds and their viability, proliferateion, osteo-chondral gene expression and the osteoblastic protein presentation were tested. These studies are meant to establish the osteoinductive behavior of the materials towards stem cells.

4.2 Materials and Methods

4.2.1 Materials

Cellulose acetate (Mw: 30K) (CA), and Polyvinyl Alcohol (30,000-70,000) (PVA) were procured from Sigma -Aldrich (St. Louis, MO, USA). Poly (lactic-co-glycolic acid) 85:15 (PLGA) was purchased from lakeshore biomaterials (Birmingham, USA). Acetone, Dichloromethane, Cyclohaxane, Paraformaldehyde and Gluteraldehyde were purchased from Fisher Scientific (Fair Lawn, NJ, USA). BioRad Alkaline Phosphatase Substrate kit (Hercules, CA, USA) and Invitrogen Quant-iT PicoGreen dsDNA Assay kit (Eugene, Oregon, USA) were used in this study. Alizarin Red and Cetylpyridinium chloride was procured from Acros Organics

(New Jersey, USA). Cell culture media was DMEM (HG) purchased from Lonza (Walkersville, USA).

4.2.2 Preparation of microspheres

Oil in water solvent- evaporation, followed by sintering of formed microspheres using a solvent/non-solvent mixture was used for producing microsphere of i) Cellulose acetate (CA), ii) poly (lactic-co-glycolic acid) 85:15 (PLGA). In brief, 13 (w/v) % of CA polymer was dissolved in a solvent mixture containing methylene chloride and acetone at a ratio of 9:1 to produce microspheres. A 20 (w/v) % solution in methylene chloride was used in the case of PLGA polymer to produce the microspheres. The polymer solutions were then poured in a thin stream into an aqueous media containing 1.25(w/v) % PVA as a surfactant, with constant stirring at 250rpm to form an oil-in-water emulsion. These suspensions were stirred overnight to evaporate the solvent to obtain hardened microspheres. Isolated microspheres were washed repeatedly with deionized (DI) water, dried, and sieved into different microsphere sizes. Microspheres in the size range of 600-710 and 710-800μm were mixed at a weight ratio of 1:1 and sintered into micro porous scaffolds using either solvent-non-solvent or heat sintering based on the polymer(*352, 391*).

4.2.3 Preparation of micro-porous sintered microsphere scaffolds

Teflon molds of different dimensions were filled with CA microspheres to which a 200μL volume of an optimized solvent/non-solvent composition, acetone: cyclohexane in the ratio of 3:1 (v/v), was added to cover the microspheres. Solvent was allowed to evaporate at room temperature to obtain sintered microsphere scaffolds. Cylindrical scaffolds measuring 5mm diameter X 10mm height were used for the characterization of hydration properties while 8mm diameter X 2mm thick tablets were used for cell studies and animal experiments. The control

PLGA micro porous scaffolds with identical micro-particle sizes were produced by heat sintering at 95^{o}C for 45 minutes using Teflon molds(*352*).

4.2.4 Preparation of micro-nano structured scaffolds

A modified biomimetic approach was used to functionalize micro porous scaffolds with type I collagen. In brief, both control and test scaffolds were incubated in a 0.1 (w/v) % collagen type I solution with a pH adjusted to 4.2 at 37°C for 7 days to promote molecular collagen self-assembly. The dried scaffolds were treated with UV light for 30 min each side to achieve collagen nanofiber stability and washed repeatedly with DI water to remove buffer salts.

4.2.5 *In Vitro* human Mesenchymal Stem Cells (hMSCs) culture on scaffolds

Human bone marrow derived mesenchymal stem cells were purchased from Lonza (Lonza, Walkersville, USA) and expanded as per the protocol provided by the supplier. Cells used for all experiments were at passage 5. The basal media consisted of DMEM (HG) (Lonza, Walkersville, USA) supplemented with 10% FBS and 1% antibiotics (Penicillin-Streptomycin). The osteogenic media was composed of basal media with 0.2mM L- Ascorbic acid and 7.0mM Glycerol 2-phosphate disodium salt and 0.1μM Dexamethasone.

Scaffolds were soaked in 70% ethanol for 20min and allowed to dry in the cell culture hood. Each side of the scaffold was exposed to UV light for 20 minutes in the tissue culture hood. Scaffolds were soaked in basal media overnight prior to seeding with the hMSCs. Each scaffold was seeded with 250,000 cells in a 50μL cell suspension and incubated for 4h before additional media was added. A total of 500μL basal media was added to the samples in a 48 well plate and then switched to osteogenic media following 24h. The media was changed every other day and cultures were maintained for 21 days. One set of scaffolds was also cultured in basal media up to

21 days to evaluate hMSC proliferation using pico-green assay. All studies were done in triplicate for each time point and each group of scaffolds.

4.2.6 Cell viability

Viability of hMSCs on the scaffolds was analyzed with a live/dead cell viability kit. In brief, calcein AM enters live cells and reacts with intracellular esterase to produce a bright green fluorescence, while ethidium homodimer-1 enters only dead cells with damaged membranes and produces a bright red fluorescence upon binding to nucleic acids. Scaffolds were imaged on 3, 7, 14 and 21 days of osteoinduction using a Zeiss 780 /Laser Scanning Confocal Microscope (LSCM) at magnifications of 10X to view cells independently and along with the scaffolds. 3D reconstruction of the confocal stacks was done using Imaris software (Bitplane).

4.2.7 Cell proliferation

Rate of hMSCs proliferation after transferring to osteogenic media was quantified by measuring the amount of cellular DNA content at various culture points using a Picogreen dsDNA assay. In brief, at different culture time of 3, 7, 14 and 21 days, the cellular constructs were washed twice with PBS, transferred to new well plates and 1ml of 1% Triton X-100 solution was added to lyse the cells. The well plates underwent three freeze-thaw cycles, between -70^{o}C and room temperature, and mixed with the aid of a pipette to extract cell lysate from the 3D scaffolds prior to analysis. 125µL of sample DNA was transferred into a new well plate to which 375µL (component B) and 500µL (Component A) kit reagents were added. Well plates were covered with aluminum foil to prevent light exposure and incubated for 5min. A BioTek plate reader was used to read fluorescence (485nm/535nm). Optical readings were converted in DNA concentration using a standard curve.

4.2.8 Alkaline phosphatase activity

Alkaline phosphatase activity of hMSCs on the scaffolds was evaluated as a marker of osteoblast phenotype progression using an ALP substrate kit. A 100µL of cell lysate was transferred into a well plate to which a 400µL of P-NPP (para- nitro phenol phosphate) substrate and buffer solution were added and incubated at 37ºC for 30min. After 30 minutes, 500µL of 0.4N of sodium hydroxide was added to stop the reaction. The intensity of the color produced though the reaction is proportional to ALP activity. The optical density of the solution was measured at 405nm using a BioTek plate reader. The results for ALP activity were optical density and these were normalized to scaffold volume.

4.2.9 Mineralized matrix deposition by cells

Mineralized matrix deposition by osteoinduced hMSCs on the scaffolds were evaluated as marker of mature osteoblast phenotype using an Alizarin Red staining method for calcium deposition at 21 days of osteoinduction. This colorimetric analysis is based on solubilizing the red matrix precipitate with cetylpyridinium chloride (CPC) to yield a purple solution. In brief, at 21 days of osteoinductive cell culture, cellular constructs were fixed in 70% ethanol for 1h, at room temperature and then stained with 40mM Alizarin Red (Sigma) solution for 10 min at room temperature. After washing 5-10 times with distilled water to remove the adsorbed/absorbed dye, chemically bound red matrix precipitate was solubilized in 1mL of 10% CPC until color was stable. The optical density of the solution was read at 562nm using BioTek plate reader. The results for calcium deposition were also normalized to scaffold volume.

4.2.10 Gene expression

The RNA from scaffolds was extracted using RNeasy Plus Universal Mini Kit (Quiagen, Valencia, CA, USA) as per the manufacturer's protocol. Briefly, each scaffold was washed with sterile PBS (pH 7.4) and then RNA extraction was carried out using RNeasy Plus Universal ^{R} kit (Quiagen, Valencia, CA, USA). Briefly, Quiazol ^{R}/ chloroform extraction yielded an aqueous layer. This layer was loaded on to columns and washed using buffers successively to collect RNA in a micro centrifuge tube and suspended in 30µL of RNase-free water. The RNA was measured using a nanodrop spectrophotometer and 1.5µg RNA was used for DNAse treatment, to eliminate any remnant genomic DNA contamination. A DNA-free^{TM} Kit (ambion, life technologies, Foster City, CA, USA) was used and the manufacturer's protocol was used to digest the cDNA.

This DNAse treated RNA was used to reverse transcribe into cDNA using iSript advanced reverse transcription kit (Bio-rad, Hercules, California, U.S.A.), using the manufacturer's protocol. To each sample, 4µL of reaction buffer and 1µL of advanced reverse transcriptase enzyme were added. Following incubation at 42°C for 30 minutes and enzyme inactivation at 85°C for 5 minutes, the cDNA was ready for gene expression analysis.

Prime- PCR (Bio- Rad, Hercules, California, U.S.A.), gene arrays where primers of osteochondral genes were used for the gene expression analysis. Validated SYBR green primers of the following genes were analyzed: GAPDH, TBP, HPRT1 (internal control genes expressions were normalized to), Coll1A1, Coll1A2, Coll3A1, Coll2A1, BGLAP, MMP-13, Coll10A1, Sox9, RUNX-2, ALPL, IBSP, BMP-2, DMP-1, SPARC (ON), MMP-9, MMP-13, IHH. To each of the test wells, 10µL of 2X Sos Advanced SYBR green mix, 10µl of cDNA with ultrapure water (equivalent to 12.5ng) was added. All controls to check for purity of starting material

including gDNA contamination, and RNA integrity were included and passed the quality control criteria. Samples used were cells seeded and osteoinduced on PLGA, PLGAc, CA and CAc. PLGA was kept at 1.0 and the gene expression fold changes were with reference to PLGA.

4.2.11 Osteogenic marker Immunostaining

The scaffolds seeded with hMSCs were harvested at 21 days of osteoinduction and washed with PBS (pH 7.4) prior to fixation with 4% paraformaldehyde (PFA) in PBS (pH 7.4) at room temperature for 10 minutes. The samples were then washed with PBS (pH 7.4) and permeabilized using 0.1% Triton X-100 in 1X PBS (pH 7.4) for 10 minutes. Samples were washed again with PBS (pH 7.4) and subsequently incubated in 3% bovine serum albumin (BSA) in 1X PBS (pH 7.4) solution for 30 min to block non- specific antibody binding. Primary antibodies at specific concentrations (Colleen Rabbit anti human (abcam, Cambridge, MA, U.S.A.) at 1:200 dilution; and bone sialoprotein Rabbit anti human (Millipore, Billerica, MA, U.S.A. at a dilution of 1:100)) were dissolved in 1% BSA/ PBS (pH 7.4) buffer. Scaffolds were incubated in primary antibody solution for one hour at room temperature. This was followed by rinsing of samples with PBS (pH 7.4). Dylight 594- Goat- anti- Rabbit secondary antibody (Jackson immune, West Grove, PA, U.S.A.) at a dilution of 1:400 was dissolved in 1% BSA/ PBS (pH 7.4) buffer along with Alexafluor 488- Phalloidin (Invitrogen, Eugene, Oregon, USA) at a 1:40 dilution were added to scaffold construct for one hour. This was followed by rinsing of samples 3 times with PBS (pH 7.4). NucBlue (DAPI) at a 2 drops/ ml of PBS (pH 7.4) was used for staining the cellular nuclei. This was followed by confocal imaging with z- stacking for each of the scaffolds for visualization of the marker (red)/ cytoskeleton (green) and nuclei (blue).

4.2.12 Statistical analysis

All data are reported as the mean ± standard deviation (SD) of results from at least three independent runs. In case of experiments with two groups a student t- test was performed. In the case of experiments with multiple groups and multiple time points a 2- way- ANOVA with Bonferroni posttest was performed. In the case of experiments that focused on one time point and several groups, a one- way- ANOVA with Tukey posttest was performed. 95% Confidence interval was employed to arrive at the p values. The denotation of significances given by p values are- *$p<0.001$ (extremely significant), $^{\#}p<0.01$ (very significant), $^{@}p<0.05$ (significant). Analyses were performed using GraphPad Prism Software (GraphPad Software, San Diego, CA).

4.3 Results

4.3.1 Characterization of hMSC response

Good cell viability on PLGA, PLGAc, CA and CAc from day 3 to day 21 was evident (**Figure 4.3**). In the current study all structures were seeded at a high cell density to study the osteogenic phenotype development and hence the cell proliferation rates were constant due to confluency (**Figure 4.1 a, b, c and Figure 4.4**). The alkaline phosphatase activity (ALP), as a precursor of osteoblast maturation, and mineralization determined by alizarin red staining (ALZ), as a marker of late stages of osteoblastic maturation, were evaluated at 21 days. The ALP activity was highest on CAc and it was significantly greater than CA. However, this was not the case with PLGAc and PLGA, as there was no difference between the two groups in ALP activity (**Figure 4.1d**). Mineralization was higher on collagen-coated groups than on their uncoated counterparts. However mineralization on CAc was significantly greater than mineralization on PLGAc (**Figure 4.1 e,f**). These findings indicate that the osteoblastic phenotype progression may be greater on CAc than the other groups including PLGAc.

To further understand if there is a difference in osteochondral progression of seeded hMSCs, the expression of osteochongral genes and proteins were analyzed (**Figure 4.5** and **Figure 4.2**). Collage 1 (Coll1), an important ECM component of bone was significantly upregulated in all groups in contrast to PLGA. The CAc group had the highest collagen expression and it was remarkably greater than PLGAc and CA (**Figure 4.2a**). Osteonectin (ON), a protein associated with the collagen ECM, also showed a similar trend with cells on CAc showing the highest levels of expression (**Figure 4.2b**). Bone sialoprotein (BSP), a mature marker of osteoblasts, was upregulated considerably on CA and CAc in contrast to PLGA and PLGAc. Interestingly CAc performed better than CA, but cells on PLGAc and PLGA showed no significant difference in

BSP expression (**Figure 4.2c**). Additionally, an important osteoblastic transcription factor Runx2 was seen to be significantly upregulated on CAc in contrast to all other groups (**Figure 4.2d**). Furthermore we examined genes for osteochondral progression (**Figure 4.5**), such as alkaline phosphatase (ALPL), Collagen III (Coll3A1), Matrix metalloproteinase 13 (MMP13), Sox9 and Collagen10A1 (Coll10A1). We saw an upregulation of these genes on the natural polymers (CA and CAc) in contrast to the synthetic polymers (PLGA and PLGAc). CAc showed the highest expression of all the genes indicating greatest osteoinduction of seeded hMSC. To visualize phenotype expression and cellularity within scaffolds, immunostains were performed for osteoblastic markers such as Coll1 and BSP along with phalloidin for cytoskeletal F-actin and Nucblue for cell nuclei. While the cells and markers were distributed evenly on the CA and CAc groups, PLGAc showed better cellular distribution than PLGA. The cells and markers were confined to the microspheres, with very little cellularity in the pores (**Figure 4.2e,f**). Thus osteoblastic maturation was greatest on CAc followed by CA, indicating the effectiveness of natural polymeric micro-nano structured scaffolds towards osteoinduction of stem cells. The CAc scaffolds induced greater osteogenic progression than PLGAc as the biomimetic nature of CAc was more conducive than PLGAc.

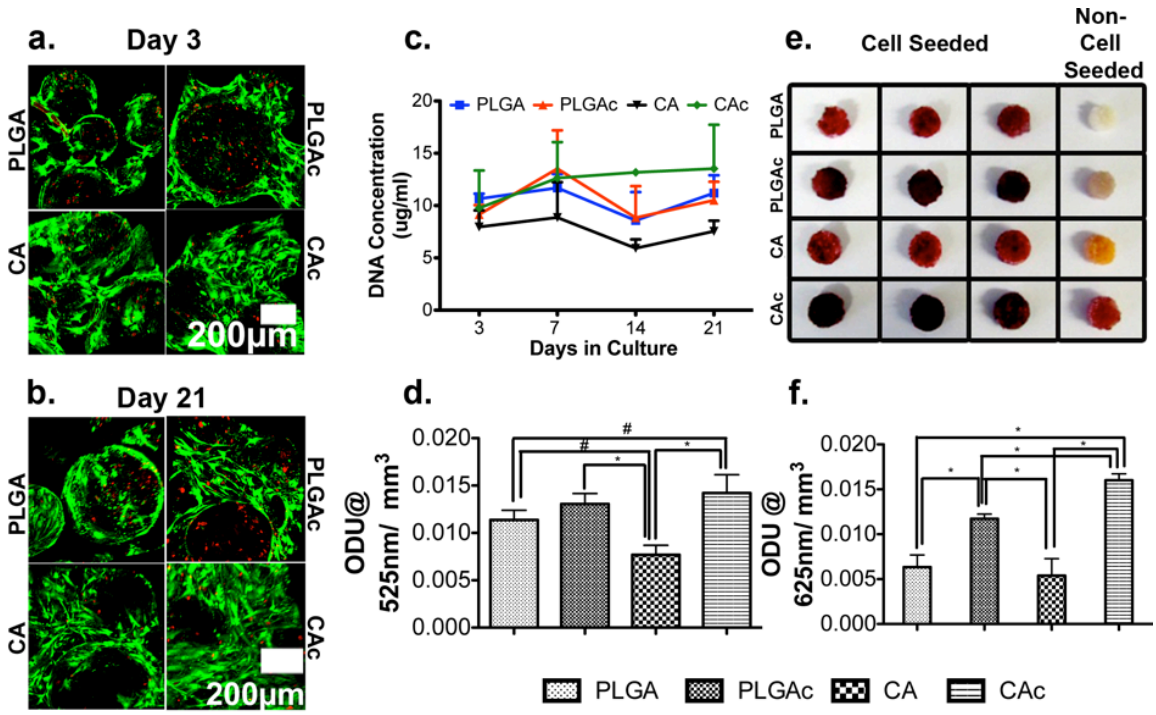

Figure 4.1 Viability, proliferation and osteoblastic markers of seeded hMSCs

In vitro phenotype development by hMSCs seeded on to scaffolds under osteoinduction. Viability of seeded cells over time on PLGA (top left), PLGAc (top right), CA (bottom left) and CAc (bottom right) with live (green)/ dead (red) staining at a) Day 3 and b) Day 21. Scalebar = 200µm. c) DNA content by pico- green assay over 21 days in culture d) Alkaline phosphatase activity at 21 days of osteoinduction on PLGA, PLGAc, CA and CAc. Mineralization at 21 days of osteoinduction on scaffolds measured by e) visual micrographs of alizarin red stained scaffolds (PLGA, PLGAc, CA and CAc- top to bottom) and f) Colorimetric quantification of calcium deposition on PLGA, PLGAc, CA and CAc. One – way ANOVA with Tukey post test, with 95% confidence intervals, *P<0.001, #P<0.01, @P<0.05.

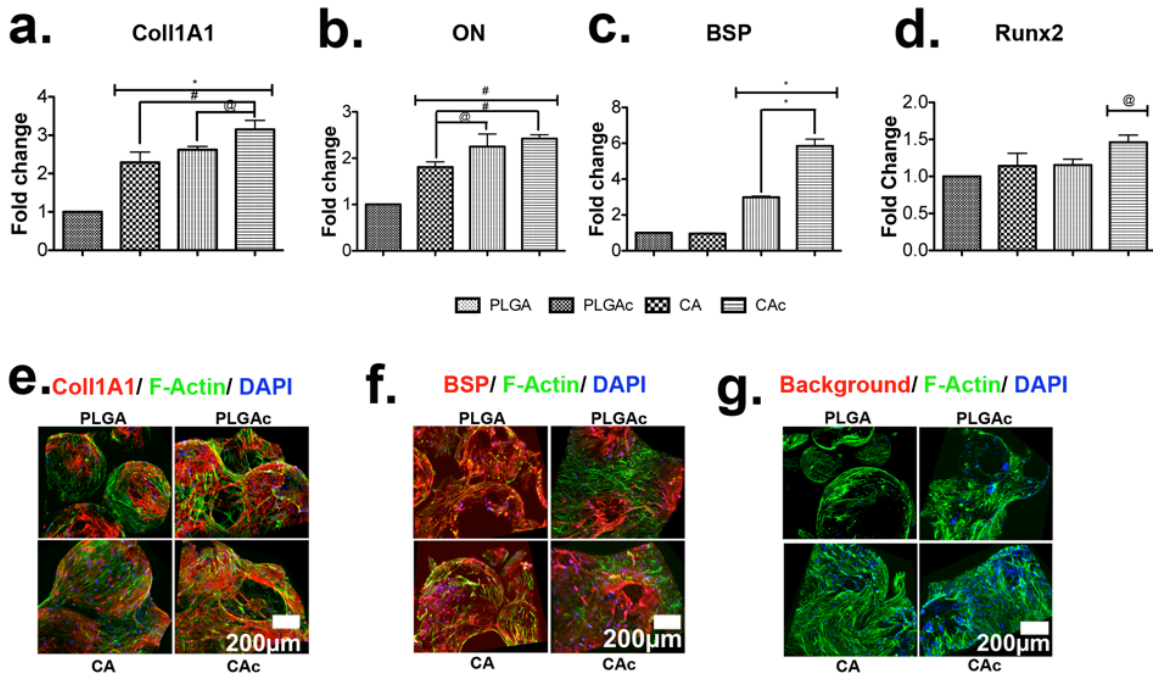

Figure 4.2 Osteoblastic gene and protein expression by hMSCs

Osteoblast markers expressed by osteoinduced hMSCs on PLGA, PLGAc, CA and CAc at 21 days. Osteogenic gene expression of a) Collagen1A1 (Coll1A1), b) Osteonectin (ON), c) Bone Sialoprotein (BSP) and d) Runx2. Immunostaining for osteoblastic protein markers (Marker- red/ F-actin (Phalloidin)- green/ Nucleus (Nucblue DAPI)- blue) staining of PLGA (top left), PLGAc (top right), CA (bottom left) and CAc (bottom right) e) Collagen1/ F- actin/ Nuclei staining f) Bone sialoprotein/ F- actin/ Nuclei and g) No primary control (Background -red/ F- actin (Phalloidin)- green/ Nuclei (DAPI)- blue) scalebar = 200µm. One – way ANOVA with Tukey post test, with 95% confidence intervals, $^{*}P<0.001$, $^{\#}P<0.01$, $^{@}P<0.05$.

4.4 Discussion

Cells adhere to materials through adsorbed ligands, by binding to these ligands via their integrin receptors(*423*). The classical view in material-protein interaction argues that a hydrophobic matrix, due to its favourable surface energy, adsorbs higher quantity of proteins from the surrounding environment. These absorbed proteins play an important function in regulating cellular events(*424-426*). However, the absolute quantity of adsorbed proteins onto a material could not be correlated to cell adhesion(*427*). Many reports identify the importance of matrix hydrophilicity as an essential feature for achieving cell adhesion and long term biocompatibility(*428*). Studies focused on improving the matrix hydrophilicity, without altering its chemistry or surface roughness, led to greater cellular adhesion demonstrating that cellular responses were optimal on slightly hydrophilic materials(*377*). Though experimental evidence is minimal, it is believed that hydrophilic matrices may lead to a more native-like conformation of the adsorbed proteins in turn producing better cellular responses(*429*). The differential response of collagen self-assembly on CA and PLGA polymers could be an attributing factor for the observed D-banding patterns on the CA matrix alone.

The chemical functional groups on a material can influence cellular responses immensely. For instance Curran *et al.* cultured bone marrow derived mesenchymal stem cells (MSCs) on glass substrates modified to contain the functional groups: like $-CH_3$, -SH, –COOH, –OH, and $–NH_2$, under basal, osteogenic and chondrogenic conditions. They found that the $-CH_3$ functional groups helped maintain the multipotency of MSCs, while the –OH and $–NH_2$ groups were conducive for osteogenic differentiation, and the –COOH and –SH groups on the substrate supported chondrogenic differentiation. These differences were observed both under basal and stimulated conditions(*413*). Many other studies have used materials that varied only by the

chemical functional groups on the biomaterial's surface and all of them have shown that the chemical functionalities on the material surface can have a profound influence on stem cell behavior(*37, 340*). These changes can be attributed to the resulting material surface energy and hydration characteristic that determine the conformation of adsorbed proteins and in turn cellular adhesion(*414*). In the present study, polysaccharide CA provides aforementioned functionalities and control PLGA polyester lacks these groups to study the osteochondral phenotype progression of seeded stem cells. Apart from this, the observed micro scale roughness of CA groups over the smooth morphology of PLGA, could also act as an inductive factor for osteogenic differentiation of stem cells(*430*).

In order to understand the effect of the properties of the material towards stem cell differentiation, hMSCs were seeded on all the polymers and differentiated into osteoblastic lineage. The hMSCs showed good viability for the period in culture on both the polyesters and the polysaccharides. However, the cells spread on the microspheres and the interpore spaces of CA and CAc, and PLGAc but not in the case of PLGA. The inclusion of integrin ligand such as collagen or the presence of a hydrophilic polymer that allows for integrin ligands from the media to be presented in the right conformation may have lead to better cell spreading on the CA, CAc and PLGAc matrices against the microsphere focused cellularity of PLGA (**Figure 4.1 a, b, c and Figure 4.4**). PLGA is shown to have a contact angle above 90**°,** but CA has a much lower contact angle of around 55°. It has been seen that several studies that a contact angle between 35-65**°,** may be more conducive for cell adhesion than a contact angle above 90**°(*431, 432*).** Hence the CA materials showed greater cell adhesion and spread than PLGA, owing to their hydrophilic nature.

The presence of collagen, which is an integrin ligand could compensate in the case of PLGAc, leading to greater uniformity in cell distribution. However, the osteochondral progression of seeded MSCs was higher on CA and CAc both in terms of gene and protein levels and distribution (**Figure 4.2, 4.5**). The long bones of our body are formed by endochondral ossification. In this process the MSCs undergo a transition through the formation of a condensed chondrogenic template to facilitate the formation of bone. The material properties may have attributed to better cell adhesion by integrin signaling on the MSCs seeded on CA and CAc. These could translate into better cell- cell contact as well. This is likely to be more conducive for cellular condensation and hence the greater osteochondral progression seen on CA and CAc.

Though both CAc and PLGAc possessed collage, the collagen on CAc was seen to be more biomimetic than the collagen on PLGAc. It has been shown in literature that denaturation of collagen leads to loss of mechanical stimuli needed for MSC's osteoblastic differentiation(*405, 406*). It is also known that the Hedgehog signaling pathway, seen to play an important role in osteochondral progression(*433, 434*) in the body is upregulated by type one collagen with the native structure(*435*). Hence we observed that the CAc micro-nano structured biopolymer was most osteoinductive, to an extent greater than its PLGAc counterpart.

4.5 Conclusions

We conclude that the natural polymer based micro- nano structured CAc scaffolds mediated the greatest degree of cell spreading and distribution along with greatest levels of osetoblastic differentiation of the seeded MSCs. While the PLGA platform showed similar viability and cell proliferation levels, the CA scaffolds showed better cell and osteoblastic marker distribution throughout its microspgeres and the interpore spaces. Hence these studies have shown the

potential of CA and CAc scaffolds to be osteoinductive when used in combination with MSCs. Since MSCs are a very clinically relevant cell population, the translational relevance of using CA and CAc scaffolds in combnation with MSCs may be great.

4.6 Supplemental Figures

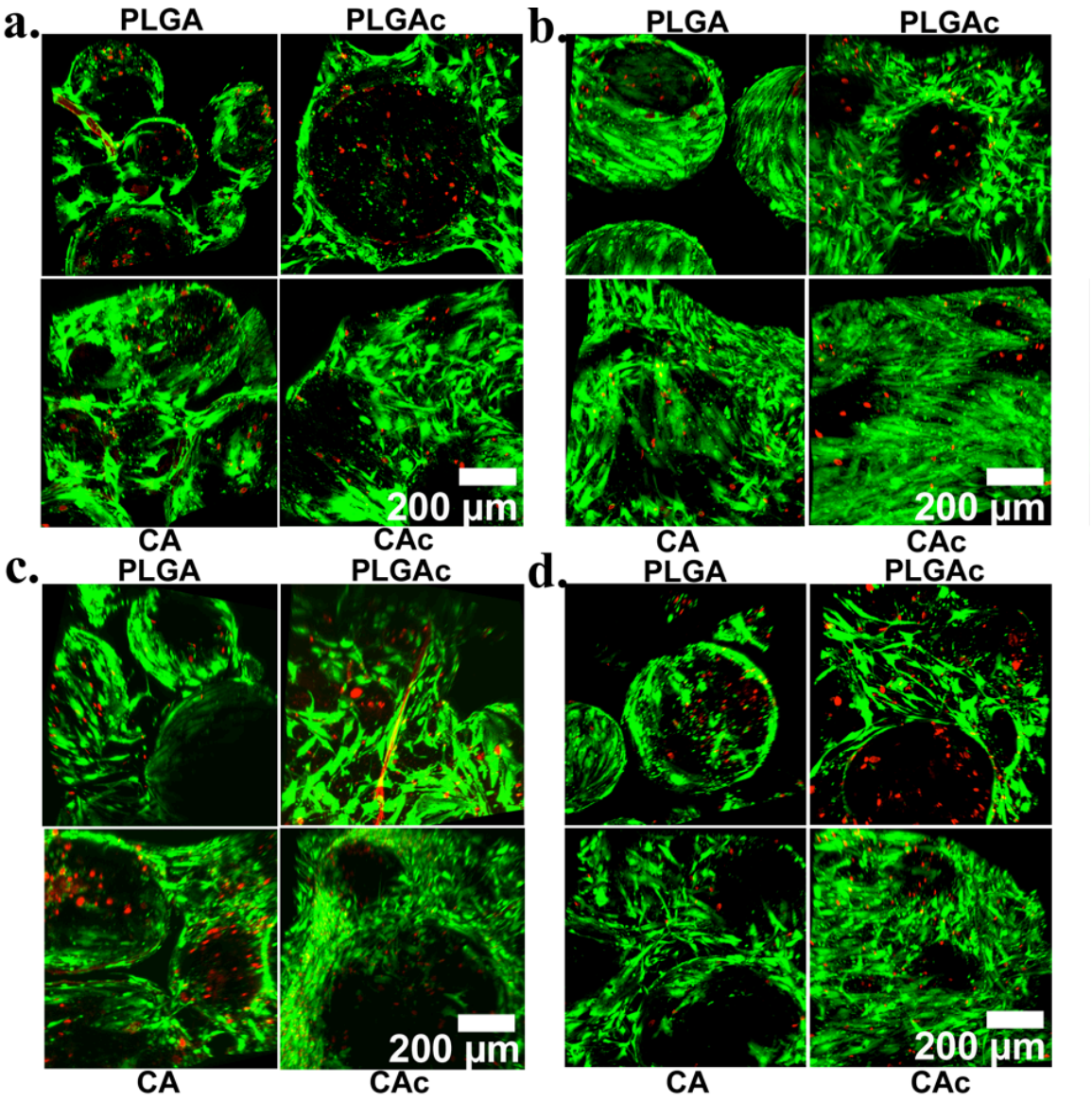

Figure 4.3 Viability of seeded hMSCSs

Live (green)/ dead (red) staining of cells on scaffolds at a) Day 3, b) Day 7, c) Day 14, d) Day 21. PLGA (top left) PLGAc (top right), CA (bottom left) and CAc (bottom right) show good viability of seeded hMSC throughout all culture time points.

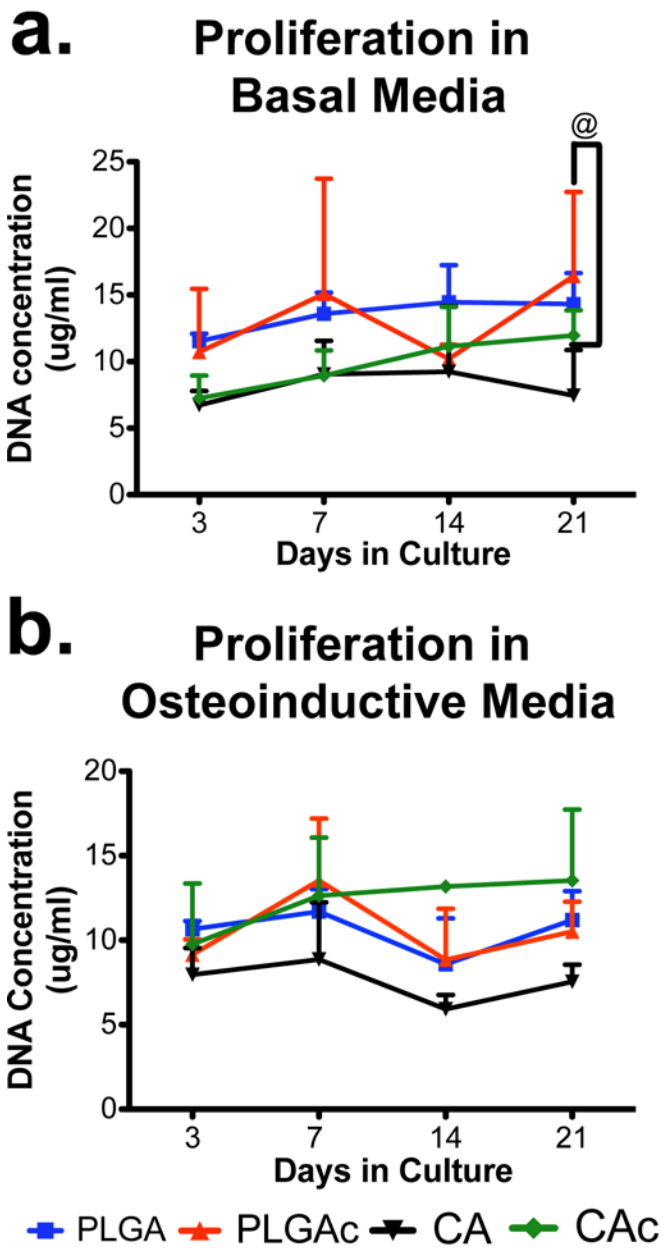

Figure 4.4 Proliferation of seeded hMSCs

a) hMSC proliferation measured by pico- green assay over 21 days of culture in basal and b) osteoinduced condition. Two- way ANOVA with Bonferroni post- test, with 95% confidence intervals, $^{*}P<0.001$, $^{\#}P<0.01$, $^{@}P<0.05$.

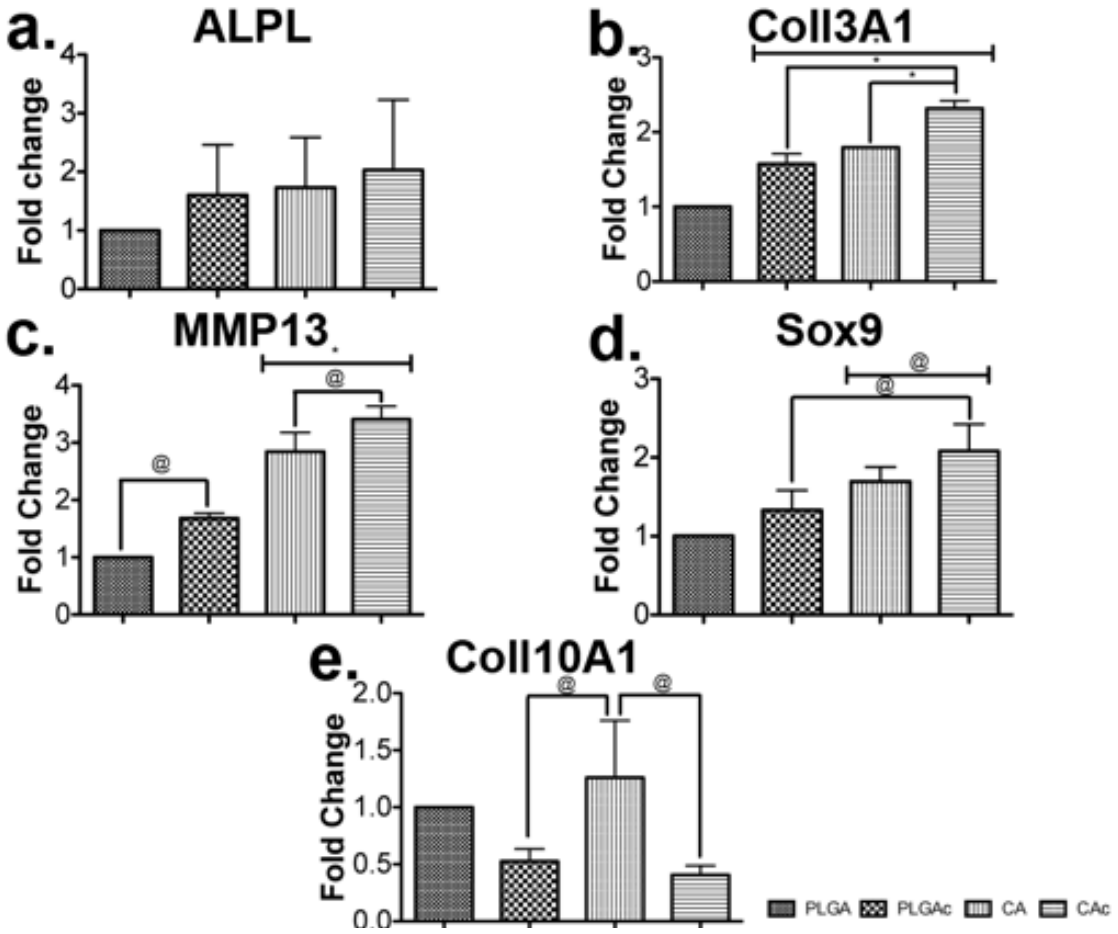

Figure 4.5 Osteochondral gene expression by seeded hMSCs

Osteochondral gene expression by osteoinduced hMSCs on PLGA, PLGAc, CA and CAc. a) ALPL- Alkaline phosphatase, b) Coll3A1- collagen 3A1, c) MMP13- Matrix metaloprotease 13, d) Sox9, e) Coll10A1- collagen 10A1. One – way ANOVA with Tukey posttest, with 95% confidence intervals, $^{*}P<0.001$, $^{\#}P<0.01$, $^{@}P<0.05$

5 Chapter 5

Charecterization of the Biocompatibility of CA-Collagen, Micro-Nano Structured Scaffolds *in vivo*

5.1 Introduction

Any foreign material that is placed into a host tends to elicit an immune reaction. When a material is first implanted into the body, it comes into contact with blood. A layer of protein from the host coats the implanted biomaterial. Various proteins like fibrin, fibrinogen, vitronectin and a host of other proteins are found in this mix, along with immunoglobulins like IgE and opsonins like compliment activated factor C3b(*436*) etc. The neutrophils home and try to resolve the new foreign body by trying to digest it with their activity. However the biomaterial is too large and once this acute phase resolved, the macrophages home to the implant and since they are also incapable of destroying the foreign body, the fusion of macrophages occurs, leading to the formation f multinucleated giant cells (MNCs), that are characteristic of a foreign body reaction (FBR). Eventually a layer of collagen produced by fibroblasts encapsulates the implant. This is known as fibroencapsulation of the biomaterial(*437*).

Biocompatibility is a complex factor that involves the immune response by the body to the implanted foreign material. Though every material tends to elicit an immune response, it is important to make sure that the FBR to a material is acceptable as per the norms laid out by regulatory agencies before implantation into the body. Though cell viability in vitro can and is used as a measure of biocompatibility, implantation into the body is necessary to understand the tissue response to the material and establish its safety for usage an implant biomaterial for tissue engineering. The (IOS) 10993 criteria for biomaterial biocompatibility mandates implantation into animals and require that the implants be non- toxic on implantation(*437*).

Taking these factors into consideration, implantation of CA, CAc and PLGA polymers under subcutaneous pouches of rats were conducted. The rats were sacrificed and the immune response in the tissue infiltrating into the scaffold matrix were determined by histological staining and histomorphometric measurements. These studies were designed to test the safety of the new CA and CAc polymeric scaffolds against an FDA approved (PLGA) polymer.

5.2 Materials and Methods

5.2.1 Subcutaneous implantation

Sprague Dawley rats of 250-300 grams of body weight were purchased from Charles River (Wilmington, MA, USA). All procedures for animal use were approved by the Institutional Animal Care and Use Committee (IACUC), at the UConn Health. Isoflurane (3%) in a gaseous mix with oxygen was used as the anesthetic. Each rat was implanted with six scaffolds, two of each kind (PLGA, CA and CAc). Briefly, the dorsal side of the rats were shaved and prepped with betadine and alcohol. A 2.5 cm long incision was created to make a subcutaneous pouch and individual scaffolds (8X2mm) were implanted into pouches. The pouches were sutured and animals were monitored regularly. At each of the 2, 4, 8 and 12 weeks of implantation time points, two rats were sacrificed using carbon dioxide overdose and four scaffolds (n=4) of each type (PLGA, CA and CAc) were removed and collected for evaluation.

5.2.2 Histological staining

The scaffold samples were harvested along with the surrounding subcutaneous tissue, washed in PBS (pH 7.4) and fixed in 4% PFA/ PBS (pH 7.4) overnight at 4°C. The scaffolds were rinsed in PBS (pH 7.4) after fixation and transferred to a 1:1 mix of OCT and 30% Sucrose solution in PBS (pH 7.4). The samples were incubated for 24h at 4°C. The samples were then transferred to

OCT alone at room temperature for an hour. The samples were flash frozen and sectioned into 10μm thick sections and captured on cryo-films. The cryo films were fixed onto slides using UV-curing adhesive. The samples were hydrated in water and Hematoxylin and eosin staining and Gomori Trichrom staining was performed.

5.2.3 Histomorphometric analysis

The hematoxylin and eosin stained samples were used for characterization of cell types infiltrating the implants. Two independent evaluators scored the samples for multinucleated giant cells (MNC) characteristic of foreign body response, macrophages, fibroblasts and blood vessels based on cell morphology, in consultation with a clinical pathologist. The gomori trichrome samples were used as guidelines for confirmation of cellular phenotype. FIJI (NIH) software was used to count the total number of cells in each type and to measure the tissue area in the pore of each group of scaffold. All the scores were normalized to the tissue area fraction. Tissue area fraction was equal to Tissue area in section (i.e. tissue area in the pores of the scaffold)/ Total area of the section. An n=3 was used for this analysis.

5.2.4 Statistical analysis

All data are reported as the mean ± standard deviation (SD) of results from at least three independent runs. In case of experiments with two groups a student t- test was performed. In the case of experiments with multiple groups and multiple time points a 2- way- ANOVA with Bonferroni posttest was performed. In the case of experiments that focused on one time point and several groups, a one- way- ANOVA with Tukey posttest was performed. 95% Confidence interval was employed to arrive at the p values. The denotation of significances given by p values are- *$p<0.001$ (extremely significant), $^{\#}p<0.01$ (very significant), $^{@}p<0.05$ (significant). Analyses were performed using GraphPad Prism Software (GraphPad Software, San Diego, CA).

5.3 Results

5.3.1 Cellularity in the scaffolds

Subcutaneously implanted PLGA, CA and CAc scaffolds in Sprague Dawley® rats retrieved at week 2, 4, 8 and 12 were processed for histology. At the earliest time point CA scaffolds had very little cellularity compared to PLGA controls. However, the CAc scaffolds presented good cellularization at the early time point (2 weeks) (**Figure 5.1a**). The collagen content of the tissue was also higher in CAc than CA (**Figure 5.1c**). As time progressed the cellularization of CA groups increased at 4 weeks (**Figure 5.1 b,d**) with the CAc scaffolds showing more cellularization than CA. However by 8 weeks all the materials looked similar in terms of their cellular and collagen content (**Figure 5.2 a, c**). At 12 weeks there was a marginal decrease in the cellularity of PLGA, but the tissue infiltration of the CA and CAc scaffolds were greater (Figure **5.2 b, d**). Quantitatively the tissue infiltration in the CA material was lower than PLGA in the earlier time points after implantation of the material (at 2 and 4 weeks). However at 8 weeks all the scaffolds had a comparable amount of tissue infiltration and by 12 weeks the CA material showed greater cellular content than the other groups (**Figure 5.3b**).

5.3.2 Immune response to scaffolds

The macrophages population on CA was considerably higher than CAc at the earliest (week 2) time point (**40X magnified images of Figure 5.1 a,c**). However these differences were insignificant with progress in time (**40X magnified images of Figure 5.1 b,d; Figure 5.2 a, c; b,d**; **Figure 5.3 c**). The multinucleated giant cells (MNCs) representing the FBR of the tissue to the biomaterial indicated a significantly higher FBR to CA than on PLGA, but not on CAc soon after implantation at around 2 weeks (**40X magnified images of Figure 5.1 a,c** and **Figure 5.3 a**). These significances did not persist at later time points (**40X magnified images of Figure 5.1 b,d;Figure 5.2 a, c)** until 12 weeks (**Figure 5.2 b, d)** when PLGA showed considerably greater number of MNCs than CA and CAc (**Figure 5.3 a)**.

5.3.3 Vascularity in scaffolds

Vascularity of all the materials were pretty low to begin with at 2 weeks but increased at a similar rate on all the materials (**Figure 5.3 d)**.

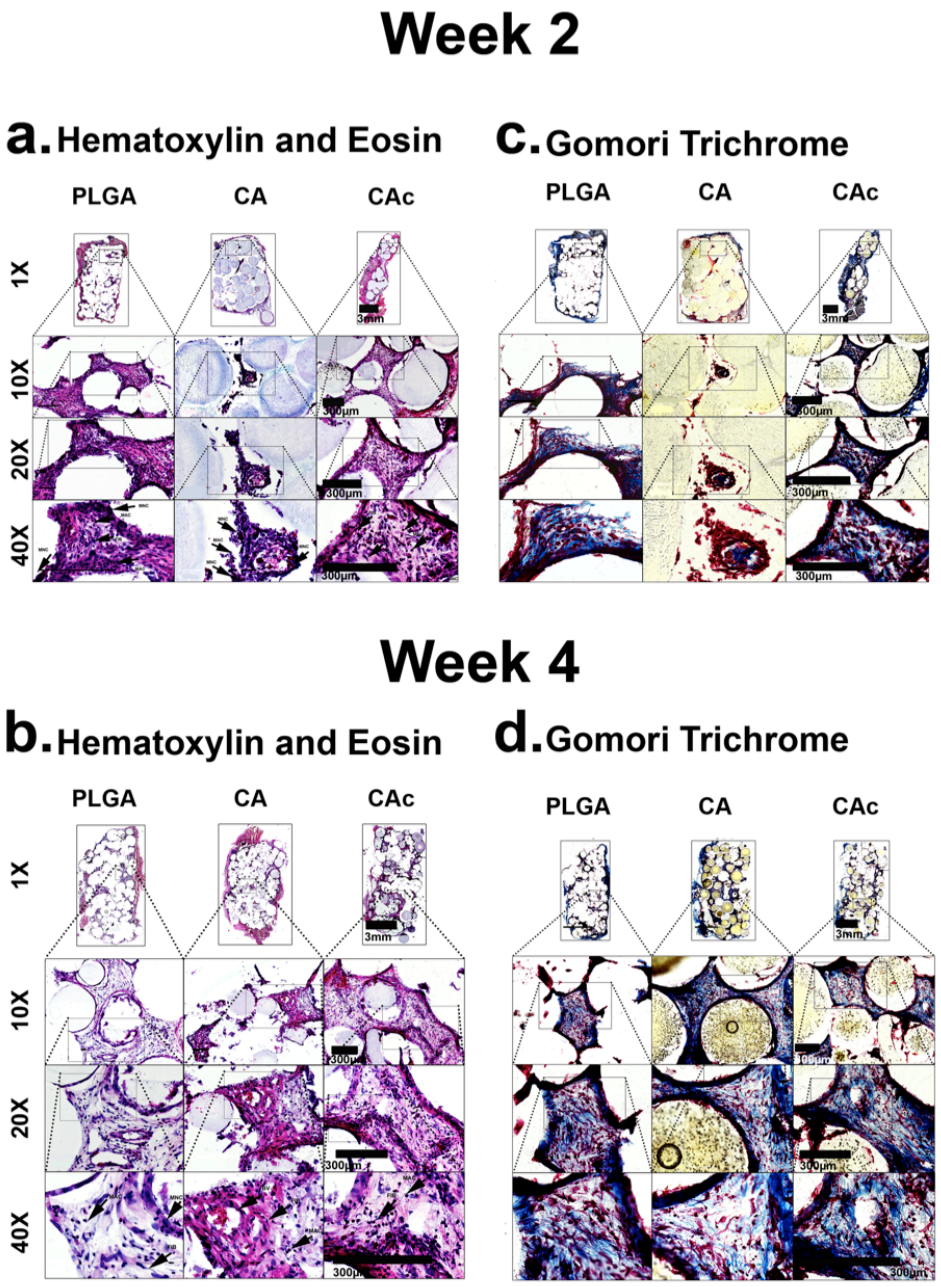

Figure 5.1 Staained histological sections at early time points

Histological staining of subcutaneously implanted PLGA, CA abnd CAc at early time points. (a, c- at 2 weeks , b, d- at 4 weeks). a), b)- Hematoxylin and eosin staining, c), d)- Gomori trichrome staining. Scalebars on 1X magnification = 3mm, scalebar on 20X and 40X magnifications= 300 µm.

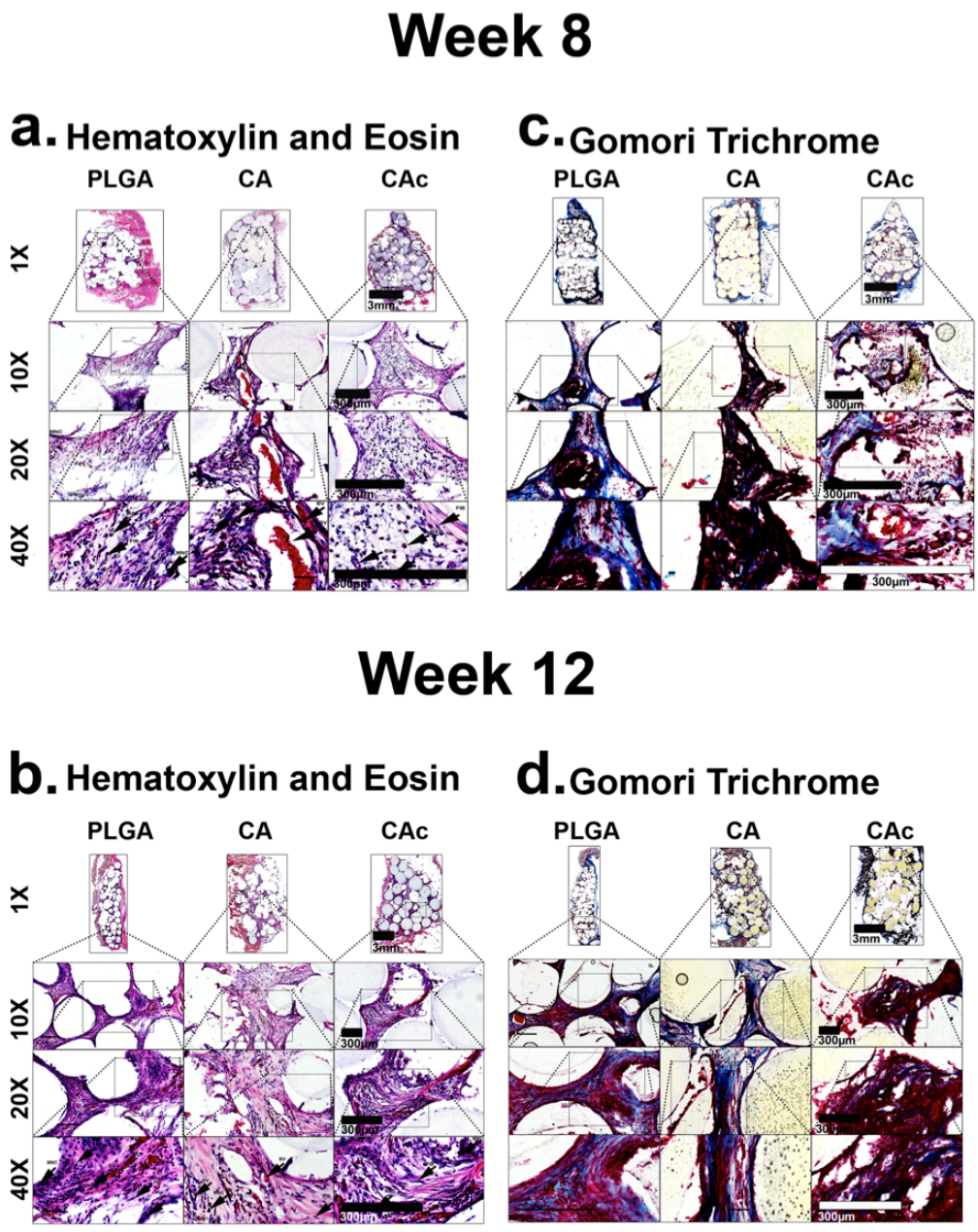

Figure 5.2 Stained histological sections at late time points

Histological staining of subcutaneously implanted PLGA, CA abnd CAc at late time points (a,c- at 8 weeks, b,d- at 12 weeks). a), b) Hematoxylin and eosin staining, c), d) Gomori trichrome staining. Scalebars on 1X magnification = 3mm, scalebar on 20X and 40X magnifications= 300 µm.

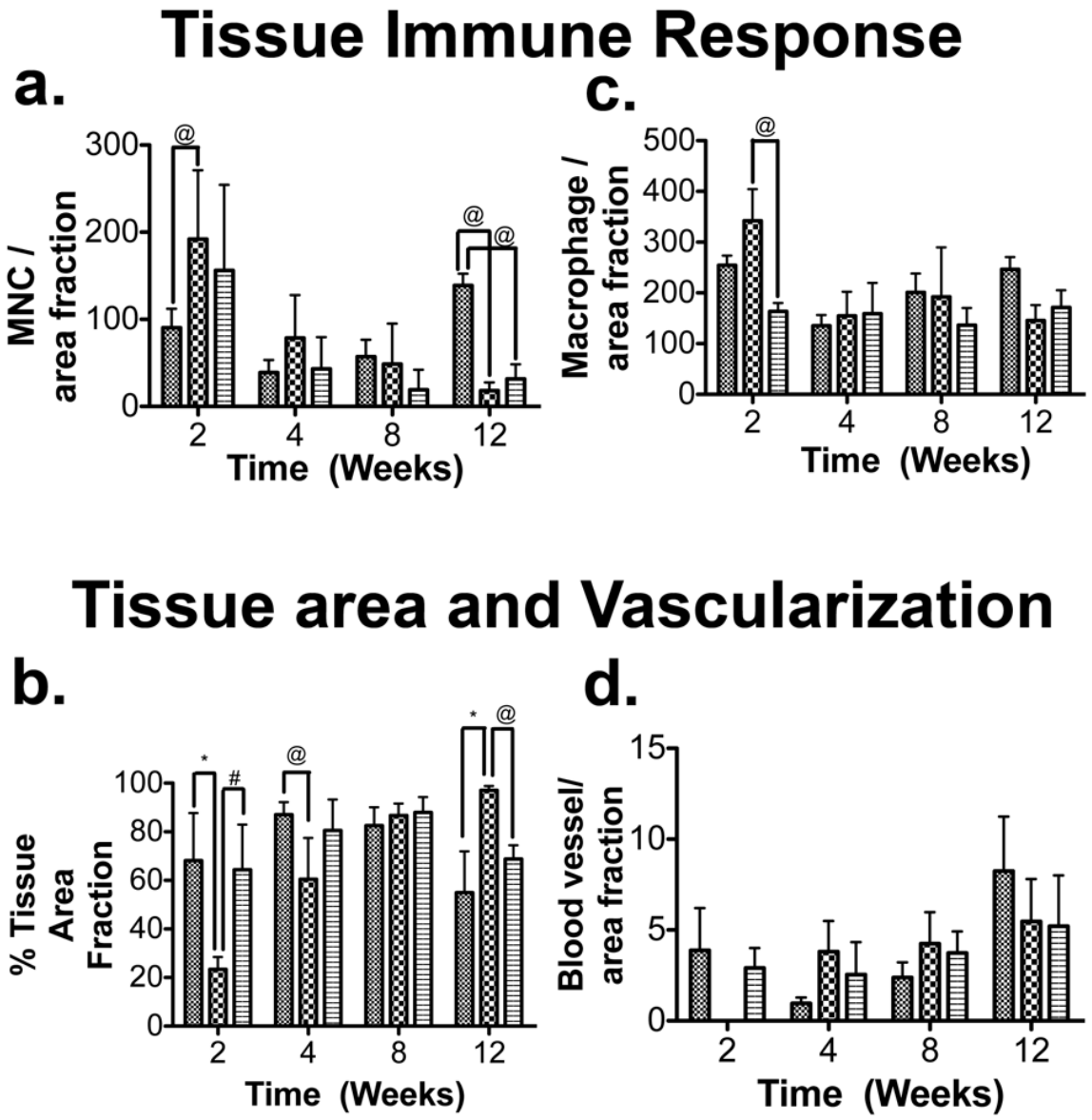

Figure 5.3 Histomorphometric analysis of subcutaneous implants

Histomorphometric analysis of implanted scaffolds over time- Immune response represented by a) multinucleated giant cells (MNCs), and, b) percentage tissue area, c) macrophages and d) number of blood vessels. Two- way ANOVA with Bonferroni post- test, with 95% confidence intervals, $^{*}P<0.001$, $^{\#}P<0.01$, $^{@}P<0.05$.

5.4 Discussion

Biocompatibility is a basic criterion for using any biomaterial in the body. Though biocompatibility was thought to be elicited by bioinert materials that did not lead to adverse reaction, presently it is defined as a biomaterial's ability to elicit an appropriate tissue response when implanted in the body(*437*). As mentioned in the introduction of this chapter, the tissue response to the natural polymeric CA and CAc materials were contrasted with the PLGA scaffolds. As per the expert opinion of clinical pathologist all the materials elicited an immune response that indicated good immune tolerance by the body. Cellulose and its derivatives are well known to be biocompatible as implants(*231*). Its blood biocompatibility had led to the formulation of hemostatic devices based on cellulose. However the CA scaffolds used by us have tested as highly hydrophilic materials (**Chapter 3**). As stated in the introduction the first step in biomaterial recognition in the body after implantation is by adsorption of several proteins and opsonins onto the surface of the biomaterial. In this regards, the C3 fragment of the compliment system plays an important role in eliciting the FBR response. For instance Elwin *et al*. showed that C3 compliment factor adsorbed in modified surfaces that were highly hydrophobic showed denaturation of the adsorbed protein(*438*). This led to exposure of the epitopes recognized by the antigens in the body. With biomaterials used as contact lenses, the more hydrophilic ones lead to greater biocompatibility and lesser protein buildup(*439*). So, in general, hydrophilic materials have been seen to induce greater bio-acceptance in the body. It was shown by Sussman *et al*, that the same material implanted as a solid piece vs as an interconnected porous scaffold can elicit very different immune response. While the solid material showed a fibrotic response the porous sctucture showed greater biocompatibility(*440*). Hydrogels that show very little protein adsorption onto their surface have also shown great biocompatibility and tissue integration

responses(*441*). Here in these studies we observed a lack of immune tolerance for the CA scaffold at the early time points of 2 and 4 weeks in comparison to PLGA. However the collagen coated counterparts did not suffer this lag time for cellularization of the biomaterial and they had a lower FBR response. CA being extremely hydrophilic could have shown a lag in the adsorption of bodily proteins stably onto its surface at the early time points of implantation in turn leading to a lag in cellular infiltration/ adhesion. However the presence of exogenous collagen may have helped with achieving initial tissue infiltration and biocompatibility of the CAc over the CA scaffolds. On the other hand, at the latest time point of 12 weeks PLGA that showed good responses in terms of cellularization and FBR started showing a reduction in tissue content and an increase in MNCs representative of an increasing FBR with time in contrast to CA. PLGA and synthetic polymers like PLLA may elicit an adverse immune response with time due to the change in the environmental pH associated with the degradation of the polymer matrix(*365*). On the other hand CA which showed slow cellularization showed long term biocompatibility. The presence of collagen in CAc may have hastened the process of cellularization and immune acceptance of the material by the body. The results of material characterization (**chapter 3**) and cellular viability (**chapter 4**) agree well with the results of long-term biocompatibility of the natural polymers seen in this chapter.

5.5 Conclusions

We conclude that CA 3D porous microsphere scaffolds show good long-term biocompatibility. Inclusion of collagen nanofibers may be beneficial in achieving biocomapatibility soon after implantation. This implies that the CA, CAc and PLGA materials can be safely implanted into animals for examining functional bone regeneration by the scaffolds.

6 Chapter 6

Characterization of Bone Formation by Natural Polymeric Materials in a Critical Sized Calvarial Defect in Combination with Bone Marrow Stromal Cells

6.1 Introduction

Bone represent one of the most transplanted organ(*5*). About 0.5 million bone grafts are carried out in the U.S. alone, (*6-8*) per annum(*5*). Though using bone from the patient itself (autografting) is considered the golden standard for achieving bone healing, it is restricted by availability and discomfort to the patient. Allografts on the other hand help overcome these limitations, but carry the threat of low remodeling due to excessive processing and possibility of disease transmission(*9*). Hence in bone tissue engineering, biomaterial scaffolds, biological factors and cells used alone or in a combination promises better bone regeneration(*9*). Here, the tissue engineered scaffolds act as a template for regeneration to occur and the properties of the biomaterial can dictate the nature of bone regeneration achieved(*33*).

It is well known that the scaffold properties such as hydrophilicity(*34*), morphology(*35*), porosity, and mechanical properties(*39*) can be used to direct effective bone healing. Both synthetic and natural polymers have been used as scaffold materials for bone regeneration. The most popular polymeric materials used commercially are PLLA and PLGA(*395*). Though synthetic polymers lend themselves to be readily modified to obtain the desired molecular weights and hence gaining control over their mechanical and degradation properties is possible, concerns are raised due to their hydrophobic nature and acidic bulk degradation products that could impact bone formation in the body(*343, 396*). Strategies such as inclusion of hydroxyapatite have given a buffering effect under such conditions(*344*).

Natural polymers such as polysaccharides and proteins on the other hand are synthesized in biological systems like plants, animals and microbes and therefore their structure and chemistry are similar to the ECM macromolecules seen in our body(*442*). Hence these natural polymers offer greater biocompatibility in tissue healing(*335, 345*). Though a number of attempts have been made to include natural polymers with synthetic polymers for bone tissue engineering(*443, 444*), very few materials made of bio-polymers alone have been successful in providing the functions of mechanical competence, porosity and bioactivity(*445*). We were successful in developing a natural polymeric platform that combined mechanical competence(*352*) with bioactivity(*391*). For example, collagen(*346, 347*), chitosan(*345*), polysaccharide(*348*) and protein based scaffolds are often presented in the form of porous sponges, fiber matrices or hydrogels. These scaffolds lack the mechanical stability and require chemical crosslinking to produce stable scaffolds. During scaffold fabrication, extensive processing and cross-linking compromises the biological functionality of these scaffolds(*349-351*). We followed a two-pronged approach by having a mechanically competent sintered microsphere 3D- porous base structure made of cellulose acetate (CA), further functionalized with self-assembled nanofibrillar collagen (CAc)(*352, 391*).

Often times, the inclusion of factors or stem cells is needed to achieve complete tissue regeneration and the biomaterial scaffold acts as a delivery vehicle(*330*). In this context, while the delivery of growth factors such as BMPs have had mixed outcome such as bone formation in non-target regions(*446, 447*), a clinically viable alternative is the use of patient derived bone marrow stromal cells (BMSCs)(*448-450*). The scaffold used to deliver the cells also acts as an instructive temporary ECM to control and direct the survival(*451*), proliferation(*452*) and differentiation(*421*) of the stem cells(*453, 454*) and ultimately dictated the quality of regenerated

bone(*455*). Hence the mechanical(*422*), pore properties(*456, 457*), chemical functionalities(*37, 413*), topographical(*39*) and nanoscale(*39, 379*) features can all influence osteogenic differentiation of BMSCs. Most of these studies however do not examine the role of these material characteristics towards regeneration *in vivo* when combined with BMSCs. It is extremely critical to understand the behavior of materials with superior physicochemical properties in the body to formulate scaffolds with potential use in human bone regeneration applications.

In this study, we compare the performance of a natural polymer based CA and (CAc) scaffolds(*352, 391*) along with the synthetic polymeric (PLGA) scaffold(*458, 459*), in terms of their ability to heal a critical sized bone defect in a two hole (bilateral) calvarial mouse model. In the first set of studies, cellulosic- CA, CAc and synthetic- PLGA 3 D-porous materials alone were implanted into the bilateral calvarial defects in mice. In the second set of studies, BMSCs from donor mice were seeded at equal numbers on to each of the matrices and implanted into the calvaria of mice.

It was hypothesized that the natural polymers may act as a better matrix for cellular infiltration, by offering greater biocompatibility. We also hypothesized that the natural polymers (CA, CAc) materials may offer a more osteoinductive environment towards the seeded BMSCs and lead to better quality of bone formation in a critical-sized defect. The bone formation was monitored at 8 weeks after implantation to determine the ability of scaffold alone in inducing bone formation and in combination with seeded BMSCs. The BMSCs from the host mice had a green fluorescent collagen reporter gene, as they became osteoblasts and the donor mice had BMSCs that had a cyan fluorescent collagen reporter gene if they became osteoblasts. Hence this tool helped us

identify the probable origin of bone formation in the materials seeded with BMSCs based on blue/ green fluorescence.

6.2 Materials and Methods

6.2.1 Materials

Cellulose acetate (Mw: 30K) (CA), and Polyvinyl Alcohol (30,000-70,000) (PVA) were procured from Sigma -Aldrich (St. Louis, MO, USA). Poly (lactic-co-glycolic acid) 85:15 (PLGA) was purchased from lakeshore biomaterials (Birmingham, USA). Acetone, Dichloromethane, Cyclohaxane, Paraformaldehyde and Gluteraldehyde were purchased from Fisher Scientific (Fair Lawn, NJ, USA).

6.2.2 Preparation of microspheres

Oil in water solvent- evaporation, followed by sintering of formed microspheres using a solvent/non-solvent mixture was used for producing microsphere of i) Cellulose acetate (CA), ii) poly (lactic-co-glycolic acid) 85:15 (PLGA). In brief, 13 (w/v) % of CA polymer was dissolved in a solvent mixture containing methylene chloride and acetone at a ratio of 9:1 to produce microspheres. A 20 (w/v) % solution in methylene chloride was used in the case of PLGA polymer to produce the microspheres. The polymer solutions were then poured in a thin stream into an aqueous media containing 1.25(w/v) % PVA as a surfactant, with constant stirring at 250rpm to form an oil-in-water emulsion. These suspensions were stirred overnight to evaporate the solvent to obtain hardened microspheres. Isolated microspheres were washed repeatedly with deionized (DI) water, dried, and sieved into different microsphere sizes. Microspheres in the size range of 200- 425μm were sintered into micro porous scaffolds using either solvent-non-solvent or heat sintering based on the polymer(*352, 391*).

6.2.3 Preparation of micro-porous sintered 3D microsphere scaffolds

Metal molds were filled with CA microspheres to which a 200μL volume of an optimized solvent/non-solvent composition, acetone: cyclohexane in the ratio of 3:1 (v/v), was added to

cover the microspheres. Solvent was allowed to evaporate at room temperature to obtain sintered microsphere scaffolds. Cylindrical scaffolds measuring 3.5mm diameter X 1mm height were used for implantation into mouse calvaria. The control PLGA micro porous scaffolds with identical micro-particle sizes were produced by heat sintering at 95^{o}C for 45 minutes using Teflon molds(*352*).

6.2.4 Preparation of collagen naonfiber infused cellulose 3D microporous scaffolds

A modified biomimetic approach was used to functionalize micro porous scaffolds with type I collagen. In brief, both control and test scaffolds were incubated in a 0.1 (w/v) % collagen type I solution with a pH adjusted to 4.2 at 37°C for 7 days to promote molecular collagen self-assembly. The dried scaffolds were treated with UV light for 30 min each side to achieve collagen nanofiber stability and washed repeatedly with DI water to remove buffer salts. Microspheres in the size range of 200-425µm diameters were sintered and infused with self-assembled collagen and used in this study (*391*).

6.2.5 Characterization of internal structure of scaffolds by SEM

Scanning electron microscopy (SEM) was used to characterize scaffold morphology and evaluate collagen fiber diameter and distribution. Scaffolds were sputter coated with Au/Pd using a Polaron E5100 sputtering system (Quorum Technologies, East Sussex, UK) to achieve an eighteen nanometer thick coating before viewing under SEM. The samples were viewed using FEI Nova NanoSEM 450 scanning electron microscope (FEI, Hillsboro, OR, USA) operated at an accelerating voltage of 2kV at various magnifications.

6.2.6 Design of calvarial implantation studies

The Institutional Animal Care and Use Committee (IACUC) at The University of Connecticut Health Center approved all procedures for animal use and all efforts were made to minimize animal suffering. 10-12 week old CD-1 wild type female mice, weighing 26-32 g were used for implantation of the scaffolds alone. The10-12 week old male transgenic mice, weighing 25-30 g used as hosts for implantation had a green fluorescence in their osteoblasts as the expression of EGFP is driven by a 3.6 kb fragment of collagen 1 promotor (Col 3.6- TPZ mice- host)(*460*). These host mice were NOD SCID and gama irradiated (NSG) to facilitate the immune acceptance of donor cells. The transgenic mice used to obtain the bone marrow stromal cells (BMSCs) to seed the scaffolds before implantation had blue fluorescence in their osteoblasts as the expression of CFP is driven by a 3.6 kb fragment of collagen 1 promotor (Col 3.6 –Cyan mice- donor)(*460, 461*). Thus the BMSCs from donor mice becoming osteoblasts fluoresce blue, while the BMSCs becoming osteoblasts fluoresce green. Thus the fluorescent reporters acted as a tool to determine the quantity of active osteoblasts formed by the donor cells and the host cells. Critical sized calvarial defects (3.5 mm diameter) were created on both the sides of the calvarium of mice and a scaffold of 3.5mm diameter X 1mm height was implanted into each of the defects. The studies contained 3 groups with control scaffold on the left side and test scaffold on the right side as given by Figure 6.2 A. In the study using no cells, six samples (n=6) were used, while twenty-four samples (n= 24) were examined in the case of studies where the scaffolds were seeded with donor cells. Each scaffold was sterilized by soaking in 70% ethanol followed by UV treatment on both the sides for 20-minutes per side. They were then washed with sterile PBS and either directly implanted (study1) or implanted after seeding donor cells as described below (study 2). Each scaffold was seeded by immersion into 1 $X10^6$ BMSCs cultured to confluence

and spun down into a pellet prior to transplantation(*462*). The samples were retrieved at 8 weeks for radiological and histological examination.

6.2.7 BMSC Culture

For experiments where the scaffolds were seeded with cells, donor mice (Col3.6- Cyan) of 6-8 weeks of age were sacrificed by carbondioxide asphyxiation and sprayed with ethanol to avoid contamination from mouse hair/ skin. The tibia and femur of these mice were isolated and briefly washed with sterile PBS. The bone epiphyses were removed to expose the marrow and then flushed with media. The media was made up by adding 1% Penicillin/ Streptomycin and 10% FBS to α-MEM. The flushed cells were filtered using a 70μm cell strainer and the filtrate was spun down by centrifugation for ten minutes at 350Xg. The pelleted cells were suspended well in the media and plated at a density of 3 X 10^6 cells/cm^2. A fifty percent media removal and replacement was completed at day 4 of plating and a hundred percent removal and replacement of media was done after 7 days of culture. Once the cells reached confluency by day 10, they were lifted with Trypsin EDTA (2.5%) solution and suspended in media with serum to achieve a cellular concentration of 1X10^6 cells/mL of media(*463*).

6.2.8 Calvarial surgery

A combination of Ketamine (135 mg/kg) and Xylazine (15 mg/kg) was administered (I.P.) were used to anesthetize the mice (CD-1 wild type mice for implantation of scaffold alone and 3.6col-TPZ mice in the case of experiments with BMSC seeded scaffolds), for the surgical implantation of the scaffolds. A clipper was used to cleanse the area and followed by topical application of 70% ethanol to removed hairs on their heads and clean the surface for the surgery. The mice heads were dissected with a clean incision to reach the cranium. A 3.5mm critical sized defect was made on each side of the cranium using a drill bit, making sure that the underlying dura

matter was not damaged. A two-hole mouse calvarial model was used and the scaffolds were placed into theses defects as per the study design (Figure 6.2 B). In the case of the cell-seeded scaffolds, the BMSCs were spun down for a minute at 10,000Xg and the pellet was seeded onto the scaffolds by immersion of the scaffold until all the cells in the pellet got onto the material. Thus each scaffold received $1X10^6$ cells (Col3.6- Cyan), in the case of the cell seeded scaffold implantation experiments. Hence each mouse received two implants on either side of their calvaria(*454*).

6.2.9 Sample harvest

The animals were sacrificed using carbon dioxide asphyxiation followed by cervical dislocation at 8 weeks post implantation of the scaffolds. An alizarin red injection (30mg/kg body weight, I.P.) was administered 24hours prior to sacrifice of the animals in order to label the newly formed bone(*463*). The skulls of the mice were dissected, washed in PBS at pH 7.4 and fixed using 10% buffered formalin for 4 days. An X-ray cabinet (Faxitron LX-60) was used for digital X-ray capture at a 43 magnification (6 s at 26 kVp). The samples were then cryosectioned for histological and immunostaining. The fixed samples were washed in PBS at pH 7.4 and transferred to 30% sucrose solution in PBS at pH 7.4 for a day. The tissue was embedded in Shandon Cryomatrix-TM placed in cryo-molds by flash freezing on dry ice. The frozen sections were stored in -20°C until sectioning. Leica CM3050S cryostat (Leica, Wetzlar) was used for obtaining 10µm thick sections of the embedded samples by employing the tape transfer technique (Cryofilm type IIC (10), Section-Lab Co. Ltd.)(*464*) The samples were imaged for mineral content (DIC- white) and new bone formation (red) in the case of unseeded scaffolds. In the case of cell seeded implants, the mineral content (white), Alizarin Complexone label (AC-red) for new bone formation, donor cells (cyan), and host cells (green) were imaged using dark

field and fluorescent microscope. Serial sections were used for immunostaining for bone sialoprotein (BSP) and Collagen (Coll1). Another set of histological sections was serially stained for alkaline phosphatase and DAPI (AP/ DAPI) to determine osteogenic activity and cellularity, and tartrate resistant acid phosphatase (TRAP) activity to determine bone resorbing osteoclastic activity. A Zeiss Axio Scan.Z1 (Carl Zeiss MicroImaging Inc.) was used to details from 4-100X magnifications. The excitation (Ex) and emission (Em) filters used were as follows: AC: Ex-545/25, Em-605/70; Col3.6TPZ: Ex- 500/20, Em-535/30; Col3.6ECFP: Ex-436/20, Em-480/40; TRAP: Ex-405/440, Em-550/560; AP: Ex-640/630, Em-690/650; Col: Ex-650/590, Em-738/663; BSP: Ex- 556/513, Em- 613/570.

6.2.10 Histomorphometric analysis of calvarial implants

In the case of unseeded scaffolds n=3 from each group were analyzed and in the case of cell seeded scaffolds n=7 was used for CA, n=7 was used for CAc and n=6 for PLGA. Some samples were eliminated due to sample slippage from defect. The image analysis was done using Fiji (NIH software). Each individual channel was used and converted into an 8-bit image. Each of these images was appropriately thresholded to quantify the signal and eliminate the noise.

6.3 Results

6.3.1 Scaffold Morphology

The 3D porous scaffolds of PLGA were golden in color (**Figure 6.1A**), while the CA (**Figure 6.1B**) and CAc (**Figure 6.1C**) were opaque and white in color. Under higher magnification, with scanning electron microscope (SEM), the PLGA 3D porous materials (**Figure 6.1 D, G, J**) showed a smooth morphology (arrows). On the other hand the morphology presented by CAc (**Figure 6.1 E, H, K**) showed many undulations on the surface (arrows). The collagen nanofibers were present on the CA microspheres in CAc (**Figure 6.1 F, I, L**). The collagen fibers formed a coating on the microsphere without accumulating at the pores of the material (arrows).

6.3.2 Radiological examination of bone formation with scaffolds alone and scaffolds along with BMSCs

The animals were sacrificed and the whole calvaria were dissected out after 8 weeks of implantation (**Figure 6.3- A, B, C** in the case of unseeded scaffolds and **Figure 6.4A- 1,2,3** in the case of scaffolds seeded with BMSCs) and examined by X-ray to evaluate the amount of bone formation in the materials. The radioopacity of the tissue formed in the case of implants alone was very low, and mostly represented a background signal only (**Figure 6.3- D, E and F**). This did not represent a significant amount of bone formation by the materials in the absence of cells. However, when the materials were seeded with $1X10^6$ BMSCs from donor mice, the scaffolds showed bone formation (**Figure 6.4A- 4, 5, 6**). While all the materials showed bone formation in the presence of BMSCs, on quantifying the radioopacity in each material group, the amount of bone formed with CA and CAc was twice as much as what was observed with PLGA (**Figure 6.4B**). This difference was statistically very significant ($P< 0.001$).

6.3.3 Histological analysis of implantation of scaffolds alone

The bone formation was not very high when the materials alone were implanted into calvarial defect and examined after 8 weeks of implantation (Top row -DIC in **Figure 6.5**, and supplemental **Figures 6.13, 6.14**). There was not much robust mineral deposition (Top row –AC red label in **Figure 6.5**, and supplemental **Figures 6.13, 6.14**). This was indicative of low degrees of bone mineral deposition. The materials showed presence of cells in their interior along (Middle row –DAPI Blue stain in **Figure 6.5**, and supplemental figures **6.13, 6.14**) with robust alkaline phosphatase activity, indicative of osteoblastic activity (Middle row –AP Red stain label in **Figure 6.5**, and supplemental figures **6.13, 6.14**). However, the PLGA scaffolds had most of the cellularity (DAPI- blue) and osteoblastic activity (AP- red) confined to the periphery of the implant (Middle rows: **Figure 6.13**, Inset **C**; **Figure 6.5**, Inset **C)**. On the other hand the cellularity (DAPI- blue) and osteoblastic activity (AP- red) were seen well inside the scaffold interior and were more evenly distributed in the case of CA (Middle rows: **Figure 6.13**, Inset **D**; **Figure 6.14**, Inset **C**) and CAc (Middle rows: **Figure 6.5**, Inset **D**; **Figure 6.14**, Inset **D**). Finally, the osteoclastic activity was also seen better distributed in CA (Final rows: **Figure 6.13**, Inset **F**; **Figure 6.14**, Inset **F**) and CAc (Final rows: **Figure 6.5**, Inset **F**; **Figure 6.14**, Inset **F**) than in PLGA (Final rows: **Figure 6.13**, Inset **E**; **Figure 6.5**, Inset **E**). Therefore, though the materials alone could not facilitate proper bone formation in the defects by themselves, the cellularization, osteoblastic and osteoclastic cellular activity in the case of PLGA were confined mostly to the periphery of the materials. In the case of CA and CAc, a well-distributed cellularity, along with uniformly spread osteoblast and osteoclast activity was seen. There was no significant difference between the test and the control materials in the quantity of cells or the osteoblast and osteoclast activity. Therefore the materials alone did not lead to appreciable bone

formation, but in the presence of BMSCs the bone formed in the test CA and CAc groups was twice that formed in PLGA

6.3.4 ECM protein deposition by scaffolds and BMSCs

The collagen I (Coll I) and bone sialoprotein (BSP) content of scaffolds loaded with BMSCs was evaluated by immunostaining (Coll I- yellow, BSP- red). Both Coll I and BSP were found in all the sections. The BSP content was similar between the groups (Bottom row and top row: **Figure 6.15, Figure 6.6, Figure 6.16** and **Figure 6.7A**). The distribution of collagen was confined to certain areas in the case of PLGA and a continuous collagenous ECM was absent. Therefore though collagen was present it did not bridge the defect well in the case of PLGA (**Figure 6.15- A, C; Figure 6.6- A, C**). However, the distribution of collagen was more

uniform throughout the matrix in the case of CA (**Figure 6.15- B, D; Figure 6.16- A, C**) and CAc (**Figure 6.6- B, D; Figure 6.16- B, D**). The intensity of the signal, when contrasted to the host bone was weaker in the case of PLGA (**Figure 6.15- A, C; Figure 6.6- A, C** vs the central insets in the rows). The intensity of collagen signal was comparable to host bone in the case of CA (**Figure 6.15- B, D; Figure 6.16- A**, C vs the central inset in the rows) and CAc (**Figure 6.6- B, D; Figure 6.16- B, D** vs the central insets in the rows). Quantitatively, the collagen content of CA and CAc was almost twice as much as the collagen presented by the regenerated tissue in PLGA (**Figure 6.7B**). The difference was very significant. All scaffolds seeded with BMSCs showed bone formation (DIC signal in **Figure 6.17, Figure 6.8, and Figure 6.18**) and new mineral deposition (AC- red signal in **Figure 6.17, Figure 6.8, and Figure 6.18**). Bone formation was confined to certain regions of the material in the case PLGA (**Figure 6.17- A, C, E, G; Figure 8- A, C, E, G**), with minimal closure of the defect at the interphase of calvarium and the dura of the mice.

On the other hand the bone formation was well distributed and a good bone bridge was formed at the interphase of the calvarium and dura in the case of CA (**Figure 6.17- B, D, F, H; Figure 6.18- A, C, E, G**) and CAc (**Figure 6.8- B, D, F, H**). Quantitatively, the bone area on CA and CAc was approximately twice that seen in PLGA implants (**Figure 6.9A**). However the quantity of bone mineral deposition (**Figure 6.9B**), donor cells (**Figure 6.9C**) and host cells (**Figure 6.9C**) in all the groups was no significantly different. In all the groups, the Col3.6- Cyan (donor) cells presented greater intensity than the Col3.6- Tpz (host cells).The donor cells also presented better merger with the AC (red), new mineral signal (smaller insets in each of the insets of **Figure 6.17, Figure 6.8**, and **Figure 6.18**).

6.3.5 Osteoblastic and osteoclastic activity in scaffolds seeded with BMSCs

The cellular content (DAPI- blue) of the scaffolds was similar between PLGA, CA and CAc (Lowest panel: **Figure 6.19, Figure 6.10, Figure 6.20, and Figure 6.12A**). The AP (red) content was also similar between the groups (Middle panel: **Figure 6.19, Figure 6.10, Figure 6.20**, and **Figure 6.12B**). However, the distribution was more uniform and a continuous layer of cells with active AP content was seen in the case of CA and CAc. The PLGA materials showed cell (DAPI) and AP distribution more in certain pockets than in the other parts of the material. There was also a lack of continuous tissue (**Figure 6.19- E, A; Figure 6.10- E, A**) and osteoblastic AP activity at the interphase of the cranium and dura in the PLGA implants (**Figure 6.19- C, A; Figure 6.10- C, A**), while a good degree of tissue and ostoblastic activity was seen in analogous regions of CA (**Figure 6.19- D, B; Figure 6.20- C, A**) and CAc (**Figure 6.10- D, B; Figure 6.20- D, B**) Though the osteoclastic bone resorption was not different between all the groups (**Figure 6.12 C**), the distribution of osteoclast activity, as given by TRAP staining was more homogenous with

CA (**Figure 6.21- B, C**) and CAc (**Figure 6.11B, Figure 6.21D**), than with PLGA (**Figure 6.11A, Figure 6.21A**)

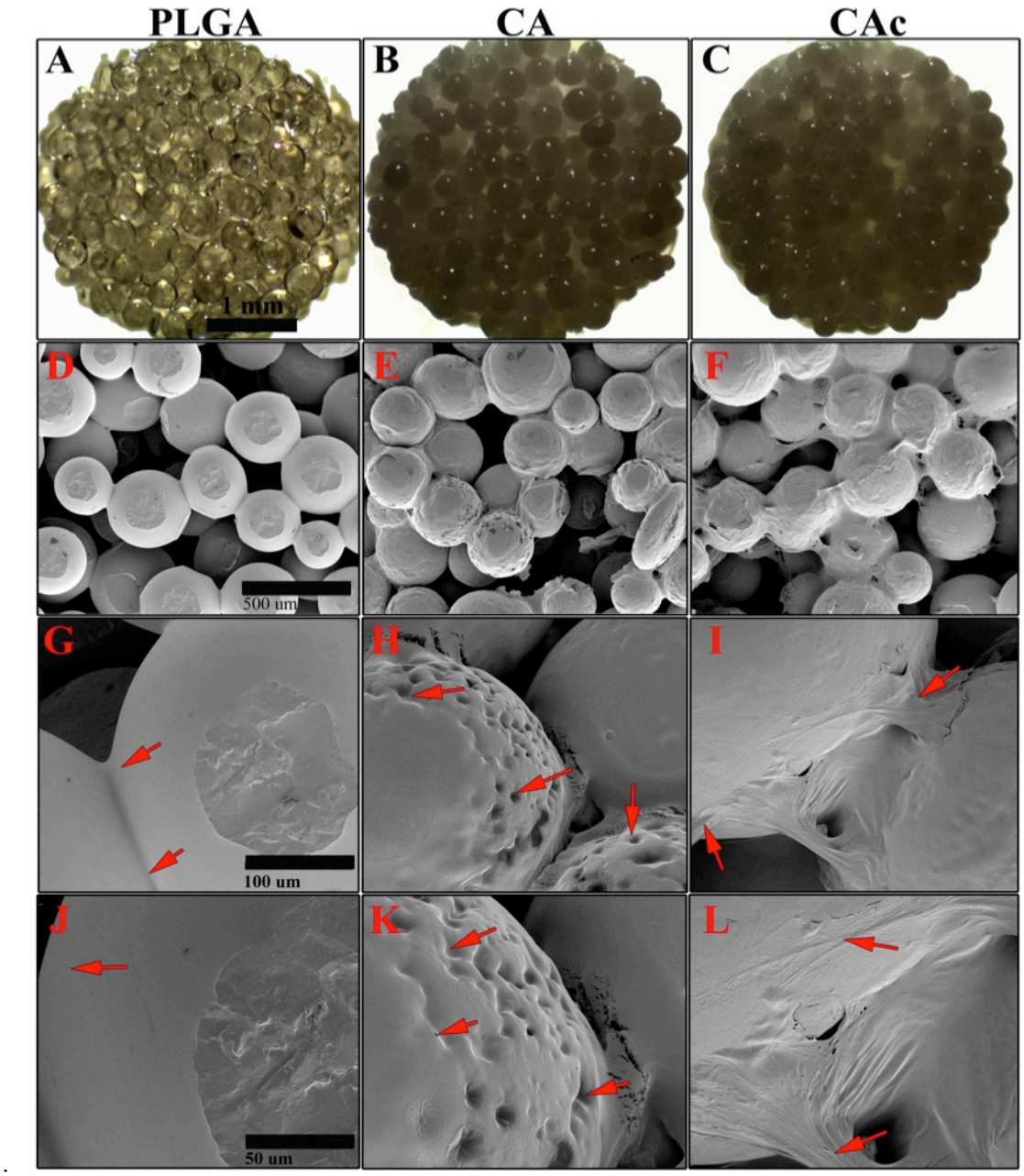

Figure 6.1 Morphology of scaffold

Examination of scaffold structure. Photographic images of 3D microporous scaffolds used (A) PLGA, (B) CA, (C) CAc, scale bar= 1mm; SEM images at 100X magnification (D) PLGA, (E) CA, (F) CAc, scale bar= 500µm; SEM images at 500X magnification (G) PLGA, (H) CA, (I) CAc, scale bar= 100µm; SEM images at 1000X magnification (J) PLGA, (K) CA, (L) CAc, scale bar= 50µm.

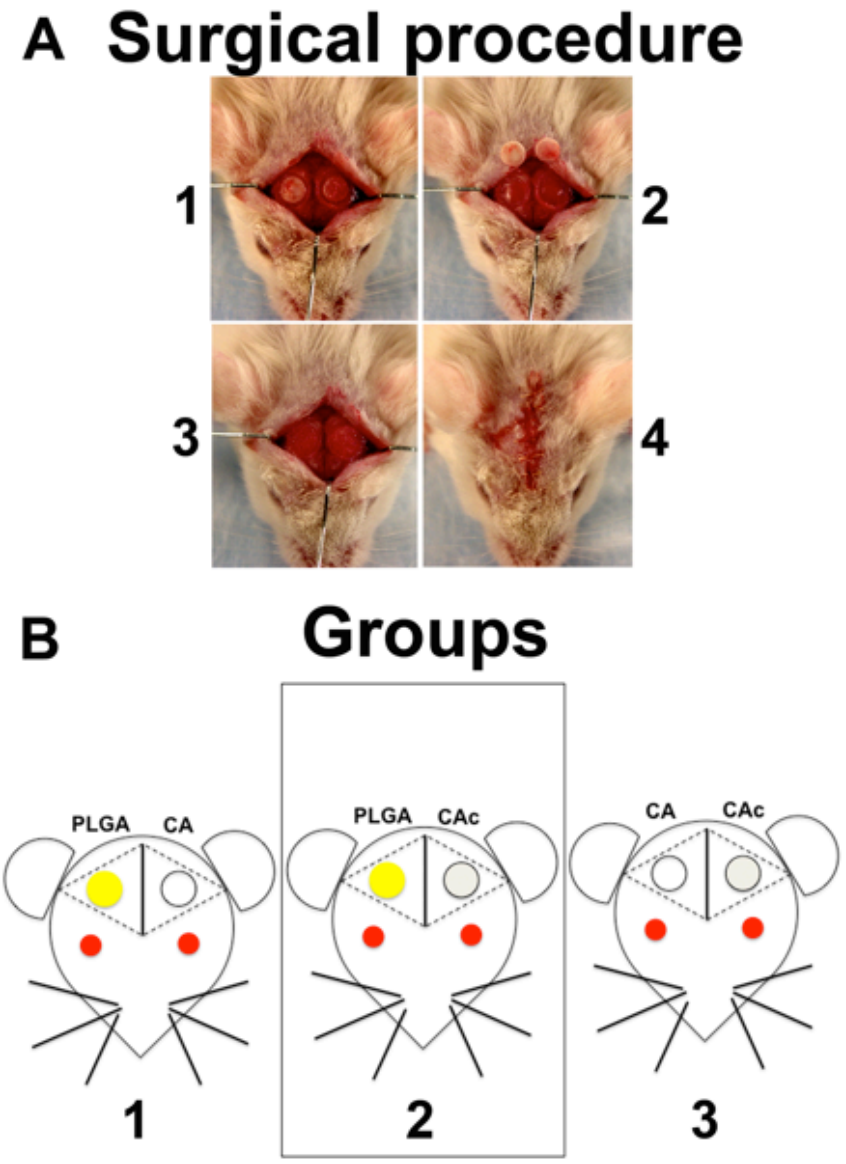

Figure 6.2 Calvarial Surgery and scaffold groups implanted

Surgical procedure and schematic of the study groups. (A) Steps in the surgical implantation: (1) Creation of two circular 3.5mm defects on the two sides of mouse calvaria, (2) removal of calvarial bone, (3) Implantation of the scaffolds into the defects, (4) Closure of the implants by suturing the skin. (B) Groups 1: left side defect was filled with PLGA and the right side defect with CA, group 2: left side defect was filled with PLGA and the right side was filled with CAc, group 3: left side was filled with CA and the right side was filled with CAc. In study 1, the materials alone were used. In study 2, $1X10^6$ Col3.6- Cyan BMSCs from donor mice were seeded on to each scaffold before implantation into host mice with Col3.6- Tpz BMSCs.

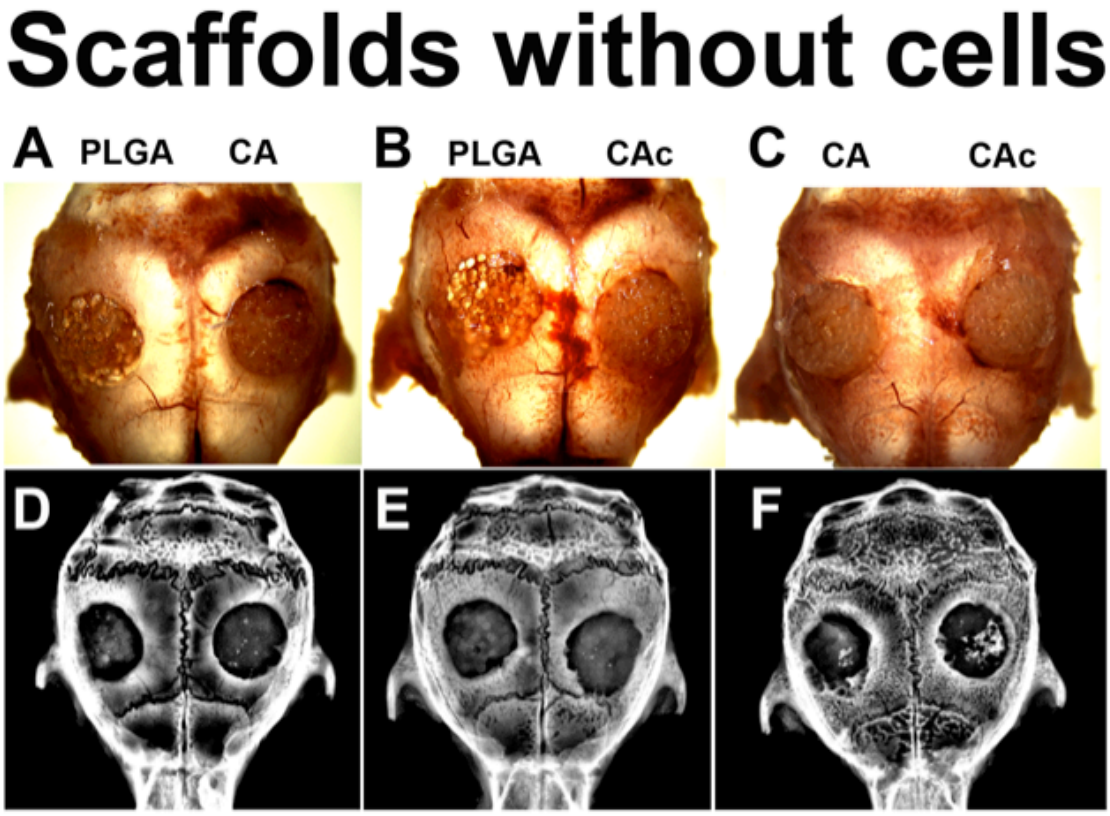

Figure 6.3 Calvarial impants with material only

Whole calvaria and X- ray radiograph of defects implanted with scaffolds alone. Whole calvarial mount of (A) group 1- PLGA vs CA, (B) group 2- PLGA vs CAc, (C) group 3- CA vs CAc.; X-ray radiographs of (D) group 1- PLGA vs CA, (E) group 2- PLGA vs CAc, (F) group 3- CA vs CAc.

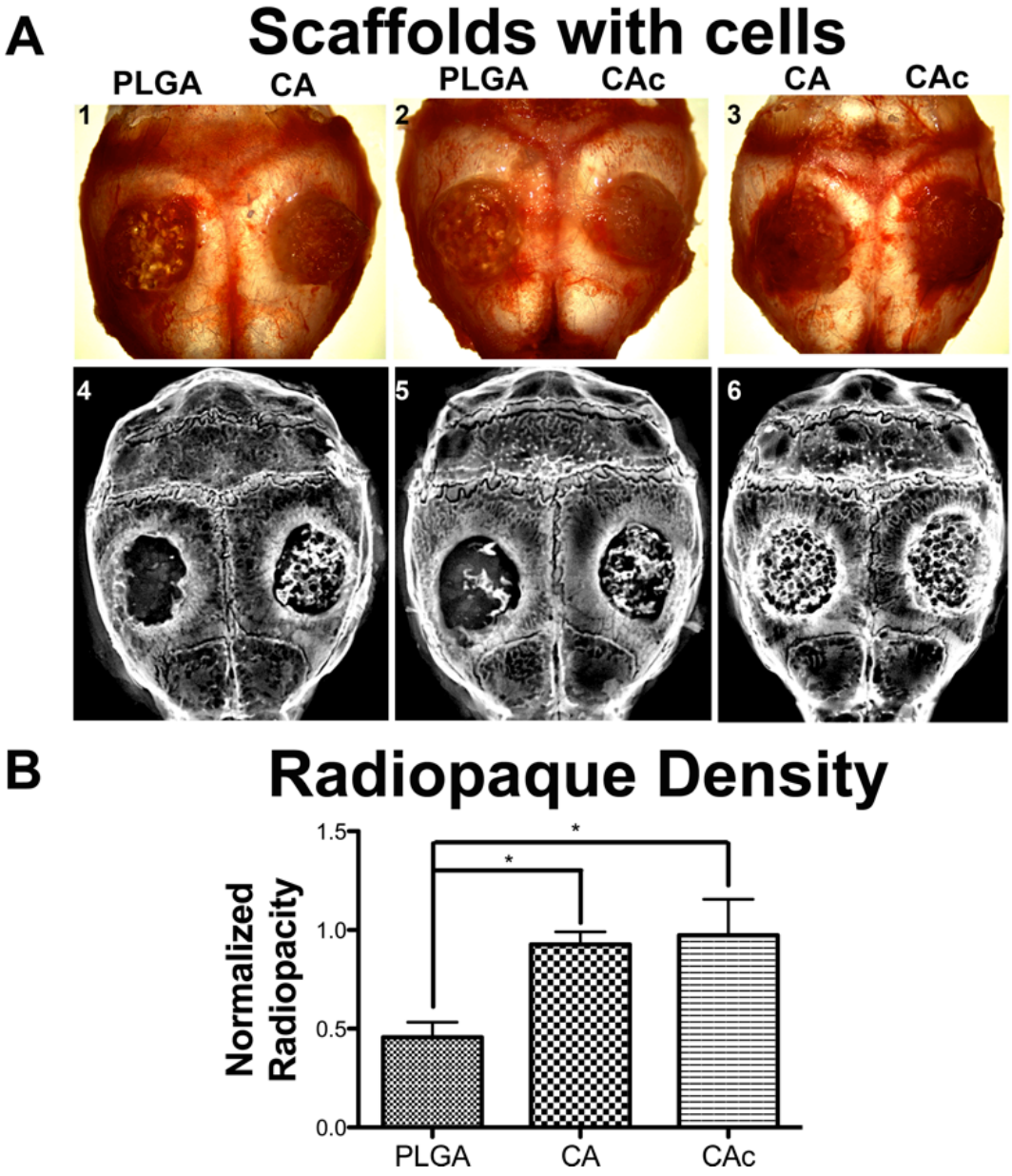

Figure 6.4 Calvarial implants with materials and donor cells

Whole calvaria and X- ray radiograph of defects implanted with scaffolds and cells. (A) Top panel: 1. Group 1- PLGA vs CA, 2. Group 2- PLGA vs CAc, 3. Group 3- CA vs CAc.; X-ray radiographs of 4. Group 1- PLGA vs CA, 5. Group 2- PLGA vs CAc, 6. Group 3- CA vs CAc. (B) Quantitative radio opacity of defect area normalized to radio opacity of host bone, both measured per unit area; PLGA, n=6; CA, n=6; CAc, n=7. One way ANOVA with Tukey post-test with 95% confidence interval, $^{*}P<0.001$, $^{\#}P<0.01$, $^{@}P<0.05$.

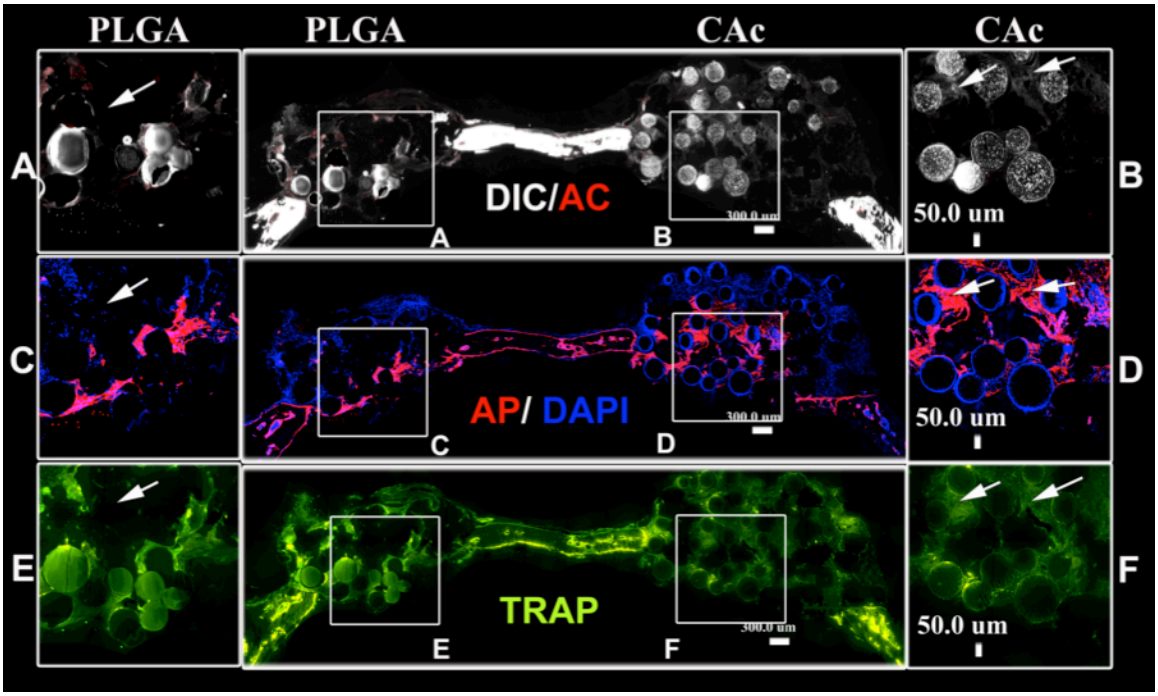

Figure 6.5 Histological sections of scaffolds without cells (Group 2)

Cell infiltration and bone forming/resorbing activity with implantation of scaffolds alone into calvarial defects. Flourescent histological cross sectional images of calvaria implanted with material alone at 8 weeks, Group 2: PLGA vs CAc, Top row: DIC- Differential interference channel image with AC- red labeled alizarin complexon marking new mineral deposition (PLGA inset A, CAc inset B); Middle row: AP- Alkaline phosphatase activity for osteoblastic activity with DAPI- cell nuclei (PLGA inset C, CAc inset D). Lowest row: TRAP- Tartrate-resistant acid phosphatase staining as a marker of osteoclastic activity (PLGA inset E, CAc inset F).

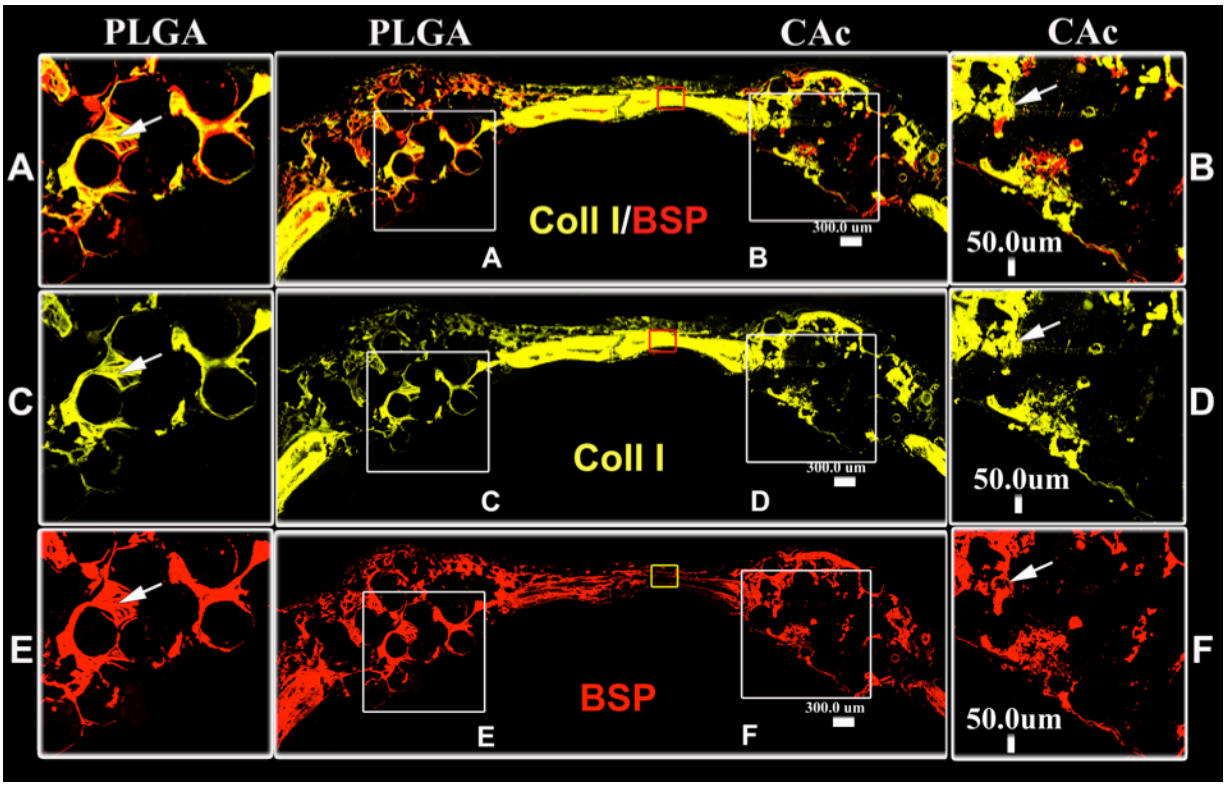

Figure 6.6 ECM markers immunostained on cell seeded scaffolds (Group 2)
Immunofluorescently stained (ECM proteins: Coll1-Collagen1/ Bone sialoprotein- BSP) histological cross sectional images of calvaria implanted with material and BMSCs at 8 weeks, Group 2: PLGA vs CAc, Top row: Coll1- yellow, BSP- red (PLGA inset A, CAc inset B); Middle row: Coll1- yellow (PLGA inset C, CAc inset D). Lowest row: BSP- red (PLGA inset E, CAc inset F).

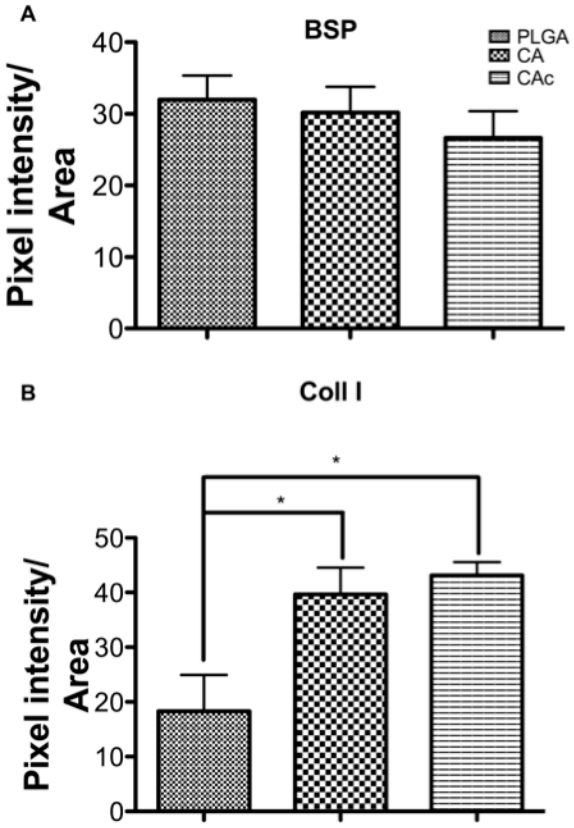

Figure 6.7 ECM protein content on seeded implants

Quantification of pixel intensity of signal normalized to the defect area (A) BSP- Bone sialoprotein (red in Figure 6.6), (B) Coll 1- Collagen 1 (yellow in Figure 6). One way ANOVA with Tukey posttest with 95% confidence intervals, $^{*}P<0.001$, $^{\#}P<0.01$, $^{@}P<0.05$.

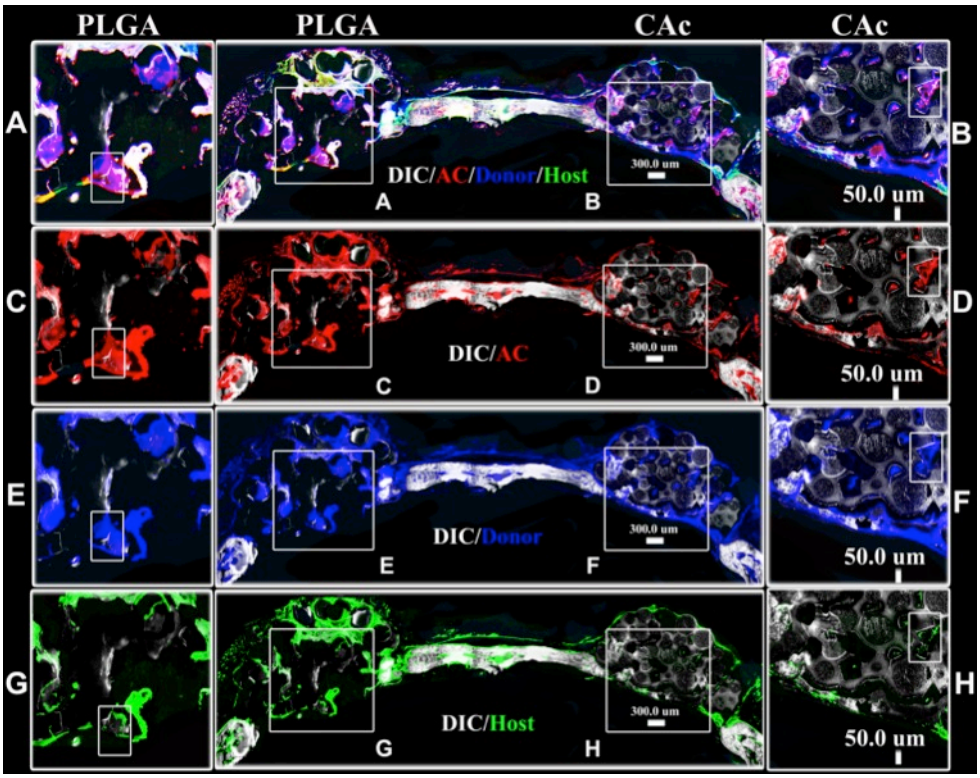

Figure 6.8 Stained histological sections of cell seeded scaffolds (Group 2)
Flourescent histological cross sectional images of calvaria implanted with material and BMSCs at 8 weeks, Group 2: PLGA vs CAc, Top row: DIC- Differential interference channel image to visualize bone and microspheres with AC- red labeled alizarin complexon marking new mineral deposition, Donor cells- Col3.6- Cyan (blue), Host cells- Col3.6-Tpz (green) (PLGA inset A, CAc inset B); Second row: DIC- Differential interference channel image to visualize bone and microspheres with AC- red labeled alizarin complexon marking new mineral deposition (PLGA inset C, CAc inset D). Third row: DIC- Differential interference channel image to visualize bone and microspheres with Donor cells- Col3.6- Cyan (blue) (PLGA inset E, CAc inset F). Fourth row: DIC- Differential interference channel image to visualize bone and microspheres with Host cells- Col3.6-Tpz (green) (PLGA inset G, CAc inset H). Mineral deposition, host and donor cell participation in bone formation by materials along with BMSCs

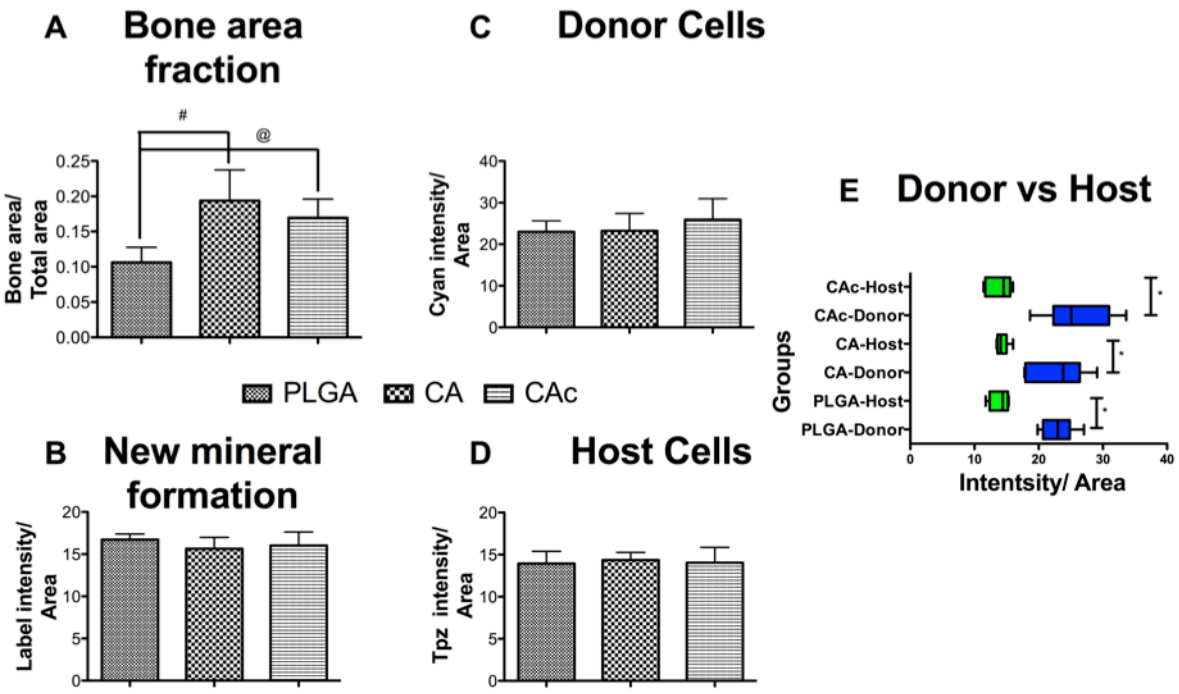

Figure 6.9 Quantification of bone formation, host and donor cells

Quantification of pixel intensity of signal normalized to area of defect (A) Bone area fraction- DIC quantification, (B) New mineral formation- AC quantification, (C) Donor cells- Col3.6-Cyan quantification, (D) Host cells- Col3.6-Tpz quantification, (E) Host (Green bars) and Donor (Blue bars) cells in each scaffold group. One way ANOVA with Tukey post-test with 95% confidence intervals, $^{*}P<0.001$, $^{\#}P<0.01$, $^{@}P<0.05$.

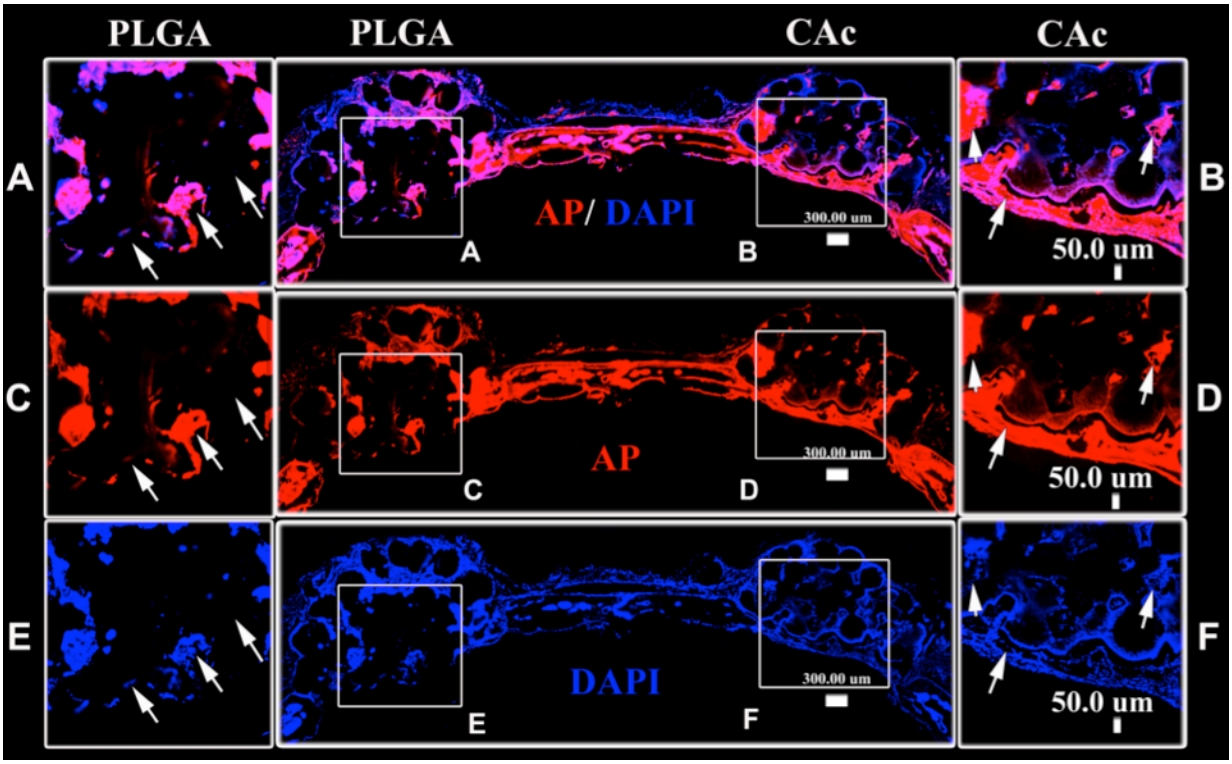

Figure 6.10 Osteoblastic activity on cell seeded scaffolds (Group 2)
Flourescent histological cross sectional images of calvaria implanted with material and BMSCs at 8 weeks, Group 2: PLGA vs CAc, Top row: AP for osteoblastic activity - red, DAPI for cell nuclei- blue (PLGA inset A, CAc inset B); Middle row: AP for osteoblastic activity- red (PLGA inset C, CAc inset D). Lowest row: DAPI for cell nuclei- blue (PLGA inset E, CAc inset F).

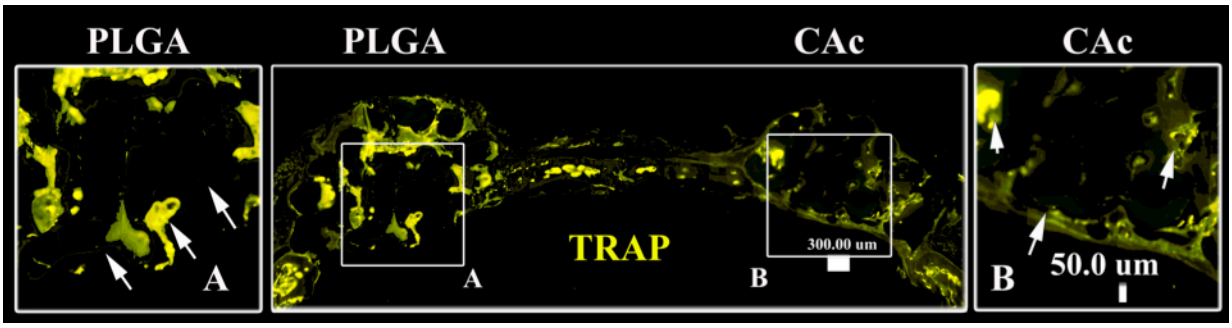

Figure 6.11 Osteoclastic activity on cell seeded scaffolds (Group2)
Flourescent histological cross sectional images of calvaria implanted with material and BMSCs at 8 weeks, Group 2: PLGA vs CAc, TRAP- Tartrate-resistant acid phosphatase staining as a marker of osteoclastic activity (PLGA inset A, CAc inset B).

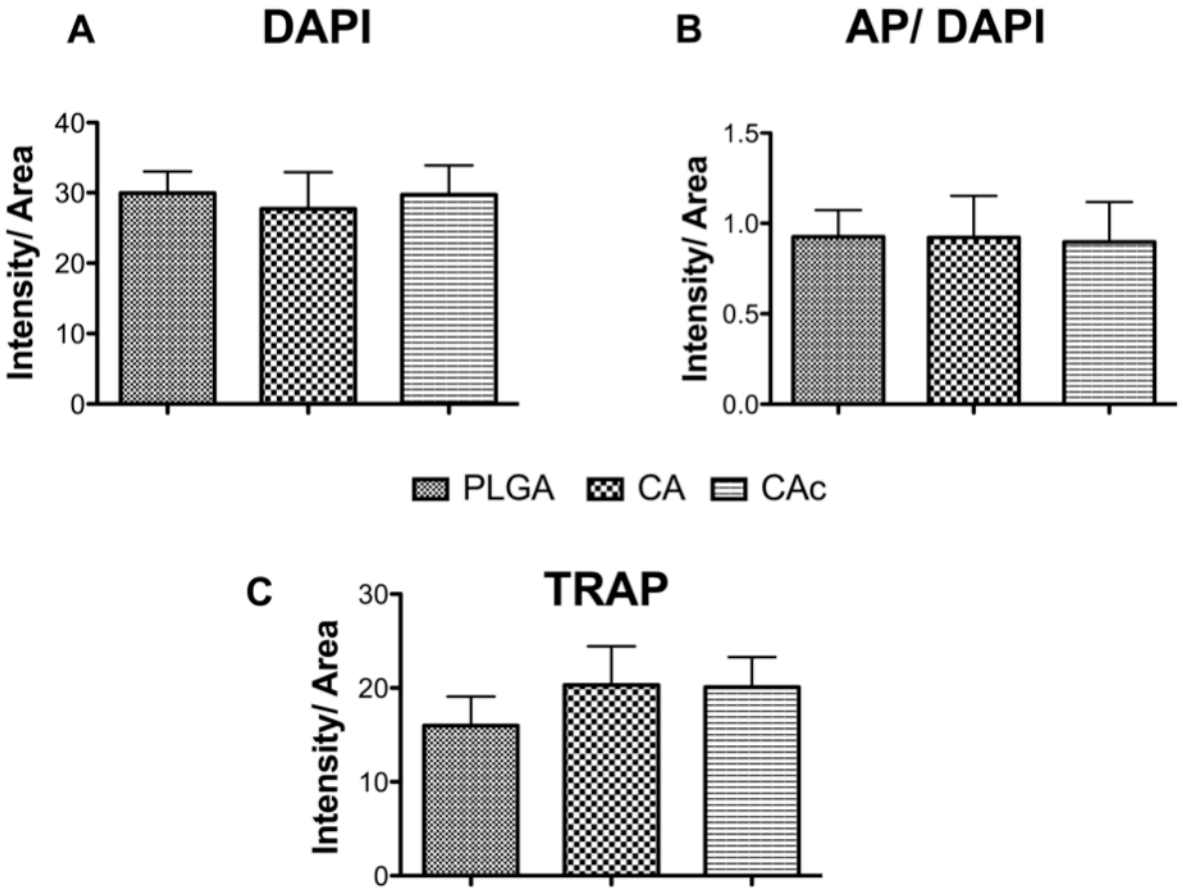

Figure 6.12 Quantification of osteoblastic and osteoclastic activity on seeded implants
Quantification of pixel intensity of signal normalized to area of defect (A)DAPI- cells, (B) AP/DAPI- osteoblastic activity, (C) TRAP- osteoclastic activity. One way ANOVA with Tukey post-test with 95% confidence intervals, $^{*}P<0.001$, $^{\#}P<0.01$, $^{@}P<0.05$.

6.4 Discussion

Scaffold based bone tissue engineering relies on the ability of this temporary ECM to direct tissue healing in a desirable direction(*40*). Though synthetic polymers are used widely for scaffolding applications, there is a clear need to formulate and characterize the performance of scaffolds made of biopolymers(*442*), such as polysaccharides and proteins, due to their inherently bioactive nature and greater cost effectiveness(*445*). Several attempts have been made to construct completely biopolymeric scaffolds(*457, 465, 466*) and blend of synthetic and natural polymers(*443, 444, 459*). Many of these were not very successful as the materials could not meet the dual goals of providing a mechanically robust support and be bioactive at the same time. For example, collagen(*346, 347*), chitosan(*345*), polysaccharide(*348*) and protein based scaffolds are often presented in the form of porous sponges, fiber matrix or hydrogels. These scaffolds lack the mechanical stability and require chemical crosslinking to produce stable scaffolds. During scaffold fabrication, extensive processing and cross-linking compromises the biological functionality of these scaffolds(*349-351*).

The system developed by us contains a cellulose derivative as the 3D sintered microsphere base, further functionalized by self-assembled collagen nanofibers for greater bioactivity. Additionally, employing BMSCs has become a clinically relevant practice and it is important that the materials used as scaffolds channel progenitor cell differentiation into the tissue type specific lineage(*449, 455*).

Here in the present study, we contrast the performance of two biopolymeric systems (cellulose acetate (CA) and cellulose acetate- collagen (CAc)) with a synthetic polymer- PLGA, both formulated similarly to present a 3D-porous scaffold structure, for their ability to facilitate healing of a critical sized calvarial defect by (a) implantation of the material alone and by (b)

implantation of the materials along with clinically relevant donor derived BMSCs. The morphology of PLGA and CA were markedly different. While PLGA showed very smooth interfaces (**Figure 6.1 G, J**), the CA materials showed many undulations indicative of rough scaffold morphology (**Figure 6.1 H, K**). The nanofibrillar collagen coated the microspheres without obstructing the pores of the scaffold structure (**Figure 6.1 I, L**). Deligianni *et al*., found that rough surfaces were more conducive for attachment and osteoblastic differentiation of BMSCs *in vitro(467)*. Lincks *et al*., also found that Titanium implants with rough surfaces may be better for orthopaedic applications(*468*) and allow for greater osteointegration of the implant. Hence we hypothesized that the natural polymers due to the rough morphology may serve as better matrices to elicit osteoblast and progenitor cell response when implanted in a critical sized defect.

Infiltration of cells into the scaffold interior has been a challenge with tissue engineered scaffolds and often times there is bone formation at the periphery of synthetic scaffolds(*459*) with limited cellularity at the core(*36*), due to constrains of diffusion(*458*) and material degradation product accumulation at the core of the scaffold(*396*). This could explain why Jiang *et al*., saw greater defect bridging in the presence of natural polymeric (chitosan and heparin) blends of PLGA, but only peripheral bone formation was observed with PLGA alone(*459*), when these polymeric scaffolds were implanted in the long bone defect of rabbits.

In the present paper, our results have demonstrated that that the natural polymer based CA and CAc 3D- porous scaffolds show greater tissue infiltration into the interior parts of the scaffold, while most of the cellularity was confined to the periphery in the case of PLGA (**Figures 6.5, 6.13and 6.14**). This could be attributed to higher biocompatible nature(*469*) of the natural polymeric materials in contrast to the synthetic polymers that can accumulate toxic

products(*470*) at their core due to their degradation properties(*471*). However, the materials were incapable of inducing complete healing of the defect by themselves (**Figure 6.3**). These results are in agreement with the observation of Gohil *et al*.(*446*), and Yu *et al*.(*454*), who also did not find considerable bone formation by collagen based materials alone, without the inclusion of growth factors or cells. Hence the CA and CAc materials showed greater tissue infiltration than PLGA, due to the higher biocompatibility of the natural polymeric systems over PLGA.

A simple and clinically feasible method of enhancing bone healing is by the inclusion of patient derived BMSCs along with the biomaterial scaffold(*449*). Therefore, equal numbers of BMSCs were seeded on all the scaffolds. The CA and CAc materials lead to bridging of the defect by bone formation at the interface of dura and the calvarium. This bridging did not occur with PLGA (DIC channel in **Figures 6.8, 6.17, and 6.18**). Moreover, the bone formation (DIC channel) and new mineral deposition (AC- red channel) was confined to specific intensely stained regions of PLGA, while it was well distributed throughout the material in CA and CAc (DIC, and AC-red channels in **Figures 6.8, 6.17, and 6.18**). The fraction of scaffold area covered by bone was significantly higher in the natural polymers (CA and CAc) than PLGA (**Figure 6.9A**). The bone formation as detected by the radio-opacity of the defect by X-ray revealed twice as much bone formation on CA and CAc in comparison to PLGA (**Figure 6.4**). Further, the collagen content and staining intensity were more and well distributed on the CA and CAc materials than PLGA (**Figure 6.6, 6.15 and 6.16**). There was also twice as much collagen produced on the BMSC seeded CA and CAc scaffolds than PLGA (**Figure 6.7B**). Thus the collagen deposited and the bone formed was denser with the CA groups than in PLGA, indicating that the quality of regenerated bone was greater when the natural polymers were used in conjunction with BMSCs than with the synthetic polymer.

PLGA scaffolds have been used in both calvarial(*330*) and long bone defect models(*459*) in literature. Cowan *et al*., employed a calvarial defect model to study the effect of PLGA by itself and after inclusion of appetite for bone formation. When stem cells (adipose derived and BMSCs) were used on these materials, only the apatite coated PLGA led to low levels of bone formation. The inclusion of the apatite may have led to a more conducive pH neutralized system to aid in bone formation by progenitors. Jiang *et al*., saw greater defect bridging in the presence of natural polymeric (chitosan and heparin) blends of PLGA, but only peripheral bone formation was observed with PLGA alone(*459*). The highly hydrophobic and degradative nature of popular synthetic polymeric scaffolds of materials like PLGA may not be as conducive for cell survival in the scaffold interior and hence these scaffolds are less likely to promote as much cellularization as naural polymers like CA. Our results agree well with these observations in literature, indicating that the use of natural polymers like CA with BMSCs may be more beneficial in achieving bone defect healing.

We had coated collagen onto CA (CAc) in the hope of seeing greater regenerative outcomes due to presence of an ECM component of bone(*472, 473*). We had allowed type 1 collagen to self-assemble into nanofibers on the CA microspheres to include a nanofibrillar bone-ECM component to enhance the performance of CA microsphere platform(*391*). We however did not see significant differences at 8 weeks post- implantation between CA and CAc, in terms of quantity or quality of the regenerated bone. This could be due to degradation of collagen from the matrix at an earlier time point. Though the coating may have helped with achieving biocompatibility at an earlier stage of implantation, on a long run there may not be much difference between the collagen coated and uncoated CA 3D porous scaffolds (unpublished

data). Hence a technique to improve the retainment of collagen for prolonged nanofiber bioactivity may be to chemically cross-link the collagen nanofibers(*474*).

When donors BMSCs were used it was also observed that the number of donor cells far exceeded the number of host cells in all the three materials tested (**Figure 6.9 C, D, E**). Though the trends show an increase in both donor and host cell types on CA and CAc, they were not significantly different in number in contrast to PLGA (**Figure 6.9E**). The donor cells (Cyan- blue signal) showed greater degree of localization with the newly deposited mineral (AC- red signal), while a relatively thin layer of host cells (Tpz- Green signal) can be seen in the same regions (Boxed areas of the insets in-**Figures 6.8, 6.17 and 6.18**). Hence the donor BMSCs may have contributed to bone formation directly themselves and indirectly by signaling the host cells to home to the region of injury. The fact that no bone formation or active remodeling occurred in the absence of BMSCs indicated that the donor cells were indispensable for proper bone formation to occur. However the quality of bone formed even in the presence of BMSCs was twice as good on the natural polymers (CA and CAc) than the synthetic polymer (PLGA), in terms of ECM collagen content, area of the defect covered by bone and hence the radio-opaque density of the regenerated bone. Additionally there was a good bone defect closure seen when CA and CAc were used along with BMSCs. Finally the pattern of cellular content, bone formation, osteoblastic (**Figure 6.10, 6.19 and 6.20**) and osteoclastic (**Figure 6.11, 6.21**) activity seem to be focused to specific loci on PLGA in contrast to a more well distributed organization on CA and CAc. Therefore this study indicates that the usage of BMSCs in combination with an osteoconductive 3D- porous natural polymeric matrix such as CA/ CAc can lead to higher quality of bone regeneration than the convention synthetic polymers like PLGA.

Synthetic polymers are known to adsorb many plasma proteins non- specifically due to their hydrophobic nature(*475*). On the other hand polysaccharides such as starch, and cellulose are known for their hydrophilic nature and for lower degrees of non-specific protein adsorption(*476*). Hence Alves *et al*. noted that plasma treatments used to make synthetic polymeric surfaces more hydrophilic and promote cell adhesion did not lead to better cell adhesion on a complete polysaccharide material(*477*). Yunfei *et al*., doped 1- 7% nano-crystalline cellulose onto PLGA. Inclusion of cellulose with PLGA led to increased hydrophilicity of the resulting nanofibers and helped with greater degree of cell adhesion onto the material than pure PLGA(*478*). While a degree of hydrophobicity is essential for protein adsorption onto materials and hence the recognition of these proteins by cells to adhere onto the material, a highly hydrophilic or a highly hydrophobic surface is not likely to support the proper conformation of adsorbed proteins and their retainment on the biomaterial surface(*34*) to elicit a healing response from the target tissue. Thus CA and CAc showed greater biocompatibility and progenitor cell differentiation potential than synthetic polymer PLGA.

Several attempts have been made to employ cellulose based structures in tissue engineering. Barbie *et al.* had conducted a 34 week implantation of cellulose into the femur of rabbits and seen a good degree of integration and minimal inflammatory reaction with the material(*479*). Cellulose and cellulose phosphate materials were also seen to support bone healing(*480*). Additionally, CA fibrous matrices supported cardiac cell growth and activity(*242*). These studies had however not utilized the mechanical competence of cellulose, a feature extremely essential for a bone scaffold. In the present study we have formulated a mechanically competent, 3D porous structure of cellulose acetate and contrasted its performance with a model synthetic polymer for its ability to heal a critical sized defect of the bone. Our results indicate that

cellulose based materials can perform better as scaffold for bone regeneration than conventional synthetic polymer matrices, when designed to possess the desirable characteristics of surface roughness, hydrophilicity, nutrient transfer and mechanical competence. This opens the possibility for Cellulose based scaffolds to be used in BTE applications.

6.5 Conclusions

In summary, we conclude that the natural polymeric CA based 3D porous scaffolds were superior to well- established synthetic PLGA scaffolds of similar dimensions in inducing healing of critical sized bone defects. The natural polymeric materials (CA and CAc) allowed better cellular infiltration than synthetic materials (PLGA) when implanted into a critical sized bone defect, indicative of the scaffold's osteoconductive nature when used alone. When equal numbers of BMSCs were seeded onto these CA, CAc and PLGA materials before implantation, we found twice as much bone and collagen formation with the biopolymeric scaffolds than PLGA. These observations indicate the higher density and quality of regenerated bone when the natural polymeric scaffolds were used in conjunction with stem cells. We however did not see an increased bone formation with the inclusion of collagen nanofibers (CAc), which contradicts our *in vitro* studies. This observation could be due to degradation of collagen at a faster rate than what is seen *in vitro*, and hence the effects of nanofibrillar collagen were negligible after 8 weeks of implantation. Finally, the donor BMSCs seeded were found in regions of new mineral deposition along with fewer host BMSCs indicating that the donor BMSCs could be involved in the formation of new bone both directly by depositing the matrix and indirectly by signaling the host BMSCs to contribute to the process. Though there were no differences in the amount of donor

BMSCs retained by the materials, the distribution of these cells were uniform throughout the scaffold on the biopolymers than on the synthetic polymer. This study proves that natural polymeric 3D- porous structures of cellulose could be used to induce effective bone formation, in combination with patient derived BMSCs and such matrices could be an effective alternative to PLA and PLGA synthetic polymers based BTE scaffolds with superior utility.

6.6 Supplemental Figures

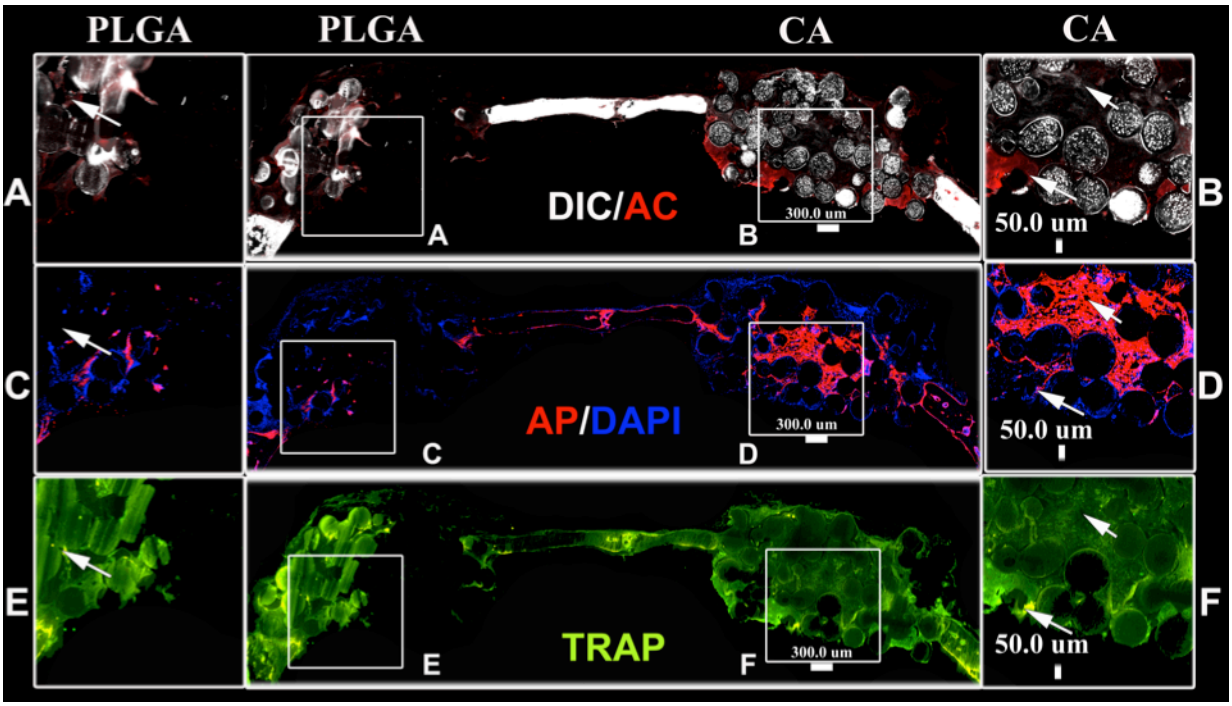

Figure 6.13 Histological sections of scaffolds without cells (Group 1)
Histological sections of scaffolds without cells (Group 1) Flourescent histological cross sectional images of calvaria implanted with material alone at 8 weeks, Group 1: PLGA vs CA, Top row: DIC- Differential interference channel image with AC- red labeled alizarin complexon marking new mineral deposition (PLGA inset A, CA inset B); Middle row: AP- Alkaline phosphatase activity for osteoblastic activity with DAPI- cell nuclei (PLGA inset C, CA inset D). Lowest row: TRAP- Tartrate-resistant acid phosphatase staining as a marker of osteoclastic activity (PLGA inset E, CA inset F).

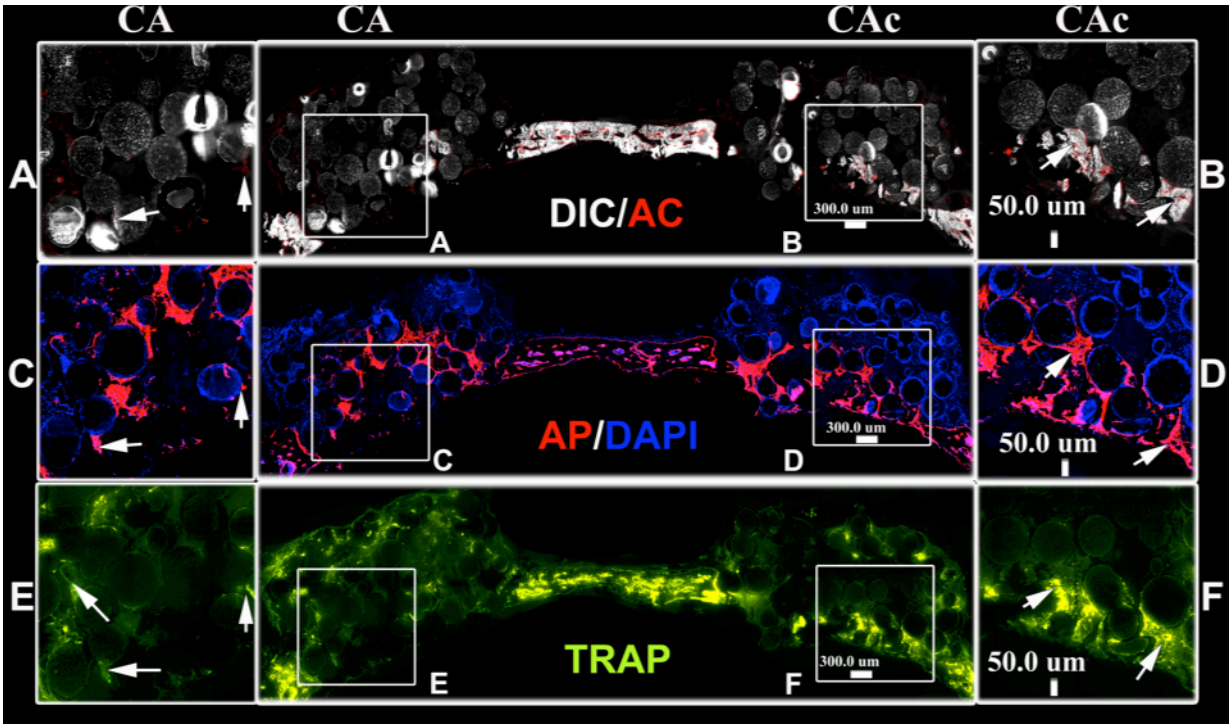

Figure 6.14 Histological sections of scaffolds without cells (Group 3)

Flourescent histological cross sectional images of calvaria implanted with material alone at 8 weeks, Group 3: CA vs CAc, Top row: DIC- Differential interference channel image with AC-red labeled alizarin complexon marking new mineral deposition (CA inset A, CAc inset B); Middle row: AP- Alkaline phosphatase activity for osteoblastic activity with DAPI- cell nuclei (CA inset C, CAc inset D). Lowest row: TRAP- Tartrate-resistant acid phosphatase staining as a marker of osteoclastic activity (CA inset E, CAc inset F).

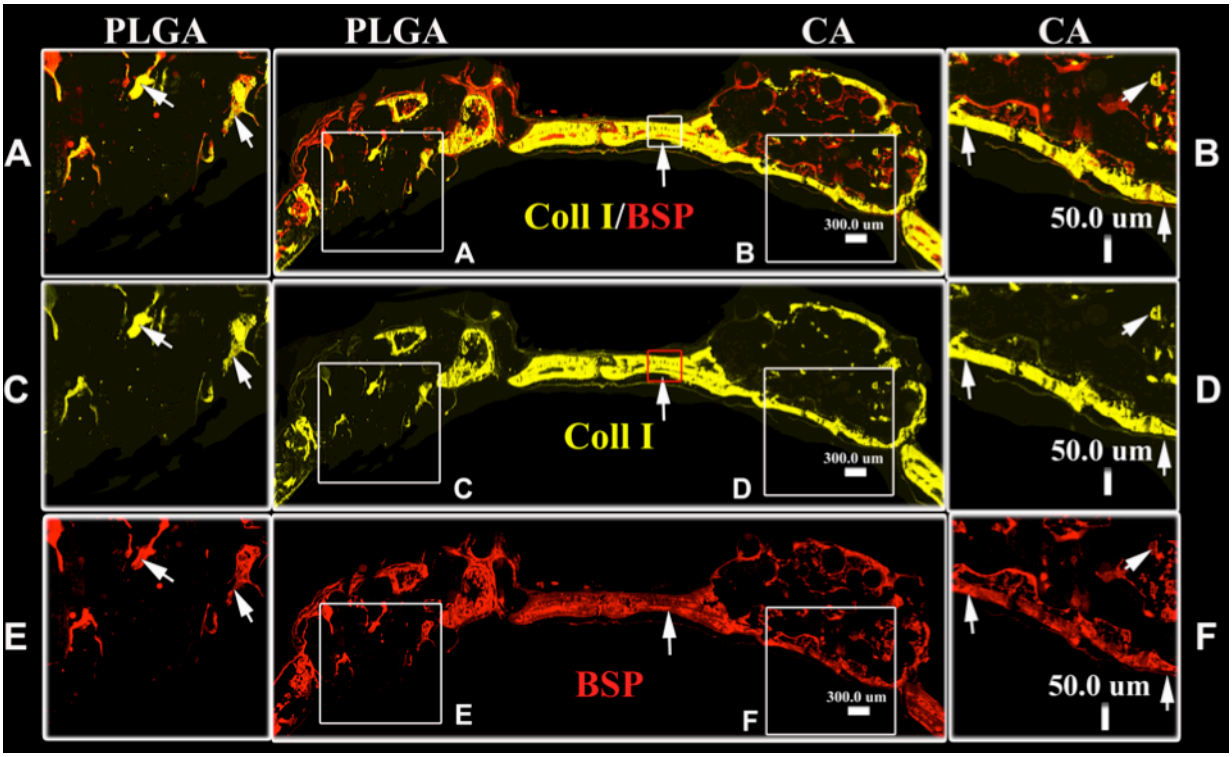

Figure 6.15 ECM markers immunostained on cell seeded scaffolds (Group 1)
Immunoflourescent stained (ECM proteins: Coll1-Collagen1/ Bone sialoprotein- BSP) histological cross sectional images of calvaria implanted with material and BMSCs at 8 weeks, Group 1: PLGA vs CA, Top row: Coll1- yellow, BSP- red (PLGA inset A, CA inset B); Middle row: Coll1- yellow (PLGA inset C, CA inset D). Lowest row: BSP- red (PLGA inset E, CA inset F).

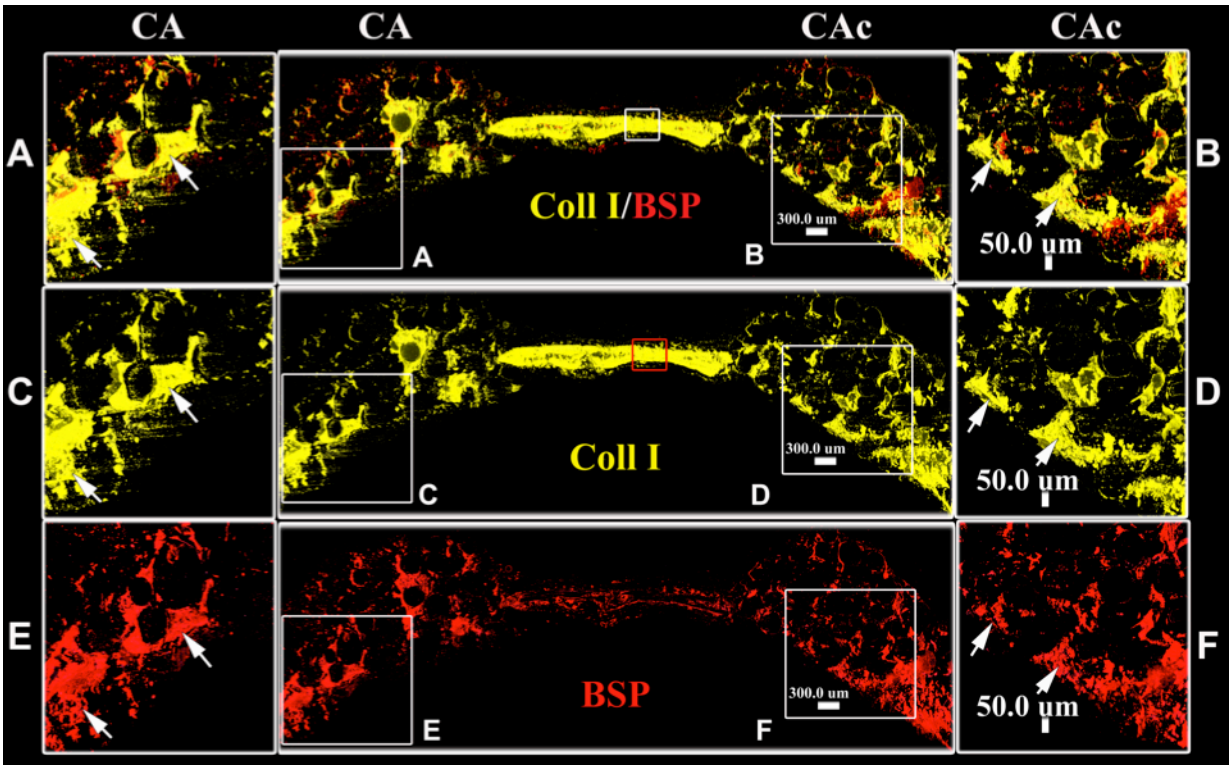

Figure 6.16 ECM markers immunostained on cell seeded scaffolds (Group 3)
Immunoflourescent stained (ECM proteins: Coll1-Collagen1/ Bone sialoprotein- BSP) histological cross sectional images of calvaria implanted with material and BMSCs at 8 weeks, Group 3: CA vs CAc, Top row: Coll1- yellow, BSP- red (CA inset A, CAc inset B); Middle row: Coll1- yellow (CA inset C, CAc inset D). Lowest row: BSP- red (CA inset E, CAc inset F).

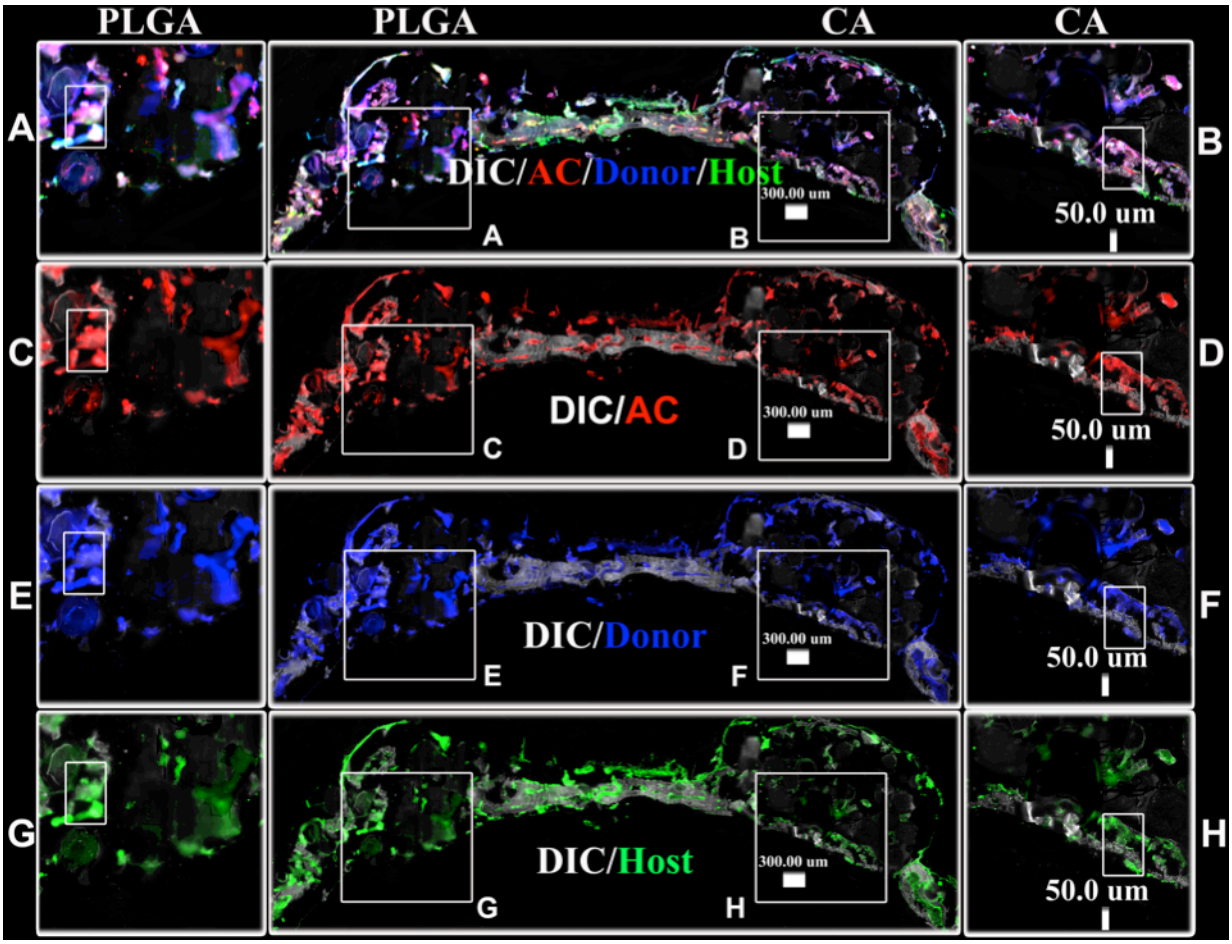

Figure 6.17 Stained histological sections of cell seeded scaffolds (Group 1)

Flourescent histological cross sectional images of calvaria implanted with material and BMSCs at 8 weeks, Group 1: PLGA vs CA, Top row: DIC- Differential interference channel image to visualize bone and microspheres with AC- red labeled alizarin complexon marking new mineral deposition, Donor cells- Col3.6- Cyan (blue), Host cells- Col3.6-Tpz (green) (PLGA inset A, CA inset B); Second row: DIC- Differential interference channel image to visualize bone and microspheres with AC- red labeled alizarin complexon marking new mineral deposition (PLGA inset C, CA inset D). Third row: DIC- Differential interference channel image to visualize bone and microspheres with Donor cells- Col3.6- Cyan (blue) (PLGA inset E, CA inset F). Fourth row: DIC- Differential interference channel image to visualize bone and microspheres with Host cells- Col3.6-Tpz (green) (PLGA inset G, CA inset H).

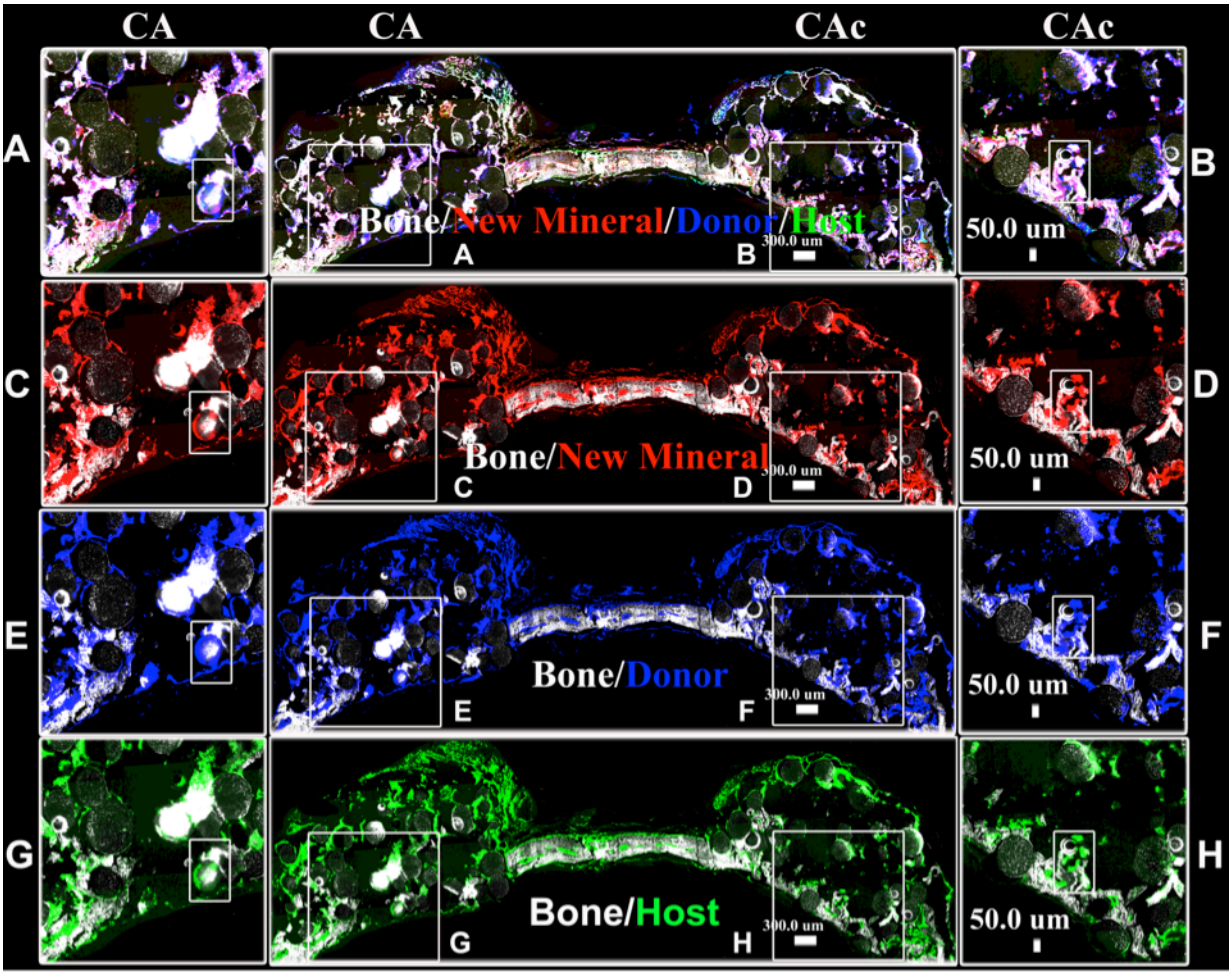

Figure 6.18 Stained histological sections of cell seeded scaffolds (Group 3)
Flourescent histological cross sectional images of calvaria implanted with material and BMSCs at 8 weeks, Group 3: CA vs CAc, Top row: DIC- Differential interference channel image to visualize bone and microspheres with AC- red labeled alizarin complexon marking new mineral deposition, Donor cells- Col3.6- Cyan (blue), Host cells- Col3.6-Tpz (green) (CA inset A, CAc inset B); Second row: DIC- Differential interference channel image to visualize bone and microspheres with AC- red labeled alizarin complexon marking new mineral deposition (CA inset C, CAc inset D). Third row: DIC- Differential interference channel image to visualize bone and microspheres with Donor cells- Col3.6- Cyan (blue) (CA inset E, CAc inset F). Fourth row: DIC- Differential interference channel image to visualize bone and microspheres with Host cells- Col3.6-Tpz (green) (CA inset G, CAc inset H).

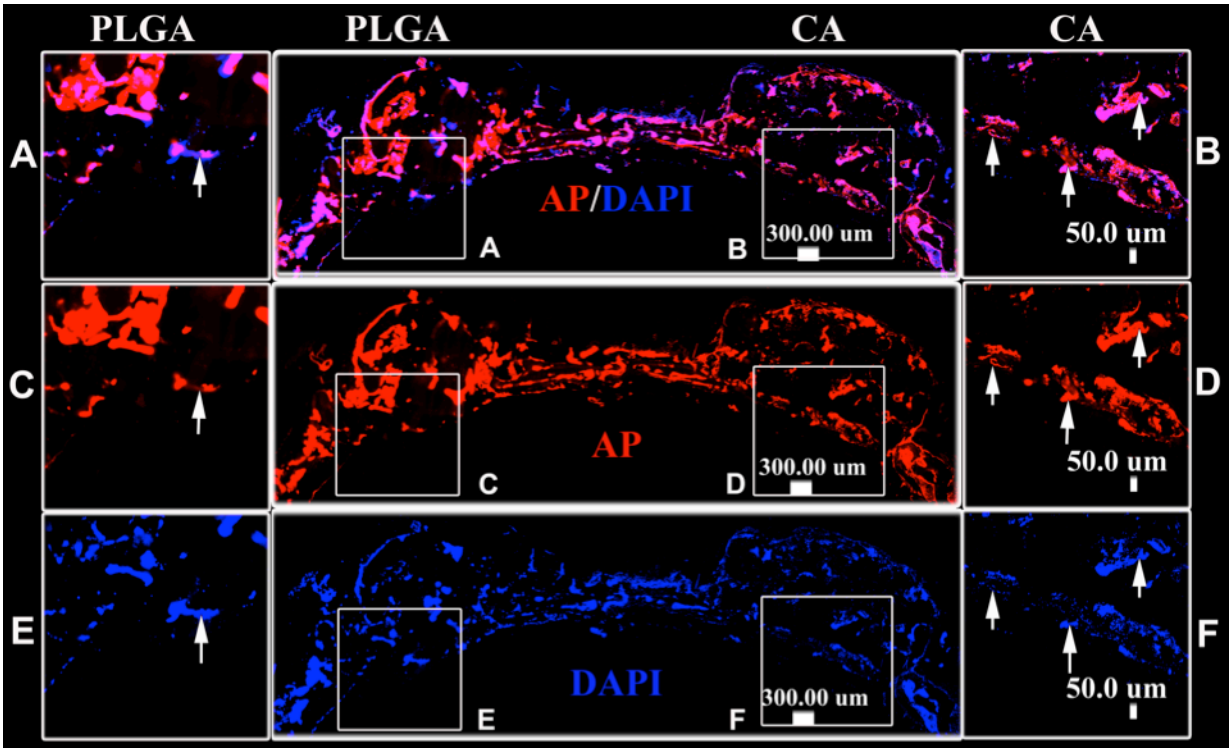

Figure 6.19 Osteoblastic activity on cell seeded scaffolds (Group 1)

Flourescent histological cross sectional images of calvaria implanted with material and BMSCs at 8 weeks, Group 1: PLGA vs CA, Top row: AP for osteoblastic activity - red, DAPI for cell nuclei- blue (PLGA inset A, CA inset B); Middle row: AP for osteoblastic activity- red (PLGA inset C, CA inset D). Lowest row: DAPI for cell nuclei- blue (PLGA inset E, CA inset F).

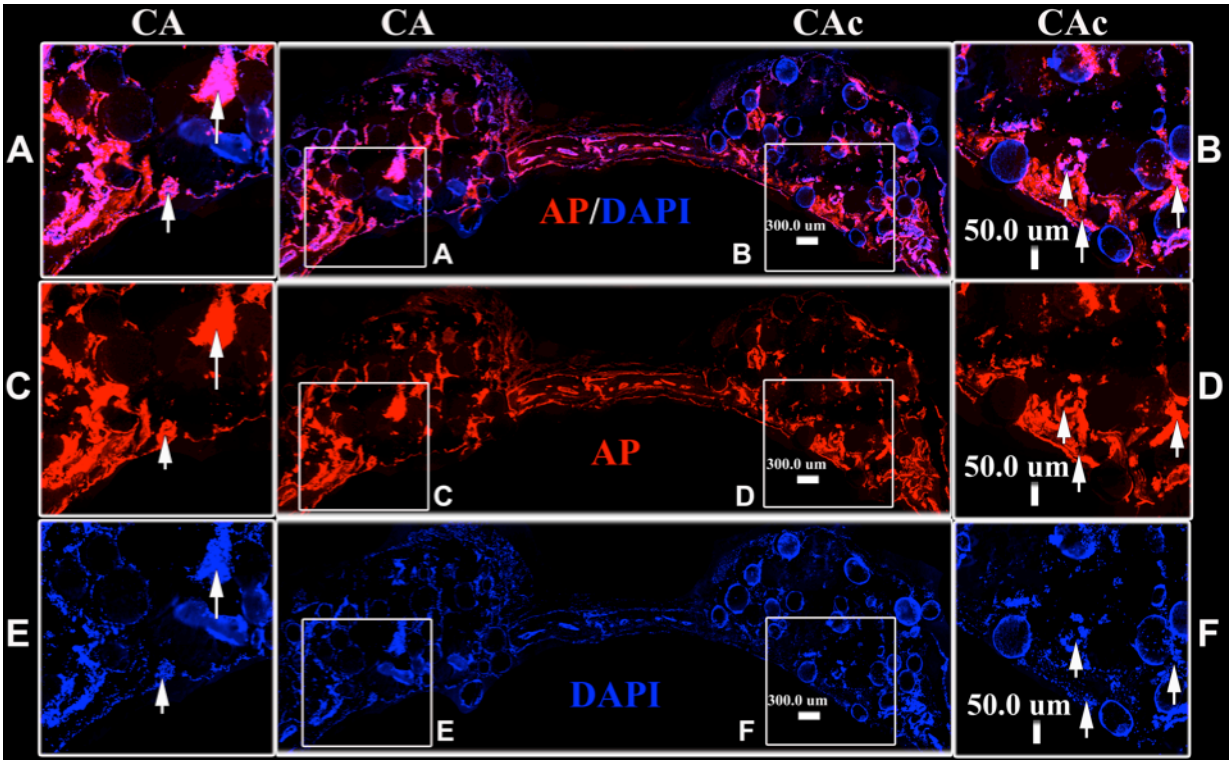

Figure 6.20 Osteoblastic activity on cell seeded scaffolds (Group 3)

Flourescent histological cross sectional images of calvaria implanted with material and BMSCs at 8 weeks, Group 3: PLGA vs CAc, Top row: AP for osteoblastic activity - red, DAPI for cell nuclei- blue (CA inset A, CAc inset B); Middle row: AP for osteoblastic activity- red (CA inset C, CAc inset D). Lowest row: DAPI for cell nuclei- blue (CA inset E, CAc inset F).

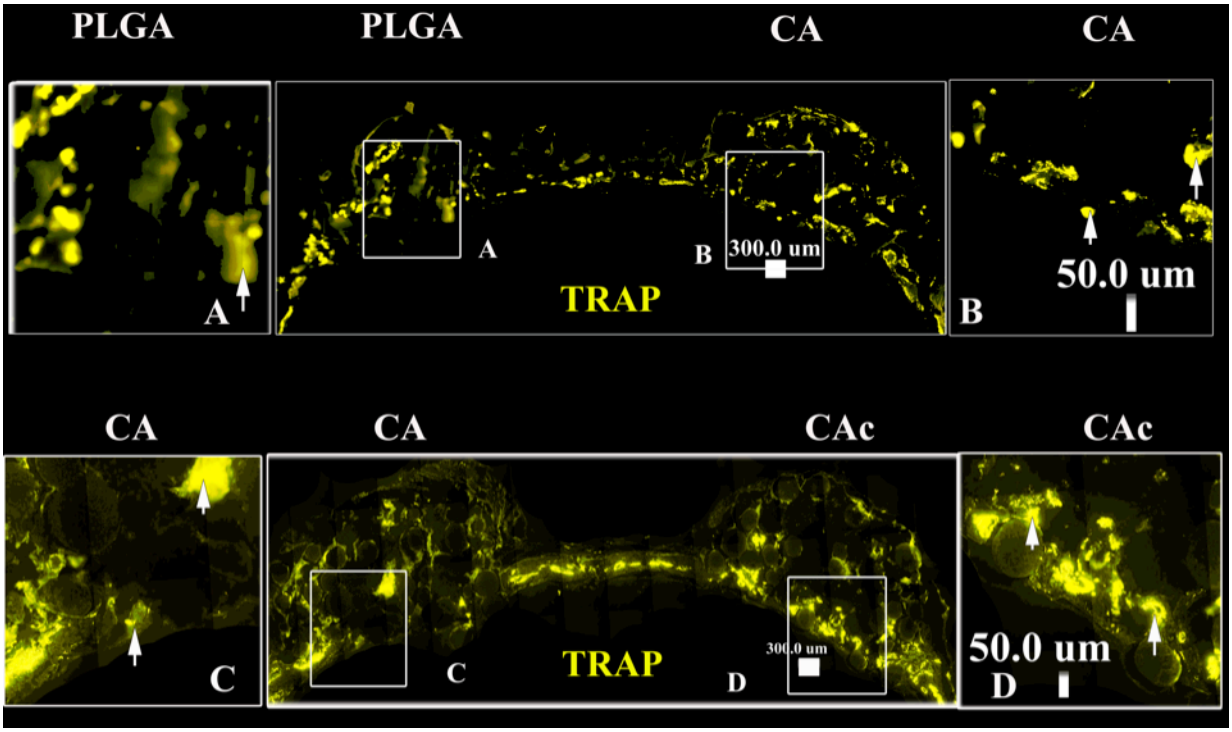

Figure 6.21 Osteoclastic activity on cell seeded scaffolds (Group 1 and 3)
Flourescent histological cross sectional images of calvaria implanted with material and BMSCs at 8 weeks, TRAP- Tartrate-resistant acid phosphatase staining as a marker of osteoclastic activity, Top row: Group 3: PLGA vs CA, (PLGA inset A, CA inset B). Bottom row: Group 1: CA vs CAc (CA inset C, CAc inset D).

7 Chapter 7

Future Directions

7.1 Stabilizing self- assembled collagen *in vivo* and uncovering the mechanism of material- protein interactions

Cellulose-collagen based matrices and related characterization for bone healing applications clearly establish their advantages over the synthetic polymer PLGA. The observed foreign body reaction at early stages to cellulose following its implantation may be lower due delay in the adsorption of bodily proteins onto the scaffold due to its increased hydrophilicity as compared to PLGA. Applying collagen coating on to the cellulose scaffold via self-assembly process may be a viable strategy to attain greater biological activity immediately after implantation. Hydrophilic nature and extensive inter- and intra-molecular hydrogen bonding of cellulose allowed a biomimetic presentation of the ECM protein collagen. This translated into greater induction of stem cell osteoblastic differentiation *in vitro* and bone healing in vivo when combined with bone marrow stromal cells. Significantly higher amount of bone was formed with cellulose-collagen scaffolds with cells as compared to PLGA control in a critical sized bone defect.

Bone healing between CA and CAc groups at 8 weeks (late) time point was at the same level. The erosion of collagen nanofibers from the scaffold in the body, due to the dynamic environment presented by MMPs could be a reason for the observed lack of difference between CA and CAc groups. It is worth investigating to crosslink collagen nanofibers to avoid their erosion to access the contributions of collagen nanofibers in long term bone healing. Many chemical collagen cross-linking mythologies have been reported that retain the bioactivity and may serve as a means to achieve this goal(*481-483*).

An important observation during the study was the biomimetic self-assembly of collagen nanofibers on the cellulose surface. Few studies have looked into the absorption of protein and their confirmation to specific material surfaces but underlying mechanisms vastly remains unknown. One of the bottlenecks to understanding the mechanism of protein assembly on material surfaces is the lack of techniques that do not modify the proteins by fluorescently tagging them or subjecting it to changes that distort their native state. Using simulation based analysis and complimenting it with real time protein folding studies materials like CA would explain the differential nature of protein adsorption and nanofiber assembly on these surfaces. For instance, it would be good to combine optical based methods employing fluorescently tagged ECM protein conformational studies(*484*) along with nano-sensors to detect the variation in electrostatic potential as it interacts with a material over time(*485*).

Collagen self-assembly on the CA scaffold was applied under static conditions in this study and approximately 90% of the collagen content was found on the scaffolds. Employing a dynamic collagen coating process with agitation and solvent evaporation may lead to presentation of the collagen with uniform nanofiber deposition throughout the scaffold architecture. Similarly MSCs were cultured on the scaffolds in a static condition prior to implantation. A dynamic cell culture approach in a bioreactor setup may help to increase the scaffold cellularity prior to implantation into an osseous defect and further improve the bone healing efficacy(*316*).

7.2 Mechanism of bone formation in calvarial defects in the presence of BMSCs

Previous studies have shown the important role of BMSCs in conjunction with scaffolds in healing the critical sized bone defect in rat calvaria(*486*). In the present study we found host

MSCs along with the donor BMSCs in the areas of dynamic bone formation. However, majority of the cell population was donor BMSCs seeded on the scaffold. In this study we did not able to quantify the contributions of each cell type towards the new bone formation. Studies could be designed to compromise donor cells ability to form bone via viral transfection to establish the contributions of donor BMSCs in bone healing. These studies may contribute to our understanding of donor BMSCs contributions in forming new bone against the trophic effect of BMSCs towards progenitor and bone cells from the host(*486*).

7.3 Scaffold degradation properties

Cellulose degradation is mediated by the enzyme as opposed to hydrolytic degradation that is seen with the PLGA. The lack of body enzymes that facilitates the cellulose degradation makes it stable at the implantation cites for the longer period of times. A detailed study should look at the effect of long term implantation of these scaffolds in a bone defect to study its degradation and its integration with the surrounding tissue. The lack of acidic degradation byproducts as seen with PLA, PGA and PLGA that compromise osseous formation and integration may benefit from the use of cellulose derived implants and scaffolds. Suitable chemical modifications to cellulose to reduce the hydrogen bonding may promote matrix erosion and hence control the scaffold replacement from cite of implantation are currently under investigation. Additionally creating hydrolytically labile ester, anhydride and amide linkages between cellulose backbone chains are also under investigation to promote cellulose erosion and degradation. In addition encapsulation of enzymes in the bulk of the CA scaffold or bending the material with a fast eroding natural or synthetic material may serve as an alternative chemical modification to promote its degradation. These efforts are focused on retaining the bulk mechanical strength of cellulose while giving the freedom to promote its degradation much like a synthetic polymer PLGA. In all these approaches

rigorous cell and biocompatibility studies should be conducted to establish the suitability of these materials for load bearing bone healing applications. Similar methodologies could be extended to other polysaccharide materials to promote their erosion and degradation in tissue healing application.

.

8 Appendix
List of Publications

8.1 Journal Articles

8.1.1 Research Articles

Aravamudhan A, Rowe DW, Kumbar SG. Evaluation of bone formation in transgenic mice by cellulose-collagen, micro-nano structured natural polymeric 3D porous scaffolds, in combination with bone marrow stromal cells (manuscript under preparation).

Aravamudhan A, Ramos DM, Jenkins NA, Dyment NA, Rowe DW, Sanders MM, Kumbar SG. Collagen nanofibril self-assembly on natural polymeric material for osteoinduction of stem cells *in vitro* and Biocompatibility *in vivo*, 6 (84), 80851-80866, 2016.

Aravamudhan A, Ramos DM, Nip J, Harmon M, James R, Deng M, Laurencin CT, Yu X, Kumbar SG. Cellulose and Collagen Derived Micro-Nano Structured Scaffolds for Bone Tissue Engineering. *J. Biomed. Nanotechnology*, 9 (4), 719-731, 2013.

Kumbar SG, Toti US, Deng M, James R, Laurencin CT, **Aravamudhan A**, Harmon M, Ramos DM. Novel mechanically competent polysaccharide scaffolds for bone tissue engineering. *Biomedical Material*, 6, 6, 065005; 2011.

8.1.2 Review Article

Aravamudhan A, Ramos DM, Nip J, Subramaniam A, James R, Harmon M, Yu X, Kumbar, S. G. Osteoinductive Small Molecules: Growth Factor Alternatives for Bone Tissue Engineering. *Current Pharmaceutical Design*, 19(19), 3420-8, 2013.

8.2 Book Chapters

Aravamudhan A, Ramos D, Nada AA, Kumbar SG, Natural Polymers: Polysaccharides and Their Derivatives for Biomedical Applications, Natural and Synthetic Biomedical Polymers; pg. 67-90, Elsevier Science; 2014.

Aravamudhan A, Olczyk J, Toti U, Deng M, Laurencin CT, Kumbar SG, Nanofibre-Based Systems for Wound Healing Applications: Electrospinning for Advanced Biomedical Applications and Therapies; pg. 135-157, iSmithers; 2012.

8.3 Conference Abstracts

8.3.1 Conference Posters

Aravamudhan A, Ramos D, Harmon M, Kumbar SG. Characterization of Cellulose Collagen based Micro Nano structured scaffolds for Osteoinductivity *in vitro* and Biocompatibility *in vivo*. Material Research Society Meeting Fall Meeting (Boston, MA); November 29- December 4, 2015, Poster # 2336912.

Aravamudhan A, Ramos D, Harmon M, Kumbar SG. Characterization of Polysaccharide Based Micro-Nano Structured Scaffolds for Osteoinductivity. Biomedical Engineering Society Annual Meeting (San Antonio, Texas); October 22-25, 2014, Poster # 492.

Aravamudhan A, Ramos D, Deng M, Toti US, Harmon M, Nip J, Laurencin CT, Kumbar SG. Induced Osteogenic Differentiation of Human Mesenchymal Stem Cells by Polyester Nanofiber Scaffolds in Combination with Resveratrol. 9th World Biomaterials Congress (Chengdu, China); June 4-5, 2012, Poster # 3137.

Aravamudhan A., Deng M, Toti US, Ramos D, Harmon M, Laurencin CT, Kumbar SG. Induced Osteogenic differentiation of human mesenchymal stem cells by polymer nanofiber scaffolds in combination with melatonin. Orthopaedic Research Society Conference (San Francisco, California, USA); February 2-4, 2012, Poster # 1598.

Aravamudhan A, Ramos D, Harmon M, Toti US, Deng M, Laurencin CT, Kumbar SG**.** Human Mesnchymal Stem Cell (hMSc) Proliferation and Differentiation on Polysaccharide Bone Grafts. Orthopaedic Research Society Conference (San Francisco, California, USA); February 2-4, 2012, Poster # 1630.

Toti US, **Aravamudhan A**, Deng M, Laurencin CT, Kumbar SG. Novel Mechanically Competent Polysaccharide Scaffolds for Bone Tissue Engineering. Annual meeting of Biomedical Engineering Society (Hartford, CT, USA); October12-15, 2011, Poster #205.

8.3.2 Conference Podium Presentations

Aravamudhan A, Kumbar S.G. Cellulose based micro- nano structured scaffolds for bone regeneration. 10th World Biomaterials Congress (Montreal,QC, Canada); May 17- 22, 2016, Presentation # 3293.

Aravamudhan A, James R, Yu X, Kumbar SG. Biodegradable Nanocomposite Based Spiral Structures for Bone Tissue Engineering. Materials Research Society Fall Meeting (Boston, MA, USA); December 1-6, 2013, Presentation # H4.07.

9 References

1. G. Calori, E. Mazza, M. Colombo, C. Ripamonti, The use of bone-graft substitutes in large bone defects: any specific needs? *Injury* **42**, S56-S63 (2011).
2. G. Calori, W. Albisetti, A. Agus, S. Iori, L. Tagliabue, Risk factors contributing to fracture non-unions. *Injury* **38**, S11-S18 (2007).
3. T. A. Einhorn, Enhancement of fracture-healing. *J Bone Joint Surg Am* **77**, 940-956 (1995).
4. C. Tzioupis, P. V. Giannoudis, Prevalence of long-bone non-unions. *Injury* **38**, S3-S9 (2007).
5. V. Campana *et al.*, Bone substitutes in orthopaedic surgery: from basic science to clinical practice. *Journal of Materials Science: Materials in Medicine* **25**, 2445-2461 (2014).
6. A. S. Greenwald *et al.*, Bone-graft substitutes: facts, fictions, and applications. *The Journal of Bone & Joint Surgery* **83**, S98-103 (2001).
7. C. G. Finkemeier, Bone-grafting and bone-graft substitutes. *J Bone Joint Surg Am* **84**, 454-464 (2002).
8. O. Faour, R. Dimitriou, C. A. Cousins, P. V. Giannoudis, The use of bone graft substitutes in large cancellous voids: any specific needs? *Injury* **42**, S87-S90 (2011).
9. A. R. Amini, C. T. Laurencin, S. P. Nukavarapu, Bone tissue engineering: recent advances and challenges. *Critical Reviews™ in Biomedical Engineering* **40**, (2012).
10. S. T. Kao, D. D. Scott, A review of bone substitutes. *Oral and maxillofacial surgery clinics of North America* **19**, 513-521 (2007).
11. H. C. Pape, A. Evans, P. Kobbe, Autologous bone graft: properties and techniques. *Journal of orthopaedic trauma* **24**, S36-S40 (2010).
12. J. Baumhauer, M. S. Pinzur, R. Donahue, W. Beasley, C. DiGiovanni, Site selection and pain outcome after autologous bone graft harvest. *Foot & ankle international* **35**, 104-107 (2014).
13. R. Miron, Y. Zhang, Osteoinduction a review of old concepts with new standards. *Journal of dental research* **91**, 736-744 (2012).
14. J. Rawlinson, Morbidity after anterior cervical decompression and fusion. The influence of the donor site on recovery, and the results of a trial of surgibone compared to autologous bone. *Acta neurochirurgica* **131**, 106-118 (1994).
15. S. D. Boden, Overview of the biology of lumbar spine fusion and principles for selecting a bone graft substitute. *Spine* **27**, S26-S31 (2002).
16. R. Calvo, D. Figueroa, C. Diaz-Ledezma, A. Vaisman, F. Figueroa, [Bone allografts and the functions of bone banks. *Revista medica de Chile* **139**, 660-666 (2011).
17. W. W. Tomford, Transmission of disease through transplantation of musculoskeletal allografts. *J Bone Joint Surg Am* **77**, 1742-1754 (1995).
18. T. E. Mroz, M. J. Joyce, M. P. Steinmetz, I. H. Lieberman, J. C. Wang, Musculoskeletal allograft risks and recalls in the United States. *Journal of the American Academy of Orthopaedic Surgeons* **16**, 559-565 (2008).
19. D. L. Wheeler, W. F. Enneking, Allograft bone decreases in strength in vivo over time. *Clinical orthopaedics and related research* **435**, 36-42 (2005).

20. S. S. Jensen, H. Terheyden, Bone augmentation procedures in localized defects in the alveolar ridge: clinical results with different bone grafts and bone-substitute materials. *International Journal of Oral & Maxillofacial Implants* **24**, (2009).
21. R. MAATZ, A. BAUERMEISTER, A method of bone maceration. *J Bone Joint Surg Am* **39**, 153-166 (1957).
22. C. T. Laurencin, S. F. El-Amin, Xenotransplantation in orthopaedic surgery. *Journal of the American Academy of Orthopaedic Surgeons* **16**, 4-8 (2008).
23. A. L. Dumitrescu, Bone grafts and bone graft substitutes in periodontal therapy. *Chemicals in Surgical Periodontal Therapy*, 73-144 (2011).
24. H. Löfgren, V. Johannsson, T. Olsson, L. Ryd, B. Levander, Rigid fusion after cloward operation for cervical disc disease using autograft, allograft, or xenograft: a randomized study with radiostereometric and clinical follow-up assessment. *Spine* **25**, 1908-1916 (2000).
25. B. Boyan, J. McMillan, C. Lohmann, D. Ranly, Z. Schwartz, Bone graft substitutes: basic information for successful clinical use with special focus on synthetic graft substitutes. *Bone Graft Substitutes*, 231-259 (2003).
26. C. D. Friedman, P. D. Costantino, S. Takagi, L. C. Chow, BoneSource™ hydroxyapatite cement: a novel biomaterial for craniofacial skeletal tissue engineering and reconstruction. *Journal of biomedical materials research* **43**, 428-432 (1998).
27. C. Yashavantha Kumar, K. Nalini, D. K. P. Jagdish Menon, B. Banerji, Calcium sulfate as bone graft substitute in the treatment of osseous bone defects, a prospective study. *Journal of clinical and diagnostic research: JCDR* **7**, 2926 (2013).
28. E. Landi *et al.*, Biomimetic Mg-substituted hydroxyapatite: from synthesis to in vivo behaviour. *Journal of Materials Science: Materials in Medicine* **19**, 239-247 (2008).
29. P. K. Yarlagadda, M. Chandrasekharan, J. Y. M. Shyan, Recent advances and current developments in tissue scaffolding. *Bio-medical materials and engineering* **15**, 159-177 (2005).
30. X. Yu, X. Tang, S. V. Gohil, C. T. Laurencin, Biomaterials for bone regenerative engineering. *Advanced healthcare materials* **4**, 1268-1285 (2015).
31. J. P. Vacanti, R. Langer, Tissue engineering: the design and fabrication of living replacement devices for surgical reconstruction and transplantation. *The Lancet* **354**, S32-S34 (1999).
32. C. T. Laurencin, Y. Khan, Regenerative engineering. *Science translational medicine* **4**, 160-169 (2012).
33. S. Bose, M. Roy, A. Bandyopadhyay, Recent advances in bone tissue engineering scaffolds. *Trends in biotechnology* **30**, 546-554 (2012).
34. L. Bacakova, E. Filova, M. Parizek, T. Ruml, V. Svorcik, Modulation of cell adhesion, proliferation and differentiation on materials designed for body implants. *Biotechnology advances* **29**, 739-767 (2011).
35. M. Lampin, R. Warocquier‐Clérout, C. Legris, M. Degrange, M. Sigot‐Luizard, Correlation between substratum roughness and wettability, cell adhesion, and cell migration. *Journal of biomedical materials research* **36**, 99-108 (1997).
36. A. R. Amini, T. O. Xu, R. M. Chidambaram, S. P. Nukavarapu, Oxygen Tension-Controlled Matrices with Osteogenic and Vasculogenic Cells for Vascularized Bone Regeneration In Vivo. *Tissue Engineering Part A* **22**, 610-620 (2016).

37. D. S. Benoit, M. P. Schwartz, A. R. Durney, K. S. Anseth, Small functional groups for controlled differentiation of hydrogel-encapsulated human mesenchymal stem cells. *Nature materials* **7**, 816-823 (2008).
38. B. G. Keselowsky, D. M. Collard, A. J. García, Integrin binding specificity regulates biomaterial surface chemistry effects on cell differentiation. *Proceedings of the National Academy of Sciences* **102**, 5953-5957 (2005).
39. G. C. Reilly, A. J. Engler, Intrinsic extracellular matrix properties regulate stem cell differentiation. *Journal of biomechanics* **43**, 55-62 (2010).
40. M. Lutolf, J. Hubbell, Synthetic biomaterials as instructive extracellular microenvironments for morphogenesis in tissue engineering. *Nature biotechnology* **23**, 47-55 (2005).
41. J. Wilson-Hench, Osteoinduction. *Progress in biomedical engineering* **4**, 29 (1987).
42. L. Lindquist, G. Carlsson, P. Glantz, Rehabilitation of the edentulous mandible with a tissue-integrated fixed prosthesis: a six-year longitudinal study. *Quintessence international (Berlin, Germany: 1985)* **18**, 89 (1987).
43. T. Albrektsson, The healing of autologous bone grafts after varying degrees of surgical trauma. A microscopic and histochemical study in the rabbit. *Bone & Joint Journal* **62**, 403-410 (1980).
44. T. Albrektsson, C. Johansson, Osteoinduction, osteoconduction and osseointegration. *European Spine Journal* **10**, S96-S101 (2001).
45. R. W. Young, 14 Nucleic Acids, Protein Synthesis and Bone. *Clinical orthopaedics and related research* **26**, 147-160 (1963).
46. M. R. Urist, Bone: formation by autoinduction. *Science* **150**, 893-899 (1965).
47. T. Albrektsson, P.-I. Brånemark, H.-A. Hansson, J. Lindström, Osseointegrated titanium implants: requirements for ensuring a long-lasting, direct bone-to-implant anchorage in man. *Acta Orthopaedica Scandinavica* **52**, 155-170 (1981).
48. P. Branemark, Osseointegrated implants in the treatment of edentulous jaw, Experience from a 10-year period. *Scand J Plast Reconstr Surg* **1**, 1-132 (1977).
49. T. Albrektsson, On long-term maintenance of the osseointegrated response. *Australian prosthodontic journal/Australian Prosthodontic Society* **7**, 15-24 (1992).
50. L. Linder *et al.*, Electron microscopic analysis of the bone-titanium interface. *Acta Orthopaedica Scandinavica* **54**, 45-52 (1983).
51. S. Li, Hydrolytic degradation characteristics of aliphatic polyesters derived from lactic and glycolic acids. *Journal of biomedical materials research* **48**, 342-353 (1999).
52. L. S. Nair, C. T. Laurencin, Biodegradable polymers as biomaterials. *Progress in polymer science* **32**, 762-798 (2007).
53. J. C. Middleton, A. J. Tipton, Synthetic biodegradable polymers as orthopedic devices. *Biomaterials* **21**, 2335-2346 (2000).
54. A. Löfgren, A.-C. Albertsson, P. Dubois, R. Jérôme, Recent advances in ring-opening polymerization of lactones and related compounds. *Journal of Macromolecular Science, Part C: Polymer Reviews* **35**, 379-418 (1995).
55. P. Gunatillake, R. Mayadunne, R. Adhikari, Recent developments in biodegradable synthetic polymers. *Biotechnology annual review* **12**, 301-347 (2006).
56. P. Törmälä, Biodegradable self-reinforced composite materials; manufacturing structure and mechanical properties. *Clinical materials* **10**, 29-34 (1992).

57. P. B. Maurus, C. C. Kaeding, Bioabsorbable implant material review. *Operative Techniques in Sports Medicine* **12**, 158-160 (2004).
58. H. H. Lu *et al.*, Anterior cruciate ligament regeneration using braided biodegradable scaffolds: in vitro optimization studies. *Biomaterials* **26**, 4805-4816 (2005).
59. J. A. Cooper, H. H. Lu, F. K. Ko, J. W. Freeman, C. T. Laurencin, Fiber-based tissue-engineered scaffold for ligament replacement: design considerations and in vitro evaluation. *Biomaterials* **26**, 1523-1532 (2005).
60. J. Bergsma *et al.*, In vivo degradation and biocompatibility study of in vitro pre-degraded as-polymerized polylactide particles. *Biomaterials* **16**, 267-274 (1995).
61. R. A. Miller, J. M. Brady, D. E. Cutright, Degradation rates of oral resorbable implants (polylactates and polyglycolates): rate modification with changes in PLA/PGA copolymer ratios. *Journal of biomedical materials research* **11**, 711-719 (1977).
62. Y. Lu, S. Chen, Micro and nano-fabrication of biodegradable polymers for drug delivery. *Advanced drug delivery reviews* **56**, 1621-1633 (2004).
63. T. K. Kim, J. J. Yoon, D. S. Lee, T. G. Park, Gas foamed open porous biodegradable polymeric microspheres. *Biomaterials* **27**, 152-159 (2006).
64. M. Borden, M. Attawia, Y. Khan, C. T. Laurencin, Tissue engineered microsphere-based matrices for bone repair:: design and evaluation. *Biomaterials* **23**, 551-559 (2002).
65. D. S. Katti, K. W. Robinson, F. K. Ko, C. T. Laurencin, Bioresorbable nanofiber‐based systems for wound healing and drug delivery: Optimization of fabrication parameters. *Journal of Biomedical Materials Research Part B: Applied Biomaterials* **70**, 286-296 (2004).
66. H. Ueda, Y. Tabata, Polyhydroxyalkanonate derivatives in current clinical applications and trials. *Advanced drug delivery reviews* **55**, 501-518 (2003).
67. M. J. Mondrinos *et al.*, Porogen-based solid freeform fabrication of polycaprolactone–calcium phosphate scaffolds for tissue engineering. *Biomaterials* **27**, 4399-4408 (2006).
68. J. Heller, J. Barr, Poly (ortho esters) from concept to reality. *Biomacromolecules* **5**, 1625-1632 (2004).
69. D. Katti, S. Lakshmi, R. Langer, C. Laurencin, Toxicity, biodegradation and elimination of polyanhydrides. *Advanced Drug Delivery Reviews* **54**, 933-961 (2002).
70. K. Leong, B. Brott, R. Langer, Bioerodible polyanhydrides as drug‐carrier matrices. I: Characterization, degradation, and release characteristics. *Journal of biomedical materials research* **19**, 941-955 (1985).
71. C. Laurencin *et al.*, Bioerodible polyanhydrides for antibiotic drug delivery: in vivo osteomyelitis treatment in a rat model system. *Journal of orthopaedic research* **11**, 256-262 (1993).
72. L. C. Li, J. Deng, D. Stephens, Polyanhydride implant for antibiotic delivery—from the bench to the clinic. *Advanced drug delivery reviews* **54**, 963-986 (2002).
73. J. Mano, Silva gA, Azevedo HS, Malafaya PB, Sousa RA, Silva SS, et al. Natural origin biodegradable systems in tissue engineering and regenerative medicine: present status and some moving trends. *Journal of The Royal Society Interface* **4**, 999-1030 (2007).

74. L. Klouda, A. G. Mikos, Thermoresponsive hydrogels in biomedical applications. *European Journal of Pharmaceutics and Biopharmaceutics* **68**, 34-45 (2008).
75. G. G. d'Ayala, M. Malinconico, P. Laurienzo, Marine derived polysaccharides for biomedical applications: chemical modification approaches. *Molecules* **13**, 2069-2106 (2008).
76. S. Hirano, Chitin biotechnology applications. *Biotechnology annual review* **2**, 237-258 (1996).
77. S. P. Evanko, J. C. Angello, T. N. Wight, Formation of hyaluronan-and versican-rich pericellular matrix is required for proliferation and migration of vascular smooth muscle cells. *Arteriosclerosis, thrombosis, and vascular biology* **19**, 1004-1013 (1999).
78. J. L. Drury, D. J. Mooney, Hydrogels for tissue engineering: scaffold design variables and applications. *Biomaterials* **24**, 4337-4351 (2003).
79. P. H. Weigel, V. C. Hascall, M. Tammi, Hyaluronan synthases. *Journal of Biological Chemistry* **272**, 13997-14000 (1997).
80. T. C. Laurent, J. Fraser, Hyaluronan. *The FASEB Journal* **6**, 2397-2404 (1992).
81. J. Fraser, T. Laurent, U. Laurent, Hyaluronan: its nature, distribution, functions and turnover. *Journal of internal medicine* **242**, 27-33 (1997).
82. C. M. McKee *et al.*, Hyaluronan (HA) fragments induce chemokine gene expression in alveolar macrophages. The role of HA size and CD44. *Journal of Clinical Investigation* **98**, 2403 (1996).
83. O. Ishida, Y. Tanaka, I. Morimoto, M. Takigawa, S. Eto, Chondrocytes are regulated by cellular adhesion through CD44 and hyaluronic acid pathway. *Journal of Bone and Mineral Research* **12**, 1657-1663 (1997).
84. J. Hodge-Dufour *et al.*, Induction of IL-12 and chemokines by hyaluronan requires adhesion-dependent priming of resident but not elicited macrophages. *The Journal of Immunology* **159**, 2492-2500 (1997).
85. D. West, S. Kumar, Hyaluronan and angiogenesis. *The biology of hyaluronan* **143**, 187-207 (1989).
86. V. C. Lees, T. Fan, D. C. West, Angiogenesis in a delayed revascularization model is accelerated by angiogenic oligosaccharides of hyaluronan. *Laboratory investigation; a journal of technical methods and pathology* **73**, 259-266 (1995).
87. G. D. Prestwich, D. M. Marecak, J. F. Marecek, K. P. Vercruysse, M. R. Ziebell, Controlled chemical modification of hyaluronic acid: synthesis, applications, and biodegradation of hydrazide derivatives. *Journal of Controlled Release* **53**, 93-103 (1998).
88. D. D. Allison, K. J. Grande-Allen, Review. Hyaluronan: a powerful tissue engineering tool. *Tissue engineering* **12**, 2131-2140 (2006).
89. S. Eriksson, J. R. E. Fraser, T. C. Laurent, H. Pertoft, B. Smedsrød, Endothelial cells are a site of uptake and degradation of hyaluronic acid in the liver. *Experimental cell research* **144**, 223-228 (1983).
90. R. Tammi *et al.*, Hyaluronan enters keratinocytes by a novel endocytic route for catabolism. *Journal of Biological Chemistry* **276**, 35111-35122 (2001).
91. K. Kyyrönen *et al.*, Methylprednisolone esters of hyaluronic acid in ophthalmic drug delivery: in vitro and in vivo release studies. *International journal of pharmaceutics* **80**, 161-169 (1992).

92. M. F. Saettone, P. Chetoni, M. T. Torracca, S. Burgalassi, B. Giannaccini, Evaluation of muco-adhesive properties and in vivo activity of ophthalmic vehicles based on hyaluronic acid. *International journal of pharmaceutics* **51**, 203-212 (1989).
93. N. Yerushalmi, A. Arad, R. Margalit, Molecular and cellular studies of hyaluronic acid-modified liposomes as bioadhesive carriers for topical drug delivery in wound healing. *Archives of biochemistry and biophysics* **313**, 267-273 (1994).
94. D. Coradini, C. Pellizzaro, G. Miglierini, M. G. Daidone, A. Perbellini, Hyaluronic acid as drug delivery for sodium butyrate: Improvement of the anti‐proliferative activity on a breast‐cancer cell line. *International journal of cancer* **81**, 411-416 (1999).
95. T. Segura *et al.*, Crosslinked hyaluronic acid hydrogels: a strategy to functionalize and pattern. *Biomaterials* **26**, 359-371 (2005).
96. J. A. Burdick, C. Chung, X. Jia, M. A. Randolph, R. Langer, Controlled degradation and mechanical behavior of photopolymerized hyaluronic acid networks. *Biomacromolecules* **6**, 386-391 (2005).
97. B. P. Toole, in *Seminars in cell & developmental biology*. (Elsevier, 2001), vol. 12, pp. 79-87.
98. L. Cen, K. Neoh, Y. Li, E. Kang, Assessment of in vitro bioactivity of hyaluronic acid and sulfated hyaluronic acid functionalized electroactive polymer. *Biomacromolecules* **5**, 2238-2246 (2004).
99. J. H. Collier, J. P. Camp, T. W. Hudson, C. E. Schmidt, Synthesis and characterization of polypyrrole–hyaluronic acid composite biomaterials for tissue engineering applications. *Journal of biomedical materials research* **50**, 574-584 (2000).
100. D. Campoccia *et al.*, Semisynthetic resorbable materials from hyaluronan esterification. *Biomaterials* **19**, 2101-2127 (1998).
101. A. P. Hollander, E. Kon, Hyaluronan-based scaffolds (Hyalograft1 C) in the treatment of knee cartilage defects: preliminary clinical findings. *Tissue Eng. Cartil. Bone* **249**, 203 (2003).
102. L. A. Solchaga *et al.*, Repair of osteochondral defects with hyaluronan-and polyester-based scaffolds. *Osteoarthritis and cartilage* **13**, 297-309 (2005).
103. M. Radice *et al.*, Hyaluronan‐based biopolymers as delivery vehicles for bone‐marrow‐derived mesenchymal progenitors. *Journal of biomedical materials research* **50**, 101-109 (2000).
104. B. Zavan *et al.*, Extracellular matrix-enriched polymeric scaffolds as a substrate for hepatocyte cultures: in vitro and in vivo studies. *Biomaterials* **26**, 7038-7045 (2005).
105. K. Hemmrich *et al.*, Implantation of preadipocyte-loaded hyaluronic acid-based scaffolds into nude mice to evaluate potential for soft tissue engineering. *Biomaterials* **26**, 7025-7037 (2005).
106. S. Yamane *et al.*, Feasibility of chitosan-based hyaluronic acid hybrid biomaterial for a novel scaffold in cartilage tissue engineering. *Biomaterials* **26**, 611-619 (2005).
107. H. S. Yoo, E. A. Lee, J. J. Yoon, T. G. Park, Hyaluronic acid modified biodegradable scaffolds for cartilage tissue engineering. *Biomaterials* **26**, 1925-1933 (2005).

108. A. Ramamurthi, I. Vesely, Evaluation of the matrix-synthesis potential of crosslinked hyaluronan gels for tissue engineering of aortic heart valves. *Biomaterials* **26**, 999-1010 (2005).
109. A. Ramamurthi, I. Vesely, Ultraviolet light‐induced modification of crosslinked hyaluronan gels. *Journal of Biomedical Materials Research Part A* **66**, 317-329 (2003).
110. L. P. Amarnath, A. Srinivas, A. Ramamurthi, In vitro hemocompatibility testing of UV-modified hyaluronan hydrogels. *Biomaterials* **27**, 1416-1424 (2006).
111. B. Joddar, A. Ramamurthi, Fragment size-and dose-specific effects of hyaluronan on matrix synthesis by vascular smooth muscle cells. *Biomaterials* **27**, 2994-3004 (2006).
112. R. Ohri, S. K. Hahn, A. S. Hoffman, P. S. Stayton, C. M. Giachelli, Hyaluronic acid grafting mitigates calcification of glutaraldehyde‐fixed bovine pericardium. *Journal of Biomedical Materials Research Part A* **70**, 328-334 (2004).
113. A. Chajara, M. Raoudi, B. Delpech, H. Levesque, Inhibition of arterial cells proliferation in vivo in injured arteries by hyaluronan fragments. *Atherosclerosis* **171**, 15-19 (2003).
114. E. A. Balazs, J. L. Denlinger, Viscosupplementation: a new concept in the treatment of osteoarthritis. *The Journal of rheumatology. Supplement* **39**, 3-9 (1993).
115. K. W. Marshall, Intra-articular hyaluronan therapy. *Current opinion in rheumatology* **12**, 468-474 (2000).
116. L. Liu, Y. Liu, J. Li, G. Du, J. Chen, Microbial production of hyaluronic acid: current state, challenges, and perspectives. *Microbial cell factories* **10**, 1 (2011).
117. R. M. Lauder, Chondroitin sulphate: a complex molecule with potential impacts on a wide range of biological systems. *Complementary therapies in medicine* **17**, 56-62 (2009).
118. C. D. Nandini *et al.*, Structural and functional characterization of oversulfated chondroitin sulfate/dermatan sulfate hybrid chains from the notochord of hagfish neuritogenic and binding activities for growth factors and neurotrophic factors. *Journal of Biological Chemistry* **279**, 50799-50809 (2004).
119. C. D. Nandini, N. Itoh, K. Sugahara, Novel 70-kDa chondroitin sulfate/dermatan sulfate hybrid chains with a unique heterogenous sulfation pattern from shark skin, which exhibit neuritogenic activity and binding activities for growth factors and neurotrophic factors. *Journal of Biological Chemistry* **280**, 4058-4069 (2005).
120. T. Hardingham, A. Fosang, Proteoglycans: many forms and many functions. *The FASEB Journal* **6**, 861-870 (1992).
121. K. Sugahara, T. Mikami, Chondroitin/dermatan sulfate in the central nervous system. *Current opinion in structural biology* **17**, 536-545 (2007).
122. C. D. Nandini, K. Sugahara, Role of the sulfation pattern of chondroitin sulfate in its biological activities and in the binding of growth factors. *Advances in pharmacology* **53**, 253-279 (2006).
123. R. M. Lauder, T. N. Huckerby, G. M. Brown, M. T. Bayliss, I. A. NIEDUSZYNSKI, Age-related changes in the sulphation of the chondroitin sulphate linkage region from human articular cartilage aggrecan. *Biochemical Journal* **358**, 523-528 (2001).

124. H. Nagase, M. Kashiwagi, Aggrecanases and cartilage matrix degradation. *Arthritis Res Ther* **5**, 1 (2003).
125. L. Antonilli, E. Paroli, Role of the oligosaccharide inner core in the inhibition of human leukocyte elastase by chondroitin sulfates. *International journal of clinical pharmacology research* **13**, 11-17 (1992).
126. A. Baici, P. Bradamante, Interaction between human leukocyte elastase and chondroitin sulfate. *Chemico-biological interactions* **51**, 1-11 (1984).
127. N. Volpi, Inhibition of human leukocyte elastase activity by chondroitin sulfates. *Chemico-biological interactions* **105**, 157-167 (1997).
128. E. J. Campbell, C. A. Owen, The sulfate groups of chondroitin sulfate-and heparan sulfate-containing proteoglycans in neutrophil plasma membranes are novel binding sites for human leukocyte elastase and cathepsin G. *Journal of Biological Chemistry* **282**, 14645-14654 (2007).
129. F. Legendre, C. Baugé, R. Roche, A. Saurel, J. Pujol, Chondroitin sulfate modulation of matrix and inflammatory gene expression in IL-1β-stimulated chondrocytes–study in hypoxic alginate bead cultures. *Osteoarthritis and cartilage* **16**, 105-114 (2008).
130. S. Y. Cho *et al.*, Effects of low molecular weight chondroitin sulfate on type II collagen-induced arthritis in DBA/1J mice. *Biological and Pharmaceutical Bulletin* **27**, 47-51 (2004).
131. C.-X. Xu *et al.*, Chondroitin sulfate extracted from the Styela clava tunic suppresses TNF-α-induced expression of inflammatory factors, VCAM-1 and iNOS by blocking Akt/NF-κB signal in JB6 cells. *Cancer letters* **264**, 93-100 (2008).
132. J. Du, N. Eddington, Determination of the chondroitin sulfate disaccharides in dog and horse plasma by HPLC using chondroitinase digestion, precolumn derivatization, and fluorescence detection. *Analytical biochemistry* **306**, 252-258 (2002).
133. N. Volpi, Oral absorption and bioavailability of ichthyic origin chondroitin sulfate in healthy male volunteers. *Osteoarthritis and cartilage* **11**, 433-441 (2003).
134. S. Kusano *et al.*, HPLC determination of chondrosine in mouse blood plasma after intravenous or oral dose. *Biological and Pharmaceutical Bulletin* **30**, 1365-1368 (2007).
135. L. Barthe *et al.*, In vitro intestinal degradation and absorption of chondroitin sulfate, a glycosaminoglycan drug. *Arzneimittelforschung* **54**, 286-292 (2004).
136. A. Rubinstein, D. Nakar, A. Sintov, Chondroitin sulfate: a potential biodegradable carrier for colon-specific drug delivery. *International journal of pharmaceutics* **84**, 141-150 (1992).
137. A. Sintov, N. Di-Capua, A. Rubinstein, Cross-linked chondroitin sulphate: characterization for drug delivery purposes. *Biomaterials* **16**, 473-478 (1995).
138. O. A. Cavalcanti, C. C. da SILVA, E. A. G. Pineda, A. A. W. Hechenleitner, Synthesis and characterization of phosphated crosslinked chondroitin sulfate: Potential ingredient for specific drug delivery. *acta farmacéutica bonaerense* **24**, 234 (2005).
139. J. Pieper, A. Oosterhof, P. Dijkstra, J. Veerkamp, T. Van Kuppevelt, Preparation and characterization of porous crosslinked collagenous matrices containing bioavailable chondroitin sulphate. *Biomaterials* **20**, 847-858 (1999).

140. J. L. van Susante *et al.*, Linkage of chondroitin-sulfate to type I collagen scaffolds stimulates the bioactivity of seeded chondrocytes in vitro. *Biomaterials* **22**, 2359-2369 (2001).
141. C.-H. Chang, H.-C. Liu, C.-C. Lin, C.-H. Chou, F.-H. Lin, Gelatin–chondroitin–hyaluronan tri-copolymer scaffold for cartilage tissue engineering. *Biomaterials* **24**, 4853-4858 (2003).
142. C.-S. Ko, J.-P. Huang, C.-W. Huang, I.-M. Chu, Type II collagen-chondroitin sulfate-hyaluronan scaffold cross-linked by genipin for cartilage tissue engineering. *Journal of bioscience and bioengineering* **107**, 177-182 (2009).
143. C.-T. Lee, P.-H. Kung, Y.-D. Lee, Preparation of poly (vinyl alcohol)-chondroitin sulfate hydrogel as matrices in tissue engineering. *Carbohydrate Polymers* **61**, 348-354 (2005).
144. M. Wollenweber *et al.*, Mimicked bioartificial matrix containing chondroitin sulphate on a textile scaffold of poly (3-hydroxybutyrate) alters the differentiation of adult human mesenchymal stem cells. *Tissue engineering* **12**, 345-359 (2006).
145. S. Varghese *et al.*, Chondroitin sulfate based niches for chondrogenic differentiation of mesenchymal stem cells. *Matrix Biology* **27**, 12-21 (2008).
146. D.-A. Wang *et al.*, Multifunctional chondroitin sulphate for cartilage tissue–biomaterial integration. *Nature materials* **6**, 385-392 (2007).
147. J. F. Piai, A. F. Rubira, E. C. Muniz, Self-assembly of a swollen chitosan/chondroitin sulfate hydrogel by outward diffusion of the chondroitin sulfate chains. *Acta biomaterialia* **5**, 2601-2609 (2009).
148. M. Dornish, D. Kaplan, Ø. Skaugrud, Standards and Guidelines for Biopolymers in Tissue‐Engineered Medical Products. *Annals of the New York Academy of Sciences* **944**, 388-397 (2001).
149. P. J. VandeVord *et al.*, Evaluation of the biocompatibility of a chitosan scaffold in mice. *Journal of biomedical materials research* **59**, 585-590 (2002).
150. K. S. Chow, E. Khor, Novel fabrication of open-pore chitin matrixes. *Biomacromolecules* **1**, 61-67 (2000).
151. G. Paradossi, E. Chiessi, M. Venanzi, B. Pispisa, A. Palleschi, Branched-chain analogues of linear polysaccharides: a spectroscopic and conformational investigation of chitosan derivatives. *International journal of biological macromolecules* **14**, 73-80 (1992).
152. K. Y. Lee, W. S. Ha, W. H. Park, Blood compatibility and biodegradability of partially N-acylated chitosan derivatives. *Biomaterials* **16**, 1211-1216 (1995).
153. K. Kamiyama, H. Onishi, Y. Machida, Biodisposition characteristics of N-succinyl-chitosan and glycol-chitosan in normal and tumor-bearing mice. *Biological and Pharmaceutical Bulletin* **22**, 179-186 (1999).
154. Y.-M. Chen, Y.-C. Chung, L. Woan Wang, K.-T. Chen, S.-Y. Li, Antibacterial properties of chitosan in waterborne pathogen. *Journal of Environmental Science and Health, Part A* **37**, 1379-1390 (2002).
155. S.-G. Hu, C.-H. Jou, M. Yang, Protein adsorption, fibroblast activity and antibacterial properties of poly (3-hydroxybutyric acid-co-3-hydroxyvaleric acid) grafted with chitosan and chitooligosaccharide after immobilized with hyaluronic acid. *Biomaterials* **24**, 2685-2693 (2003).

156. M. N. R. Kumar, A review of chitin and chitosan applications. *Reactive and functional polymers* **46**, 1-27 (2000).
157. J. Kim *et al.*, Preparation of doxorubicin-containing chitosan microspheres for transcatheter arterial chemoembolization of hepatocellular carcinoma. *Journal of microencapsulation* **24**, 408-419 (2007).
158. C. N. Mhurchu, C. Dunshea‐Mooij, D. Bennett, A. Rodgers, Effect of chitosan on weight loss in overweight and obese individuals: a systematic review of randomized controlled trials. *Obesity reviews* **6**, 35-42 (2005).
159. O. Felt, P. Buri, R. Gurny, Chitosan: a unique polysaccharide for drug delivery. *Drug development and industrial pharmacy* **24**, 979-993 (1998).
160. M. P. Patel, R. R. Patel, J. K. Patel, Chitosan mediated targeted drug delivery system: a review. *Journal of Pharmacy & Pharmaceutical Sciences* **13**, 536-557 (2010).
161. S. Kumbar, A. Kulkarni, T. Aminabhavi, Crosslinked chitosan microspheres for encapsulation of diclofenac sodium: effect of crosslinking agent. *Journal of microencapsulation* **19**, 173-180 (2002).
162. V. Mourya, N. N. Inamdar, Trimethyl chitosan and its applications in drug delivery. *Journal of Materials Science: Materials in Medicine* **20**, 1057-1079 (2009).
163. Y.-H. Lin *et al.*, Preparation and characterization of nanoparticles shelled with chitosan for oral insulin delivery. *Biomacromolecules* **8**, 146-152 (2007).
164. M.-C. Chen *et al.*, The characteristics, biodistribution and bioavailability of a chitosan-based nanoparticulate system for the oral delivery of heparin. *Biomaterials* **30**, 6629-6637 (2009).
165. N. Arya, S. Chakraborty, N. Dube, D. S. Katti, Electrospraying: a facile technique for synthesis of chitosan‐based micro/nanospheres for drug delivery applications. *Journal of Biomedical Materials Research Part B: Applied Biomaterials* **88**, 17-31 (2009).
166. Y.-H. Lin *et al.*, Preparation of nanoparticles composed of chitosan/poly-γ-glutamic acid and evaluation of their permeability through Caco-2 cells. *Biomacromolecules* **6**, 1104-1112 (2005).
167. S. W. Shalaby, J. A. DuBose, M. Shalaby, Chitosan based systems. *Absorbable and Biodegradable Polymers*, 77 (2004).
168. S. A. Agnihotri, T. M. Aminabhavi, Chitosan nanoparticles for prolonged delivery of timolol maleate. *Drug development and industrial pharmacy* **33**, 1254-1262 (2007).
169. T. Sonia, C. P. Sharma, in *Chitosan for biomaterials I*. (Springer, 2011), pp. 23-53.
170. S.-J. Seo *et al.*, Xyloglucan as a synthetic extracellular matrix for hepatocyte attachment. *Journal of Biomaterials Science, Polymer Edition* **15**, 1375-1387 (2004).
171. A. Gamian, M. Chomik, C. A. Laferrière, R. Roy, Inhibition of influenza A virus hemagglutinin and induction of interferon by synthetic sialylated glycoconjugates. *Canadian journal of microbiology* **37**, 233-237 (1991).
172. D. W. Jenkins, S. M. Hudson, Review of vinyl graft copolymerization featuring recent advances toward controlled radical-based reactions and illustrated with chitin/chitosan trunk polymers. *Chemical Reviews* **101**, 3245-3274 (2001).
173. Z. Ding *et al.*, Immobilization of chitosan onto poly-L-lactic acid film surface by plasma graft polymerization to control the morphology of fibroblast and liver cells. *Biomaterials* **25**, 1059-1067 (2004).

174. A. Zhu, M. Zhang, J. Wu, J. Shen, Covalent immobilization of chitosan/heparin complex with a photosensitive hetero-bifunctional crosslinking reagent on PLA surface. *Biomaterials* **23**, 4657-4665 (2002).
175. S. Mao *et al.*, Synthesis, characterization and cytotoxicity of poly (ethylene glycol)-graft-trimethyl chitosan block copolymers. *Biomaterials* **26**, 6343-6356 (2005).
176. E. Khor, L. Y. Lim, Implantable applications of chitin and chitosan. *Biomaterials* **24**, 2339-2349 (2003).
177. T.-W. Chung, Y.-F. Lu, S.-S. Wang, Y.-S. Lin, S.-H. Chu, Growth of human endothelial cells on photochemically grafted Gly–Arg–Gly–Asp (GRGD) chitosans. *Biomaterials* **23**, 4803-4809 (2002).
178. L. Li, Y.-L. Hsieh, Chitosan bicomponent nanofibers and nanoporous fibers. *Carbohydrate research* **341**, 374-381 (2006).
179. N. Bhattarai, D. Edmondson, O. Veiseh, F. A. Matsen, M. Zhang, Electrospun chitosan-based nanofibers and their cellular compatibility. *Biomaterials* **26**, 6176-6184 (2005).
180. E. Ruel-Gariepy, J.-C. Leroux, In situ-forming hydrogels—review of temperature-sensitive systems. *European Journal of Pharmaceutics and Biopharmaceutics* **58**, 409-426 (2004).
181. A. D. Augst, H. J. Kong, D. J. Mooney, Alginate hydrogels as biomaterials. *Macromolecular bioscience* **6**, 623-633 (2006).
182. B. Christensen, Alginates as biomaterials in tissue engineering. *Carbohydrate Chemistry: Chemical and Biological Approaches* **37**, 227-258 (2011).
183. Y. A. Mørch, S. Holtan, I. Donati, B. L. Strand, G. Skjåk-Bræk, Mechanical properties of C-5 epimerized alginates. *Biomacromolecules* **9**, 2360-2368 (2008).
184. S. Holtan, P. Bruheim, G. Skjåk-Bræk, Mode of action and subsite studies of the guluronan block-forming mannuronan C-5 epimerases AlgE1 and AlgE6. *Biochemical Journal* **395**, 319-329 (2006).
185. Ý. Mørch, I. Donati, B. L. Strand, G. Skjåk-Bræk, Molecular engineering as an approach to design new functional properties of alginate. *Biomacromolecules* **8**, 2809-2814 (2007).
186. H. J. Kong, M. K. Smith, D. J. Mooney, Designing alginate hydrogels to maintain viability of immobilized cells. *Biomaterials* **24**, 4023-4029 (2003).
187. I. Donati, S. Paoletti, in *Alginates: Biology and applications*. (Springer, 2009), pp. 1-53.
188. H. Holme, H. Foros, H. Pettersen, M. Dornish, O. Smidsrød, Thermal depolymerization of chitosan chloride. *Carbohydrate Polymers* **46**, 287-294 (2001).
189. H. K. Holme, K. Lindmo, A. Kristiansen, O. Smidsrød, Thermal depolymerization of alginate in the solid state. *Carbohydrate Polymers* **54**, 431-438 (2003).
190. O. Jeon, K. H. Bouhadir, J. M. Mansour, E. Alsberg, Photocrosslinked alginate hydrogels with tunable biodegradation rates and mechanical properties. *Biomaterials* **30**, 2724-2734 (2009).
191. M. Ashley, A. McCullagh, C. Sweet, Making a good impression:(a'how to'paper on dental alginate). *Dental update* **32**, 169-170, 172, 174-165 (2005).
192. I. R. Matthew, R. M. Browne, J. W. Frame, B. G. Millar, Subperiosteal behaviour of alginate and cellulose wound dressing materials. *Biomaterials* **16**, 275-278 (1995).

193. M. A. LeRoux, F. Guilak, L. A. Setton, Compressive and shear properties of alginate gel: effects of sodium ions and alginate concentration. *Journal of biomedical materials research* **47**, 46-53 (1999).
194. H. J. Kong, D. J. Mooney, The effects of poly (ethyleneimine)(PEI) molecular weight on reinforcement of alginate hydrogels. *Cell transplantation* **12**, 779-785 (2003).
195. J. L. Drury, R. G. Dennis, D. J. Mooney, The tensile properties of alginate hydrogels. *Biomaterials* **25**, 3187-3199 (2004).
196. D. F. Emerich, C. Halberstadt, C. Thanos, Role of nanobiotechnology in cell-based nanomedicine: A concise review. *Journal of Biomedical Nanotechnology* **3**, 235-244 (2007).
197. E. Alsberg *et al.*, Regulating bone formation via controlled scaffold degradation. *Journal of dental research* **82**, 903-908 (2003).
198. K. Y. Lee, K. H. Bouhadir, D. J. Mooney, Evaluation of chain stiffness of partially oxidized polyguluronate. *Biomacromolecules* **3**, 1129-1134 (2002).
199. K. Y. Lee, K. H. Bouhadir, D. J. Mooney, Degradation behavior of covalently cross-linked poly (aldehyde guluronate) hydrogels. *Macromolecules* **33**, 97-101 (2000).
200. A. Mosahebi, M. Wiberg, G. Terenghi, Addition of fibronectin to alginate matrix improves peripheral nerve regeneration in tissue-engineered conduits. *Tissue engineering* **9**, 209-218 (2003).
201. P. Prang *et al.*, The promotion of oriented axonal regrowth in the injured spinal cord by alginate-based anisotropic capillary hydrogels. *Biomaterials* **27**, 3560-3569 (2006).
202. R. Pasqualini, E. Koivunen, E. Ruoslahti, Alpha v integrins as receptors for tumor targeting by circulating ligands. *Nature biotechnology* **15**, 542-546 (1997).
203. K. H. Bouhadir, G. M. Kruger, K. Y. Lee, D. J. Mooney, Sustained and controlled release of daunomycin from cross‐linked poly (aldehyde guluronate) hydrogels. *Journal of pharmaceutical sciences* **89**, 910-919 (2000).
204. K. H. Bouhadir, E. Alsberg, D. J. Mooney, Hydrogels for combination delivery of antineoplastic agents. *Biomaterials* **22**, 2625-2633 (2001).
205. R. J. Laham *et al.*, Local perivascular delivery of basic fibroblast growth factor in patients undergoing coronary bypass surgery results of a phase I randomized, double-blind, placebo-controlled trial. *Circulation* **100**, 1865-1871 (1999).
206. Q. Sun *et al.*, Sustained vascular endothelial growth factor delivery enhances angiogenesis and perfusion in ischemic hind limb. *Pharmaceutical research* **22**, 1110-1116 (2005).
207. K. Lee *et al.*, in *Transplantation proceedings*. (Elsevier, 2004), vol. 36, pp. 2464-2465.
208. S. He, M. Zhang, Z. Geng, Y. Yin, K. Yao, Preparation and characterization of partially oxidized sodium alginate. *Chinese Journal of Applied Chemistry* **22**, 1007 (2005).
209. C. Gomez, M. Rinaudo, M. Villar, Oxidation of sodium alginate and characterization of the oxidized derivatives. *Carbohydrate Polymers* **67**, 296-304 (2007).
210. F.-L. Mi, H.-W. Sung, S.-S. Shyu, Drug release from chitosan–alginate complex beads reinforced by a naturally occurring cross-linking agent. *Carbohydrate Polymers* **48**, 61-72 (2002).

211. S. Alban, A. Schauerte, G. Franz, Anticoagulant sulfated polysaccharides: Part I. Synthesis and structure–activity relationships of new pullulan sulfates. *Carbohydrate Polymers* **47**, 267-276 (2002).
212. G. Sen, R. P. Singh, S. Pal, Microwave‐initiated synthesis of polyacrylamide grafted sodium alginate: Synthesis and characterization. *Journal of Applied Polymer Science* **115**, 63-71 (2010).
213. A. Sand, M. Yadav, K. Behari, Synthesis and characterization of alginate‐g‐vinyl sulfonic acid with a potassium peroxydiphosphate/thiourea system. *Journal of applied polymer science* **118**, 3685-3694 (2010).
214. W. Pluemsab, N. Sakairi, T. Furuike, Synthesis and inclusion property of α-cyclodextrin-linked alginate. *Polymer* **46**, 9778-9783 (2005).
215. M.-C. Carre, C. Delestre, P. Hubert, E. Dellacherie, Covalent coupling of a short polyether on sodium alginate: synthesis and characterization of the resulting amphiphilic derivative. *Carbohydrate polymers* **16**, 367-379 (1991).
216. I. Ugi, The α‐Addition of Immonium Ions and Anions to Isonitriles Accompanied by Secondary Reactions. *Angewandte Chemie International Edition in English* **1**, 8-21 (1962).
217. C. Galant, A.-L. Kjøniksen, G. T. Nguyen, K. D. Knudsen, B. Nyström, Altering associations in aqueous solutions of a hydrophobically modified alginate in the presence of β-cyclodextrin monomers. *The Journal of Physical Chemistry B* **110**, 190-195 (2006).
218. B. A. Justice, N. A. Badr, R. A. Felder, 3D cell culture opens new dimensions in cell-based assays. *Drug discovery today* **14**, 102-107 (2009).
219. S.-J. Shin *et al.*, "On the fly" continuous generation of alginate fibers using a microfluidic device. *Langmuir* **23**, 9104-9108 (2007).
220. K. H. Lee, S. J. Shin, Y. Park, S. H. Lee, Synthesis of cell‐laden alginate hollow fibers using microfluidic chips and microvascularized tissue‐engineering applications. *Small* **5**, 1264-1268 (2009).
221. C. A. Bonino *et al.*, Electrospinning alginate-based nanofibers: From blends to crosslinked low molecular weight alginate-only systems. *Carbohydrate Polymers* **85**, 111-119 (2011).
222. M. Bongio, J. J. van den Beucken, S. C. Leeuwenburgh, J. A. Jansen, Development of bone substitute materials: from 'biocompatible'to 'instructive'. *Journal of Materials Chemistry* **20**, 8747-8759 (2010).
223. M. Dvir-Ginzberg, T. Elkayam, S. Cohen, Induced differentiation and maturation of newborn liver cells into functional hepatic tissue in macroporous alginate scaffolds. *The FASEB Journal* **22**, 1440-1449 (2008).
224. D. Roy, M. Semsarilar, J. T. Guthrie, S. Perrier, Cellulose modification by polymer grafting: a review. *Chemical Society Reviews* **38**, 2046-2064 (2009).
225. H.-P. Fink, D. Hofmann, B. Philipp, Some aspects of lateral chain order in cellulosics from X-ray scattering. *Cellulose* **2**, 51-70 (1995).
226. A. Hebeish, J. T. Guthrie, in *The Chemistry and Technology of Cellulosic Copolymers*. (Springer, 1981), pp. 326-342.

227. O. Pajulo *et al.*, Viscose cellulose sponge as an implantable matrix: changes in the structure increase the production of granulation tissue. *Journal of biomedical materials research* **32**, 439-446 (1996).
228. M. Märtson, J. Viljanto, T. Hurme, P. Saukko, Biocompatibility of cellulose sponge with bone. *European surgical research* **30**, 426-432 (1998).
229. M. Märtson, J. Viljanto, T. Hurme, P. Laippala, P. Saukko, Is cellulose sponge degradable or stable as implantation material? An in vivo subcutaneous study in the rat. *Biomaterials* **20**, 1989-1995 (1999).
230. M. B. Turner, S. K. Spear, J. D. Holbrey, R. D. Rogers, Production of bioactive cellulose films reconstituted from ionic liquids. *Biomacromolecules* **5**, 1379-1384 (2004).
231. T. Miyamoto, S. i. Takahashi, H. Ito, H. Inagaki, Y. Noishiki, Tissue biocompatibility of cellulose and its derivatives. *Journal of biomedical materials research* **23**, 125-133 (1989).
232. W. K. Czaja, D. J. Young, M. Kawecki, R. M. Brown, The future prospects of microbial cellulose in biomedical applications. *Biomacromolecules* **8**, 1-12 (2007).
233. G. Helenius *et al.*, In vivo biocompatibility of bacterial cellulose. *Journal of Biomedical Materials Research Part A* **76**, 431-438 (2006).
234. G. T. Ciacco, T. F. Liebert, E. Frollini, T. J. Heinze, Application of the solvent dimethyl sulfoxide/tetrabutyl-ammonium fluoride trihydrate as reaction medium for the homogeneous acylation of Sisal cellulose. *Cellulose* **10**, 125-132 (2003).
235. T. Heinze, T. Liebert, Unconventional methods in cellulose functionalization. *Progress in polymer science* **26**, 1689-1762 (2001).
236. T. Heinze, T. F. Liebert, K. S. Pfeiffer, M. A. Hussain, Unconventional cellulose esters: synthesis, characterization and structure–property relations. *Cellulose* **10**, 283-296 (2003).
237. C. Altaner, J. Puls, B. Saake, Enzyme aided analysis of the substituent distribution along the chain of cellulose acetates regioselectively modified by the action of an Aspergillus niger acetylesterase. *Cellulose* **10**, 391-395 (2003).
238. S.-J. Lee, C. Altaner, J. Puls, B. Saake, Determination of the substituent distribution along cellulose acetate chains as revealed by enzymatic and chemical methods. *Carbohydrate polymers* **54**, 353-362 (2003).
239. A. Althin *et al.* (Google Patents, 1998).
240. S. Sternberg, D. R. Lynn. (Google Patents, 2000).
241. K. J. Edgar *et al.*, Advances in cellulose ester performance and application. *Progress in Polymer Science* **26**, 1605-1688 (2001).
242. E. Entcheva *et al.*, Functional cardiac cell constructs on cellulose-based scaffolding. *Biomaterials* **25**, 5753-5762 (2004).
243. M. I. Ugwoke *et al.*, Scintigraphic evaluation in rabbits of nasal drug delivery systems based on carbopol 971p® and carboxymethylcellulose. *Journal of controlled release* **68**, 207-214 (2000).
244. R.-N. Chen, H.-O. Ho, C.-Y. Yu, M.-T. Sheu, Development of swelling/floating gastroretentive drug delivery system based on a combination of hydroxyethyl cellulose and sodium carboxymethyl cellulose for Losartan and its clinical relevance in healthy volunteers with CYP2C9 polymorphism. *European Journal of Pharmaceutical Sciences* **39**, 82-89 (2010).

245. A. H. Shojaei, Buccal mucosa as a route for systemic drug delivery: a review. *J Pharm Pharm Sci* **1**, 15-30 (1998).
246. K. Pal, A. Banthia, D. Majumdar, Development of carboxymethyl cellulose acrylate for various biomedical applications. *Biomedical Materials* **1**, 85 (2006).
247. A. T. Reza, S. B. Nicoll, Characterization of novel photocrosslinked carboxymethylcellulose hydrogels for encapsulation of nucleus pulposus cells. *Acta Biomaterialia* **6**, 179-186 (2010).
248. H. Chen, M. Fan, Novel thermally sensitive pH-dependent chitosan/carboxymethyl cellulose hydrogels. *Journal of Bioactive and Compatible Polymers* **23**, 38-48 (2008).
249. J. Liuyun, L. Yubao, X. Chengdong, Preparation and biological properties of a novel composite scaffold of nano-hydroxyapatite/chitosan/carboxymethyl cellulose for bone tissue engineering. *Journal of biomedical science* **16**, 1 (2009).
250. P. G. Wuts, T. W. Greene, *Greene's protective groups in organic synthesis*. (John Wiley & Sons, 2006).
251. A. L. Schwan, M. L. Kalin, K. E. Vajda, T.-J. Xiang, D. Brillon, Oxidative fragmentations of selected 1-alkenyl sulfoxides. Chemical and spectroscopic evidence for 1-alkenesulfinyl chlorides. *Tetrahedron letters* **37**, 2345-2348 (1996).
252. K. Rahn, M. Diamantoglou, D. Klemm, H. Berghmans, T. Heinze, Homogeneous synthesis of cellulose p‐toluenesulfonates in N, N‐dimethylacetamide/LiCl solvent system. *Die Angewandte Makromolekulare Chemie* **238**, 143-163 (1996).
253. D. Klemm, B. Heublein, H. P. Fink, A. Bohn, Cellulose: fascinating biopolymer and sustainable raw material. *Angewandte Chemie International Edition* **44**, 3358-3393 (2005).
254. H. A. Krässig, V. Stannett, in *Fortschritte der Hochpolymeren-Forschung*. (Springer, 1965), pp. 111-156.
255. G. S. Chauhan, S. Mahajan, L. K. Guleria, Polymers from renewable resources: sorption of Cu 2+ ions by cellulose graft copolymers. *Desalination* **130**, 85-88 (2000).
256. K. Gupta, K. Khandekar, Temperature-responsive cellulose by ceric (IV) ion-initiated graft copolymerization of N-isopropylacrylamide. *Biomacromolecules* **4**, 758-765 (2003).
257. S. Vitta, E. Stahel, V. Stannett, The preparation and properties of acrylic and methacrylic acid grafted cellulose prepared by ceric ion initiation. Part I. Preparation of the grafted cellulose. *Journal of Macromolecular Science—Chemistry* **22**, 579-590 (1985).
258. A. Waly, F. Abdel‐Mohdy, A. Aly, A. Hebeish, Synthesis and characterization of cellulose ion exchanger. II. Pilot scale and utilization in dye‐heavy metal removal. *Journal of applied polymer science* **68**, 2151-2157 (1998).
259. K. El‐Salmawi, M. Zaid, S. Ibraheim, A. El‐Naggar, A. Zahran, Sorption of dye wastes by poly (vinyl alcohol)/poly (carboxymethyl cellulose) blend grafted through a radiation method. *Journal of applied polymer science* **82**, 136-142 (2001).
260. G. Odian, *Principles of polymerization*. (John Wiley & Sons, 2004).
261. R. Harkness, Biological functions of collagen. *Biological Reviews* **36**, 399-455 (1961).

262. G. Veit *et al.*, Collagen XXVIII, a novel von Willebrand factor A domain-containing protein with many imperfections in the collagenous domain. *Journal of Biological Chemistry* **281**, 3494-3504 (2006).
263. M. D. Shoulders, R. T. Raines, Collagen structure and stability. *Annual review of biochemistry* **78**, 929 (2009).
264. G. Kleinmann *et al.*, Collagen shields as a drug delivery system for the fourth-generation fluoroquinolones. *Ophthalmologica* **221**, 51-56 (2006).
265. F. G. Lyons *et al.*, The healing of bony defects by cell-free collagen-based scaffolds compared to stem cell-seeded tissue engineered constructs. *Biomaterials* **31**, 9232-9243 (2010).
266. J. Heino, The collagen receptor integrins have distinct ligand recognition and signaling functions. *Matrix Biology* **19**, 319-323 (2000).
267. C. M. Tierney *et al.*, The effects of collagen concentration and crosslink density on the biological, structural and mechanical properties of collagen-GAG scaffolds for bone tissue engineering. *Journal of the mechanical behavior of biomedical materials* **2**, 202-209 (2009).
268. M. M. Martino *et al.*, Engineering the growth factor microenvironment with fibronectin domains to promote wound and bone tissue healing. *Science translational medicine* **3**, 100ra189-100ra189 (2011).
269. S. Gomes, I. B. Leonor, J. F. Mano, R. L. Reis, D. L. Kaplan, Natural and genetically engineered proteins for tissue engineering. *Progress in polymer science* **37**, 1-17 (2012).
270. T. A. Petrie *et al.*, Multivalent integrin-specific ligands enhance tissue healing and biomaterial integration. *Science translational medicine* **2**, 45ra60-45ra60 (2010).
271. G. F. Smith, Fibrinogen–fibrin conversion. The mechanism of fibrin-polymer formation in solution. *Biochemical Journal* **185**, 1-11 (1980).
272. M. W. Mosesson, K. R. Siebenlist, D. A. Meh, The structure and biological features of fibrinogen and fibrin. *Annals of the New York Academy of Sciences* **936**, 11-30 (2001).
273. B. Blombäck, B. Hessel, D. Hogg, Disulfide bridges in NH 2-terminal part of human fibrinogen. *Thrombosis research* **8**, 639-658 (1976).
274. W. D. Spotnitz, Fibrin sealant: past, present, and future: a brief review. *World journal of surgery* **34**, 632-634 (2010).
275. I. Schvartz, D. Seger, S. Shaltiel, Vitronectin. *The international journal of biochemistry & cell biology* **31**, 539-544 (1999).
276. I. Schleicher *et al.*, Surface modification by complexes of vitronectin and growth factors for serum-free culture of human osteoblasts. *Tissue engineering* **11**, 1688-1698 (2005).
277. S. Reichl, Films based on human hair keratin as substrates for cell culture and tissue engineering. *Biomaterials* **30**, 6854-6866 (2009).
278. A. Tachibana, S. Kaneko, T. Tanabe, K. Yamauchi, Rapid fabrication of keratin–hydroxyapatite hybrid sponges toward osteoblast cultivation and differentiation. *Biomaterials* **26**, 297-302 (2005).
279. M. Heim, L. Römer, T. Scheibel, Hierarchical structures made of proteins. The complex architecture of spider webs and their constituent silk proteins. *Chemical Society Reviews* **39**, 156-164 (2010).

280. F. Sehnal, M. Zˇurovec, Construction of silk fiber core in Lepidoptera. *Biomacromolecules* **5**, 666-674 (2004).
281. S. Sofia, M. B. McCarthy, G. Gronowicz, D. L. Kaplan, Functionalized silk‐based biomaterials for bone formation. *Journal of biomedical materials research* **54**, 139-148 (2001).
282. K. Rezwan, Q. Chen, J. Blaker, A. R. Boccaccini, Biodegradable and bioactive porous polymer/inorganic composite scaffolds for bone tissue engineering. *Biomaterials* **27**, 3413-3431 (2006).
283. V. Maquet, A. R. Boccaccini, L. Pravata, I. Notingher, R. Jérôme, Porous poly (α-hydroxyacid)/Bioglass® composite scaffolds for bone tissue engineering. I: preparation and in vitro characterisation. *Biomaterials* **25**, 4185-4194 (2004).
284. A. R. Boccaccini, V. Maquet, Bioresorbable and bioactive polymer/Bioglass® composites with tailored pore structure for tissue engineering applications. *Composites Science and Technology* **63**, 2417-2429 (2003).
285. Z. Xiong, Y. Yan, S. Wang, R. Zhang, C. Zhang, Fabrication of porous scaffolds for bone tissue engineering via low-temperature deposition. *Scripta Materialia* **46**, 771-776 (2002).
286. J. Blaker, J. Gough, V. Maquet, I. Notingher, A. Boccaccini, In vitro evaluation of novel bioactive composites based on Bioglass®‐filled polylactide foams for bone tissue engineering scaffolds. *Journal of Biomedical Materials Research Part A* **67**, 1401-1411 (2003).
287. S. Verrier, J. J. Blaker, V. Maquet, L. L. Hench, A. R. Boccaccini, PDLLA/Bioglass® composites for soft-tissue and hard-tissue engineering: an in vitro cell biology assessment. *Biomaterials* **25**, 3013-3021 (2004).
288. A. Boccaccini *et al.*, PDLLA foams with TiO2 nanoparticles and PDLLA/TiO2-Bioglass foam composites for tissue engineering scaffolds. *J. Mater. Sci*, (2005).
289. J. M. Holzwarth, P. X. Ma, Biomimetic nanofibrous scaffolds for bone tissue engineering. *Biomaterials* **32**, 9622-9629 (2011).
290. C. Laurencin, H. Lu, Y. Khan, Processing of polymer scaffolds: polymer-ceramic composite foams. *Methods of tissue engineering*, 705-714 (2002).
291. C. Schiller, M. Siedler, F. Peters, M. Epple, Functionally graded materials of biodegradable polyesters and bone-like calcium phosphates for bone replacement. *Ceramic Transactions(USA)* **114**, 97-108 (2001).
292. J. Taboas, R. Maddox, P. Krebsbach, S. Hollister, Indirect solid free form fabrication of local and global porous, biomimetic and composite 3D polymer-ceramic scaffolds. *Biomaterials* **24**, 181-194 (2003).
293. D. W. Hutmacher, Scaffolds in tissue engineering bone and cartilage. *Biomaterials* **21**, 2529-2543 (2000).
294. H. H. Lu, S. F. El‐Amin, K. D. Scott, C. T. Laurencin, Three‐dimensional, bioactive, biodegradable, polymer‐bioactive glass composite scaffolds with improved mechanical properties support collagen synthesis and mineralization of human osteoblast‐like cells in vitro. *Journal of Biomedical Materials Research Part A* **64**, 465-474 (2003).

295. J. L. Brown, L. S. Nair, C. T. Laurencin, Solvent/non‐solvent sintering: A novel route to create porous microsphere scaffolds for tissue regeneration. *Journal of Biomedical Materials Research Part B: Applied Biomaterials* **86**, 396-406 (2008).
296. X. Deng, J. Hao, C. Wang, Preparation and mechanical properties of nanocomposites of poly (D, L-lactide) with Ca-deficient hydroxyapatite nanocrystals. *Biomaterials* **22**, 2867-2873 (2001).
297. J. L. Brown, M. S. Peach, L. S. Nair, S. G. Kumbar, C. T. Laurencin, Composite scaffolds: bridging nanofiber and microsphere architectures to improve bioactivity of mechanically competent constructs. *Journal of Biomedical Materials Research Part A* **95**, 1150-1158 (2010).
298. J. Roether *et al.*, Development and in vitro characterisation of novel bioresorbable and bioactive composite materials based on polylactide foams and Bioglass® for tissue engineering applications. *Biomaterials* **23**, 3871-3878 (2002).
299. J. F. Mano, R. A. Sousa, L. F. Boesel, N. M. Neves, R. L. Reis, Bioinert, biodegradable and injectable polymeric matrix composites for hard tissue replacement: state of the art and recent developments. *Composites Science and Technology* **64**, 789-817 (2004).
300. E. Sachs, M. Cima, P. Williams, D. Brancazio, J. Cornie, Three dimensional printing: rapid tooling and prototypes directly from a CAD model. *Journal of Engineering for Industry* **114**, 481-488 (1992).
301. B. M. Wu *et al.*, Solid free-form fabrication of drug delivery devices. *Journal of Controlled Release* **40**, 77-87 (1996).
302. M. K. Agarwala *et al.*, Structural quality of parts processed by fused deposition. *Rapid Prototyping Journal* **2**, 4-19 (1996).
303. J. M. Williams *et al.*, Bone tissue engineering using polycaprolactone scaffolds fabricated via selective laser sintering. *Biomaterials* **26**, 4817-4827 (2005).
304. A. Ronca, L. Ambrosio, D. Grijpma, Preparation of designed poly (D, L-lactide)/nanosized hydroxyapatite composite structures by stereolithography. *Acta biomaterialia* **9**, 5989-5996 (2013).
305. Y. Luo, C. Wu, A. Lode, M. Gelinsky, Hierarchical mesoporous bioactive glass/alginate composite scaffolds fabricated by three-dimensional plotting for bone tissue engineering. *Biofabrication* **5**, 015005 (2012).
306. R. J. Mart, R. D. Osborne, M. M. Stevens, R. V. Ulijn, Peptide-based stimuli-responsive biomaterials. *Soft Matter* **2**, 822-835 (2006).
307. G. A. Silva *et al.*, Selective differentiation of neural progenitor cells by high-epitope density nanofibers. *Science* **303**, 1352-1355 (2004).
308. M. G. Ryadnov, D. N. Woolfson, Engineering the morphology of a self-assembling protein fibre. *Nature materials* **2**, 329-332 (2003).
309. V. Jayawarna *et al.*, Nanostructured Hydrogels for Three‐Dimensional Cell Culture Through Self‐Assembly of Fluorenylmethoxycarbonyl‐Dipeptides. *Advanced Materials* **18**, 611-614 (2006).
310. M. M. Stevens, Biomaterials for bone tissue engineering. *Materials today* **11**, 18-25 (2008).
311. D. H. Reneker, I. Chun, Nanometre diameter fibres of polymer, produced by electrospinning. *Nanotechnology* **7**, 216 (1996).

312. P. Katta, M. Alessandro, R. Ramsier, G. Chase, Continuous electrospinning of aligned polymer nanofibers onto a wire drum collector. *Nano letters* **4**, 2215-2218 (2004).
313. K. Li *et al.*, Composite mesoporous silica nanoparticle/chitosan nanofibers for bone tissue engineering. *RSC Advances* **5**, 17541-17549 (2015).
314. E. Alsberg, K. Anderson, A. Albeiruti, R. Franceschi, D. Mooney, Cell-interactive alginate hydrogels for bone tissue engineering. *Journal of dental research* **80**, 2025-2029 (2001).
315. C. PAUTKE *et al.*, Characterization of osteosarcoma cell lines MG-63, Saos-2 and U-2 OS in comparison to human osteoblasts. *Anticancer research* **24**, 3743-3748 (2004).
316. X. Yu, E. A. Botchwey, E. M. Levine, S. R. Pollack, C. T. Laurencin, Bioreactor-based bone tissue engineering: the influence of dynamic flow on osteoblast phenotypic expression and matrix mineralization. *Proceedings of the National Academy of Sciences of the United States of America* **101**, 11203-11208 (2004).
317. L. L. Hench, J. M. Polak, Third-generation biomedical materials. *Science* **295**, 1014-1017 (2002).
318. G. Z. Jin *et al.*, Bone tissue engineering of induced pluripotent stem cells cultured with macrochanneled polymer scaffold. *Journal of Biomedical Materials Research Part A* **101**, 1283-1291 (2013).
319. P. W. Andrews, Toward safer regenerative medicine. *Nature biotechnology* **29**, 803-805 (2011).
320. C. Colnot, Cell sources for bone tissue engineering: insights from basic science. *Tissue Engineering Part B: Reviews* **17**, 449-457 (2011).
321. S. Agacayak, B. Gulsun, M. Ucan, E. Karaoz, Y. Nergiz, Effects of mesenchymal stem cells in critical size bone defect. *Eur Rev Med Pharmacol Sci* **16**, 679-686 (2012).
322. F. Granero‐Moltó *et al.*, Regenerative effects of transplanted mesenchymal stem cells in fracture healing. *Stem cells* **27**, 1887-1898 (2009).
323. A. De Luca *et al.*, Role of the EGFR ligand/receptor system in the secretion of angiogenic factors in mesenchymal stem cells. *Journal of cellular physiology* **226**, 2131-2138 (2011).
324. J. Shao, W. Zhang, T. Yang, Using mesenchymal stem cells as a therapy for bone regeneration and repairing. *Biological research* **48**, 1 (2015).
325. Z. Y. Li, C. Q. Wang, G. Lu, X. Y. Pan, K. L. Xu, Effects of bone marrow mesenchymal stem cells on hematopoietic recovery and acute graft-versus-host disease in murine allogeneic umbilical cord blood transplantation model. *Cell biochemistry and biophysics* **70**, 115-122 (2014).
326. P. A. Zuk *et al.*, Human adipose tissue is a source of multipotent stem cells. *Molecular biology of the cell* **13**, 4279-4295 (2002).
327. S. Tholpady, A. Katz, R. Ogle, Mesenchymal stem cells from rat visceral fat exhibit multipotential differentiation in vitro. *The Anatomical Record Part A: Discoveries in Molecular, Cellular, and Evolutionary Biology* **272**, 398-402 (2003).
328. H. Hattori *et al.*, Bone formation using human adipose tissue‐derived stromal cells and a biodegradable scaffold. *Journal of Biomedical Materials Research Part B: Applied Biomaterials* **76**, 230-239 (2006).
329. K. C. Hicok *et al.*, Human adipose-derived adult stem cells produce osteoid in vivo. *Tissue engineering* **10**, 371-380 (2004).

330. C. M. Cowan *et al.*, Adipose-derived adult stromal cells heal critical-size mouse calvarial defects. *Nature biotechnology* **22**, 560-567 (2004).
331. S. Lendeckel *et al.*, Autologous stem cells (adipose) and fibrin glue used to treat widespread traumatic calvarial defects: case report. *Journal of Cranio-Maxillofacial Surgery* **32**, 370-373 (2004).
332. F. Barrere, T. Mahmood, K. De Groot, C. Van Blitterswijk, Advanced biomaterials for skeletal tissue regeneration: Instructive and smart functions. *Materials Science and Engineering: R: Reports* **59**, 38-71 (2008).
333. R. W. Bucholz, Nonallograft osteoconductive bone graft substitutes. *Clinical orthopaedics and related research* **395**, 44-52 (2002).
334. S. Chung, M. W. King, Design concepts and strategies for tissue engineering scaffolds. *Biotechnology and applied biochemistry* **58**, 423-438 (2011).
335. J. L. Arias, M. a. S. Fernández, Polysaccharides and proteoglycans in calcium carbonate-based biomineralization. *Chemical Reviews* **108**, 4475-4482 (2008).
336. I. Ahmed *et al.*, Morphology, cytoskeletal organization, and myosin dynamics of mouse embryonic fibroblasts cultured on nanofibrillar surfaces. *Molecular and cellular biochemistry* **301**, 241-249 (2007).
337. C. Lohmann *et al.*, Surface roughness modulates the response of MG63 osteoblast‐like cells to 1, 25‐(OH) 2D3 through regulation of phospholipase A2 activity and activation of protein kinase A. *Journal of biomedical materials research* **47**, 139-151 (1999).
338. Y. Mei *et al.*, Combinatorial development of biomaterials for clonal growth of human pluripotent stem cells. *Nature materials* **9**, 768-778 (2010).
339. B. G. Keselowsky, D. M. Collard, A. J. García, Surface chemistry modulates focal adhesion composition and signaling through changes in integrin binding. *Biomaterials* **25**, 5947-5954 (2004).
340. J. E. Phillips, T. A. Petrie, F. P. Creighton, A. J. García, Human mesenchymal stem cell differentiation on self-assembled monolayers presenting different surface chemistries. *Acta biomaterialia* **6**, 12-20 (2010).
341. P. X. Ma, R. Zhang, Synthetic nano-scale fibrous extracellular matrix. *Journal of biomedical materials research* **46**, 60-72 (1999).
342. K. M. Woo, V. J. Chen, P. X. Ma, Nano‐fibrous scaffolding architecture selectively enhances protein adsorption contributing to cell attachment. *Journal of biomedical materials research Part A* **67**, 531-537 (2003).
343. P. A. Gunatillake, R. Adhikari, Biodegradable synthetic polymers for tissue engineering. *Eur Cell Mater* **5**, 1-16 (2003).
344. S. P. Nukavarapu *et al.*, Polyphosphazene/nano-hydroxyapatite composite microsphere scaffolds for bone tissue engineering. *Biomacromolecules* **9**, 1818-1825 (2008).
345. C. M. Valmikinathan *et al.*, Photocrosslinkable chitosan based hydrogels for neural tissue engineering. *Soft Matter* **8**, 1964-1976 (2012).
346. P. Arpornmaeklong, P. Pripatnanont, N. Suwatwirote, Properties of chitosan–collagen sponges and osteogenic differentiation of rat-bone-marrow stromal cells. *International journal of oral and maxillofacial surgery* **37**, 357-366 (2008).

347. U. Geissler *et al.*, Collagen type I - coating of Ti6Al4V promotes adhesion of osteoblasts. *Journal of biomedical materials research* **51**, 752-760 (2000).
348. C. M. Valmikinathan, S. Defroda, X. Yu, Polycaprolactone and bovine serum albumin based nanofibers for controlled release of nerve growth factor. *Biomacromolecules* **10**, 1084-1089 (2009).
349. C. Yao *et al.*, [Experimental research of astragalus polysaccharides collagen sponge in enhancing angiogenesis and collagen synthesis]. *Zhongguo xiu fu chong jian wai ke za zhi= Zhongguo xiufu chongjian waike zazhi= Chinese journal of reparative and reconstructive surgery* **25**, 1481-1485 (2011).
350. C. L. Casper, W. Yang, M. C. Farach-Carson, J. F. Rabolt, Coating electrospun collagen and gelatin fibers with perlecan domain I for increased growth factor binding. *Biomacromolecules* **8**, 1116-1123 (2007).
351. Y. Duan *et al.*, Preparation of collagen-coated electrospun nanofibers by remote plasma treatment and their biological properties. *Journal of Biomaterials Science, Polymer Edition* **18**, 1153-1164 (2007).
352. S. Kumbar *et al.*, Novel mechanically competent polysaccharide scaffolds for bone tissue engineering. *Biomedical Materials* **6**, 065005 (2011).
353. M. Kofron, J. Cooper, S. Kumbar, C. Laurencin, Novel tubular composite matrix for bone repair. *Journal of Biomedical Materials Research Part A* **82**, 415-425 (2007).
354. C. J. Brinker, Y. Lu, A. Sellinger, H. Fan, Evaporation-induced self-assembly: nanostructures made easy. *Advanced materials* **11**, 579-585 (1999).
355. H. W. Kim, L. H. Li, E. J. Lee, S. H. Lee, H. E. Kim, Fibrillar assembly and stability of collagen coating on titanium for improved osteoblast responses. *Journal of Biomedical Materials Research Part A* **75**, 629-638 (2005).
356. M. Deng *et al.*, Miscibility and in vitro osteocompatibility of biodegradable blends of poly [(ethyl alanato)(p-phenyl phenoxy) phosphazene] and poly (lactic acid-glycolic acid). *Biomaterials* **29**, 337-349 (2008).
357. M. L. Decaris, B. Y. Binder, M. A. Soicher, A. Bhat, J. K. Leach, Cell-derived matrix coatings for polymeric scaffolds. *Tissue engineering Part A* **18**, 2148-2157 (2012).
358. C. T. Laurencin, T. Jiang, S. G. Kumbar, L. S. Nair, Biologically active chitosan systems for tissue engineering and regenerative medicine. *Current topics in medicinal chemistry* **8**, 354-364 (2008).
359. K. A. Athanasiou, C.-F. Zhu, D. Lanctot, C. Agrawal, X. Wang, Fundamentals of biomechanics in tissue engineering of bone. *Tissue engineering* **6**, 361-381 (2000).
360. K. A. Athanasiou, C. M. Agrawal, F. A. Barber, S. S. Burkhart, Orthopaedic applications for PLA-PGA biodegradable polymers. *Arthroscopy: The Journal of Arthroscopic & Related Surgery* **14**, 726-737 (1998).
361. K. Sawakami *et al.*, Polymethylmethacrylate augmentation of pedicle screws increases the initial fixation in osteoporotic spine patients. *Clinical Spine Surgery* **25**, E28-E35 (2012).
362. M. D. Kofron *et al.*, The Implications of Polymer Selection in Regenerative Medicine: A Comparison of Amorphous and Semi - Crystalline Polymer for Tissue Regeneration. *Advanced Functional Materials* **19**, 1351-1359 (2009).

363. M. Borden, S. El-Amin, M. Attawia, C. Laurencin, Structural and human cellular assessment of a novel microsphere-based tissue engineered scaffold for bone repair. *Biomaterials* **24**, 597-609 (2003).
364. A. C. Stähelin, A. Weiler, All-inside anterior cruciate ligament reconstruction using semitendinosus tendon and soft threaded biodegradable interference screw fixation. *Arthroscopy: The Journal of Arthroscopic & Related Surgery* **13**, 773-779 (1997).
365. O. Böstman, Osteoarthritis of the ankle after foreign-body reaction to absorbable pins and screws. *Bone & Joint Journal* **80**, 333-338 (1998).
366. A. Weiler, S. Scheffler, N. Südkamp, Current aspects of anchoring hamstring tendon transplants in cruciate ligament surgery. *Der Chirurg; Zeitschrift für alle Gebiete der operativen Medizen* **71**, 1034 (2000).
367. M. Deng *et al.*, In situ Porous Structures: A Unique Polymer Erosion Mechanism in Biodegradable Dipeptide‐Based Polyphosphazene and Polyester Blends Producing Matrices for Regenerative Engineering. *Advanced functional materials* **20**, 2794-2806 (2010).
368. M. Deng *et al.*, Biomimetic Structures: Biological Implications of Dipeptide‐Substituted Polyphosphazene‐Polyester Blend Nanofiber Matrices for Load‐Bearing Bone Regeneration. *Advanced Functional Materials* **21**, 2641-2651 (2011).
369. F. Nudelman *et al.*, The role of collagen in bone apatite formation in the presence of hydroxyapatite nucleation inhibitors. *Nature materials* **9**, 1004-1009 (2010).
370. A. Travan *et al.*, Polysaccharide-coated thermosets for orthopedic applications: from material characterization to in vivo tests. *Biomacromolecules* **13**, 1564-1572 (2012).
371. M. Borden, M. Attawia, Y. Khan, S. El-Amin, C. Laurencin, Tissue-engineered bone formation in vivo using a novel sintered polymeric microsphere matrix. *Bone & Joint Journal* **86**, 1200-1208 (2004).
372. T. Jiang, W. I. Abdel-Fattah, C. T. Laurencin, In vitro evaluation of chitosan/poly (lactic acid-glycolic acid) sintered microsphere scaffolds for bone tissue engineering. *Biomaterials* **27**, 4894-4903 (2006).
373. T. Jiang, Y. Khan, L. S. Nair, W. I. Abdel‐Fattah, C. T. Laurencin, Functionalization of chitosan/poly (lactic acid‐glycolic acid) sintered microsphere scaffolds via surface heparinization for bone tissue engineering. *Journal of Biomedical Materials Research Part A* **93**, 1193-1208 (2010).
374. T. Białopiotrowicz, B. Jańczuk, The wettability of a cellulose acetate membrane in the presence of bovine serum albumin. *Applied surface science* **201**, 146-153 (2002).
375. L. Chan, K. Chow, P. Heng, Investigation of wetting behavior of nonaqueous ethylcellulose gel matrices using dynamic contact angle. *Pharmaceutical research* **23**, 408-421 (2006).
376. B. Valamehr *et al.*, Hydrophobic surfaces for enhanced differentiation of embryonic stem cell-derived embryoid bodies. *Proceedings of the National Academy of Sciences* **105**, 14459-14464 (2008).
377. A. Ranella, M. Barberoglou, S. Bakogianni, C. Fotakis, E. Stratakis, Tuning cell adhesion by controlling the roughness and wettability of 3D micro/nano silicon structures. *Acta biomaterialia* **6**, 2711-2720 (2010).

378. S. Kumbar, R. James, S. Nukavarapu, C. Laurencin, Electrospun nanofiber scaffolds: engineering soft tissues. *Biomedical Materials* **3**, 034002 (2008).
379. E. K. Yim, E. M. Darling, K. Kulangara, F. Guilak, K. W. Leong, Nanotopography-induced changes in focal adhesions, cytoskeletal organization, and mechanical properties of human mesenchymal stem cells. *Biomaterials* **31**, 1299-1306 (2010).
380. K. Tuzlakoglu, M. I. Santos, N. Neves, R. L. Reis, Design of nano-and microfiber combined scaffolds by electrospinning of collagen onto starch-based fiber meshes: a man-made equivalent of natural extracellular matrix. *Tissue Engineering Part A* **17**, 463-473 (2010).
381. P. Habibovic, K. de Groot, Osteoinductive biomaterials—properties and relevance in bone repair. *Journal of tissue engineering and regenerative medicine* **1**, 25-32 (2007).
382. R. Bodmeier, O. Paeratakul, Mechanical properties of dry and wet cellulosic and acrylic films prepared from aqueous colloidal polymer dispersions used in the coating of solid dosage forms. *Pharmaceutical research* **11**, 882-888 (1994).
383. R. Ayala *et al.*, Engineering the cell–material interface for controlling stem cell adhesion, migration, and differentiation. *Biomaterials* **32**, 3700-3711 (2011).
384. A. K. Kundu, A. J. Putnam, Vitronectin and collagen I differentially regulate osteogenesis in mesenchymal stem cells. *Biochemical and biophysical research communications* **347**, 347-357 (2006).
385. M. Galindo *et al.*, The bone-specific expression of Runx2 oscillates during the cell cycle to support a G1-related antiproliferative function in osteoblasts. *Journal of Biological Chemistry* **280**, 20274-20285 (2005).
386. S. Gronthos, S. Chen, C. Y. Wang, P. G. Robey, S. Shi, Telomerase accelerates osteogenesis of bone marrow stromal stem cells by upregulation of CBFA1, osterix, and osteocalcin. *Journal of Bone and Mineral Research* **18**, 716-722 (2003).
387. D. M. Thomas *et al.*, The retinoblastoma protein acts as a transcriptional coactivator required for osteogenic differentiation. *Molecular cell* **8**, 303-316 (2001).
388. E. e. Golub, Enzymes in mineralizing systems: state of the art. *Connective tissue research* **35**, 183-188 (1996).
389. M. J. Glimcher, Mechanism of calcification: Role of collagen fibrils and collagen‐phosphoprotein complexes in vitro and in vivo. *The Anatomical Record* **224**, 139-153 (1989).
390. P. Pooyan, R. Tannenbaum, H. Garmestani, Mechanical behavior of a cellulose-reinforced scaffold in vascular tissue engineering. *Journal of the mechanical behavior of biomedical materials* **7**, 50-59 (2012).
391. A. Aravamudhan *et al.*, Cellulose and collagen derived micro-nano structured scaffolds for bone tissue engineering. *Journal of biomedical nanotechnology* **9**, 719-731 (2013).
392. M. D. Kofron, J. A. Cooper, Jr., S. G. Kumbar, C. T. Laurencin, Novel tubular composite matrix for bone repair. *Journal of biomedical materials research.Part A* **82**, 415-425 (2007).
393. P. X. Ma, Biomimetic materials for tissue engineering. *Advanced drug delivery reviews* **60**, 184-198 (2008).

394. M. V. Jose, V. Thomas, K. T. Johnson, D. R. Dean, E. Nyairo, Aligned PLGA/HA nanofibrous nanocomposite scaffolds for bone tissue engineering. *Acta biomaterialia* **5**, 305-315 (2009).
395. P. Gentile, V. Chiono, I. Carmagnola, P. V. Hatton, An overview of poly (lactic-co-glycolic) acid (PLGA)-based biomaterials for bone tissue engineering. *International journal of molecular sciences* **15**, 3640-3659 (2014).
396. J. M. Anderson, M. S. Shive, Biodegradation and biocompatibility of PLA and PLGA microspheres. *Advanced drug delivery reviews* **64**, 72-82 (2012).
397. F. B. Basmanav, G. T. Kose, V. Hasirci, Sequential growth factor delivery from complexed microspheres for bone tissue engineering. *Biomaterials* **29**, 4195-4204 (2008).
398. G. Anand, S. Sharma, A. K. Dutta, S. K. Kumar, G. Belfort, Conformational transitions of adsorbed proteins on surfaces of varying polarity. *Langmuir* **26**, 10803-10811 (2010).
399. Y. Yamashita, T. Endo, Deterioration behavior of cellulose acetate films in acidic or basic aqueous solutions. *Journal of applied polymer science* **91**, 3354-3361 (2004).
400. R. L. Sammons, N. Lumbikanonda, M. Gross, P. Cantzler, Comparison of osteoblast spreading on microstructured dental implant surfaces and cell behaviour in an explant model of osseointegration. *Clinical oral implants research* **16**, 657-666 (2005).
401. B. Boyan *et al.*, Osteoblast-mediated mineral deposition in culture is dependent on surface microtopography. *Calcified tissue international* **71**, 519-529 (2002).
402. C. Lohmann *et al.*, Maturation State Determines the Response of Osteogenic Cells to Surface Roughness and 1, 25‐Dihydroxyvitamin D3. *Journal of Bone and Mineral Research* **15**, 1169-1180 (2000).
403. L. Wang *et al.*, Integrin β 1 silencing in osteoblasts alters substrate-dependent responses to 1, 25-dihydroxy vitamin D 3. *Biomaterials* **27**, 3716-3725 (2006).
404. L. Bacakova *et al.*, *Nanocomposite and nanostructured carbon-based films as growth substrates for bone cells*. (INTECH Open Access Publisher, 2011).
405. L. Xu, A. L. Anderson, Q. Lu, J. Wang, Role of fibrillar structure of collagenous carrier in bone sialoprotein-mediated matrix mineralization and osteoblast differentiation. *Biomaterials* **28**, 750-761 (2007).
406. S.-W. Tsai *et al.*, MG63 osteoblast-like cells exhibit different behavior when grown on electrospun collagen matrix versus electrospun gelatin matrix. *PloS one* **7**, e31200 (2012).
407. J. B. Lee *et al.*, Modification of PLGA nanofibrous mats by electron beam irradiation for soft tissue regeneration. *Journal of Nanomaterials* **2015**, 136 (2015).
408. D. Naumann, D. Helm, H. Labischinski, P. Giesbrecht, The characterization of microorganisms by Fourier-transform infrared spectroscopy (FT-IR). *Modern techniques for rapid microbiological analysis*, 43-96 (1991).
409. L. Bačáková, M. Lapčíková, D. Kubies, F. Rypáček, in *Tissue Engineering, Stem Cells, and Gene Therapies*. (Springer, 2003), pp. 179-189.
410. E. Filová *et al.*, Vascular endothelial cells on two‐and three‐dimensional fibrin assemblies for biomaterial coatings. *Journal of Biomedical Materials Research Part A* **90**, 55-69 (2009).

411. L. Grausova *et al.*, Bone and vascular endothelial cells in cultures on nanocrystalline diamond films. *Diamond and Related Materials* **17**, 1405-1409 (2008).
412. L. Grausova *et al.*, Molecular markers of adhesion, maturation and immune activation of human osteoblast-like MG 63 cells on nanocrystalline diamond films. *Diamond and Related Materials* **18**, 258-263 (2009).
413. J. M. Curran, R. Chen, J. A. Hunt, The guidance of human mesenchymal stem cell differentiation in vitro by controlled modifications to the cell substrate. *Biomaterials* **27**, 4783-4793 (2006).
414. B. G. Keselowsky, D. M. Collard, A. J. García, Surface chemistry modulates fibronectin conformation and directs integrin binding and specificity to control cell adhesion. *Journal of Biomedical Materials Research Part A* **66**, 247-259 (2003).
415. K. Lee, E. A. Silva, D. J. Mooney, Growth factor delivery-based tissue engineering: general approaches and a review of recent developments. *Journal of the Royal Society Interface* **8**, 153-170 (2011).
416. C. Li, C. Vepari, H.-J. Jin, H. J. Kim, D. L. Kaplan, Electrospun silk-BMP-2 scaffolds for bone tissue engineering. *Biomaterials* **27**, 3115-3124 (2006).
417. W. L. Murphy, M. C. Peters, D. H. Kohn, D. J. Mooney, Sustained release of vascular endothelial growth factor from mineralized poly (lactide-co-glycolide) scaffolds for tissue engineering. *Biomaterials* **21**, 2521-2527 (2000).
418. I. Martin *et al.*, Enhanced cartilage tissue engineering by sequential exposure of chondrocytes to FGF‐2 during 2D expansion and BMP‐2 during 3D cultivation. *Journal of cellular biochemistry* **83**, 121-128 (2001).
419. P. C. Bessa, M. Casal, R. Reis, Bone morphogenetic proteins in tissue engineering: the road from laboratory to clinic, part II (BMP delivery). *Journal of tissue engineering and regenerative medicine* **2**, 81-96 (2008).
420. A. Aravamudhan *et al.*, Osteoinductive small molecules: growth factor alternatives for bone tissue engineering. *Current pharmaceutical design* **19**, 3420-3428 (2013).
421. F. Guilak *et al.*, Control of stem cell fate by physical interactions with the extracellular matrix. *Cell stem cell* **5**, 17-26 (2009).
422. A. J. Engler, S. Sen, H. L. Sweeney, D. E. Discher, Matrix elasticity directs stem cell lineage specification. *Cell* **126**, 677-689 (2006).
423. A. J. García, D. Boettiger, Integrin–fibronectin interactions at the cell-material interface: initial integrin binding and signaling. *Biomaterials* **20**, 2427-2433 (1999).
424. D. L. Elbert, J. A. Hubbell, Surface treatments of polymers for biocompatibility. *Annual Review of Materials Science* **26**, 365-394 (1996).
425. A. Krishnan, P. Cha, Y.-H. Liu, D. Allara, E. A. Vogler, Interfacial energetics of blood plasma and serum adsorption to a hydrophobic self-assembled monolayer surface. *Biomaterials* **27**, 3187-3194 (2006).
426. E. A. Vogler, Protein adsorption in three dimensions. *Biomaterials* **33**, 1201-1237 (2012).
427. J. Comelles, M. Estévez, E. Martínez, J. Samitier, The role of surface energy of technical polymers in serum protein adsorption and MG-63 cells adhesion. *Nanomedicine: Nanotechnology, Biology and Medicine* **6**, 44-51 (2010).

428. J. D. Bryers, C. M. Giachelli, B. D. Ratner, Engineering biomaterials to integrate and heal: the biocompatibility paradigm shifts. *Biotechnology and bioengineering* **109**, 1898-1911 (2012).
429. Z. Ma, Z. Mao, C. Gao, Surface modification and property analysis of biomedical polymers used for tissue engineering. *Colloids and Surfaces B: Biointerfaces* **60**, 137-157 (2007).
430. M. O. Klein *et al.*, Submicron scale‐structured hydrophilic titanium surfaces promote early osteogenic gene response for cell adhesion and cell differentiation. *Clinical implant dentistry and related research* **15**, 166-175 (2013).
431. K. Webb, V. Hlady, P. A. Tresco, Relative importance of surface wettability and charged functional groups on NIH 3T3 fibroblast attachment, spreading, and cytoskeletal organization. *Journal of biomedical materials research* **41**, 422 (1998).
432. J. Wei *et al.*, Adhesion of mouse fibroblasts on hexamethyldisiloxane surfaces with wide range of wettability. *Journal of Biomedical Materials Research Part B: Applied Biomaterials* **81**, 66-75 (2007).
433. B. St-Jacques, M. Hammerschmidt, A. P. McMahon, Indian hedgehog signaling regulates proliferation and differentiation of chondrocytes and is essential for bone formation. *Genes & development* **13**, 2072-2086 (1999).
434. C. Scotti *et al.*, Recapitulation of endochondral bone formation using human adult mesenchymal stem cells as a paradigm for developmental engineering. *Proceedings of the National Academy of Sciences* **107**, 7251-7256 (2010).
435. S. M. Zunich *et al.*, Osteoblast-secreted collagen upregulates paracrine Sonic hedgehog signaling by prostate cancer cells and enhances osteoblast differentiation. *Molecular cancer* **11**, 1 (2012).
436. J. M. Anderson, Biological responses to materials. *Annual review of materials research* **31**, 81-110 (2001).
437. B. D. Ratner, Healing with medical implants: The body battles back. *Science translational medicine* **7**, 272fs274 (2015).
438. H. Elwing *et al.*, Conformational changes of a model protein (complement factor 3) adsorbed on hydrophilic and hydrophobic solid surfaces. *Journal of colloid and interface science* **125**, 139-145 (1988).
439. K. L. Menzies, L. Jones, The impact of contact angle on the biocompatibility of biomaterials. *Optometry & Vision Science* **87**, 387-399 (2010).
440. E. M. Sussman, M. C. Halpin, J. Muster, R. T. Moon, B. D. Ratner, Porous implants modulate healing and induce shifts in local macrophage polarization in the foreign body reaction. *Annals of biomedical engineering* **42**, 1508-1516 (2014).
441. L. Zhang *et al.*, Zwitterionic hydrogels implanted in mice resist the foreign-body reaction. *Nature biotechnology* **31**, 553-556 (2013).
442. J. Mano *et al.*, Natural origin biodegradable systems in tissue engineering and regenerative medicine: present status and some moving trends. *Journal of the Royal Society Interface* **4**, 999-1030 (2007).
443. T. Jiang, W. I. Abdel-Fattah, C. T. Laurencin, In vitro evaluation of chitosan/poly(lactic acid-glycolic acid) sintered microsphere scaffolds for bone tissue engineering. *Biomaterials* **27**, 4894-4903 (2006).

444. T. Jiang, S. G. Kumbar, L. S. Nair, C. T. Laurencin, Biologically active chitosan systems for tissue engineering and regenerative medicine. *Current topics in medicinal chemistry* **8**, 354-364 (2008).
445. A. Aravamudhan, D. M. Ramos, A. A. Nada, S. G. Kumbar, Natural polymers: polysaccharides and their derivatives for biomedical applications. *Natural and Synthetic Biomedical Polymers*, 67-89 (2014).
446. S. V. Gohil, D. J. Adams, P. Maye, D. W. Rowe, L. S. Nair, Evaluation of rhBMP‐2 and bone marrow derived stromal cell mediated bone regeneration using transgenic fluorescent protein reporter mice. *Journal of Biomedical Materials Research Part A* **102**, 4568-4580 (2014).
447. M. Yamamoto, Y. Takahashi, Y. Tabata, Controlled release by biodegradable hydrogels enhances the ectopic bone formation of bone morphogenetic protein. *Biomaterials* **24**, 4375-4383 (2003).
448. E. Gómez‐Barrena *et al.*, Bone regeneration: stem cell therapies and clinical studies in orthopaedics and traumatology. *Journal of cellular and molecular medicine* **15**, 1266-1286 (2011).
449. E. M. Horwitz *et al.*, Transplantability and therapeutic effects of bone marrow-derived mesenchymal cells in children with osteogenesis imperfecta. *Nature medicine* **5**, 309-313 (1999).
450. P. Bianco *et al.*, The meaning, the sense and the significance: translating the science of mesenchymal stem cells into medicine. *Nature medicine* **19**, 35-42 (2013).
451. D. E. Discher, D. J. Mooney, P. W. Zandstra, Growth factors, matrices, and forces combine and control stem cells. *Science* **324**, 1673-1677 (2009).
452. F. G. Giancotti, E. Ruoslahti, Integrin signaling. *Science* **285**, 1028-1033 (1999).
453. S. Martino, F. D'Angelo, I. Armentano, J. M. Kenny, A. Orlacchio, Stem cell-biomaterial interactions for regenerative medicine. *Biotechnology advances* **30**, 338-351 (2012).
454. X. Yu *et al.*, Controlling the structural organization of regenerated bone by tailoring tissue engineering scaffold architecture. *Journal of Materials Chemistry* **22**, 9721-9730 (2012).
455. K. Beitzel *et al.*, Properties of biologic scaffolds and their response to mesenchymal stem cells. *Arthroscopy: The Journal of Arthroscopic & Related Surgery* **30**, 289-298 (2014).
456. P. Kasten *et al.*, Porosity and pore size of β-tricalcium phosphate scaffold can influence protein production and osteogenic differentiation of human mesenchymal stem cells: an in vitro and in vivo study. *Acta Biomaterialia* **4**, 1904-1915 (2008).
457. C. M. Murphy, M. G. Haugh, F. J. O'Brien, The effect of mean pore size on cell attachment, proliferation and migration in collagen–glycosaminoglycan scaffolds for bone tissue engineering. *Biomaterials* **31**, 461-466 (2010).
458. A. R. Amini, D. J. Adams, C. T. Laurencin, S. P. Nukavarapu, Optimally porous and biomechanically compatible scaffolds for large-area bone regeneration. *Tissue Engineering Part A* **18**, 1376-1388 (2012).
459. T. Jiang *et al.*, Chitosan–poly (lactide-co-glycolide) microsphere-based scaffolds for bone tissue engineering: In vitro degradation and in vivo bone regeneration studies. *Acta biomaterialia* **6**, 3457-3470 (2010).

460. I. Bilic‐Curcic *et al.*, Visualizing levels of osteoblast differentiation by a two‐color promoter‐GFP strategy: Type I collagen‐GFPcyan and osteocalcin‐GFPtpz. *Genesis* **43**, 87-98 (2005).
461. I. Kalajzic *et al.*, Use of type I collagen green fluorescent protein transgenes to identify subpopulations of cells at different stages of the osteoblast lineage. *Journal of Bone and Mineral Research* **17**, 15-25 (2002).
462. Y. H. Wang, Y. Liu, K. Buhl, D. W. Rowe, Comparison of the action of transient and continuous PTH on primary osteoblast cultures expressing differentiation stage‐specific GFP. *Journal of Bone and Mineral Research* **20**, 5-14 (2005).
463. Y. Liu *et al.*, Isolation of murine bone marrow derived mesenchymal stem cells using Twist2 Cre transgenic mice. *Bone* **47**, 916-925 (2010).
464. X. Jiang *et al.*, Histological analysis of GFP expression in murine bone. *Journal of Histochemistry & Cytochemistry* **53**, 593-602 (2005).
465. W. I. Abdel-Fattah, T. Jiang, G. E.-T. El-Bassyouni, C. T. Laurencin, Synthesis, characterization of chitosans and fabrication of sintered chitosan microsphere matrices for bone tissue engineering. *Acta Biomaterialia* **3**, 503-514 (2007).
466. J. A. Inzana *et al.*, 3D printing of composite calcium phosphate and collagen scaffolds for bone regeneration. *Biomaterials* **35**, 4026-4034 (2014).
467. D. D. Deligianni, N. D. Katsala, P. G. Koutsoukos, Y. F. Missirlis, Effect of surface roughness of hydroxyapatite on human bone marrow cell adhesion, proliferation, differentiation and detachment strength. *Biomaterials* **22**, 87-96 (2000).
468. J. Lincks *et al.*, Response of MG63 osteoblast-like cells to titanium and titanium alloy is dependent on surface roughness and composition. *Biomaterials* **19**, 2219-2232 (1998).
469. J. M. Dang, K. W. Leong, Natural polymers for gene delivery and tissue engineering. *Advanced drug delivery reviews* **58**, 487-499 (2006).
470. O. Bostman, U. Paivarinta, M. Manninen, P. Rokkanen, Polymeric debris from absorbable polyglycolide screws and pins. Intraosseous migration studied in rabbits. *Acta Orthopaedica Scandinavica* **63**, 555-559 (1992).
471. F. von Burkersroda, L. Schedl, A. Göpferich, Why degradable polymers undergo surface erosion or bulk erosion. *Biomaterials* **23**, 4221-4231 (2002).
472. L.-S. Liu, A. Y. Thompson, M. A. Heidaran, J. W. Poser, R. C. Spiro, An osteoconductive collagen/hyaluronate matrix for bone regeneration. *Biomaterials* **20**, 1097-1108 (1999).
473. A. M. Ferreira, P. Gentile, V. Chiono, G. Ciardelli, Collagen for bone tissue regeneration. *Acta biomaterialia* **8**, 3191-3200 (2012).
474. K. Weadock, R. M. Olson, F. H. Silver, Evaluation of collagen crosslinking techniques. *Biomaterials, medical devices, and artificial organs* **11**, 293-318 (1983).
475. K. Sempf *et al.*, Adsorption of plasma proteins on uncoated PLGA nanoparticles. *European Journal of Pharmaceutics and Biopharmaceutics* **85**, 53-60 (2013).
476. C. Alves, R. Reis, J. Hunt, Preliminary study on human protein adsorption and leukocyte adhesion to starch-based biomaterials. *Journal of Materials Science: Materials in Medicine* **14**, 157-165 (2003).
477. C. M. Alves *et al.*, Modulating bone cells response onto starch-based biomaterials by surface plasma treatment and protein adsorption. *Biomaterials* **28**, 307-315 (2007).

478. Y. Mo *et al.*, Preparation and properties of PLGA nanofiber membranes reinforced with cellulose nanocrystals. *Colloids and Surfaces B: Biointerfaces* **132**, 177-184 (2015).
479. C. Barbie, D. Chauveaux, X. Barthe, C. Baquey, J. Poustis, Biological behaviour of cellulosic materials after bone implantation: preliminary results. *Clinical materials* **5**, 251-258 (1990).
480. J. Fricain *et al.*, Cellulose phosphates as biomaterials. In vivo biocompatibility studies. *Biomaterials* **23**, 971-980 (2002).
481. M. E. Nimni, D. Cheung, B. Strates, M. Kodama, K. Sheikh, Chemically modified collagen: a natural biomaterial for tissue replacement. *Journal of biomedical materials research* **21**, 741-771 (1987).
482. M. Kikuchi *et al.*, Glutaraldehyde cross-linked hydroxyapatite/collagen self-organized nanocomposites. *Biomaterials* **25**, 63-69 (2004).
483. L. Ma, C. Gao, Z. Mao, J. Zhou, J. Shen, Enhanced biological stability of collagen porous scaffolds by using amino acids as novel cross-linking bridges. *Biomaterials* **25**, 2997-3004 (2004).
484. B. S. Lee, Y. S. Chi, K.-B. Lee, Y.-G. Kim, I. S. Choi, Functionalization of poly (oligo (ethylene glycol) methacrylate) films on gold and Si/SiO2 for immobilization of proteins and cells: SPR and QCM studies. *Biomacromolecules* **8**, 3922-3929 (2007).
485. W. Qiu, E. Skafidas, Detection of Protein Conformational Changes with Multilayer Graphene Nanopore Sensors. *ACS applied materials & interfaces* **6**, 16777-16781 (2014).
486. A. I. Caplan, J. E. Dennis, Mesenchymal stem cells as trophic mediators. *Journal of cellular biochemistry* **98**, 1076-1084 (2006).